Lightweight Cellular Concrete as Flexible Pavement Subbase Material: Field Performance and Sustainability Study

by

Abimbola Grace Oyeyi

A thesis
presented to the University of Waterloo
in fulfillment of the
thesis requirement for the degree of
Doctor of Philosophy
in
Civil Engineering

Waterloo, Ontario, Canada, 2022

Examining Committee Membership

The following served on the Examining Committee for this thesis. The decision of the Examining Committee is by majority vote.

External Examiner:	Ahmed Shalaby Professor, Department of Civil Engineering University of Manitoba
Supervisor(s):	Susan Tighe Professor, Department of Civil & Environmental Engineering University of Waterloo
Supervisor(s):	Shunde Yin Professor, Department of Civil & Environmental Engineering University of Waterloo
Internal Member:	Hassan Baaj Professor, Department of Civil & Environmental Engineering University of Waterloo
Internal Member:	Vimy Henderson Professor, Department of Civil & Environmental Engineering University of Waterloo

Internal-External Member: Kaan Inal
Professor, Department of Mechanical & Mechatronics Engineering
University of Waterloo

Author's Declaration

This thesis consists of material all of which I authored or co-authored: see Statement of Contributions included in the thesis. This is a true copy of the thesis, including any required final revisions, as accepted by my examiners.

I understand that my thesis may be made electronically available to the public.

Statement of Contribution

Chapter 2 of this thesis contains parts of a paper co-authored by myself, Frank Mi-Way Ni, and my supervisor (Dr. Tighe). Dr. Ni and I developed the methodology and research design of the paper with input from Dr. Tighe. Dr. Ni and I also completed the writing of the paper.

Section 6.3 of this thesis has been incorporated into a paper submitted for publication. The paper is co-authored by myself, Emmanuel A. Badewa, Frank Mi-Way Ni, and my supervisor (Dr. Tighe). I developed the methodology and research design of the paper, with input from Dr. Tighe, while Dr. Ni assisted in data collection. Emmanuel and I worked on data processing and analysis. I completed the paper writing while Mr. Badewa, Dr. Ni and Dr. Tighe edited and reviewed the paper.

Sections 6.9 and 7.3.1.1 of this thesis have been incorporated into a paper submitted for publication. The paper is co-authored by myself, Frank Mi-Way Ni, and my supervisor (Dr. Tighe). I developed the methodology and research design of the paper, with input from Dr. Tighe, while Dr. Ni assisted in data collection and analysis. I completed the paper writing while Dr. Ni and Dr. Tighe edited and reviewed the paper.

Chapter 8 of this thesis contains parts of a paper submitted for publication. The paper is co-authored by me, Jessica Achebe, Frank Mi-Way Ni, and my supervisor (Dr. Tighe). I developed the paper's research design with help from Dr. Ni. Dr Achebe and I developed the methodology and collectively analyzed the data with input from Dr. Tighe. I completed the writing of the paper. The co-authors also provided editing and review during the paper's production.

Abstract

Enhancing the long-term performance of road infrastructure is an important goal for engineers in Canada, especially with changing climatic conditions. This has brought about varying approaches in design and construction techniques with alternative materials. Some factors considered in selecting these materials include advantages in terms of sustainability, lower costs, ease of construction, and increased structural capacity. Lightweight Cellular Concrete (LCC) is one such material that could be a viable option in Canada, where the pavement structure is subject to the freeze-thaw effect yielding weaker subgrades. Previous research acknowledges that as a subbase material, it could yield promising results as it has shown good freeze-thaw resistance, ease of placement as it is semi-liquid, and potential sustainability benefits such as the reduction in the use of virgin materials through the usage of industrial by-products, less pollution, and lower lifecycle costs. However, there is a need to quantify these benefits and develop unified standards and specifications for using this material in the pavement structure in Canada.

This study evaluated three densities of LCC with two production methods (wet and dry mix) in terms of constructability, field performance, and sustainability. This involved pre and post-construction monitoring of test and control sections to evaluate the performance of the LCC layer. Two test sections were built in the Region of Waterloo, Ontario. One of the trial roads (Erbsville) incorporated 250 mm and 350 mm of 475 kg/m^3 LCC as subbase material and compared it with a control constituting of 450 mm granular B subbase. The second test section (Notre Dame Drive) employed 200 mm LCC with densities of 400, 475, and 600 kg/m^3 compared with a 150 mm granular A subbase.

Constructability evaluation involved field testing, onsite, and instrumentation monitoring during construction. Field performance tracking was achieved across varying climatic conditions using pre-installed instrumentation to monitor stress and strain responses, layer temperature, moisture, and LCC maturity. Precipitation and ambient temperature conditions were monitored using a weather station at both field test locations. Also, pavement material properties from the field sections were tested at the CPATT laboratory. The tests performed included dynamic modulus for the asphalt concrete, unconfined compressive strength, modulus of elasticity and Poisson's ratio, and water absorption tests for LCC, California Bearing Ratio (CBR) test for the pavement unbound layers.

Furthermore, stiffness and structural capacity were evaluated using the Falling Weight Deflectometer (FWD) and Lightweight deflectometer. Roughness assessment was done with SurPro and Dipstick equipment. Regular visual inspections were conducted to capture distresses on the pavement sections. Finally, Lifecycle Assessment (LCA) and Lifecycle

Cost Analysis (LCCA) were performed to quantify economic and environmental outcomes compared with current industry standards.

The results revealed that applying a Lightweight Cellular Concrete subbase within the pavement structure is a feasible alternative to traditional subbase material, especially when subgrade insulation is required and weak subgrades are encountered. It showed that excessive vehicles and trucks over the LCC pavement sections before asphalt paving could be detrimental to LCC pavement performance by inducing higher stresses and strains. Lightweight Cellular Concrete with densities between 400 and 600 kg/m^3 has excellent insulation properties within the pavement structure. It can reduce subgrade pressure due to traffic by up to three times compared to unbound granular material and strain responses by four times. These attributes were seen to increase with an increase in density. Layer temperature and moisture were influenced by ambient temperature and precipitation events and, in turn, influenced pavement stress and strain responses. A structural coefficient of 0.22 was determined for 475 kg/m^3 and proposed as a benchmark for designing LCC pavements with a density between 400 and 600 kg/m^3.

Lifecycle assessment results showed that LCC pavements could lower environmental costs by reducing total life CO_2 emissions by up to 16% while significantly reducing the environmental impact of SO_2, CO, NO_x, PM_{10}, and total PM compared to unbound granular pavements. Environmental impact was seen to increase with an increase in LCC density. Total life costs of the LCC sections were 10% to 13% more than pavement sections with granular A and 4% to 6% more than granular B pavements. However, when only the initial construction and maintenance phase were considered, the LCC sections were 3% to 6% less expensive than the granular A pavement and 9% to 12% less than the granular B pavement. The 400 and 475 kg/m^3 LCC pavements had comparable costs.

This study provided an understanding of the pavement behavior of lightweight cellular concrete subbase and developed pavement layer temperature regression models for LCC and unbound granular subbase pavements with very good predictability. It presents a way to assess LCC pavements' environmental and economic impacts and recommends design, construction specifications, and guidelines for using lightweight cellular concrete subbase within flexible pavements.

Acknowledgements

I would like to express my sincere gratitude to my supervisor Professor Susan Tighe for this amazing opportunity, her support, encouragement, and patience throughout my Ph.D. study. My appreciation to my co-supervisor Prof. Shunde Yin for his kind support.

I would like to acknowledge my Ph.D. committee members Professor Hassan Baaj, Professor Kaan Inal, Professor Vimy Henderson from University of Waterloo, and my external examiner Professor Ahmed Shalaby from the University of Manitoba for participating in my Ph.D. defense and helping to improve this work.

I would like to thank Brad Dolton, Steve Bent, Dr Jim Li, Albert Fang, Jerry Janik, and Dan Hanley from CEMATRIX (Canada) Inc. for their valuable feedbacks and support on this research.

My heartfelt gratitude goes to the Civil and Environmental Engineering Department staff, particularly Peter Volcic, Richard Morrison, Douglas Hirst, Terry Ridgway, Victor Lewis and Victoria Tolton for their professional advice and support in the laboratory, on the field and administratively.

Special thanks to Luke Misurka and Jeff Nyhesius from the Region of Waterloo for their tremendous support before, during and after construction of the field sections. Also, many thanks to Steed and Evans and Seegmiller for all the help on the field during construction and testing especially Andre Schaap and Dale Serediak.

Further thanks to all my CPATT professors and colleagues for their help with field laboratory work and emotional support. Thank you, Professor Pejoohan Tavassoti, Dr. Abdulrahman Hamid, Tamanna Kabir, Dr. Luke Zhao, Dr. Eskedil Melese, Dr. Taher Baghaee Maghaddam, Dr. Dan Pickel, Dr. Shenglin Wang, Dandi Zhao, Rob Aurilio, Peggie Wang, Haya Almutairi, Dr. Hanaa Al-Bayati, Frank Lui, Adam Schneider, Dr. Saeid Salehiashani, Paula Barbi, Jianq Kang, Dr. Ata Nahidi and Ali Qabur.

Special thanks to my friend and colleague, Dr. Frank Mi-Way Ni for his immeasurable help, support, and encouragement. To my friends and their families, Remi Oyediji, Emmanuel Badewa, Dr. Ibrahim Ogunsanya, Kay Awe, Sergey Averyanov, Dr. Jessica Achebe and Dr. Dotun Adenigbo, thank you. I would also like to acknowledge my church family Our God Hears Foursquare church for their love and support throughout my program. Thank you Pastors Funso and Bim (of blessed memory) Akinniyi. Thank you Pastors Sam and Fise Ekpenyong.

I want to thank my mom, my siblings (Wumi, Wale, and Dapo), and their families as well as my other sisters (Mafo and Maade) for their love and support. For my other parents,

Dad and Mom Oyeyi, thank you. To my Husband (Tony) and my babies (David and Anna), you made the process worthwhile; thank you so much for your patience, understanding, and love throughout the research period.

To God! I am absolutely nothing without You! Thank you for life and grace to do this work and live worthy of the calling!

I would like to acknowledge the following sponsoring partners of this research project:

- The Centre for Pavement and Transportation Technology (CPATT), Norman W. McLeod Chair, University of Waterloo.
- The Natural Sciences and Engineering Research Council of Canada (NSERC) Collaborative Research and Development Program.
- CEMATRIX (Canada) Inc.
- The Region of Waterloo

Dedication

Mom, this is for you. Thank you for the many sacrifices, prayers, and love!

Table of Contents

List of Figures

List of Tables

List of Abbreviations

AADT: Average Annual Daily Traffic

AADTT: Average Annual Daily Truck Traffic

AASHTO: American Association of State Highway and Transportation Officials

AC: Asphalt Concrete

ACI: American Concrete Institute

ARA: Applied Research Associates

ASTM: American Society for Testing and Material

BCA: British Concrete Association

CO: Carbon monoxide

CO_2: Carbon dioxide

CPATT: Centre for Pavement and Transportation Technology

CSA: Canada Standard Association

EUAC: Equivalent Uniform Annual Cost

EPS: Expanded Polystyrene

FWD: Falling Weight Deflectometer

FHWA: Federal Highway Administration

GA: Granular A

GB: Granular B

GBE: Granular Base Equivalency

HMA: Hot Mix Asphalt

IRI: International Roughness Index

LCC: Lightweight Cellular Concrete

LCA: Life Cycle Assessment

LCCA: Life Cycle Cost Analysis

LWD: Lightweight Deflectometer

MD: Marginal Damage

MEPDG: Mechanistic-Empirical Pavement Design Guide

MOE: Modulus of Elasticity

NCHRP: National Cooperative Highway Research Program

NO_x: Nitogen oxides

NPV: Net Present Value

NPW: Net Present Worth

OPSS: Ontario Provisional Standard Specification

PCI: Pavement Condition Index

PG: Performance Grading

PM: Particulate Matter

QA: Quality Assurance

QC: Quality Control

RAP: Reclaimed Asphalt Pavement

RCA: Recycled Concrete Aggregate

RCR: Road Condition Rating

RMSE: Root Mean Square Error

SO_2: Sulphur dioxide

SP: SuperPave

SWP: Soil Water Potential

MTO: Ministry of Transportation Ontario

TAC: Transportation Association of Canada

WESLEA: Waterways Experiment Station Linear Elastic Analysis

UCPRC: University of California Pavement Research Center

UCS: Unconfined Compressive Strength

XPS: Extruded Polystyrene

Chapter 1

Introduction

The Canadian government aims to "build a safe, secure, green, creative, and integrated transportation system that supports trade and economic growth, a cleaner environment, and the well-being of all Canadians" through its Transportation 2030 Strategic Plan [45]. A significant portion of the transportation infrastructure in Canada is the road pavement structure, with a total length of 1.04 million km [246]. Therefore, the onus is on engineers to develop innovative yet long-lasting pavement structures without compromising on cost-effectiveness and the environment. As a result, there have been research into varying approaches in design and construction techniques with alternative materials. Some primary considerations in material selection include responses to changes in climatic conditions, cost, effect on the environment, ease of use, and structural capacity.

Also, due to severe climatic conditions with frost and rapid temperature variations, weaker subgrades which are soft and frost susceptible, are produced [102] , as is the case for Canada. Frequently, Canadian roads and highways are constructed over weak subgrades consisting of peat, organics, or soft soil deposits, which cause them to undergo continual and long-term settlements [153]. This will usually require frequent repairs, leading to even more settlements due to additional loading on the pavement structure. Traditional full-depth maintenance is also not cost-effective, especially for depths greater than one meter. An alternative of full reconstruction is also expensive, disruptive to road users, and not sustainable due to the generation of large quantities of excess materials and the use of virgin material [153].

To mitigate the problem of weaker subgrades in addition to refining its characteristics, improving the subbase layer with new materials should be considered. As the subbase is a significant part of the pavement structure, which helps transmit loading from upper

layers to the subgrade, major innovations in material compositions and the ability to do their job adequately are necessary. Traditionally, the unbound crushed stone material is utilized to perform these functions. However, since it involves the use of virgin material, it poses a problem of depletion of natural resources and constituting additional environmental hazards due to its production and transportation and increased cost incurred. This also does not solve the settlement problem, as its weight also burdens the subgrade [155].

Lightweight materials are being researched to improve the subbase layer, especially when weak soils are encountered. The primary purpose of lightweight materials is to function as alternative construction materials to reduce the weight of fills significantly, thereby mitigating excessive settlements and bearing failures, minimizing the generation of waste, and delivering better-performing pavements that require fewer maintenance interventions [13, 153]. This can provide more economically viable designs [13].

Lightweight Cellular Concrete (LCC) is a lightweight material being considered a viable option to achieve the transportation goal of longer-lasting, more sustainable pavements. It is also known as foamed concrete, foam concrete, or reduced density concrete and consists of cement slurry, foam, and compressed air, which influences its lightweight [63]. It has wet densities ranging from 250 to 1600 kg/m^3 with below-the-ground installation wet densities usually between 400 kg/m^3 and 600 kg/m^3.

Lightweight Cellular Concrete use dates to the early 19th century; however, in-depth studies about the material composition, physical properties, and production were only carried out in the 1950s [252]. Since then, there has been ongoing research on how to improve the characteristics and use of LCC. The usage has increasingly become a preferable option in construction than regular concrete, especially in applications requiring lighter materials and excellent workability. This is due to specific improved properties such as its lower structural dead weight, free-flowing and self-compacting nature, lower thermal conductivity, ease of recyclability, and ultimately a lower lifecycle cost [135]. It has a lower density, which can be recycled in the future. Furthermore, it uses industrial by-products such as slag, silica fume, and fly-ash to customize its structural and flexural strength [135].

The use of LCC has evolved over the years from void fillings to ground stabilization and, more recently, as a structural component in the infrastructure. Because LCC has a wide range of density, typically between 300 to 1600 kg/m^3, it gives flexibility that could enable its use in numerous applications [172]. Specifically, it has been used for filling large voids, floor screeding, insulating foundations thermally, strengthening bridges, backfilling, and as pre-cast blocks [189]. Also, it has been applied for soil stabilization, pipe beddings, sound walls, insulation, filling abandoned pipes, tanks, and mines, and as arrester material at the end of the runway, which crushes and stops overshooting aircraft [63, 103].

The use of LCC as part of the pavement structure is also gaining recognition, especially in areas with weaker subgrades. Numerous applications in Canada within the pavement structure have been recorded, such as the bus lane in Calgary, Alberta, and Caledon, Ontario, primarily to solve settlement problems due to weak subgrades [153, 63].

With LCCs applications and previous studies, there is still limited information and guidelines for use in the pavement structure. Previous studies have mainly concentrated on mechanical properties via laboratory testing; however, there is no comprehensive field performance data for its application in road construction. Also, although LCC has been reported as being able to reuse waste material and itself recyclable, which provides an excellent indication of its sustainability benefits, there is a need to quantify these benefits, especially with recent emphasis on sustainable construction.

1.1 Research Hypothesis

- Lightweight Cellular Concrete as a subbase material can prolong the useable life of pavements by providing longer-lasting pavements than the traditional unbound granular material.
- Lightweight Cellular Concrete can be efficiently planned, designed, and constructed for successful performance based on structural and environmental responses, surface, stiffness, and roughness evaluations.
- Lightweight Cellular Concrete can replace traditional unbound granular B as subbase without compromising pavement performance.
- The use of lightweight cellular concrete as pavement subbase material provides greater sustainability benefits than the traditional unbound granular material.
- The application of lightweight cellular concrete as pavement subbase material is more cost-effective in the long term than the traditional unbound granular materials.

1.2 Research Scope and Objectives

This research aims to evaluate the field performance of Lightweight Cellular Concrete as an alternative material for the pavement subbase layer in Canada. Hence, integrating laboratory testing and field performance data to develop guidelines for its use. In achieving this goal, the specific research objectives were as follows.

- Evaluate the use of LCC as subbase material in terms of constructability using a combination of field testing, inspection, and instrumentation monitoring.
- Examine the field performance of using LCC as subbase material compared to unbound granular subbase material.
- Perform a Lifecycle Assessment (LCA) and Lifecycle Cost Analysis (LCCA) of Lightweight Cellular Concrete and compare it with current industry unbound granular subbase material.
- Develop guidelines for using LCC as a subbase material for pavement construction in Canada.

1.3 Methodology of study

The assessment plan for this study can be broken into different portions and described as follows based on the objectives and scope of the research:

- An in-depth review of Lightweight Cellular Concrete is presented, including a review of pavement subbase and insulating materials.
- Through construction, instrumentation monitoring, and post-construction testing, the performance of Lightweight Cellular Concrete pavement responses was evaluated and compared to the conventional pavement structure. Three LCC densities (400 kg/m^3, 475 kg/m^3 and 600 kg/m^3) were considered in this study. These densities were selected based on previous work by Ni [174] and industrial experience. Research showed that below ground applications such as road construction typically applied LCC densities between 300 and 600 kg/m^3. However, densities of 300 kg/m^3 have been associated with instability issues. Furthermore, past pavement field applications in Canada have mostly used the 475 kg/m^3, therefore it was important to further assess it and densities below and above 475 kg/m^3. Two typical unbound granular materials (Granular A and B) currently used in Ontario, Canada as base and subbase were selected for the Control sections.
- Evaluation of installed layer material properties through laboratory testing was performed.

- AASHTO 93, Granular Based Equivalency, and software-based pavement design were used to predict pavement performance, with input parameters derived from laboratory findings. The lightweight cellular concrete subbase pavement was compared to the traditional pavement structure.
- Estimating the life cycle economic and environmental implications of incorporating Lightweight Cellular Concrete as a pavement subbase was completed.
- Guidelines for the use of Lightweight Cellular Concrete subbase were developed.

1.4 Thesis Organization

Eleven chapters supported with tables and figures make up this thesis.

The context, aims and scope of this study are all described in **Chapter 1**. In this chapter, a broad methodology is also discussed.

The lightweight cellular concrete literature study in **Chapter 2** covers its material characteristics, comparison of pavement insulation and subbase materials, and finally outlines the current gaps.

The approach used in this study is described in detail in **Chapter 3**. This covers the evaluation considerations and approaches to evaluate laboratory and field data.

Details on the design and construction of the test sections are presented in **Chapter 4**. The challenges encountered during construction and a preliminary constructability analysis are described concerning how LCC pavements respond to construction operations.

The laboratory findings of this investigation are presented in **Chapter 5**. Several properties are offered, including mechanical, durability, and dynamic properties. This chapter also covers the outcomes of pavement performance prediction. The MEPDG and WESLEA pavement analysis software was used for this.

Chapter 6 investigates the pavement performance of Lightweight cellular concrete and unbound aggregate subbase material by examining the pressure, strain, moisture, and temperature data obtained from installed instrumentation and weather station.

Chapter 7 also investigates pavement performance, but in this case by examining post-construction evaluations such as pavement stiffness, roughness, and distress.

The life cycle assessment of lightweight cellular concrete is covered in **Chapter 8**, along with comparisons to unbound granular A and B.

The lifecycle cost analysis of lightweight cellular concrete is addressed in Chapter 9, along with a description of the methodology used and information on sensitivity analysis.

The primary contributions of this research are summarized in **Chapter 10**, which also highlights the future potential for research and summarizes the results and recommendations.

Chapter 11 presents recommended guidelines for using lightweight cellular concrete within the pavement structure as a subbase layer.

Chapter 2

Literature Review

2.1 Current Practices

2.1.1 Typical Pavement Subbase Layer

The typical flexible pavement in Canada constitutes one or more bituminous material layers (binder course and surface course), placed over a base course and a subbase course over the subgrade [234]. Figure 2.1 shows the typical flexible pavement structure in Canada. All the layers perform differing functions for the proper functioning of the pavement structure; hence, necessary to continually improve their characteristics to provide longer-lasting and performing pavements. Usually, the subbase refers to the first layer of processed aggregate laid on the subgrade, which has lower cost and quality than the base course materials [234]. The subbase layer serves as a cushion, the final loading point before the subgrade; thus, it spreads and transfers the load from the previous layers above it to the subgrade. The subbase should also provide good drainage properties and frost protection to the subgrade [234].

In Canada, both flexible and rigid pavement types typically use granular material as subbase, which could either be unbound or treated. The quality of these aggregates greatly influences pavement performance over its service life. Aggregate properties that might affect the layer performance include shear strength, frost susceptibility, durability, stiffness, and toughness [193]. Factors critical to the appearance of distresses for this material include shear strength, density, fine content, gradation, moisture level, particle angularity and surface texture, freeze-thaw cycling, and drainage ability [25].

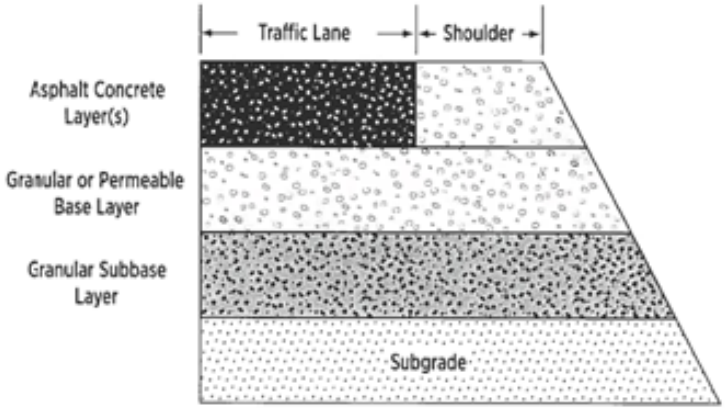

Figure 2.1: Typical cross section of a rural conventional asphalt concrete pavement [234]

This layer has historically been made of granular material; however other materials could be used instead. This is because Canadian transportation agencies are looking for more innovative pavement construction options, including recycling, reusing, and using by-product materials [234]. Other potential subbase materials have been evaluated in Canada, and some are still being assessed. Depending on the desired performance outcome, the materials are chosen based on features and attributes such as excellent thermal conductivity, freeze-thaw resistance, thermal insulation, and structural weight reduction. Other materials have also been used because of the desire to reduce the usage of virgin material, reduce costs, and improve structural and pavement performance. The traditional unbound granular material has been mixed with different materials in several approaches to improve performance. Table 2.1 shows some of the types of subbase materials that have been studied and are currently used.

The Ontario Provincial Standard Specification (OPSS) 1010, Material Specification for Aggregates, permits the use of several types of recycled or reclaimed materials, including 100% Recycled Concrete Aggregate (RCA) and 30% Recycled Asphalt Pavement (RAP), as substitutes for natural aggregates except in granular B type II. Studies evaluating the use of RAP as a substitute for natural aggregate in Canada for base and subbase material have found that RAP and RCA provide comparable characteristics to natural aggregate. Moore et.al, (2014) [169] found that if properly manufactured, RCA can be a suitable replacement for natural aggregates. This was also the case for an earlier study by National Cooperative Highway Research Program (NCHRP) in 2013. However, the study also established that processed RCA could differ from natural aggregates in terms of its higher angularity, lower specific gravity, and increased water absorption. Although RAP was also found to perform

Table 2.1: Some types of materials for pavement subbase in Canada

Type	**Material composition**	**Reason for use**	**Reference**
Unbound Granular material	Crushed stones	Most widely used, it serves to drain moisture and provide a non-frost susceptible layer over the subgrade	[234]
Treated unbound granular material	Unbound granular can be stabilized with Bituminous (Expanded Asphalt or Emulsion) material or cementitious materials)	Enhance strength and durability of the layer under traffic loading	[234]
Natural aggregate and RAP	30% by mass Reclaimed Asphalt Pavement and Natural aggregates (crushed stones)	Reduce waste disposal and use of virgin material, enhance resilient modulus, improve drainage properties of the layer	[222]; [249]; [228]
Natural aggregate and Recycled Concrete Aggregate RCA	Crushed Concrete and Natural aggregate	Reduce waste disposal and use of virgin material, enhance resilient modulus, improve drainage properties of the layer	[222]; [249]; [228]
RAP and RCA	Reclaimed Asphalt Pavement and Crushed Concrete	Enhance reuse of existing material hence reducing waste and use of virgin materials	[222]
Recycled Concrete Aggregate (RCA)	Crushed Concrete	Reduce weight, waste, and use of natural resources	[222], [169]; [228]
Recycled waste glass or ceramic and natural aggregates	15% by mass glass waste blended with natural aggregate	Reduce waste and use of natural resources. Lightweight applications such as improving thermal insulation	[223]; [228]
Iron Blast furnace slag or nickel slag aggregate	Blast furnace slag or Nickel slag aggregates	Use of industrial by-products, reduce waste, and use of natural resources. Used for lightweight applications	[228]
Lightweight Cellular Concrete	Cement, water, foam, compressed air	Reduce weight on the subgrade, ease of use, reduce waste and use of virgin material	[63]; [174]

comparatively to natural aggregates, there are still concerns as it yields lower bearing capacity and has the potential to expand and oxidize as it ages.

To further assess the effect of using a high percentage of RAP as a supplement to virgin material in subbase [168], the LWD and FWD+GPR were used to investigate the short- and long-term field performance of RAP compared to natural aggregate. They used a blend of 50% RAP and 50% natural aggregate as their subbase layer and found that mixes with higher blended RAP depicted similar short-term and slightly higher long-term performance.

A more recent study in Canada [222] evaluated the performance of RAP and RCA for application in the pavement structure, especially as a replacement for crushed rock in Granular B type II material, through field and laboratory testing. Five different mix types were evaluated; 100% crushed rock; 25% RCA with 75% crushed rock; 50% RCA with 50% crushed rock; 100% RCA; 70% RCA with 30% RAP. Results showed that mixes had similar resilient modulus and good drainage characteristics. RCA mixes had similar CBR values at 100%; however, the mix containing 30% RAP had a lower CBR value. The study concluded that RCA and RAP could be a good substitute in a range of proportions without adversely affecting the layers' physical strength and permeability characteristics. However, the weight of these materials is still a burden on the subgrade, leading to settlements.

Table 2.2 outlines the characteristics of unbound aggregates currently used in Canada compared with other recommended subbase materials. The potential use of alternatives is hugely dependent on the goal, such as insulation, protection, and improved structural capacity, to mention a few.

Table 2.2: Summary of material properties of LCC and other subbase material [174]

	LCC-400	**LCC-475**	**LCC-600**	**Granular B**	**Lean concrete**	**Cement stabilized aggregate**	**Soil cement**	**Lime stabilized soils**
Gradation Requirement	N	N	N	Y	N	N	N	N
Compressive Strength (MPa)	0.7 – 1.0	1.1 – 1.5	1.5 – 2.2	–	1.72	1.72	1.72	1.72
MOE (MPa)	600 – 850	800 – 1,300	1,300 – 1,700	250	13,790	6,895	3,447	310
Poisson's Ratio	0.14 – 0.28	0.19 – 0.31	0.18 – 0.30	0.35	0.15	0.1 – 0.2	0.15 – 0.35	0.15 – 0.2
Tensile Strength (MPa)	0.16	0.2	0.3	-	-	-	-	-
Modulus of Rupture (MPa)	0.20 – 0.25	0.27 – 0.30	0.37 – 0.45	-	3.1	1.38	0.69	0.17

2.1.2 Typical Pavement Insulation Materials

Differential frost heave and an increase in soil moisture content occur due to pavements in cold regions being exposed to extremely low temperatures for lengthy periods during the winter and freezing thaw cycles in the spring. These have negative impacts on the pavement structure, causing premature cracking and lowering the bearing capacity of pavements; as a result, these pavements have shorter service lives and higher maintenance costs [161, 162, 215, 243]. Insulation layers are frequently utilized in cold climates to reduce frost penetration within pavements [107].

These layers are often applied on top of the subgrade. They have been shown to inhibit heat transfer between the base and subgrade layers, resulting in lower frost depths than traditional pavements with an added cost efficiency advantage [91, 33]. Furthermore, more environmentally friendly insulation layers are being used. Insulation layers such as polystyrene, bottom ash, foamed glass aggregates, foamed concrete, wood residues, and tire chips have been employed within the pavement structure in cold regions [196, 272]. In addition to their insulating function, several of these materials also serve as a pavement subbase. Table 2.3 summarizes some information about these insulation materials. In contrast, unbound granular layers are not typically regarded as insulating layers due to their thermal conductivity properties. Table 2.4 presents thermal conductivity values for various unbound granular materials for reference.

The main drawback of using insulation layers within pavements is increased temperature variation to the upper layers. This could lead to temperature decreases within these layers, which could adversely affect the asphalt concrete performance and the formation of icing at the pavement surface, which is a safety concern in cold regions [272]. Although one efficient way to reduce this challenge would be to increase the thickness of the base layer above the insulation layer, there remains the concern of the negative impact on the surface layer temperature when an insulation layer is introduced [55].

Previous research has shown that 5 cm of polystyrene layer can significantly reduce thaw depth and frost heave and limit pavement displacements compared to traditional pavement designs [96, 75, 237]. Comparing XPS and EPS, Pouliot and Savard (2003) [205] found that the thickness of EPS will have to be increased by 20% to have similar thermal performance as XPS, with EPS more sensitive to moisture [53]. Investigation of bottom ash also showed that in addition to reducing frost heave in winter, it improved pavement bearing capacity through the year, limited fatigue cracking compared to typical pavement sections, and provided a more sustainable layer because it is a recycled material [238].

Table 2.3: Typical Pavement Insulation Materials

Type	Description	Benefits	Challenges	Thermal conductivity	Ref.
Polystyrene	Expanded Polystyrene (EPS) - Has interconnected voids	Super lightweight can reduce frost depth and limit frost heave. Has interconnected voids that aid water penetration	EPS has lower strength and higher water absorption than XPS. Potential to create transverse cracks. Can cause the most negative influence on the surface layer compared to others. Labour intensive installation, bulky, fuel spill can lead to loss of frost protection, insulation degradation over time due to moisture, and non-recyclable	0.02 - 0.04 W/ (m.K) 0.036 W/ (m.K) average for EPS and 0.03W/ (m.K) for XPS	[223, 53, 107, 272]
	Extruded Polystyrene Boards (XPS) - Uniform closed cell rigid structure with no voids.	Super lightweight can reduce frost depth by up to 70% for 10cm EPS, limit frost heave and pavement settlement, and have better insulation properties than EPS.			
Wood residues	Sawdust and wood chips	Can reduce frost penetration depth and frost heave. Saw dust has better mechanical and thermal properties than wood chips.	Relatively lower strength. Thermal properties are sensitive to moisture content; water should be prevented from penetrating the layer	0.25 W/ (m.K) 0.16 (dry) W/ (m.K)	[66, 272]
Foam glass aggregates	Produced from mixed powdered recycled glass plus 2% foaming agent, baked at high temperatures. It has a closed cell structure	Reduce waste and use of natural resources through recycling, and lower GHG emissions by 22% compared to EPS. Over ten times lighter than unbound aggregates, lightweight applications can improve thermal insulation, limiting subgrade frost action, providing adequate drainage, and limiting the loss of bearing capacity. Easier and less expensive to transport. Not flammable and resistant to oil spill	Leachate quality is dependent on the source of recycled glass. Requires three times the thickness of XPS for similar insulation. Ten times lower the strength of natural aggregate	0.15 - 0.25 W/ (m.K)	[223, 266]
Bottom ash	By product of coal combustion, a size smaller than 0.5mm	Similar performance to typical granular materials, more environmentally friendly due to being a recycled material, cost-effective (dependent on availability), reduce frost heave by up to 23% for 1 m thickness, improves pavement bearing capacity, limits fatigue cracking, good constructability	When dry has minimal internal stability that can cause it to displace easily under traffic loads. Has high concentrations of metals (Boron and Lead). Environmental approval requires to use.	0.006 (W/m.K) 0.025 -0.075 W/m.K	[107, 80, 272]
Tire chips	Shredded scrap tires. Size less than 2 -in	Excellent insulation properties in addition to high permeability lead to excellent drainage properties. Potential to bear more traffic than conventional pavement for thicknesses over 35cm	Relatively lower strength.	0.1 - 0.6 W/ (m.K)	[66, 272]
Foamed concrete	Cement, preformed foam, water, atimes fine aggregates, and pozzolanic material. Has a homogenous air bubble structure	Lightweight can decrease frost depth by up to 59% for densities between 480 to 960 kg/m^3. Less pavement deformation by up to 20% and allow up to 180% more traffic than conventional pavements.	Requires curing time, leading to construction delay—instability at densities below 300 kg/m^3.	0.076 - 0.66 W/ (m.K) 0.1 -0.66 W/ (m.K) for 880kg/m^3 0.076 - 0.101W/(m.K) for 400 - 600 kg/m^3	[32], [187], [189], [46], [63], [174], [272]
High plastic Clay	Moderate plastic clays with liquid limits above 35 and granular soils with 20% fines	Sound insulation properties mitigate frost heave.	The material must be relatively dry and unsaturated. Requires adequate thickness of capillary break layer of clean granular material. Constructability challenges. Success dependent on the drainage system		[80]

Table 2.4: Thermal conductivity reference values extracted from literature [57]

Sedimentary category	**Thermal Conductivity (as indicated in VDI 4640)**		
	Min (W/mK)	**Max (W/mK)**	**Recommended value (W/mK)**
Gravel dry	0.4	0.9	0.4
Gravel water-saturated	2.0	3.0	2.4
Sand dry	0.3	0.9	0.4
Sand moist	1.0	1.9	1.4
Sand water-saturated	2.0	3.0	2.4
Clay/silt dry	0.4	1.0	0.5
Clay/silt water-saturated	1.1	3.1	1.8
Till/loam	1.1	2.9	2.4
Peat, soft lignite	0.2	0.7	0.4

Extruded polystyrene boards (XPS) and bottom ash (B.Ash) were also further proven to be effective insulators in protecting the subgrade from freezing in a study [107] in Alberta, Canada. At a depth of 70 cm from the pavement surface, 10 cm and 5 cm of XPS, and 1 m of B.Ash, were laid on the subgrade. Compared to a standard pavement section (control) without an insulation layer and the B.Ash, the 10 cm XPS had the superior insulating property, lowering frost depth by 70% and reducing excessive moisture within the subgrade. B.Ash, on the other hand, reduced frost depth by 23%. The base layer temperature of the 10 cm XPS, on the other hand, was found to be substantially lower in the winter months than in the other portions, resulting in differential icing, which could be dangerous due to the forming of slippery conditions on the pavement surface [54, 55].

In addition, sawdust and tire chips have been found to have similar thermal performance compared to a standard flexible pavement section by providing lower frost penetration and reducing frost heave. However, better mechanical performance in terms of deflection and vertical strain was noted for tire chips [66].

Segui et al., (2019) [223] performed a laboratory and field study on the use of foamed glass lightweight aggregate (FGA) in road construction as a potential lightweight aggregate for thermal insulation to reduce freeze-thaw damage on road infrastructure. The study found that using an FGA layer provided adequate pavement insulation compared with conventional expanded polystyrene. FGA also exhibited good drainage characteristics without adversely impacting the environment. Yousefi (2019) [266] further observed that when FGA is used as fill material in flexible pavement structures, it could provide higher or similar structural capacity while reducing environmental impacts compared to XPS.

More recently, in comparison to standard flexible pavements, lightweight cellular concrete (LCC) has been found to offer good insulating qualities. In comparing the insulation properties of LCC with XPS, FGA, and tire chips via Finite element modelling (FEM), Zhuo (2021) [272] found that the overall positive effect on the subgrade layer and adverse impact on the base layer, XPS and FGA would perform better than LCC while LCC better than tire chips. However, selecting the appropriate density of LCC poses a significant challenge for the application in insulated pavements [272]. Increasing foamed concrete density will improve compressive strength but reduce insulating properties. A balance in mechanical and insulation characteristics is required, so care must be taken in selecting suitable parameters [122]. For a 480 kg/m^3 density, Zhuo (2021) [272] suggests a minimum layer thickness of 500 mm to ensure an unfrozen subgrade [272]. This depicts another reason LCC's use in pavement construction could be helpful.

The relationship between some of these insulating materials and their stiffness are presented in Figure 2.2 for Polystyrene, and Figure 2.3 for LCC. Materials with higher stiffness are preferable to add structural stability to the pavement structure in addition to their insulating properties. Among these insulation materials, foamed concrete has a higher stiffness and could be most suitable in terms of structural capacity.

Although previous studies have established LCCs' merits as an insulation layer, nothing is known about their actual field insulating benefits when used as a pavement structural layer. Also, it would be necessary to evaluate design options that balance the insulation and mechanical benefits of incorporating LCC as a structural layer. It is essential to understand actual field temperature variations within the pavement structure and, consequently, the thermal and durability impacts on pavements. Furthermore, it would be interesting to see how this compares with other insulation layers in terms of performance and environmental impact.

2.2 Lightweight Cellular Concrete

Cellular concrete is defined as cement slurry (Portland cement or Portland limestone cement with water), which consists of foam (a minimum of 20% per volume), and compressed air [63, 52]. A comprehensive definition of Lightweight Cellular Concrete is given in ASTM C796. With the aid of gas-forming chemicals or foaming agents, lightweight cellular concrete made of lime-pozzolan, lime-silica, lime-pozzolan, cement-pozzolan, portland cement, or pastes containing mixtures of these ingredients can be created. Autoclave curing is typically used for cellular concretes that contain binder ingredients besides or in addition to Portland cement.

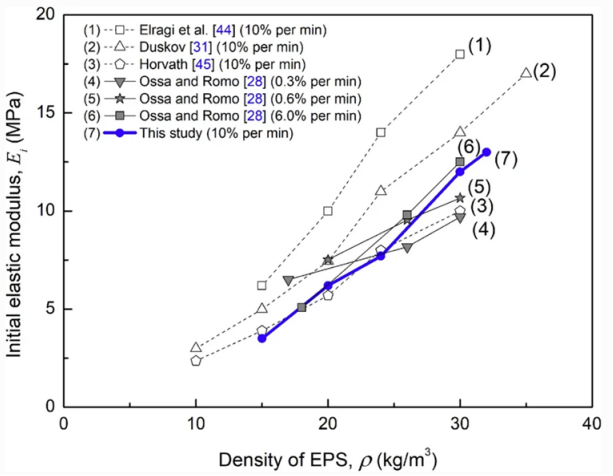

Figure 2.2: Relationships of an initial elastic modulus (E_i) with different densities of EPS pavement [154]

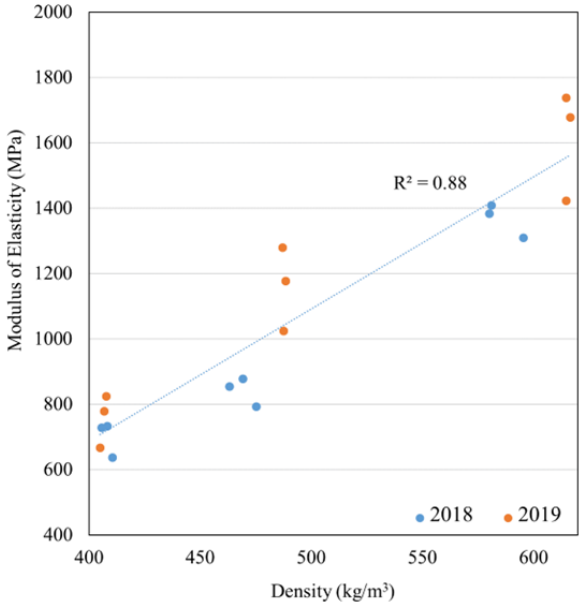

Figure 2.3: Modulus of Elasticity at different LCC density [174]

LCC typically has a wet density ranging from 250 to 1600 kg/m^3, with below-the-ground wet density installation usually between 400 and 600 kg/m^3 [63]. LCC's lightweight and

characteristics' is highly dependent on its constituents. Therefore Legatski (1994) [136] classified cellular concrete thus.

- **Neat-Cement Cellular Concrete:** This type contains cement, water, and preformed foam. It does not have aggregates, and the cement content limits its use. Application cast densities do not exceed 800 kg/m^3; however, pozzolanic materials such as fly ash can be used to substitute cement to increase this density without producing much heat of hydration.
- **Sanded Cellular Concrete:** This contains cement, sand, water, and fine aggregate (sand). Its use depends on cement content, water/cement ratio, and sand characteristics. It usually has cast densities of 800 to 2,080 kg/m^3.
- **Lightweight Aggregate Cellular Concrete:** This is similar to sanded cellular concrete, but sand is replaced with lightweight aggregate. This is to increase the strength/density ratio of the mix.
- **Cellular Concrete modified with admixture:** For this type of cellular concrete, admixtures are added to the mix to customize and improve properties. For example, cement dispersing agents are added to enhance compressive strength by reducing the cement/water ratio at a given density. Chopped fibers like glass, steel, polypropylene, polyester, and nylon are added to increase tensile strength and reduce drying shrinkage. Fly ash can substitute cement to reduce cost without affecting properties and improve compressive strength, flowability, hydration heat, and permeability. Latex can be used to impart specialized properties. Other forms of waste materials like rubber and plastic can be incorporated to control the strength, density, and heat of hydration.

Furthermore, Ozlutas, (2015) [189] categorized lightweight cellular concrete by density as follows:

- Ultra-low density: with plastic density below 600 kg/m^3.
- Low density: with plastic density from 600 to 1000 kg/m^3.
- High density: With plastic density above 1000 kg/m^3.

2.2.1 Material composition

With a concentration of 300 to 400 kg/m^3, Portland cement (PC) is the principal cementitious component of cellular concrete. However, depending on the strength or density required, the cement content can be increased or decreased [120]. PC is frequently blended with various elements to modify the qualities of cellular concrete. For example, fly ash, blast furnace slag, or silica fume are added to PC to improve compressive and flexural strength, reduce cost, the heat of hydration, drying shrinkage, thermal conductivity, and sustainability [63, 130, 132]. Kearsley and Wainwright, (2001) [130] stated that fly ash might replace PC up to 75% without compromising strength. Quick hardening PC is also utilized for rapid strength growth. However, when adding extra materials, consideration must be given to production temperatures, water content, and foam instability [160, 122]. For reducing setting times, Calcium Sul aluminate Cement (CSA) has been reported to work with additional benefits [158]. CSA cement also has the sustainable benefits of reducing CO_2 emissions due to lower temperature requirements during production compared with PC. Construction with CSA cement has shown high freeze-thaw and chemical attack resistance, but depending on the w/c ratio, they can carbonate faster and lead to strength loss [125].

Fine sand, typically 2 mm maximum size, is recommended for use only in LCC with dry densities equal or greater than 600 kg/m^3. In lower density LCC, fillers like fly ash can be used instead [32]. Carbon nanotubes (CNTs) have also been incorporated into the LCC mix as support fillers. They are found to develop more homogenous cell structures with closed cell bubbles [265]. However, CNTs can form clumps and ultimately cause foam instability; this will require dispersion in water which might not prove effective [189].

The cement-to-water ratio used for LCC ranges from 0.4 to 1.25 [128]. It must be noted that the quantity of water required depends on the material's composition and use, which relies on consistency and stability [209]. Excess moisture leads to segregation, while lower quantity produces a stiff mix leading to early breaking [170].

A foaming agent is usually added to the base mix (cement slurry) to produce the bubble structure in the LCC material. Foaming agents could either be blended with the base mix after they have been made separately or mixed along with the ingredients for the base mix [40], with the former being the preferred method in practice. The main requirements are that the foaming agent is stable and firm to resist mortar pressure [138]. Foam could be wet or dry; however, studies have reported stability issues with the wet foam producing bubble sizes of between 2 mm to 5 mm. But dry foam is said to have more reliability in terms of stability with a bubble size of 1 mm [6]. Examples of foaming agents include detergents, resin soap, hydrolyzed protein, saponin, Neopar, foam tech, Mearlcrte, and

Elashzell [171].

2.2.2 Material Properties of Lightweight Cellular Concrete

The qualities of LCC are determined by its microstructure and composition, which are influenced by the binder, pore production method, and curing procedure [172]. Pore area ratio, the average thickness of bubble wall, circularity, and solidity all exhibit high connections with LCC mechanical properties; according to the study by [268]. LCC qualities were divided into two categories by Ramamurthy, Nambiar, and Ranjani (2009) [171]: fresh state properties and hardened state properties.

Fresh State Properties

In its fresh state, LCC is flowable and self-compacting. Material consistency and stability are two factors considered to assess these properties. Consistency refers to the LCC material's spreadability and flowability, which can be measured using the marsh cone and spread cone test [121]. Stability, on the other hand, depends on the consistency of the base mix and refers to the consistency at which the ratio of the measured density to the design density nearly equals one with no indication of segregation and bleeding [139]. The measured density is expected to be within + /- 50 kg/m^3 of the design plastic density to achieve good stability [139]. Stability is an important characteristic that ensures LCC's fine and uniform texture when hardening [209].

Fly ash can be used as a filler to increase uniformity and flowability. According to a study [121], coarse fly ash improved spreadability 2.5 times more than cement-sand mix. Foam stability was shown to be reduced in mixtures containing fly ash, necessitating the use of higher quantities of foaming agents. An increase in the amount of the mix's foam affects its uniformity [126]. It is critical to exercise caution regarding the water-solid ratio, which must meet consistency and stability standards [209].

Environmental circumstances (winds, evaporation, vibration, and temperature), material composition (foaming agent, constituent proportion), construction quality, and foam instability in terms of quality and volume are all factors that influence the stability of cellular concrete (Figure 2.4) [119]. Compared to regular concrete, LCC's early stages would produce higher heat of hydration which lasts longer. According to [122], peak LCC temperature was found to drop by 40% when cement quantity was reduced from 600 to 300 kg/m^3. Generally, the volume of the pour, cement content, concrete density, and

Figure 2.4: Example of instability of ultra-low density foamed concrete on site [119]

the amount, kind, and properties of the cement/filler/aggregate used are all factors that influence the hydration of LCC [36, 122, 236].

Furthermore, the time it takes for LCC to set (rate of hardening) is critical since it affects the construction schedule. Although there is no standard test technique for assessing the setting time of LCC, Brady et al.,(2001) [36] found that the ASTM C266 test method for cement could be used to determine the setting time of cellular concrete. The stiffening of cellular concrete has been seen after five hours of casting at 20 °C [136]. On the other hand, the normal setting period for cellular concrete is between 12 and 24 hours [36].

Hardened State Properties

The attributes of the hardened state include physical, mechanical, and functional aspects. These are discussed subsequently.

Physical properties

Because LCC can be made in a wide range of densities, physical qualities, and mix design must be considered [136]. These physical properties are described in this section. LCC has up to 10% higher drying shrinkage than ordinary concrete. When 30% of fly ash, which reduces the heat of hydration of LCC [49], and lightweight aggregates are added to the LCC mix, it results in a reduction of LCC drying shrinkage [118]. For damp cured

Table 2.5: Typical properties of hardened foamed concrete [32]

Dry Density (kg/m^3)	Compressive Strength (MPa)	Drying Shrinkage (%)	Modulus of Elasticity (MPa)	Thermal Conductivity (W/mK)
400	0.5-1.0	0.30-0.35	800-1,000	0.1
600	1.0-1.5	0.22-0.25	1,000-1,500	0.11
800	1.5-2.0	0.20-0.22	2,000-2,500	0.17-0.23
1000	2.5-3.0	0.15-0.18	2,500-3,000	0.23-0.30
1200	4.5-5.5	0.09-0.11	3,500-4,000	0.38-0.42
1400	6.0-8.0	0.07-0.09	5,000-6,000	0.50-0.55
1600	7.5-10.0	0.06-0.07	10,000-12,000	0.62-0.66

concrete, autoclaving LCC can reduce drying shrinkage by 12 to 50%. Table 2.4 shows typical drying shrinkage valves for comparable LCC density values determined by BCA (1994) [32].

The injection of a predetermined amount of air as prepared foam to the cement slurry controls the density of LCC, which may be assessed as wet (cast) or hardened (dry) state density [146, 136]. Most physical attributes of LCC rely on the hardened density, which is mainly necessary for mix design and casting control [209]. The hardened density (air-dry) is around 80 kilograms per cubic meter less than the wet density [136]. When determining density, elements such as aggregate size, quantity and kind of foam agent, and sand/cement ratio influence density [159]. Material strength and thermal conductivity decrease as density decreases, although it is usually possible to select a density that provides needed strength and insulation at lower densities [136].

Mechanical Properties

Mixes with uniform distribution of air voids, circular air voids, and optical spacing between voids can produce LCC with good mechanical properties [209]. Empirical relationships between mechanical properties have been developed and show that these properties are interrelated. Research by Ni (2021) [174] proposed relationships between LCC density between 400 to 600 kg/m^3 and compressive strength (Table 2.5). They also presented the relationship between LCC compressive strength and other mechanical properties (Table 2.6). These mechanical properties are discussed in this section.

The compressive strength represents the resistance of a material to breaking due to compression from applied loads. Compressive values for hardened LCC are primarily a function of its density and can range from 0.5 to 10 MPa [32]. Factors influencing LCC compressive strength include specimen size and shape, the direction of loading, method of pore formation, characteristics of ingredients used, age, water content, cement-sand ratio,

Table 2.6: Relationship between LCC density and mechanical properties [174]

Mechanical Property	Equation	Coefficient of determination (R^2)
Compressive Strength	D = 0.0051×UCS - 0.9728	0.83
Modulus of Elasticity	D = 4.04×MOE - 930.09	0.88
Splitting Tensile Strength	D = 0.0008×ST - 0.1635	0.93
Modulus of Rupture	D = 0.0009×MR - 0.1386	0.92

Table 2.7: Relationship between LCC compressive strength and mechanical properties [174]

Mechanical Property	Equation	Coefficient of determination (R^2)
Modulus of Elasticity	MOE = 677.43×UCS + 122.16	0.99
Splitting Tensile Strength	ST = 0.11×UCS + 0.06	0.93
Modulus of Rupture	MR = 0.14×UCS + 0.10	0.93

water-sand ratio, curing process, and type of foaming agent [136]. According to Narayanan and Ramamurthy (2000) [172] Unconfined Compressive Strength (UCS) increases linearly with density increase and inversely with moisture content. Kearsley (1996) [128] also stated that compressive strength decreases exponentially with a reduction in density. There is an increase in strength at higher water/cement ratios within consistency and stability limits [130]. Their study also showed that up to 67% of cement could be replaced with classified or unclassified fly ash without a noticeable reduction in strength. However, these mixes will require longer times to achieve maximum strength. Increased strength is observed if cement is replaced with silica fume long-term. However, fly ash as fillers in higher density LCC depicts higher strength-to-density ratio with limited effect on lower densities [170]. Ramamurthy, Nambiar and Ranjani, (2009) [209] suggest that autoclaving also increases compressive strength.

Flexural strength measures the maximum stress within a material as it yields, while tensile strength measures the material's resistance under tension. Flexural strength to compressive strength ratio for LCC ranges from 0.25 to 0.35 [252], while Tensile strength is typically 10 to 15% of compressive strength [136]. Splitting tensile strength for LCC is observed to be lower than comparable normal weight and lightweight aggregate. However, mixes with sand depict higher tensile values than those with fly ash. Also, adding fibers to low-density LCC can double tensile strength and prove cost-efficient [136]

Modulus of Elasticity (MOE) measures the material's tendency to deform along an axis when an opposing force is applied to that axis. It is a function of density and compressive strength [136]. Typical values are presented in Table 2.4. LCC is reported to have MOE

values four times lower than standard concrete. LCC mixes with fly ash as fine aggregate exhibit lower MOE than mixes with sand [120]. However, to improve MOE, polypropylene fibers can be added to the mix [121]. At lower temperatures, stiffness increases linearly as compressive strength increases especially for higher density LCC.

The Poisson ratio is the ratio of a material's transverse strain to axial strain and is a significant factor in determining strain, stress, and displacement in the pavement structure [234]. A study by Tiwari et al., (2017) [245] found Poisson ratio for LCC to range from 0.2 to 0.3 for LCC densities between 230 kg/m^3 to 800 kg/m^3. Lee et al., (2004) also reported that Poisson's ratio of LCC with densities of 1,000 kg/m^3 and 1,400 kg/m^3 ranged between 0.13 to 0.16 and 0.18 to 0.19, respectively. Ni (2021) [174], in a recent study, found Poisson's ratio for densities between 400 to 600 kg/m^3 to range between 0.14 to 0.31.

Functional Properties

The thermal conductivity of a material is "the time rate of transfer of heat by conduction, through a unit thickness, across a unit area for a unit difference of temperature"[136] p.537. Typical values for cellular concrete can be found in Table 2.4. Measured thermal conductivity values for dry density LCC between 600 – 1600 kg/m^3 were found to be between 0.1 and 0.7 W/mK [121]. Cellular concrete is reported to exhibit excellent thermal insulation behavior due to its microstructure [209]. Giannakau and Jones (2002) [87] found that LCC ground-supported slab foundation provided adequate strength while having better thermal insulation and lower sorptivity properties in studying the effect of Cellular concrete on low-rise buildings. Thermal insulation decreases with a decrease in density and improves with a decrease in temperature. A reduction of 26% in thermal conductivity was observed for densities between 640 and 1440 kg/m^3 when temperatures were reduced from 22 to -196 °C [211].

Durability properties

Water absorption of LCC largely depends on the paste phase and non-interconnectedness of some artificial pores, meaning they can't take part in water absorption [170]. Water absorption decreases with density because of lower paste volume; however, water vapor and oxygen absorption have increased porosity and fly ash content [129]. LCC permeability coefficient is proportional to unit weight and inversely proportional to pore ratio [40]. On the other hand, Sorptivity appears to be a better measure for porous materials as it better explains the water absorption and transport in the material via capillary and can be easily measured [260]. LCC's Sorptivity depends upon pore structure, filler type, and permeation mechanism [209]. It is observed to increase with an increase in foam volume and the addition of fly ash into the mixes rather than sand [121].

In terms of resistance to an aggressive environment, lower density LCC has been observed to have good freeze-thaw resistance due to the hollow voids restraining the expansion forces from frozen water [36]. LCC's Freeze-thaw characteristic depends on its initial penetration depth, absorption, and absorption rate [120]. Tikalsky, Pospisil and MacDonald, (2004) [244] reported the compressive strength of four low-density LCC specimens after being subjected to freeze-thaw cycles. Mixtures for these low densities exhibited excellent freeze-thaw resistance. This was attributed to the fact that they had 28-day compressive strength above 1 MPa, which might have enabled their durability during the freeze-thaw cycle. However, higher density specimens with less than 1MPa 28-day compressive strength were not durable.

Low-density cellular concrete with high fly ash content has been observed to have excellent Frost-Heave resistance. Although the quality of the fly ash largely influences this property [136]. LCC also has good chemical attack resistance, enhanced corrosion resistance at lower densities, and its cell-like structure and porosity help prevent rapid moisture penetration [121].

2.2.3 Production and Placement methods

Typically, cellular concrete mixes are produced and placed onsite. However, the process could involve transporting trucks with cement slurry to the site. For higher density applications over 800 kg/m^3, transit mix trucks are acceptable for mixing and transporting to the site. On site, preformed foam is added just before placement is done. In the case of lower densities, less than 800 kg/m^3, the paddle type or shear mixers are commonly used for batching and mixing slurry. The preformed foam is then added prior to or during placement using a positive displacement pump [136]. Dolton et.al., (2016) [63], classified production and placement methods for road construction into two thus (Figure 2.5).

Wet mix process: In this method, cement and sand slurry are batched offsite by a ready-mix company and transported to the site. On-site, slurry in the cellular concrete equipment is injected with foam, after which the material is pumped into place. However, care must be taken to ensure that material temperature, viscosity, and density are according to specifications.

Dry mix process: All material components for this process are mixed on-site. Firstly, cement and sand slurry are mixed in the cellular concrete equipment, and foam is injected into this mixture before it is poured into place. This method is usually used for high-volume productions.

A specialized contractor with previous experience should do production and installation. If the slurry is supplied, density should be verified before use, or if mixed onsite, equipment should be thoroughly cleaned prior to use [153]. Slurry production from bulk powder on site should have a water and bulk powder tolerance within 2% of the mix design value.

Figure 2.5: Dry and Wet Mix LCC Equipment [153]

Placement can be done in freezing temperatures (below 0 °C) if LCC material is prevented from freezing until the required strength is gained [153]. Prior site-specific evaluations can achieve this for sub-zero temperatures and use hydration aids such as polyethylene sheets and insulating tarps, which can maintain LCC temperature above 4 °C. Placement can also be done under light rain; however, it becomes impossible during heavy pours. Stable surface before fall and Groundwater control is also essential during placement of LCC until granular base material is placed above it.

2.2.4 Testing procedures and Quality Control (QC)

Testing and QC procedures for LCC should be consistent with or surpass requirements according to the American Society for Testing and Materials (ASTM), Canadian Standards Association (CSA), and American Concrete Institute (ACI) [153]. ASTM testing important for LCC includes C495, C796, and C869. An Experienced quality engineer should be employed for verification and project specifications, and requirements should be included in contract documents.

The two main quality control parameters are the material density and compressive strength of hardened material (Table 2.7). Wet density and temperature of the mix

Table 2.8: Typical QC Program suitable for placing LCC for roadworks [153]

Material Property	**Frequency**	**Acceptance criteria**	**Comments /Additional Requirements**
Density	One per batch or every 10 m^3. For Continuous production every 50 m^3 or once per 20 minutes	Within 10% of design density	
Compressive strength	One sample per 100 m^3	Meets or exceeds design strength	Cast in 75 × 150 mm cylindrical molds Store in an undisturbed condition within 15 m of casting area Initial curing temperature of 25 to 30 °C for 24 to 96 hours Cure in 80% to 100% humidity room at 18 to 27 °C

should be monitored during production and placement, with necessary adjustments made to density when required [136, 153]. This will help monitor the consistency of the discharged mix. Accurate batching of the ingredients is very important [136]. Cement and sand are weighed into the batch, water is metered, and preformed foam is injected into the mixture by a calibrated nozzle. Mixing should be done to suit the type of mixture, the reason for application, method of placement, and the constituent material. Casting techniques also vary depending on their use.

To measure compressive strength, sets of standard 75 mm diameter by 150 mm high test cylinders should be cast and monitored per specifications. When unique or new materials are used as a substitute for typical components, trial batches should be produced to ensure optimum LCC mixture [153].

2.2.5 Test Standards

Although LCC is used in numerous countries, there is yet to be an internationally recognized standard for test methods and guidelines for its use. However, there is documented evidence of its properties and behavior [189]. Some countries have come up with specifications for use. For example, a Japanese standard covers the most recently updated test method for volume change of cellular concrete (JIS A 1162:1973). Ozlutas (2015) [189] also reported a list of the specifications for foamed concrete in the UK by bodies such as BCA, which provide guidelines on the properties, advantages, and application of the

foamed concrete.

In North America, a few guides provide information about cellular concrete material, design, and applications. Some of these specifications and guidelines are listed in Table 2.8. The American Concrete Institute (ACI) published two guides for cellular concrete with densities above 800 kg/ m^3 (ACI 523.3R) and less than 800 kg/ m^3 (ACI 523.1R - specifically for roof deck application). These guidelines provide a general overview of cellular concrete's properties, production procedures, and applications. There are also two standards for foaming agents (ASTM C796 and ASTM C869) and one for determining compressive strength (ASTM C495) by the American Society for Testing and Materials. Conversely, there is currently no test standard, guideline, or specification for using Lightweight cellular concrete in Canada. Also, non of these guidelines provide information specifically for pavement subbase applications and densities below 600 kg/m^3.

2.2.6 Potential Sustainability Benefits of Lightweight Cellular Concrete

According to the World Commission on Environment and Development [133], sustainable development is defined as development that satisfies current demands without jeopardizing the capacity of future generations to meet their own needs. As a result, one way to achieve the sustainability aim is through sustainable construction. The "triple bottom line" idea, which recognizes sustainable development in terms of the environment, economics, and society, is used in the Leadership in Energy and Environmental Design (LEED) framework. The process of recycling, reuse, and reduction results in sustainability when these three factors are in balance.

The leading indicators for sustainable pavement, according to Uzarowski and Moore (2008) [251], include minimizing the use of natural resources, reducing energy consumption, reducing greenhouse gas (GHG) emissions, limiting pollution (air, water, earth, noise, etc.), improving health, safety, and risk prevention, and ensuring a high level of user comfort and safety. The potential benefits of using LCC are outlined are as follows.

- It can include 80 to 90 percent voids at low densities, which reduces the need for virgin materials and the amount of waste created
- There is no need for compaction because LCC flows freely, which reduces construction-related noise pollution and uses less energy. After all, compaction is no longer necessary [121].

Table 2.9: Specifications for Lightweight Cellular Concrete in North America

Publishing body	**Title of Specification**	**Brief Description**
ACI SP-29 [144]	Lightweight Concrete	Provides information on the importance and acceptance of structural lightweight concrete in construction, particularly for building structures.
ACI 523.1R [2]	Guide for Cast-in-Place Low-Density Cellular Concrete	Gives details on materials, properties, design, processing, and use of cast-in-place low-density LCC with oven-dry densities of < 800 kg/m^3).
ACI 523.2R [37]	Guide for Precast Cellular Concrete Floor, Roof, and Wall Units	Precast LCC floor, roof, and wall units with oven-dry unit weights ≤ 800 kg/m^3 are discussed in terms of materials, fabrication, characteristics, design, and handling.
ACI 523.3R [110]	Guide for Cellular Concretes Above 50 lb/ft 3 (800 kg/m^3)	The materials, characteristics, design, production, and installation of cellular concretes with as-cast densities > 800 kg/m^3 are addressed.
ASTM C495 [15]	Standard Test Method for Compressive Strength of Lightweight Insulating Concrete	Provides test methods and procedures for determining the compressive strength of cellular concrete.
ASTM C869 [18]	Standard Specification for foaming Agents Used in Making Preformed Foam for Cellular Concrete	Give a method for assessing the performance of a particular foaming agent
ASTM C513 [41]	Standard Test Method for Obtaining and Testing Specimens of Hardened Lightweight Insulating Concrete for Compressive Strength	Includes the collection, preparation, and testing of specimens of hardened, lightweight, insulating concrete constructed with lightweight aggregate or preformed foam.
Taylor and Halsted (2021) [239]	Guide to Lightweight Cellular Concrete for Geotechnical Applications	Materials, qualities, design, correct handling, and applications of LCC for geotechnical purposes are covered.

Table 2.10: Comparison of material consumption of eCO_2 of 600 and 300 kg/m^3 foamed concretes for Combe Down case study [189]

Foamed Concrete Density (kg/m^3)	**600**	**300**	**300 (30% Fly Ash)**
Portland cement, kg/m^3	375	200	140
Water, kg/m^3	225	120	120
Portland cement, kt/600,000 m^3	225	120	84
Water, Kt/600,000 m^3	135	72	72
eCO_2, Kt eCO_2/ 600,000 m^3	209.4	105	73.8
Reduction in eCO_2, Kt		**104.4**	**135.6**

- Low strength makes it easily excavated and removed [52].
- The use of non–renewable natural resources is reduced by eliminating coarse aggregates and fine aggregates at densities below 600kg/m^3 [32].
- It uses industry by-products, reducing the amount of waste disposed of, such as slag and fly ash [63, 123]. Fly-ash can also replace Portland cement up to 75% in lower density LCC, which reduces embodied CO_2 (eCO_2) (Table 2.9). In addition, it enhances properties such as lower thermal conductivity, lower dry shrinkage, and reduces the heat of hydration [122, 118, 87, 130].
- It can be recycled and used to produce more foamed concrete as it has been shown to improve compressive strength through hydration of cement particles [123].
- It has been shown to have good freeze-thaw resistance [209], fire resistance, good sound absorption, and excellent thermal insulating properties, which get even better with lower plastic densities [52, 121].

From the preceding, lightweight cellular concrete (especially lower densities) reflects potential benefits for its contribution to sustainable construction. The problem with using LCC at ultra-plastic densities is that it can be unstable because of the separation of solids and air voids in its fresh state before it sets. However, this is usually associated with densities below 300 kg/m^3, which have been shown to be susceptible to this kind of failure [167]. It is important to assess these benefits further and quantify them. This will create a better understanding of the material, improve these advantages, and increase and expand LCC applications [189].

Table 2.11: Summary of Foamed concrete applications based on density [219]

Density (kg/m^3)	Application
300-600	Replacement of existing soil, soil stabilization, raft foundation.
500-600	Currently being used to stabilize a redundant, geotechnical rehabilitation and soil settlement. Road construction.
600-800	Widely used in void filling, as an alternative to granular fill. Some such applications include filling of old sewerage pipes, wells, basement, and subways.
800-900	Primarily used in production of blocks and other non-load bearing building element such as balcony railing, partitions, parapets, etc.
1100-1400	Used in prefabrication and cast-in-place wall, either load bearing or non-load bearing and floor screeds.
1100-1500	Housing applications.
1600-1800	Recommended for slabs and other load-bearing building element where higher strength required.

2.2.7 Applications of Lightweight Cellular Concrete

Typical applications of LCC are like regular concrete that require modest loads over smaller periods [136]. This is due to its lower weight and strength compared to regular concrete. However, with advancements in material compositions and technology, its use is expanding to cover more areas. Some applications of LCC include its use from backfill, void fill, road subbase, flat roofs, precast, blocks [189]. Additionally, LCC can be used for floor fills (1600 to 1700 kg/m^3), sloping roof screeds (480 to 640 kg/m^3), filling voids to support slabs, roadways (480 kg/m^3), reducing lateral loads on wall structures and as specially designed precast cellular concrete –common in Europe [136]. Due to its wide density range, LCC applications vary. Sari and Sani (2017) [219] classified LCC application corresponding to its density (Table 2.10).

2.2.8 Field Performance of LCC in Pavements

LCC has been implemented in several roadway sections worldwide as an alternative for support over unstable soils. In Canada, this has been done in areas like Vancouver, British Columbia, at the intersection of Vancouver and View Street, and Dixie Road, Peel Region, Ontario, to name a few.

In studying the performance of LCC installed in Victoria on Vancouver and view street, Dolton et. al., (2016) [63] reported that due to excessive total differential settlement in the

area, the roadways and sidewalks experienced surface distresses and damage to underlying utilities. In 2008, LCC with a wet density of 475 kg/m^3 was utilized as the subbase for 143 meters on Vancouver Street and 215 meters on View Street. During construction, QA/QC testing found that cast density ranged from 435 to 486 kg/m^3, with an average of 462 kg/m^3. Cylinders were also cast according to ASTM C495 for LCC compression strength, with values averaging 1.0 MPa (range 0.8 to 1.1 MPa) in 28 days. Over fourteen pour days, a total of 2,246 m^3 of LCC was poured. Before traffic was allowed on the road, gravel backfill was laid on the LCC and compacted with no vibration. The LCC was 500 mm thick, with 150 mm of 20 mm crushed granular base course and 75 mm of asphalt concrete on top.

Structural evaluation using Benkelman beam (VEhecle with 80 kN test load on single rear dual tire axles per the ASTM D4695 was completed by February of 2008. Deflection analysis was in accordance with Asphalt Institute MS-17 method. Due to winter conditions, no seasonal correction factor was applied for Maximum Pavement Spring Rebound (MPSR). Compared with adjacent pavement not re-constructed with LCC, results showed more consistency with lower MPSR (36% lower). For FWD testing following ASTM D4694 by the same company, three load levels were used to determine the deflection response (40, 50, and 75 kN approximately) at each load section. No spring correction factor was applied. Results reflected consistent static deflection for the LCC sections, with that of the non-LCC section 111% times higher than that of the LCC section. The elastic moduli of the LCC were also reported to be 445 MPa (Std 146 MPa) and 341 MPa (std 99 MPa), which are higher than the typical values for gravel [186].

In Peel Region, Ontario, continuous settlement of a 120-meter-long rural road (Dixie Road) built on five meters of peat necessitated re-construction in 2010 [88]. LCC was chosen as a subbase material because it would have the least amount of environmental impact on the nearby wetlands. The other option was to utilize sheet piling and remove all the peat, but this did not appear to be cost-effective or environmentally friendly. Using the dry-mix production equipment, a total of 1,000 m^3 of LCC with a wet density of 475 kg/m^3 was poured down the 120 m. Over the subgrade, a 650 mm layer of LCC was laid, followed by 150 mm of aggregate and 140 mm of Asphalt Concrete. The construction was relatively quick, with the road only being closed for a week.

Field performance analysis using visual inspection, Ground Penetrating Radar (GPR), and Falling Weight Deflectometer (FWD) were performed by Griffiths and Popik (2013) [88]. The detailed visual condition survey of the area reflected an overall good condition comparable to the adjacent section with traditional subbase material. A total of three longitudinal slight severity cracks and one moderate severity heave were identified. Pavement thickness was obtained using the GPR, and FWD deflection data taken at 10 m intervals

were analyzed using these thicknesses in conjunction with construction drawings. The asphalt layer was found to be fairly consistent at an average thickness of 150 mm (range of 126 to 178 mm). The thickness of the granular base was found to be very variable all through, ranging between 68 mm to 235 mm with an average thickness of 120 mm. Each FWD test included four drops, the first being a seating load and the following three at roughly 30, 40, and 75 kN.

The composite elastic modulus of the LCC pavement section was found to range between 714 and 737 MPa, which was higher than the adjacent non-LCC section, which ranged between 514 and 670 MPa. The composite pavement strength corresponds to the higher structural number for the LCC section, which ran between 175 to 224 mm, while that of the adjacent section ranged between 128 to 154 mm. Another parameter determined from FWD analysis was the structural coefficient. The calculations showed that the LCC material had a structural coefficient of 0.2, using 0.38 and 0.12 for the asphalt and base layers. Also, a more recent visual inspection in 2017 revealed the presence of several cracks; however, no severe permanent deformation was found.

The Brentwood bus lane in Calgary, Alberta, also had significant frost-heave and became nearly inaccessible [64]. In July of 2000, this road was reconstructed utilizing LCC as the subbase material on two different pour days. Initially, the road's subbase was saturated in silty deposits that reached a depth of more than 30 meters. Due to the subgrade, California Bearing Ratio (CBR) of 0.8 percent, 200 mm of LCC layer was put on 50 mm of drainage rock (sub drains installed beneath curb and gutter) and geotextile fabric. A 150 mm granular base course and a 125 mm hot mix asphalt surface layer were put over the LCC layer. In October 2001, a Benkelman Beam Deflection Test revealed 0.30 mm of deflection, far less than the 0.89 mm tolerance for such a road [64]. This road has not needed any repair since it was rebuilt. According to a recent visual assessment, the LCC part is similarly in good shape.

Highway 9 in King, Ontario, the pavement had to be reconstructed in 2014 owing to ongoing settlement caused by high levels of organic (peat) material deep in the pavement structure [153]. Previous repairs (the most recent in 2009) that used asphalt padding resulted in even more settling because of increased loading. This required more regular maintenance, resulting in increased costs. LCC was chosen as a cost-effective and long-term solution to limit settlement and eliminate safety issues and maintenance costs. The excavation was carried out over a 100-meter stretch to receive 1,100 mm of LCC material, 200 mm of granular 'O' (OPSS), and 200 mm of hot mix asphalt. For this job, a total of 905 m^3 of LCC was poured. LCC material avoided the need for deep sub-excavation of organic material (only 1.5 m excavation was necessary).

Due to the lower excavation depth, traffic staging was simplified, material disposal was minimized, backfill requirements were reduced, and construction time and impact on the surrounding wet land canals were reduced. Field inspection one year after construction revealed that the road was in excellent condition. Also, a visual examination in August 2017 revealed no severe cracks or rutting on the road.

A study assessing a pavement constructed in 2009 in Edmonton incorporating 250 mm of LCC, with 150 mm granular A and 100 mm asphalt over it, saw that the LCC section experienced deflections ranging from 0.034 to 0.059 mm and within acceptable limits of the maximum allowable deflection for the city post construction. After construction, the granular/LCC section had a higher combined elastic modulus than the Control granular section seven years later, despite deflection values being 30 percent greater than the corresponding Control with granular B material. The 30 percent deflection gap persisted after construction because the LCC portion was built over softer soils than the granular B section. Seven years later, the outcomes were still comparable. This investigation concluded that the LCC sections' shallower and softer soils, which may require greater thickness to be structurally adequate like the control, may cause more significant deflection [65].

LCC road applications are also proving to be successful around the world. For example, in the United Kingdom, approximately 13,000 m^3 of LCC with a density ranging from 410 kg/m^3 to 590 kg/m^3 was used as the subbase material in place of the original peat on Route 14 [59]. In Schaumburg, Illinois, LCC, with densities of 400 kg/m^3 and 500 kg/m^3, was utilized as the Central Road subbase layer [67]. LCC usage minimized the unit cost, reduced construction time, and performed better than the prior organic soils in supporting the pavements.

An experimental study by [176] comparing three different densities of LCC with granular B subbase discovered that the LCC pavements for the three densities provided three times more allowable number of load repetition in terms of fatigue and rutting compared to granular B material as subbase layer. Furthermore, this allowable load repetition was observed to increase with LCC density. This is consistent with conclusions by Taylor and Halsted (2021) [239] that the improved bearing capacity with LCC bases and subbase makes it an excellent alternative for pavement applications.

Despite this, most LCC studies mentioned above have minimal data on post-construction field performance evaluation and none for instrumented LCC sections. In contrast, this research examines LCC's response to traffic loads using continuous performance data.

2.3 LCC Pavement Design and Analysis Methods

As a result of its lightweight and insulating properties, LCC is commonly used to reduce or prevent roadway settlement and frost action. Key design considerations include density selection and thickness. Typically, below-ground applications range between 400 and 600 kg/m^3 [63]. Depending on the project requirements, LCC can be used in various densities. Design criteria for load reduction, buoyancy, insulation, and strength must all be considered when choosing a density.

Pavement thickness is a critical design parameter in pavement design. Determining pavement layer thickness depends on several factors such as material properties, environmental conditions, and traffic conditions [234]. The thickness of the asphalt concrete and granular base layers over the LCC is usually based on the expected traffic and potential for differential icing. These layers are typically in accordance with minimum design requirements for the location it is being incorporated, and thickness is determined based on the preferred pavement design method. For example, thickness for asphalt concrete and granular base layer in the AASHTO 93 method should be determined based on their structural number under different ESALs and reliability. For MEPDG, the designed thickness should meet provincial performance criteria. Three methods currently used within Canada have been suggested for designing LCC subbase pavements [174]. These methods are outlined below.

2.3.1 AASHTO 93 Method

This pavement design strategy considers the link between traffic loading, structural capacity, and pavement functional performance [234]. The relative strength contribution of each layer to a structural number is the foundation for thickness design. Therefore, extracting the structural number of each layer's material in the AASHTO 93 pavement design technique is critical. As a result, determining the structural number of LCC with the goal of thickness design is critical. However, AASHTO 93 does not provide a structural number for the LCC subbase.

Nonetheless, a Falling Weight Deflectometer (FWD) test in the field can be used to determine the structural number of the LCC subbase. The FWD is a non-destructive test device that can calculate the moduli of the pavement layer in reverse and must be used in line with ASTM D4694. The effective structural number of the existing pavement can be estimated once the moduli of each pavement layer have been determined.

An effective structural number of 0.20 was obtained for 475 kg/m^3 density LCC in a field test conducted in Ontario, Canada [88]. This may be considered a typical average value when developing a pavement construction with the 475 kg/m^3 density LCC as a subbase. Comparatively, structural layer coefficients for asphalt and granular foundation layers are typically 0.38 and 0.12, respectively.

2.3.2 Mechanistic-Empirical Design Method

LCC material as a pavement layer is currently not supported by the AASHTOWare program based on the Mechanistic-Empirical pavement design approach. However, because LCC is a cementitious material, Ni (2021) [174] suggests using the AASHTOWare to classify LCC as a cement stabilized base or chemically treated material. When utilized as a base layer for structural support, cement-treated and other pozzolanic stabilized materials should be treated as separate layers [11]. If the LCC layer is designed to give long-term strength and endurance, it might also be regarded as an unbound material with constant layer modulus and moisture insensitivity [174]. The LCC layer could also be categorized as a chemically stabilized structural layer.

2.3.3 Granular Base Equivalency (GBE) Method

LCC subbase pavements can also be assessed using the Granular Base Equivalency (GBE) [174]. The strength of the paving materials is measured in terms of their thicknesses by GBE. The GBE converts each layer thickness to an equivalent Granular base thickness, hence expressing the contribution of each layer to the pavement's structural capacity or strength [182] . Equation 2.1 is used to determine GBE.

$$H_e = a_1h_1 + a_2h_2 + a_3h_3 \tag{2.1}$$

Where, H_e is the equivalent granular thickness, a_1, a_2, a_3 are the strength coefficients of the asphalt layer, base layer, and subbase layer and h_1, h_2, h_3 are the actual thicknesses of the asphalt layer, base layer, and subbase layer.

According to Ni (2021) [174], typical design parameters relevant to the location of the road section in Canada can be used to establish the strength coefficient (equivalency factors) for a regular pavement (control section) using the traditional granular material as a subbase layer. Similarly, conventional and laboratory material properties are employed for LCC pavement sections. Potential stress and strain values beneath the control section's

Table 2.12: Input parameters for typical pavement design and comparable LCC designs [174]

	Surface	Base	Subbase				Subgrade
	(HMA)	Granular A	Granular B	LCC600	LCC475	LCC400	Soil
Average E(MPa)	3,445	250	200	1,490	1,001	728	30
Poisson's Ratio	0.35	0.35	0.35	0.2	0.21	0.25	0.45
Thickness(cm)	15	15	52	18	24	29	-
GBE strength coefficient	2	1	0.67	1.91	1.46	1.22	-

and LCC's subbase are necessary to calculate the required baseline pavement thickness that would give the same GBE value as the control section for a roadway with LCC as subbase material. Pavement design tools like WESLEA and KENPAVE can be used to mimic these. The simulated strain values and thicknesses for the control and LCC sections are then interpolated to find thicknesses that give the same degree of strain. Table 2.11 provides LCC equivalent factors for densities of 400 – 600 kg/m^3 based on Ni's (2021) [174] study.

2.4 Pavement Performance Evaluation

Incorporating new material into the pavement structure requires an evaluation of its performance in the laboratory and field to determine if it would be suitable for use. Pavement evaluation involves obtaining subjective and objective data such as field measurements or observations that are documented for use in the future [182]. Data acquired helps show how well the pavement serves its required purpose, how its condition has changed over time, and how long it can still perform with respect to the needed maintenance. According to [182] it is crucial to evaluate pavement performance for the following reasons: To provide input for calculating the pavement performance, provide information for pavement design, check the pavement conditions to ensure the level of service, and trigger preventive or corrective treatments, provide input to calculate funding allocation and support the efforts of research and development. Four types of pavement evaluation are currently performed by the Ministry of Transportation Ontario (MTO). They include pavement distress, pavement roughness, pavement structure, pavement transverse profile, and texture evaluation. Several factors influence flexible pavement properties, which could serve as an indication of its performance.

In evaluating the roughness of flexible pavements, studies have shown that pavement profile can be significantly influenced by environmental factors, subgrade properties, and along wheel paths, traffic loading [202]. Stoffels et al., (2006) [231] investigated the effect of subgrade moisture on roughness change for 43 AC LTPP pavements sections. These sections were included in the Seasonal Monitoring Program (SMP) and considered soil information, freezing index (FI), freeze-thaw cycles, and subgrade moisture content. The results showed that subgrade moisture significantly influenced wave bands within specific depths for freezing and non-freezing zones. An increase in roughness progression was influenced by the percentage of subgrade passing 0.002 mm sieve, variation in moisture, and moisture levels, especially moisture depths close to the top of the subgrade in non-freezing zones. Also, Von Quintus, Eltahan and Yau, (2001) [255] concluded that the initial smoothness of new AC pavements greatly influences roughness progression, while transverse cracks affected roughness over time for AC and AC overlaid pavements after developing distress-based prediction models for them.

Investigating the effect of wet days and freeze-thaw cycles on pavement roughness, Lu and Tolliver (2012) [150] developed an exponential function of pavement age representing an increase in IRI on LTPP sites. They found that increases in freeze-thaw cycles result in roughness increase, and more significant roughness deterioration was observed for wet than dry regions. Studying the before and after roughness change of 65 overlaid sections in Canada over a year, Tighe et.al., (2001) [241] found that overlay thickness and climatic factors significantly influenced pavement roughness. Subgrade type also affected conditions considerably, such as finer grain subgrades than coarse grains. They concluded that a higher roughness increase would occur on thin overlay thickness pavements over fine-grained subgrade, carrying high traffic and located in wet and low-freeze zones.

Study by Chatti et al., (2001) [48] evaluating structural, material, and environmental factors on roughness on LTPP sites also buttressed that fine-grained subgrade resulted in higher roughness changes as well as the type of base material, layer thicknesses, and climatic conditions. FHWA (2017) [202] analyzed the data on the rate of roughness change at the center lane for 201 LTPP sites using linear regression. They found higher roughness values for pavements over fine than coarse-grained subgrades with seasonal variations having a greater influence on the former. Paterson (1989) [194] developed a model for the increase in roughness incorporating structural effects, surface distress, and environmental-age factors. His analysis found that roughness occurred due to different factors and could happen even when the pavement is structurally sound. Data showed that the rate of increase in roughness change became more significant over time with factors like rut depth, traffic, pavement strength, cracking, patching, pothole, age, and environmental factors.

Furthermore, visually evaluating pavements is one fundamental way of assessing pave-

ment performance. It usually requires assessing various surface characteristics such as the severity and extent of distress. Studies have shown that the most common distresses associated with flexible pavements include ravelling, cracking, rutting/permanent deformation, potholes, flushing, distortion, ripping, and shoving, to mention a few [184]. Such factors include pavement temperature, moisture variations, and traffic loads [234].

Factors influencing the strength of flexible pavement include the quality of materials used and environmental factors such as temperature. Strength is usually expressed as its Modulus of Elasticity (MOE). A study by [235] showed that MOE increases at lower and decreases at higher temperatures.

2.5 Life Cycle Assessment

Life Cycle Assessment (LCA) is an evaluation technique used to analyze and quantify the environmental impacts of a product, process, or system by assessing all input and output throughout its lifecycle [95]. Inputs and outputs include but are not limited to materials, production process, costs, and energy and consumption. The pavement life cycle comprises the material production, design, construction (new construction as well as preservation, maintenance, and rehabilitation activities), use, and end-of-life stages associated with a pavement structure.

This method has been used in evaluating pavements, and the pavement lifecycle stages and some typical inputs and outputs for pavements are presented in Figure 2.6. The pavement life cycle includes the material production, design, construction (new construction as well as preservation, maintenance, and rehabilitation activities), use, and end-of-life stages associated with a pavement structure.

2.6 Life Cycle Cost Analyses

Life cycle costing of pavements involves compiling the initial costs and future costs associated with the pavement structure. According to the International Organization for Standardization (2008) [82], Life Cycle Cost Analyses (LCCA) is defined as an.

"Economic assessment considering all agreed projected significant and relevant cost flows over a period of analysis expressed in monetary value. The projected costs are those needed to achieve defined levels of performance, including reliability, safety, and availability."

The LCCA tells the direct financial implication of the project. It is usually used as an assessment tool in public procurement to push for more sustainable practices [197]. Typically, an LCCA analysis consists of elements such as establishing the design alternatives, determining the analysis period, determining the discount rate according to the economic development of the country or the state, estimating the specific cost, and finally, the analysis of results [241, 258, 263].

For LCCA, two crucial indicators play vital roles [241, 264]. First is Net Present Worth (NPW), which converts the cost of pavement maintenance for different years into the present year using the discount value, thereby making the comparison. The other important indicator is the Equivalent Uniform Annual Cost (EUAC), which is calculated based on the value of Net Present Value (NPV) and distributes the cost into the pavement life cycle.

Zhuo (2021) [272] used the Finite Element Model (FEM) to forecast the performance of four types of insulation materials based on analogous thermal and mechanical structures and discovered that the ordinary pavement without insulation was the most expensive to achieve identical thermal performance. The LCC pavement was the most costly insulated pavement, followed by tire chips pavements, foamed glass aggregates pavement, and XPS pavement. However, only the initial construction costs were examined in this analysis. It was also contemplated that forms would be necessary to place the LCC, but this is not always the case, as the sides of excavation can serve as forms. Also, a seven-day delay in curing the LCC was specified in the analysis. Setting time for below-ground treatments has been estimated to be as little as twelve hours; therefore, potentially, construction could commence after 24 hours in some cases, depending on weather and other factors [188]. In addition, data on the lifecycle cost of LCC as a structural subbase component of pavement construction is presently unavailable.

2.7 Research Gaps

Due to the importance of Canada's transportation infrastructure, an enormous emphasis has been placed on long-term performance and sustainable pavements. Diminishing supplies of virgin aggregates has also resulted in ministries of transportation and agencies moving towards using alternative materials such as lightweight cellular concrete. The use of LCC is expanding and gaining more grounds for use in the pavement structure. More in-depth study of LCC is required to expand the scope of its use further. Unfortunately, limited information on pavement-related performance concerning changing climatic and loading conditions is available. Previous studies have primarily focused on its material

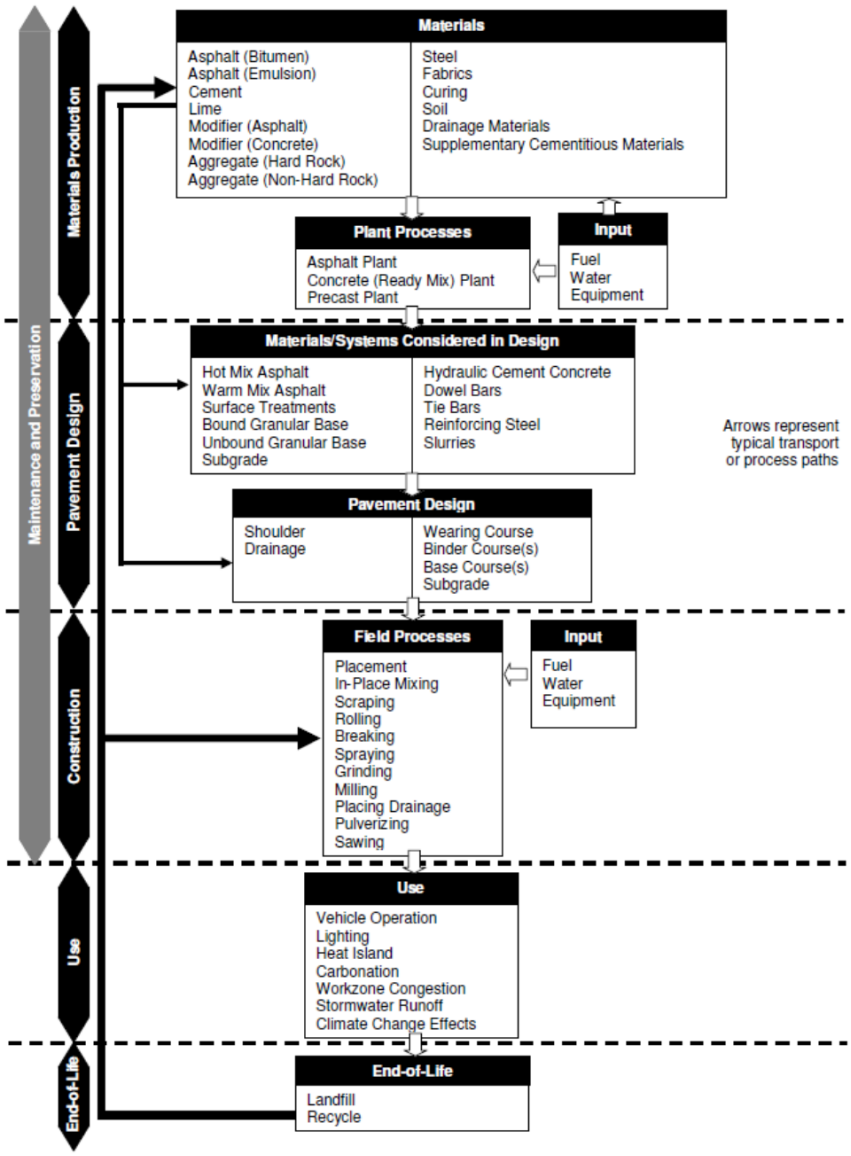

Figure 2.6: Representation of pavement life-cycle stages [94]

and engineering properties through laboratory testing and some limited form of visual and load inspection in the field. Detailed evaluation of field performance will guide how to modify specifications to promote better long-term performance. There is also a need to integrate laboratory and field results to develop more comprehensive performance analyses

and predictions.

Using LCC in the pavement structure as subbase material is not common practice. Without a known, accepted international standard, it is vital to calibrate its properties to suit local conditions. Though proportioning methods and guides have been proposed for given density and strength, there is no standard mix proportioning strategy [209]. There is a need to develop unified standards, specifications, and guidelines for using LCC in the pavement structure in Canada.

Furthermore, there is no distinct class for LCC in the MEPDG used in Canada. LCC may only be viewed as an unbound layer with a constant Modulus of Elasticity or a cement stabilized layer when using the MEPDG. To increase the MEPDG's performance prediction reliability, MEPDG must be calibrated to suit these unique material qualities and validated. There is also a requirement to investigate the simplicity of employing LCC in the pavement structure and optimize the construction process to feed into the design guideline and specification, which necessitates an in-depth constructability study.

In addition, past research has shown that LCC provides cost-effectiveness and reduces environmental impact. These advantages are bolstered by examples such as simplicity of application, reduced usage of virgin material, and the use of industrial by-products such as fly ash. On the other hand, these studies do not quantify the benefits and only provide limited data and analysis to back them up. Life Cycle Assessment (LCA) and Life Cycle Cost Analysis (LCCA) are required to evaluate further and quantify possible sustainability benefits.

Chapter 3

Research Methodology

3.1 Introduction

This chapter outlines the methods employed in investigating the performance of lightweight cellular concrete as a subbase alternative to unbound granular materials. Three aspects of LCC's performance were considered: its constructability, actual field performance, and sustainability.

3.1.1 Constructability

For this research, the term 'Constructability" refers to the ease and efficiency with which the contractor could complete the construction and how the installed LCC pavements responded to construction activities. Since earlier research identified constructability as a benefit of LCC [153], this study aimed to quantify this benefit and compare it to the typical subbase material. Constructability is crucial as it enables the review of processes from start to finish to help identify obstacles that could lead to project delays, prevent errors, cause cost overruns, and impact pavement performance.

3.1.2 Field Performance Tracking

The actual response of the pavement structure to traffic loading, climatic conditions, and other external factors are significant considerations in evaluating the performance of the

LCC pavement. Field performance is a broad term with an aspect incorporating the durability of the pavement structure. Any change that negatively affects the ability of the pavement to perform satisfactorily as compared with the traditional pavement structure poses a durability concern. For LCC pavements, the most common field performance considerations include the ability to resist freeze-thaw damage, premature cracking, pavement stiffness, instability of LCC layer which a loss of air content can cause, differential settlement of pavement structure, permeability properties, pavement longitudinal, and transverse profile.

3.1.3 Sustainability

Past studies have revealed that LCC could be a sustainable construction material, therefore this study seeks to assess this attribute. For this research, "sustainability' refers to a sustainable approach that focuses on constructing and maintaining the pavement infrastructure without the excessive use of resources through three critical factors in the process of decision making: environmental, social, and economic [95].

Two aspects are considered; cost, which covers the economy, and the environment. Two aspects of cost were considered for the use of LCC. The first aspect was the initial cost of construction. The second aspect of the cost being considered was the Life-Cycle Cost. LCCA is the cost of the pavement over its useable life and incorporates the initial construction cost, cost of maintenance, and repair over its life. The Life cycle cost forms another basis for determining the feasibility of using the LCC material over the traditional granular material. The LCC pavement should have a significantly longer service life than the granular stone base pavement. The feasibility of the option will depend on whether the increase in life and the reduction in the frequency of maintenance and repairs are enough to offset the higher initial cost and be lower through the life span. The key environmental aspect was air pollution and its implication on the environment.

Figure 3.1 outlines the research methodology, and subsequent sections give detailed descriptions of the techniques employed in this study.

3.2 Evaluation Techniques

The three primary considerations already discussed were evaluated using techniques discussed subsequently. These considerations are closely related; therefore, the results found using the following methods may be relevant to one or more of the considerations.

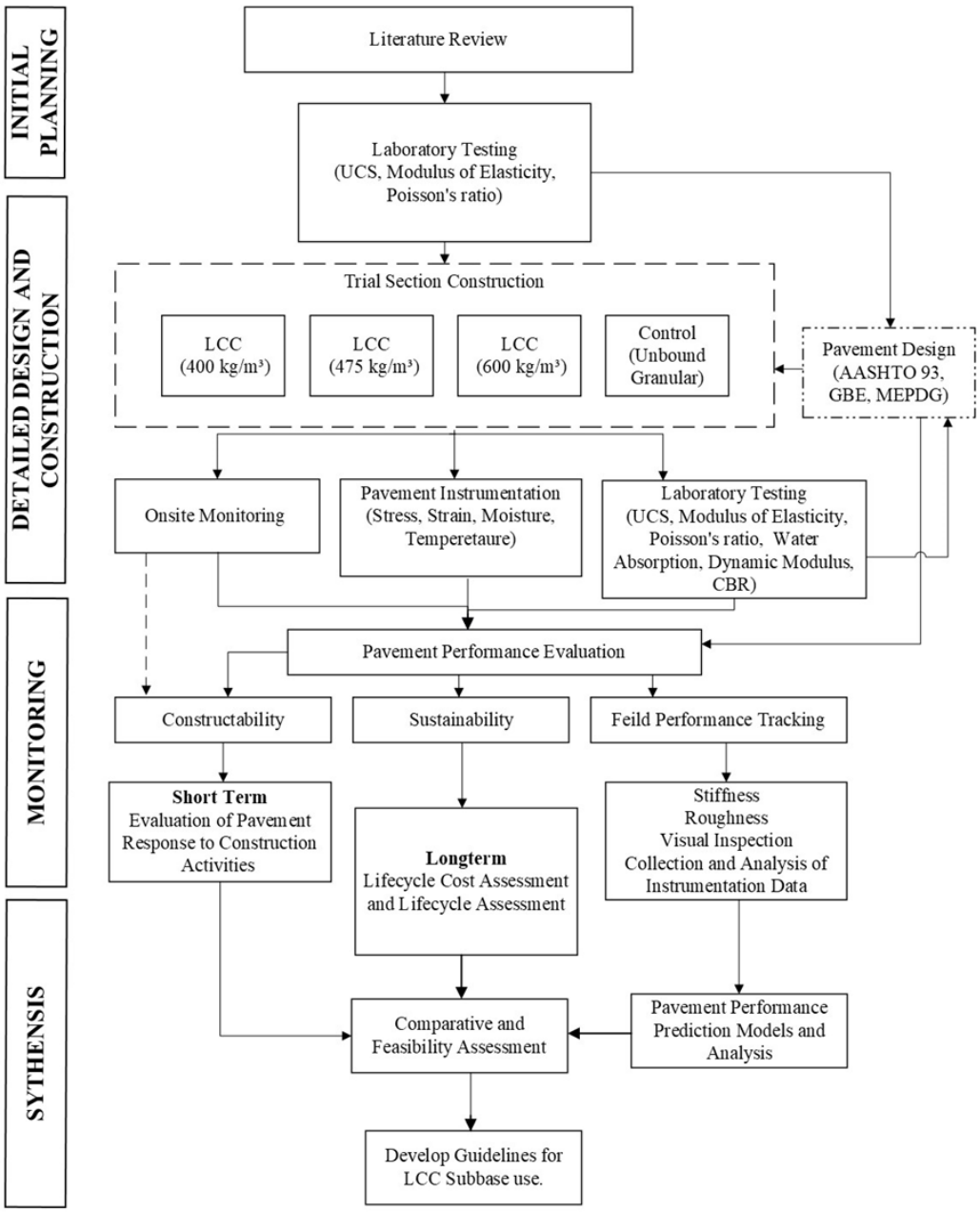

Figure 3.1: Research flow chart

3.2.1 Instrumentation

All LCC and Control sections were instrumented to monitor actual pavement response to temperature, moisture, strain, and pressure changes. Table 3.1 gives details of the type, number, and description of the instrumentation, and Figure 3.2 shows the sensors used.

Table 3.1: Sensor summary

Sensor type	**Model**	**Measurements made**	**Number installed**		**Sampling frequency**
			Erbsville	**Notre Dame**	**(readings/min)**
Earth pressure cell	LPTPC09-V	VW frequency (Hz)	3	4	5
		Thermistor resistance (ohm)			
Maturity sensor (Command center)	301006-X85	Temperature-Time Factor (TTF-hr)	2	6	1 per hour
		Temperature (°C)			
		Ultimate strength (MPa)			
Asphalt strain gauge	ASG 152/ PSS13002ASG	µstrain, mV/V	14	4	12
Concrete Strain gauge	PSS13001 CSG	µstrain, mV/V	-	6	-
Soil compression gauge	PSS13003 SCG 4-wire	Displacement, mV/V	-	2	-
Thermistor string	T107 series	Temperature (°C)	3 strings (7 sensors each)	-	12
Temperature probes	TH0003	Temperature (°C)	-	16	12
Moisture probe	Watermark 200SS	Thermistor resistance (ohm)	9	12	12
		Water potential (CB or KPa)			
Rain gauge	NovaLynx 260-2500	Precipitation (mm)	1	1	1 per hour
Solar radiation shield/ Temperature data logger	Hobo pendant UA-003-36	Temperature (°C)	1	1	1 per hour

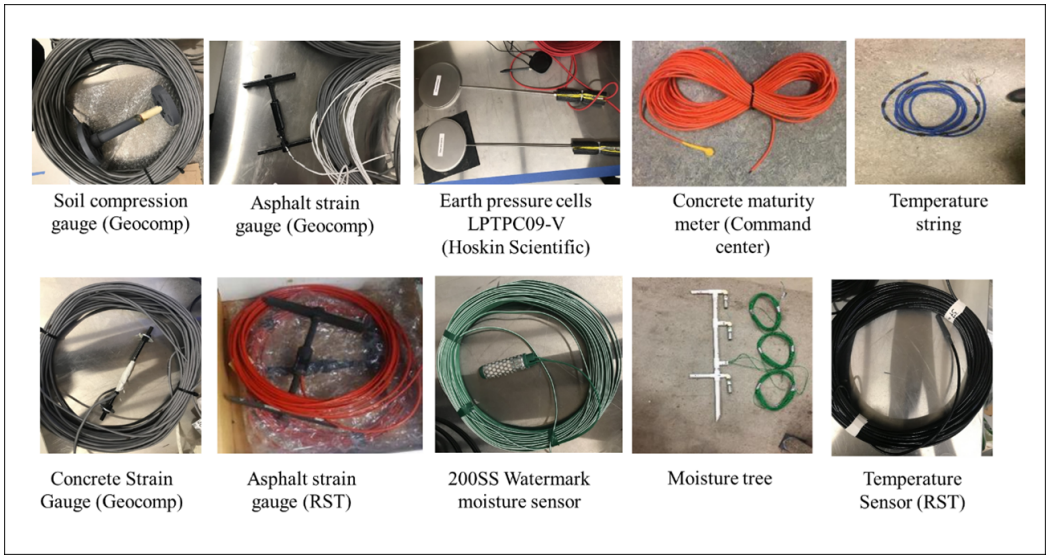

Figure 3.2: Types of installed sensors

Dataloggers

For monitoring purposes, a low-speed datalogger was required to gather moisture, temperature, and stresses at low frequency for lengthy periods, up to a few years. Figure 3.3 shows a Campbell low-speed datalogger with a multiplexer used to obtain data from the sensors.

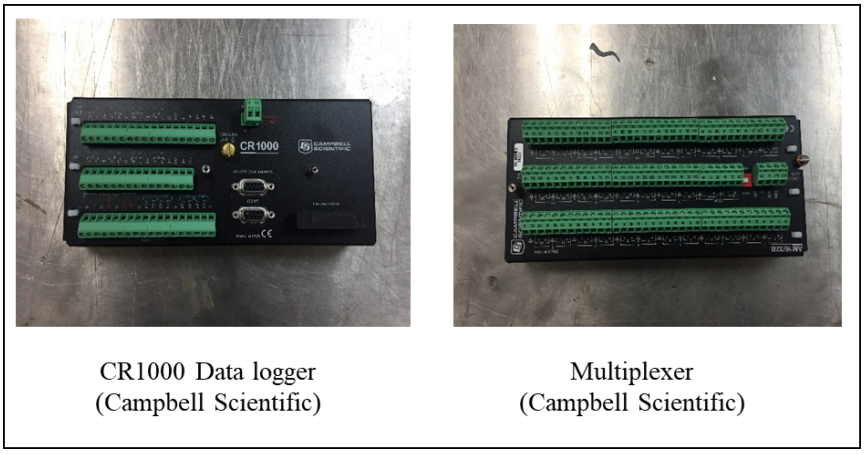

Figure 3.3: Data logger and Multiplexer

Weather station

A weather station consisting of a rain gauge and a solar radiation shield was installed at the field section locations. The purpose of this was to record atmospheric weather events at the site. In the solar radiation shield, there is a data logger that records rainfall and temperature events. The initial setting was to read the temperature every ten minutes; however, this was subsequently changed to hourly readings. The weather station is presented in Figure 3.4.

Figure 3.4: Rain gauge and Solar radiation shield

Earth Pressure Cell

The earth pressure cells employed in this study consisted of two circular steel plates welded around the periphery, with the space between the plates filled with hydraulic fluid. The cell is connected via a stainless-steel tube to a transducer forming a closed hydraulic system [69]. As the weight of a vehicle is applied to the pavement surface layer through its tires (axle load), vertical stresses in the layer are generated, which could lead to rutting. When the stress compresses the cell, the pressure can be measured and transformed into an electric signal. The earth pressure cell consists of a 3 KΩ thermistor that calculates the pressure readings based on the cell fluid viscosity characteristics [201]. These were connected to the CR1000 data logger via a vibrating wire analyzer with measurements taken every five minutes and then fifteen minutes subsequently using the program developed.

Strain Gauge

This study used two types of strain gauges: asphalt strain and concrete strain gauges. The program developed to record strain measurements of the materials surrounding the sensors included the CR1000 applying an excitation voltage to the full bridge strain gauge installed in the pavement. It then performs strain calculations on the measurement. The resulting value is the measured voltage in units of microstrain [43]. The installed strain gauge has a nominal resistance of 350 Ω.

Soil Compression gauges

Soil Compression Gauges (SCG) with a 4-wire potentiometer and a temperature range of -1 to 60 °C were used in this study to monitor horizontal and vertical displacements beneath the granular subbase layer. Typically, SCGs are used in soils and subgrade materials because they are toughened to survive the extreme conditions in soils, building fill material during installation and compaction, and waterproofing. These gauges can assess dynamic response using displacement transducers with travel ranges of 1 to 6 inches [86]. Displacement readings were then converted to microstrain using Equation 3.1.

$$S = \frac{D_m}{G_L} \times 10^6 \tag{3.1}$$

where S is strain (in μ), D_m is the measured displacement and G_L is the original gauge length.

Thermistor Strings

Two types of temperature sensors were used in this study. A thermistor string, consisting of seven temperature sensors, was included in one of the field sections, and single points temperature sensors were included in the second section. This provided subsurface information on temperature variation at different elevations within the pavement structure. Hence, it would enable a comparison of pavement and atmospheric temperature, temperature profile using LCC and granular B materials, and for use in analyzing the moisture sensor data. The temperature sensors were connected to the CR1000 data logger through one single-ended input channel and a voltage excitation channel, with measurements taken by the sensors every five seconds and then five minutes. To obtain accurate readings, temperature sensors must be entirely surrounded by the material; thus, temperature sensors

were embedded close to the mid-point of each layer of the pavement. The daily average temperature value is obtained over a twenty-four-hour period. The daily maximum and minimum temperatures are also recorded. The sensors are designed to resist heat, and the cables are waterproof, which increases the durability of the instrument.

Moisture Probe

The moisture sensors included in this trial section are typically used for agricultural applications. They have been selected for use in this research because they can record measurements when not totally surrounded by soil. LCC and granular material have several voids, meaning air is adjacent to the moisture sensors in specific locations. To read these sensors, a CR1000 data logger was used. A program was developed to record the moisture measurements of the sensors' surrounding materials. An excitation voltage is sent from the CR1000 to the moisture sensors; a voltage is measured after a pause of three milliseconds. The CR1000 records the measured voltage divided by the excitation voltage, which is then converted to resistance and adjusted to 21 °C using Equation 3.2 for a uniform basis of comparison. After this, the resistance is converted to Soil Water Potential (SWP) in centibars (cb) units which is equivalent to kPa via Equation 3.3 [98].

$$R_{21} = \frac{R_m}{(0.018(T_m - 21))} \tag{3.2}$$

where, R_{21} is the resistance adjusted to 21 °C, Rm is the resistance reading determined from the raw data collected by the CR1000, in kΩ and Tm is the temperature of the soil surrounding the moisture gauge in °C.

$$SWP = 7.407 \times R_{21} - 3.704 \tag{3.3}$$

SWP is the soil water potential measured in centibars (cb) and SWP (or Tension) describes water availability. When water is readily available, the centibar values are closer to zero, with a zero-value signifying fully saturated, but when minimal water is available, the values become higher [98]. Temperature readings used with the moisture sensors were obtained from the installed thermistor strings, which corresponded to moisture sensors in the same layer. Temperature and moisture readings were collected every five minutes.

Concrete maturity meter

The temperature within the LCC must be correlated with its compressive strength over 28 days in determining the maturity curve using the maturity method. One maturity sensor was installed in the middle of 150 × 300 mm cylindrical samples for each density and taken to the laboratory from the field to achieve this. This specimen was left undisturbed in the field for twenty-four hours before moving to avoid changing the material's structure. At the CPATT laboratory, it was demolded on the seventh day and put in the humidity chamber at 85% humidity. The recorded temperature from the sensor in the specimen was correlated with compressive strength results obtained in the laboratory. The maturity curve was determined based on strength and Temperature-Time Factor (TTF).

3.2.2 Onsite Construction Monitoring

The research team was on-site during construction. The process was documented from start to finish using notes of observations, photographs, and videos of the process. Key areas that were noted included time taken for each activity, the number of crew members involved in each activity, time of the day of construction, the weather conditions, types of equipment used and operation time, transportation time and distance for materials, duration of road closure for construction activity and challenges encountered. The onsite construction monitoring provided the most insight into the constructability of using LCC for road pavements. Challenges faced, as well as all possible solutions attempted, were documented. Notes on the practicality of these solutions were also made. All these eventually feed into guidelines that were developed for the use of LCC within pavements.

3.2.3 Material Property Characterization

Laboratory testing was performed to characterize the material used in the field during construction. This was to serve as quality control and input parameters when predicting the as-built pavement performance.

Lightweight Cellular Concrete

A. Unconfined Compressive Strength (UCS)

Specimens of size 75 × 150 mm were used for this test. The samples collected were tested at 1, 3, 7, 14, and 28 days. The test was performed in a stress-controlled setup

where the load was applied at a constant rate. All testing was conducted per ASTMC796 [16] and C495 [15]. The samples were left undisturbed on-site, transported to the CPATT laboratory twenty-four hours after casting and placed in the humidity chamber at an 85% humidity level. Four samples on day one were tested, and the results were recorded. Before testing, the samples were demolded and surface grinded. The maximum load was reached in considerable time. Equation 3.4 was employed to determine the unconfined compressive strength.

$$UCS = \frac{P}{A} \tag{3.4}$$

where UCS is the unconfined compressive strength, MPa, P is the maximum load recorded, kN and, A is the cross-sectional area of the specimen, mm^2.

The test setup is presented in Figure 3.5. Similarly, the samples on subsequent days were taken out the same day from the humidity chamber, demolded and grinded, then tested. Based on quality control data, the average LCC 28-day compressive strength was recorded as well as the minimum and maximum. Compressive strength and density are the leading indicators of the quality of the mixture [136].

B. Modulus of Elasticity (MOE) and Poisson's Ratio

150 x 300 mm samples were used for this test following ASTM C469 [21]. Samples were placed in the humidity chamber (humidity level 85%) up until the 28^{th} day. On day 28, the samples were demolded, and the surface grinded. Before testing, the unconfined compressive strength test was performed for two of these samples to determine the ultimate load of the LCC with this size specimen. MOE testing requires the maximum load applied on the sample to be 40% of its ultimate load, hence the need for the unconfined compressive test. The testing further requires six cycles of loading per sample. Poisson's ratio was estimated using a frame that read longitudinal and lateral deformation during load application. The test setup is shown in Figure 3.5. For Modulus of Elasticity, Equation 3.5 is utilized.

$$E = \frac{(S_2 - S_1)}{(\varepsilon_2 - 0.00005)} \tag{3.5}$$

where E is the chord modulus of elasticity, MPa, S_2 is the stress corresponding to 40% of ultimate load, MPa, S_1 is the stress corresponding to a longitudinal strain, ε_1, of 50 millionths, MPa, ε_2 is the longitudinal strain produced by stress S_2. For Poisson's ratio Equation 3.6 is used.

Unconfined Compressive Strength test setup

Modulus of Elasticity and Poisson's ratio test setup

Figure 3.5: UCS and Modulus of Elasticity/Poisson Ratio test set up

$$\mu = \frac{(\varepsilon_{t2} - \varepsilon_{t1})}{(\varepsilon_2 - 0.00005)} \tag{3.6}$$

where μ is Poisson's ratio, ε_{t2} is the transverse strain at midheight of the specimen produced by stress S_2, ε_{t1} is the transverse strain at midheight of the specimen produced by stress S_1.

C. Water Absorption

A water absorption test was performed on 150 × 300 mm samples at seven and twenty-eight days following (ASTM C1585) [19]. Three samples were removed from the storage container for the seven-day testing and demolded on the 7^{th} day. The samples were weighed and trimmed before being immersed in water. Since the LCC samples are very light and would float in water, a piece of wood with weights on it was used to hold them down in the water (Figure 3.6). This modified procedure was followed to simulate pavement field conditions as Ni proposed (2021) [174]. Samples remained in the water for 24 hours with water temperature maintained at 20 °C +/- 3 °C. Afterward, samples were weighed again to obtain the percentage of water absorbed. The wet mass of the sample was recorded

30 seconds after it was removed from the water. The water absorption was calculated by Equation 3.7.

Specimens soaked in water

Weighing specimen after soaking

Figure 3.6: Water Absorption testing setup

$$Absorption, \% \ by \ volume = 100 \times \frac{V_w}{V_c} \tag{3.7}$$

where V_w is the volume of water absorbed by the test specimen in 24 h, in m^3, and V_c is the volume of the test specimen (cylinder), in m^3.

The twenty-eight-day samples were demolded on day seven along with other samples and placed in the humidity chamber with a humidity level of 85% until day 28. The same procedure as day seven testing was followed.

Asphalt Concrete Dynamic (Complex) Modulus

The characteristics of an asphalt mixture can provide information that can help anticipate its performance in the field. Loose asphalt concrete mix collected on the field was transferred to the CPATT laboratory. To simulate the field mixing and placement impacts, loose HMA mixtures were exposed to a short-term temperature of 143 °C before compaction, as per AASHTO R 30-02 (2010) [179].

For this test, the SuperPave Gyratory Compactor was used to produce test specimens following AASHTO PP 60-13 [180]; the mixtures were compacted to 152 mm in diameter

and approximately 170 mm in height. The samples were cored and cut into dimensions of 150 mm height and 100 mm diameter with air void content of 7 ± 1% for the dynamic modulus samples. Afterward, the specimens were grinded to obtain a smooth, levelled surface.

Dynamic (Complex) modulus test was conducted at different temperatures (-10, 4, 21.1, 37, and 54.4 °C) and various load frequencies (25, 10, 5, 1, 0.5, 0.1 Hz) to examine the change in the stiffness. This was evaluated using the CPATT Material Testing System (MTS) according to the protocol outlined in AASHTO TP 62-07 [181], Standard Test Method for Determining Dynamic Modulus of Hot-Mix Asphalt Concrete Mixtures. A repeated compressive and sinusoidal force was applied to the test specimens. The deformation of the test specimen was measured using three Linear Variable Differential Transducers (LVDTs). In this test, triplicate cylinder specimens were used. The lowered frequency was assessed using a master curve (Hz).

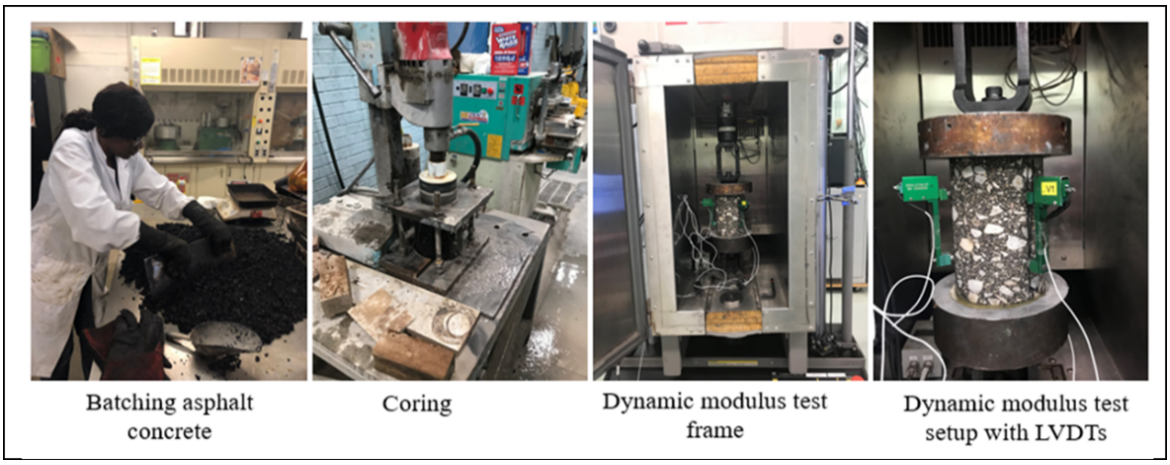

Figure 3.7: MTS loading frame with Dynamic Modulus test setup

Unbound Layers

A. Moisture Content and Sieve Analysis

The optimum water content (OPC) of the base, subbase, and subgrade material was determined under ASTM D 698 [56], procedure C. This procedure is used for materials with 30% or less retention on the 19 mm sieve. This was determined by performing a sieve analysis to determine the gradation of the unbound layers [20]. The materials fulfilling this

procedure C requirement are compacted in a 152.4 mm (6-inch) diameter mold in three layers, each compacted with 56 blows with a 24.5 N rammer falling from a height of 305 mm. For each specimen, 6 kg of material was used. Figure 3.8 shows the sieve analysis setup, sample mixing setup and the compacted sample after compaction at OPC.

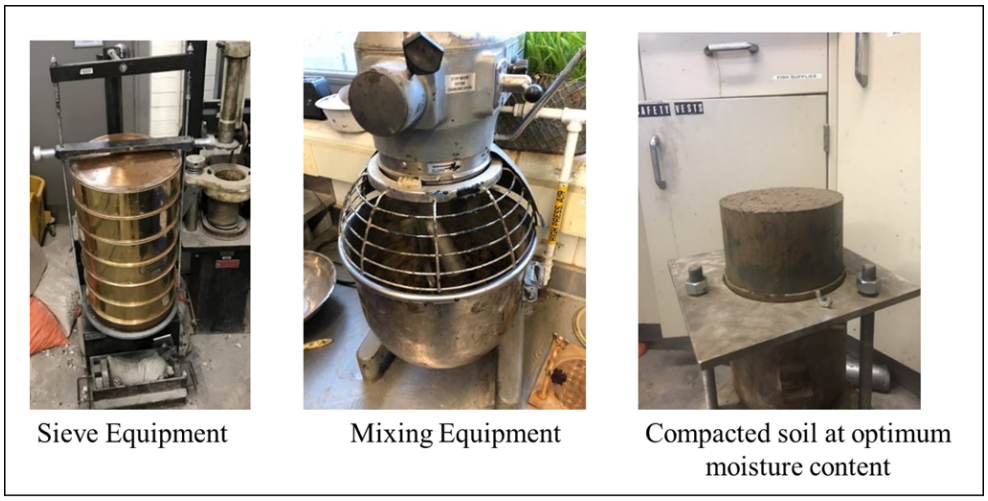

Figure 3.8: Sieve analysis and moisture content setup

B. California Bearing Ratio

The California Bearing Ratio (CBR) for the unbound layers was determined per ASTM D1883 [18]. For this test, specimens were prepared using ASTM D 698 [56]. After the specimen was compacted in three layers with 56 blows per layer, a 152.4 mm diameter mold, the specimen was levelled with a straight edge and then weighed. The base plate in the mold was removed, and the specimen was turned upside so that the levelled surface became the base. Weights of up to 4.5 kg according to the specification were placed on the specimen, which was soaked in water for four days. A tripod scale was used to take readings every day until day four, just before testing, to monitor any material swelling. Initial scale reading was noted on day one, and the difference in the readings for day four was recorded as the swell in mm. Figure 3.9 shows the CBR testing setup and specimen after testing.

Stress exerted on the specimen at different penetration levels was computed using Equation 3.8 below. The CBR was calculated with Equations 3.9 and 3.10 for 2.5 mm and 5.08 mm penetration depths. The bearing ratio reported is usually the one at 2.5 mm penetration; however, a test rerun is required to verify when the ratio at 5.08 mm is greater.

$$S = \frac{L}{A_p} \times 100 \tag{3.8}$$

where S is Stress in (MPa), L is measured loading force in (kN), and A_p is the area of the piston in (mm^2)

$$CBR_{2.5} = \frac{S_{2.5}}{6.9} \times 100 \tag{3.9}$$

$$CBR_{5.08} = \frac{S_{5.08}}{10} \times 100 \tag{3.10}$$

where $CBR_{2.5}$ is the bearing ratio at 2.5 mm penetration, $CBR_{5.08}$ is the bearing ratio at 5.08 mm penetration, $S_{2.5}$ is the calculated stress at 2.5 mm penetration depth in MPa, $S_{5.08}$ is the calculated stress at 5.08 mm penetration depth in MPa, 6.9 and 10 are the standard stresses at 2.5 mm and 5.08 mm penetration depth respectively in MPa. The test was repeated as per specification whenever the CBR value was greater at 5.08 penetration.

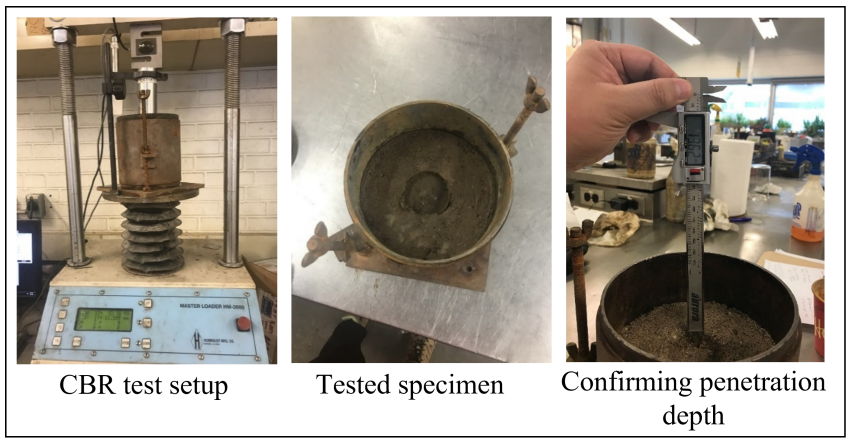

Figure 3.9: California Bearing Ratio test setup

3.2.4 Pavement Stiffness Evaluation

Falling Weight Deflectometer

The Falling Weight Deflectometer (FWD) test is one of the post-construction testing carried out by Wood Plc and PSI Technologies to measure the field pavement performance.

FWD measures the vertical deflection response of the surface to an impulse load applied to the pavement surface (and the testing was performed in accordance with ASTM D4695–03 [24]; D4694–09 [23]. Using geophone sensors, this testing tool uses a falling weight from a defined height to impart deflections on the pavement surface, then measures these deflections at specific distances from the impact point. The FWD data was used to estimate the pavement structural capacity and determine whether the pavement was being overloaded. To do this, deflections from the FWD were used for back calculations to assess the: elastic modulus of each layer, the overall stiffness of the pavement system, the modulus of subgrade reaction, the effective thickness, structural number, or soil support value, and the bearing capacity or load carrying capacity of a pavement

This information shows the pavement capacity and performance life and helps plan future rehabilitation techniques [155]. The testing equipment was a suitable trailer towed by a vehicle, as shown in Figure 3.11. Data collected included load characteristics, load frequency, the geometry of loaded area and deflection sensor location, time of test, location of test points, and air and pavement temperatures.

Erbsville Structural Evaluation

The EXP Heavy Weight Deflectometer (HWD) was used to perform the Falling Weight Deflectometer (FWD) test at Erbsville. The testing equipment used a falling weight from a predetermined height to impart deflections on the pavement surface, then measured using geophone sensors at various distances from the impact location. For traditional asphalt pavement testing, four drops per point of dynamic load between 30 kN and 70 kN were applied to the pavement surface and normalized to 40 kN. To measure deflection at those places, nine geophones with a sensor spacing of 0 mm, 200 mm, 300 mm, 450 mm, 600 mm, 900 mm, 1200 mm, 1500 mm, and 1800 mm (as per Strategic Highway Research Program requirements) were utilized. In addition, individual layer material attributes were back-calculated. Throughout the experiment, surface, sub-surface, and ambient temperatures were recorded, which is required for back-calculation. A thermal gun and subsurface instrumentation installed were used to measure the temperatures. The FWD test was conducted on all three sections of the Erbsville field road stretch on the lane's centerline at two-meter intervals.

Equation 3.11 was used to calculate composite pavement moduli, as stated by MTO in the National Cooperative Highway Research Program (NCHRP) study [206]. Each drop's deflection profile was employed in the calculation.

$$E_0 = \frac{f \times (1 - v^2) \times \sigma_0}{d_0} \tag{3.11}$$

where E_0 is the composite modulus of the entire pavement system beneath the load plate, f is the factor for stress distribution (using 2), v is the Poisson's ratio, σ_0 is the peak pressure of FWD impact load under the load plate, a is the radius of FWD load plate and d_0 is the peak center FWD deflection reading.

In compliance with the AASHTO 1993 Pavement Design Guide, the Subgrade Resilient Moduli were calculated using Equation 3.12, which considered geophone deflection at 1200mm from the loading point.

$$M_r = C \times \frac{0.24P}{d_r \times r} \tag{3.12}$$

where, M_r is the subgrade modulus, in psi, P is the applied load, in pounds, d_r is the deflection measured at a radial distance r, in inches, r is the radial distance at which the deflection is measured, in inches, and C is the correction factor for design (0.33 was employed).

The existing pavement structural number was also calculated based on the AASHTO 1993 Pavement Design Guide with Equation 3.13.

$$SN_{eff} = 0.0045 \times D \times E_p^{\frac{1}{3}} \tag{3.13}$$

where D is the total thickness of all pavement layers of existing pavement above the subgrade (inch), E_P is the effectively combined modulus of all pavement layers above the subgrade (psi).

Notre Dame Structural Evaluation

A similar methodology as described for performing the FWD testing at Erbsville was followed. However, in this case, the structural coefficients of the pavement sections were not determined. It is expected to be performed after the final lift of asphalt is placed. Figure 3.10 presents the testing locations.

The $AREA_{60}$ method was used to evaluate the structural capacity of the pavement sections at this location using Equation 3.14.

$$AREA_{60} = 4 + 6 \times \frac{d_8}{d_0} + 5 \times \frac{d_{12}}{d_0} + 6 \times \frac{d_{18}}{d_0} + 9 \times \frac{d_{24}}{d_0} + 18 \times \frac{d_{36}}{d_0} + 12 \times \frac{d_{60}}{d_0} \tag{3.14}$$

where d_0, d_8, d_{12}, d_{18}, d_{24}, d_{36}, and d_{60} indicate deflection at distances mm (inch) 0, 203 mm (8), 457 mm (12), 610 mm (24), 914 mm (36), and 1,524 (60), for the nine-sensor configuration. The calculated $AREA_{60}$ and Maximum deflection values were used

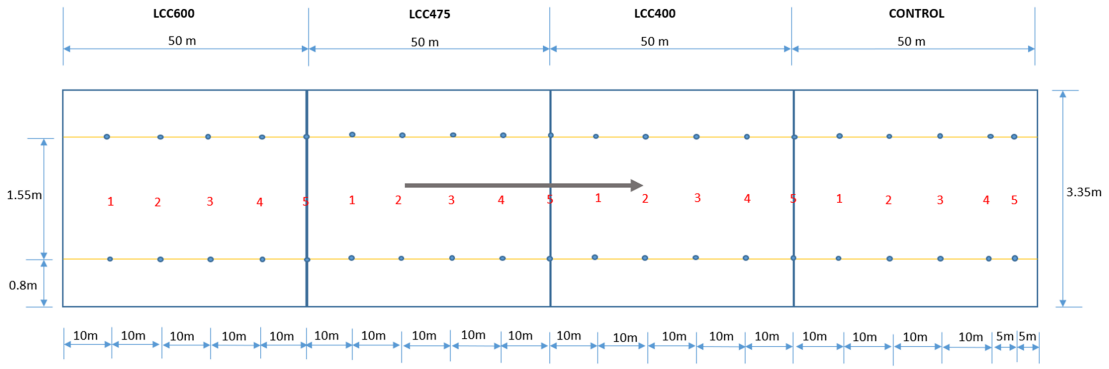

Figure 3.10: Falling Weight/Lightweight deflectometer testing layout (Notre Dame Drive)

to compare the structural capacity of the pavement sections following the FHWA guideline [17]; [202]).

Lightweight Deflectometer

This is a portable falling weight deflectometer that can be used to perform a similar test as described for FWD in section 3.3.2.1. However, because it is portable, it can be used when the FWD is unavailable and allows for the test to be done more often. For this test, a falling weight held at a constant height by a release mechanism is manually dropped onto the pavement surface, thereby transmitting load (Figure 3.11). Deflection readings were obtained and back-calculated to get the pavement stiffness. Because this test is manually performed, it can be subject to human error; thus, care was taken to minimize this error by ensuring that at least three drops with consecutively constant or close outcomes were achieved at a location before moving to the following location. Also, care was taken to drop the load correctly from the required height. Equation 3.15 was used to compute the LWD stiffness based on the elastic half-space (Boussinesq's Solution) theory.

$$E(MPa) = \frac{\pi \times (1 - \mu^2) \times r \times \sigma_0}{2 \times d} \tag{3.15}$$

where μ is the soil's Poisson ratio, r is the plate radius in mm, σ_0 is the maximum force in kN and d is the maximum deflection in m. The LWD testing locations for Erbsville are presented in Figure 3.12, while the exact testing location as the FWD test for Notre Dame Drive (Figure 3.10) was also used for LWD.

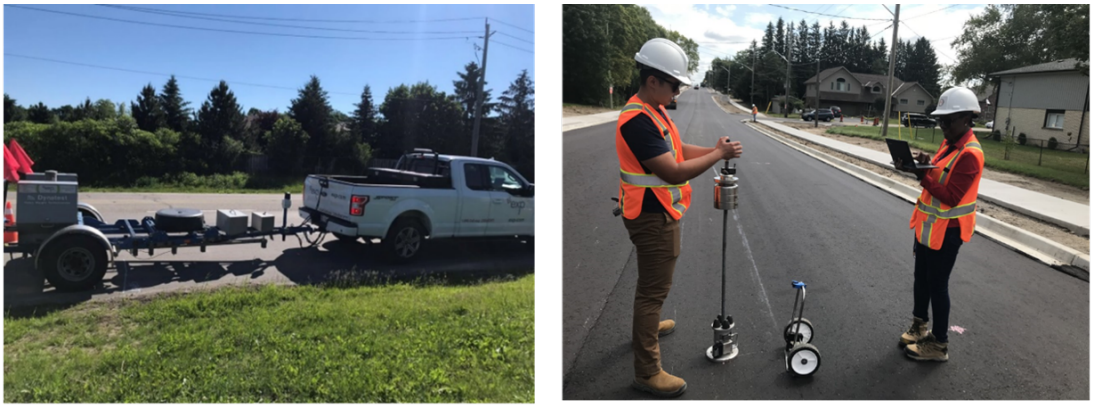

Falling Weight Deflectometer testing at Erbsville

Lightweight Deflectometer testing at Notre Dame Drive

Figure 3.11: Pavement stiffness evaluation equipment

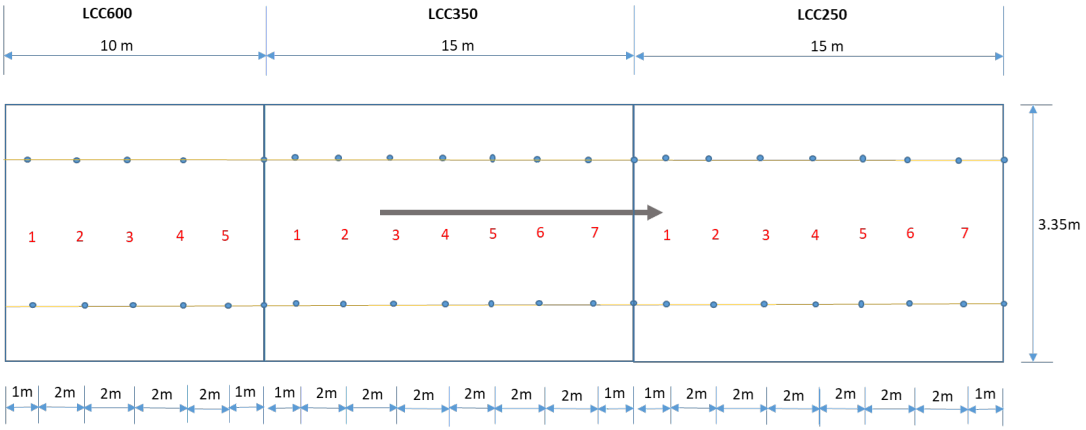

Figure 3.12: Lightweight deflectometer testing layout (Erbsville Drive)

3.2.5 Truck Driving Test

A truck driving test was carried out to monitor pavement responses under controlled axle load. This will help evaluate and compare the pavement bearing capacity for the Control and LCC sections. One typical type of large-size truck (tandem rear axle configuration) in Canada was chosen to conduct the load tests. Two scenarios with two different load configurations were considered. The first scenario studied a loaded truck (with granular A material), and the second scenario was an unloaded truck. Both scenarios may cause

noticeable damage to the pavement surface structure. The testing on the Erbsville road gathered mostly static load impact on the pavement layers by allowing the truck to stand on the pavement surface for about two minutes. On Notre Dame Drive road, the truck moved very slowly at a 1.5 km/hr speed over the pavement surface. The tire-pavement interface for each truck tire was found to have an area of 0.06 m^2. The corresponding average pressure beneath the tires was calculated for both scenarios. Details used in this analysis are presented in Table 3.2. It should be noted that this average value likely underestimates the pressure under the rear tandem axles that could support the majority of the loaded truck's mass. However, individual axle weight data was not available.

Table 3.2: Truck characteristics

Scenario	**Erbsville**				**Notre Dame**			
	Weight (kg)	NT	Load (kN)	MTP (kPa)	Weight (kg)	NT	Load (kN)	MTP (kPa)
Loaded	35,080	10	344	573	34,620	14	340	405
Unloaded	13,650	10	134	223	13,840	14	136	162

Note: NT: Number of tires, MTP: Mean tire pressure

The truck specifications are presented in Figures 3.13 and 3.14. The truck consisted of one steering axle, one single axle (raised for the Erbsville testing), and one tandem axle with dual tires per side 0.5 m apart. At the time of this test for Notre Dame Drive, only 100 mm Asphalt Concrete for all the sections, had been placed.

3.2.6 Roughness Evaluation

Pavement roughness is the measure of the surface irregularities that impact ride quality and is of great safety concern [182], hence a measure of the deviation of the road surface from its original plain. There are three ways of evaluating this; Subjective method, where a vehicle is driven over the pavement, and a ride comfort rating (RCR) is assigned based on discretion; Objective method, where a device takes mechanical measurements like the automated road analyzer (ARAN®); Profiler method in which the longitudinal profile of the road is taken using a tool such as SurPro. The International Roughness Index (IRI) is commonly used to assess pavement roughness. It is estimated by evaluating the longitudinal profile of the road section [256]. A change in roughness over time because of a change in longitudinal profile serves as a good indication of pavement performance. Profile data using the road profiler are typically generated at intervals of 25 mm. An IRI value of

Figure 3.13: Loaded truck during the truck driving test

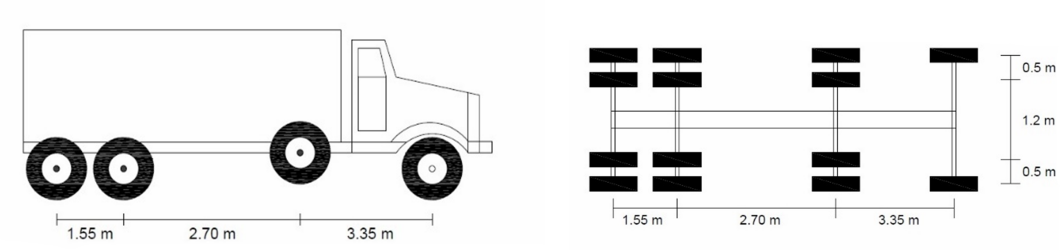

Figure 3.14: Truck configuration

0 m/km signifies absolute smoothness and 10 m/km roughness of an unpaved road. This study adopted two walking profilers, the SurPro and Dipstick, as presented in Figure 3.14.

3.2.7 Visual Inspection

Visual inspection was performed at regular intervals in accordance with ASTM D6433 -18 [22] throughout the study period for the field sections. The aim of this was to evaluate pavement distresses. This indicates the performance of the LCC and control section sub-base layers. When assessing the pavement, the following distress was considered: Fatigue (alligator) cracking, reflective cracking, bumps and sags, corrugation, depression, edge cracking, longitudinal and transverse cracking, and rutting.

a. Dipstick b. SurPro

Figure 3.15: SurPro and Dipstick IRI testing equipment

For each distress, its severity (low, medium, and high) and its density (number) were noted. This assessment could help determine the durability behavior of the LCC pavement and enhance comparative evaluation with the control section. While this condition survey is somewhat subjective, it provides a basis for comparison. The ASTM D6433 -18 offers detailed descriptions of each pavement distress type's severity level. Furthermore, measurements of any significant distress will help to provide objective values for comparison.

3.2.8 Life-Cycle Assessment

The Life Cycle Assessment (LCA) methodology specified in the ISO 14020 standard and the framework for pavement LCA provided by the FHWA report [95] was adopted for this study. The pavement life cycle stages were material production, design, construction, maintenance, and rehabilitation. The use and end-of-life stages associated with the pavements have not been considered. Further details are presented in Chapter 8.

3.2.9 Life-Cycle Cost Analysis

Determining the Life cycle cost of using LCC within the pavement structure involved compiling the initial and future expenses. Two crucial indicators were considered. Firstly, the Net Present Worth (NPW) was used to convert the cost of pavement maintenance for different years to the current year's worth using a discount value. Secondly, the Equivalent Uniform Annual Cost (EUAC), calculated based on Net Present Worth (NPW) value and distributes cost into the pavement life cycle yearly, was also used. The LCCA for the control and LCC sections were compared to see which cost-effective option. This analysis could also help determine the minimum life span, which could mean LCC pavements become more economically viable. Further details are presented in Chapter 9

3.3 Chapter Summary

Three evaluation considerations were laid out to be performed in this study. Considerations were made for constructability, sustainability, and field performance for lightweight cellular concrete subbase flexible pavements. Several evaluation techniques have been performed to obtain information on these considerations, ranging from using pre-installed instrumentation during construction for structural monitoring, temperature, and moisture that enabled field performance tracking in various environmental circumstances. Furthermore, structural performance was assessed using stiffness, roughness, and physical condition evaluation. In terms of sustainability, given previous research revealed possible environmental and cost benefits, this study conducted a Life-Cycle Assessment and Life-Cycle Cost Analysis to examine these benefits further. All of this was described in this chapter.

Chapter 4

Trial Section Design and Construction

4.1 Introduction

This chapter outlines the design and configuration of two test sections, including materials, baseline layer thickness, and layout. The purpose of the test sections was to investigate the performance of lightweight cellular concrete as a structural subbase layer. The test sections were instrumented to observe the pavement structure's stress, strain, temperature, and moisture. Three densities (400 kg/m^3, 475 kg/m^3, and 600 kg/m^3) of LCC were incorporated within the two sections to evaluate performance. A control section with traditional flexible pavement subbase layers was also included within each test site to compare LCC subbase performance with existing practice.

4.2 Erbsville Trial Road

4.2.1 Project Location

The project site is a shoulder located on the southbound shoulder of a two-lane major arterial road at the intersection of Erbsville Road and Brandenburg Blvd, in Waterloo, Ontario. The geographic Cartesian coordinates of the site are 43° 27'34.6"N 80° 34'42.3"W. The location is shown in the red box in Figure 4.1.

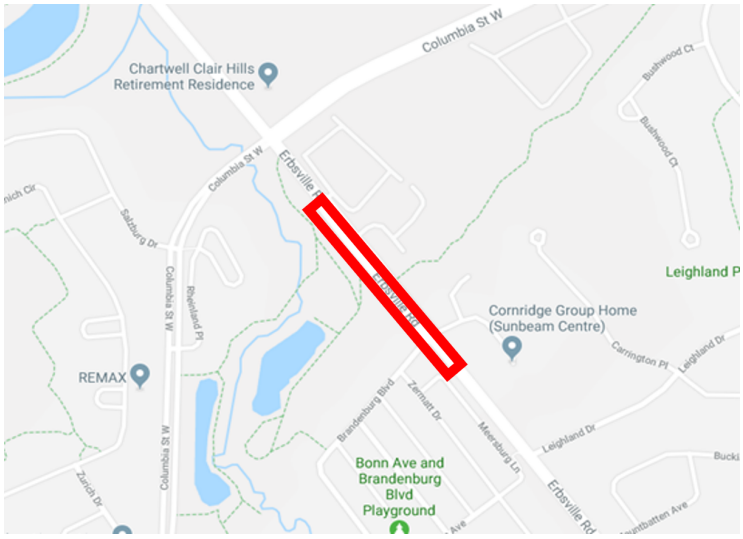

Figure 4.1: Location of trial section (Google, CNES 2018)

This shoulder also serves as a bus stop and was selected by the Region of Waterloo as a potential location for lightweight cellular concrete subbase as it experienced severe cracking and rutting issues, especially at the bus stop, as seen in Figure 4.2. The cause of these distresses is uncertain, but speculations were that it might be because of a weak subgrade. The trial section was planned for a 40-meter length from the beginning of the intersection. The area of the roadway was relatively flat and straight. Figure 5.2(b) illustrates the location going southwards.

4.2.2 Pavement Design (Granular Base Equivalency Method)

The design for this project was completed by an experienced team including members from the Region of Waterloo, CEMATRIX, and the Centre for Pavement and Transportation Technology (CPATT) at the University of Waterloo. The design took place between August and September of 2018. The trial design was completed using the Granular Base Equivalency (GBE) method adapted from work by Ni (2021) [174]. The original design for the entire road segment corresponded to that of a major arterial road in Ontario with a weak subgrade (30 MPa Resilient Modulus) and an AADTT of 2500 according to typical pavement design report classification by Applied Research Associates-ARA [10]. The operating speed for this road section is 60 km/hr. To design corresponding LCC sections, this classification was also used. Also, typical material properties were sourced from the

Pavement distress at bus stop (Erbsville)

Southbound illustration of Erbsville test road location

Figure 4.2: Location before construction

Table 4.1: GBE design coefficients [174]

	Surface	**Base**	**Subbase**				Subgrade
	Hot-mix	Granular	Granular	LCC(kg/m^3)			Soil
	Asphalt	A	B	400	475	600	
GBE strength coefficient	2	1	0.67	1.22	1.46	1.91	-

maintenance and rehabilitation manual [182].

Typical strength coefficients (equivalency factors) for the proposed pavement design, otherwise known as the Control section, were obtained from the OPAC 2000 specifications in [182] while the LCC strength coefficients derived by Ni [174] were adopted for the LCC sections. Results for the GBE strength coefficient of substituting unbound granular subbase with LCC [174] for densities of LCC ranging between 400 and 600 kg/m^3 are presented in Table 4.1. The three LCC densities were noted to have a higher strength coefficient than granular B. This would yield thinner pavements incorporating LCC as pavement subbase compared with Granular B. Thus, using the structural coefficients for the LCC densities obtained with the control design produced alternative pavement designs (Table 4.2).

Due to the limited road length available for the test section, it was decided that only one

Table 4.2: Erbsville equivalent LCC pavement designs

Layer	**Control**	**LCC(kg/m^3)**		
		400	475	600
Asphalt Concrete (mm)	150	150	150	150
Base (Granular A, mm)	150	150	150	150
Subbase (Granular B, mm)	450	-	-	-
Subbase (LCC, mm)		250	210	160

LCC density would be appropriate at this location. Based on experience and experimental results, the 475 kg/m^3 LCC density was selected. Two possible LCC layer thicknesses of 250 mm and 350 mm were also considered. Since the minimum LCC thickness of 210 mm was required for the design to be equivalent to the control, a decision was made to increase thickness to the nearest 50 mm, thereby 250 mm. Furthermore, a 100 mm thicker LCC layer was also proposed to assess the performance of varying LCC thickness. The final design would have three sections: a Control with 450 mm granular B and two LCC portions, one 350 mm thick and the other 250 mm thick, as shown in Table 4.3.

Table 4.3: Final design for Erbsville test road

Layer	**Control**	**475 kg/m^3 Sections**	
		LCC350	LCC250
Asphalt Concrete (mm)	150	150	150
Base (Granular A, mm)	150	150	150
Subbase (Granular B, mm)	450	-	-
Subbase (LCC, mm)		350	250

The detailed section view is presented in Figure 4.3. The three sections constituted similar layer material and thickness for asphalt concrete as the surface layer and granular A as the base layer; the control section was 10 m long, while the LCC350 and LCC250 sections were each 15 m long.

4.2.3 Site preparation, Excavation, and Granular B placement

Excavation, subgrade sampling, and Granular B installation for the Control section kicked up construction on October 22, 2018. The weather was pleasant for the day, with an average

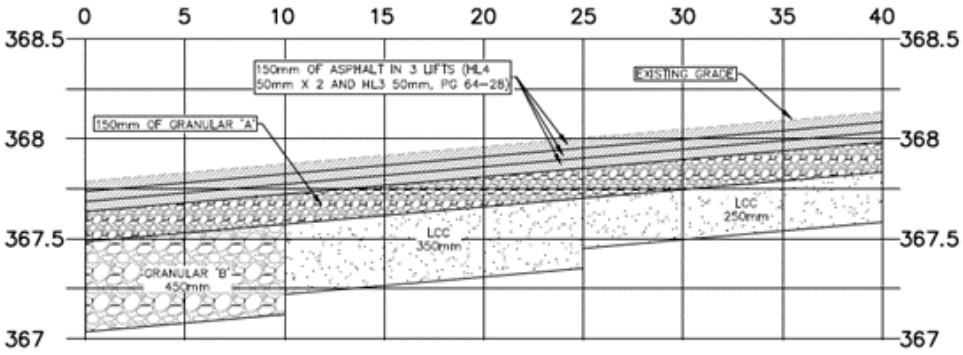

Figure 4.3: Section view of trial section

temperature of 4 °C in the morning and 8 °C in the afternoon and some sunshine. Saw cutting of the existing asphalt concrete layer was done, followed by full depth excavation to a total depth of 750 mm for the control section, 650 mm for the 650 mm section, and 550 mm for the LCC 350 and LCC 250 sections (Figure 4.4).

The exposed subgrade was rolled without vibration with a smooth steel drum roller. The subgrade was found to be damp, stable, and good to accept granular B and cellular concrete, with moderate deflection. Soil samples were collected in plastic bags at a depth of 750 mm for laboratory examination.

4.2.4 Instrumentation Installation

The general instrumentation installation is described in this section. Except for the moisture tree, instrument installation coincided with the construction process, with each instrument being installed before constructing the stratum where it would be located. The complete procedure began on October 22, 2018, with excavation and granular B placement for the control section. The LCCs were installed the next day. All construction activities concluded on November 5, 2018, with asphalt concrete paving. Figure 4.5 shows a detailed section view of each sensor, illustrating the type and placement of each sensor. All the sensors were positioned beneath the bus stop's right wheel path.

Each section's moisture and temperature sensors were installed as a single unit. In this case, a temperature string with numerous sensors per string was used. Two temperature strings had seven temperature sensors spaced at different intervals to ensure they could be located within each pavement layer. The third sensor had nine sensors spaced at 100

Figure 4.4: Site preparation and excavation

mm intervals. Three moisture sensors and one thermistor string were attached to a tree of $3/4''$ diameter PVC pipes. A hole was dug in the subgrade soil to receive the moisture tree hammered into the subgrade to ensure that at least one moisture and temperature sensor was in each layer. One moisture sensor was installed 100 mm into the subgrade, the other at the center of the subbase layer, and the third at the center of the base layer. The moisture sensors were placed at an angle (more vertically inclined) to ensure they were at the exact positions intended and read correctly.

Also, at least one temperature sensor was placed at the center of each pavement layer, including the asphalt layer. For the subgrade, three temperature sensors were located at 120 mm, 100 mm, and 50 mm in the soil of the Control. In contrast, one sensor was at a depth of 50 mm and two sensors at 100 mm depth in the soil at the LCC350 and LCC250 sections. Two temperature sensors were in the granular B layer at 40 mm and 150 mm depth, and one temperature sensor at 190 mm within the LCC 350 layer (Figure 4.6 c and b).

Each section had one earth pressure cell installed. The circular head of the cell was bedded with fine sand procured offsite, and the cell was set on the sand at a 45-degree angle. To guarantee that the handle was firmly secured, metal pegs were used to secure it to the ground (Figure 4.6 a). The sensors' wiring was run through flexible conduits to

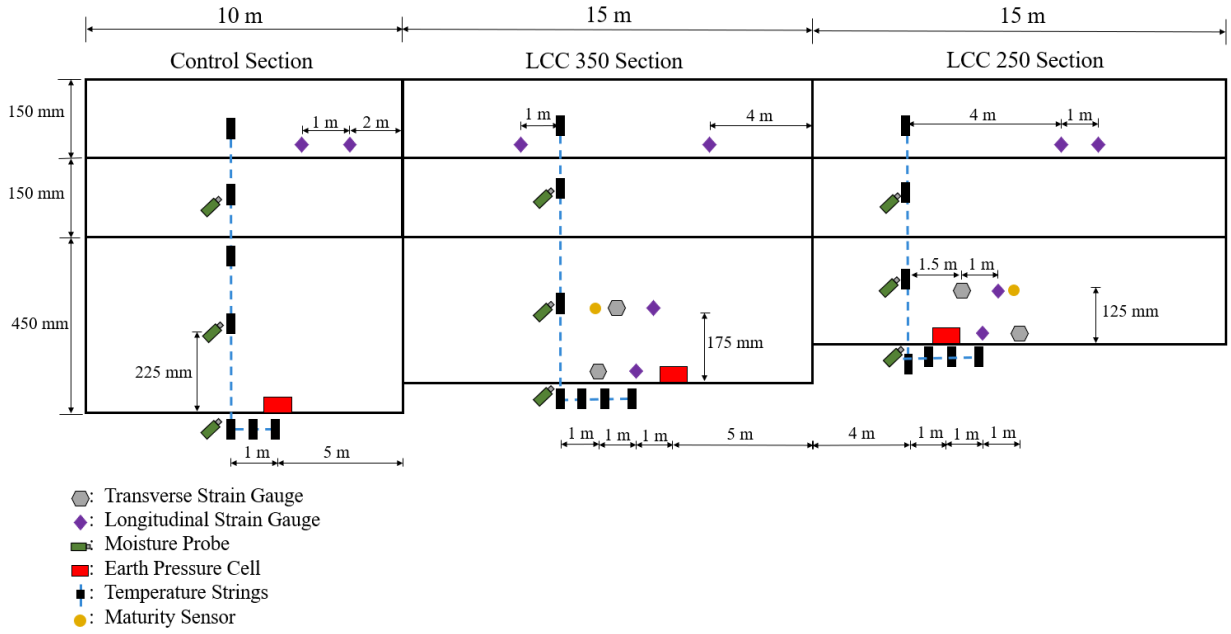

Figure 4.5: Section View for location of sensors within the pavement

the excavation's edge.

Four strain gauges were placed in the subbase layer for each LCC section, while two each were placed at the bottom of the asphalt layer for all the sections. For the two strain gauges installed at the bottom of the LCC layers, metal pegs were used to firmly fix them to the ground surface to ensure no movement during the LCC pour. One strain gauge was installed horizontally, while the other was installed in the transverse direction. For the strain gauges installed in the middle of the LCC layer, props made with $\frac{3}{4}$" diameter PVC pipes were used to hold them. Like the gauges placed at the bottom of the LCC layer, one was placed in the horizontal direction and the other in the transverse direction (Figure 4.6 e).

One concrete maturity meter was placed in each LCC layer. The concrete maturity meters were also attached to the props used for the mid-LCC strain gauges to ensure that the meters were located at the center of the LCC layer (Figure 4.6 d).

All the cabling for the sensors was run to the side of the excavation and placed in PVC flexible conduit pipes that transitioned into a 4" diameter solid PVC pipe which was laid in a trench, dug to meet the data logging unit. The instrumentation cluster is shown in Figure 4.7 e.

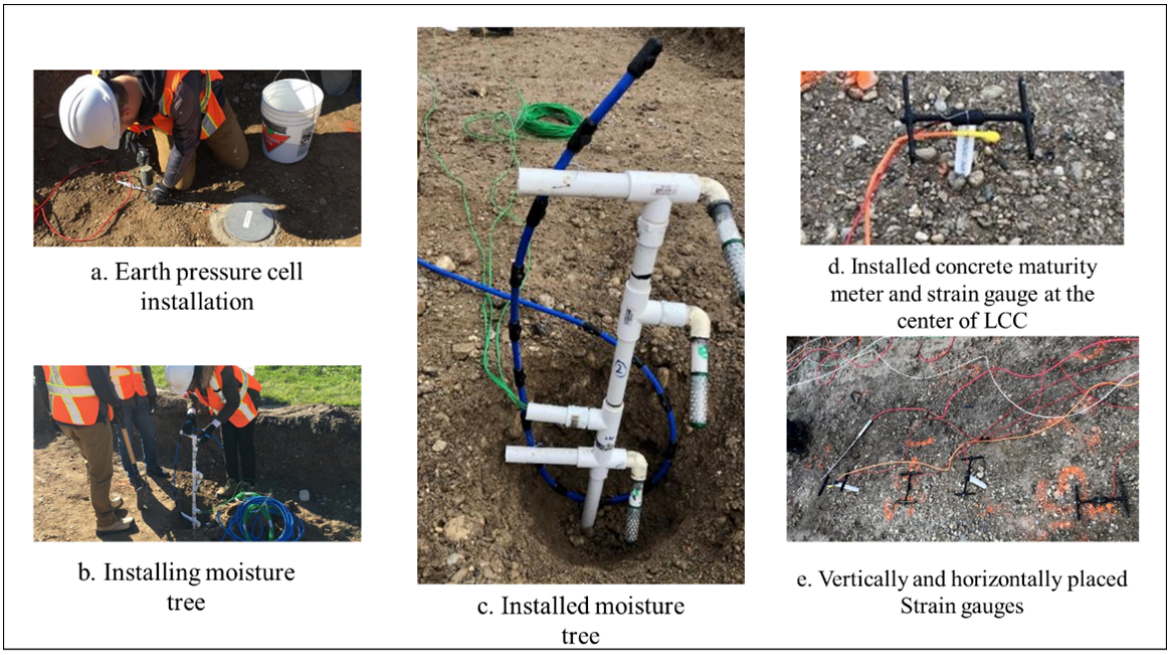

Figure 4.6: Instrumentation installation

Towards protecting the sensors during construction activities from material and equipment damage, a wooden box (Figure 4.7 d) was used to form a hedge around the sensors. This was also to help improve the visibility of sensor locations for equipment operators and further avoid damage when no one was on site. The cables were all run into a PVC flexible conduit to the edge of the excavation (Figure 4.7 b and c). After protecting the sensors, one truckload of Granular B was used to partially fill up the subbase layer at the control section, in preparation for the next day's work. Construction activities on October 22, were completed for the day at 4:30 pm. The Overall cabling and instrumentation for all sections can be seen in Figure 4.7 a.

4.2.5 Placing Lightweight Cellular Concrete (LCC) – October 23, 2018

Before the LCC was installed, the CPATT team installed the sensors on October 23. Instrumentation was installed before and during the wet intervals because it was a very rainy day, with rain commencing at 9:40 a.m. and ending around 10:30 a.m. After the rain

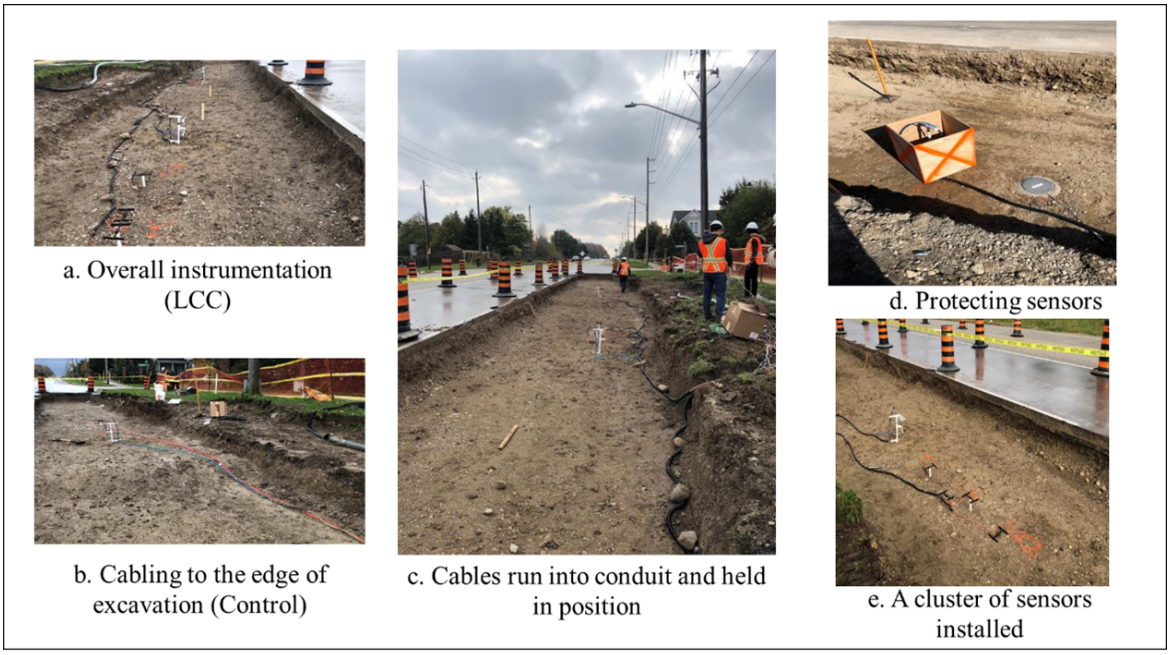

Figure 4.7: Overall instrumentation installation and cabling

had stopped for a bit, the LCC was erected. Various weather conditions were encountered throughout the day's construction operation, ranging from rain to sunshine. Despite sub-zero temperatures the night after the LCC placement, average temperatures remained at 4 °C in the morning and 8 °C in the afternoon.

The LCC was transported and poured into place for both sections using a hose from the mixing apparatus. The approach employed was the wet mix method. A ready-mix company batched cement, slag, and water slurry offsite and brought it to the job site. Onsite the slurry was injected with foam to produce the required density, after which the material was pumped into place. This was possible as the LCC material is free-flowing and self-levelling. This is illustrated in Figure 4.8 a and b.

A quality check was performed to ensure the target LCC density was reached. This was achieved by collecting samples of LCC from the nozzle of the hose in a cup, then measuring the density on a scale (Figure 4.8 e). The target LCC density for this project was 475 kg/m^3. Two batches of LCC were placed using two truckloads of cement slurry from offsite. The measured density for each batch was 493 kg/m^3 and 471kg/m^3, respectively. The mix comprised 80% Portland cement to 20% slag and a cementitious to water ratio of 0.51.

CEMATRIX and the CPATT team also collected LCC samples to perform some material property testing described in chapter 3. Before pouring the LCC material into the molds, the inner faces were lined with wax paper to enable smooth removal of the sample during demolding (Figure 4.8 c). Buckets of LCC were obtained from the pipe's nozzle and transferred into the molds. This was done cautiously to avoid messing with the LCC's air bubble structure. The samples were adequately covered afterward and placed in a big container with a lid. Bubble wraps were used around the samples to prevent movement and damage (Figure 4.8 d). Before being taken to the laboratory, the samples were kept untouched for 24 hours on site. The overall outlook of the poured LCC is shown in Figure 4.8 f.

Figure 4.8: LCC pour and sampling

4.2.6 Granular B placement

Granular B placement for the Control section was completed on October 23. Granular B samples were also collected for testing in the laboratory. Compaction of granular B achieved 100% Standard Proctor Maximum Dry Density.

4.2.7 Insulating LCC layer

Granular A was supposed to be installed on October 25. Still, the main contractor was concerned about the LCC's strength due to cold conditions, especially at night, reaching -5 °C, which might have hampered the LCC's curing. Although the LCC contractor gave the go-ahead for granular A placement after 24 hours, this was rescheduled to the next day. The LCC was covered with an insulating blanket to aid the curing process (Figure 4.9 a and b).

4.2.8 Granular A placement

Granular A was placed on October 26. The average temperature in the morning was 1 °C, increasing to an average of 8 °C by noon. The placement of Granular A started at 7:30 am. Since all the sensors for this layer were previously installed as a single unit (the moisture probe and temperature sensors), there was no need for any installation. However, the sensors exposed had to be protected during the placing. After which, the material around the sensors was manually compacted (Figure 4.9 e) to avoid them being destroyed by the mechanically operated compactor.

Granular A samples were collected (Figure 4.9 d) after spreading before the roller compactor was used to compact the layer (Figure 4.9 f). One hundred percent compaction was achieved by first using a single smooth drum roller over the granular A about twenty times back and forth movements. A double smooth drum roller twice to get a smoothen surface of the granular A layer. It should be noted that no vibration was involved during the compaction.

4.2.9 Milling adjacent pavement

The adjacent pavement was milled after Granular A placement in preparation for the asphalt concrete paving to provide room for new asphalt concrete to be poured and bonded adequately with the untampered asphalt concrete (Figure 4.10 a). However, the adjacent pavement chipped off during the removal of the existing pavement (Figure 4.10 b). This could be a potential source of crack propagation in the future.

Figure 4.9: After LCC pour and base construction

4.2.10 Datalogging Unit and Cabling

The data station was built between October 26 and November 1, and data collecting began on November 12. The sensor cables were sorted and clipped to the required length, making them easier to manage. They were fed into a 300 mm trench dug from the excavation side to the traffic box and installed on a concrete pad through a 4" diameter trench pipe (containing the uninstalled asphalt strain gauges wires). Concrete screws were used to secure the data-logging unit to the concrete base (Figure 4.10 c, d, and e).

The data-logging unit consisted of a battery, one 1000V data logger, and four multiplexers. The temperature sensors, moisture sensors, strain gauges, and pressure cells were each connected to separate multiplexers. The pressure cell used a vibrating wire analyzer with the multiplexer to enable its readings. These logging units were all attached to a plywood board and firmly fixed to the data-logging box (Figure 4.10 f). The data logger was set to take readings every five minutes; however, this frequency was increased to ten minutes.

A weather station consisting of a rain gauge and a solar radiation shield was installed

beside the data-logging unit (Figure 4.10 g). The purpose of this was to record atmospheric weather events at the location. The solar radiation shield had a data logger to record rainfall and temperature events. The initial setting was to read the temperature every ten minutes; however, this was changed to hourly readings.

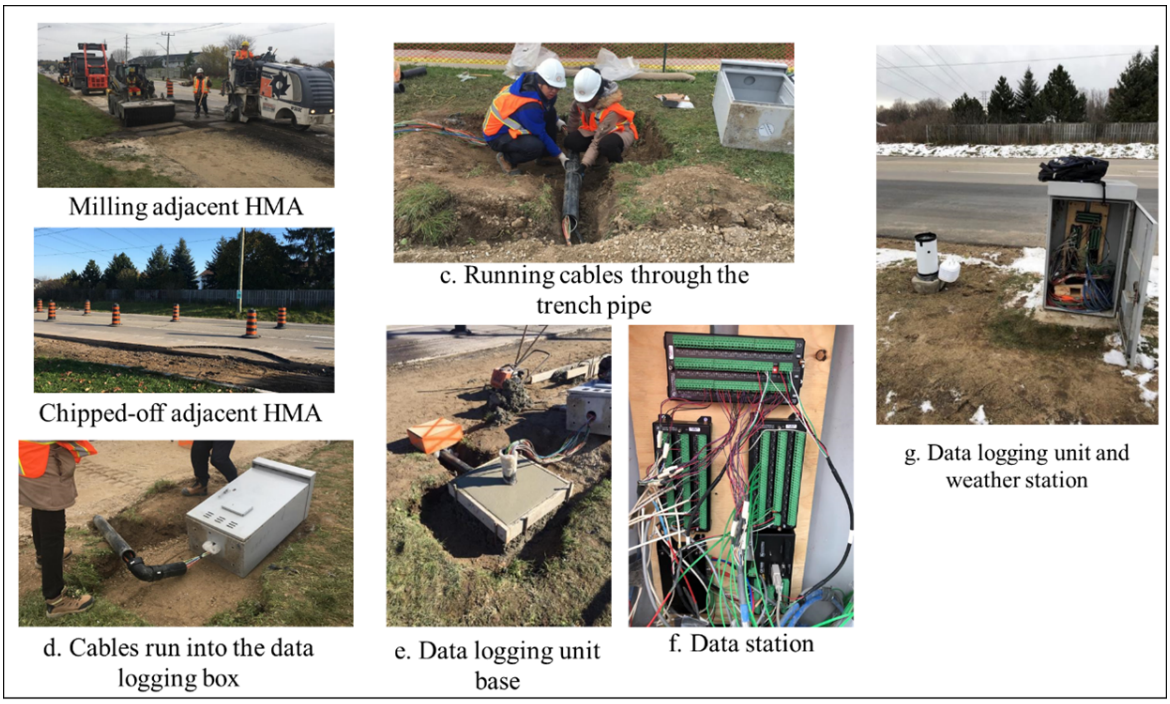

Figure 4.10: Milling adjacent HMA and installation of data logging unit

4.2.11 Asphalt Concrete (AC) Paving

Although the morning of November 5 was wet with rain drizzles, asphalt paving commenced. Three lifts of asphalt concrete were laid. Two of the base lifts HL4 were placed together in one lift, and the surface lift (HL3) was then placed. Figure 4.11 a shows the paving operation. Also, asphalt concrete samples were obtained to be tested at the CPATT laboratory. Only strain gauges and temperature sensors have been installed in the AC layer.

Two strain gauges were installed per section, all in the horizontal direction. The strain gauges were placed beneath the asphalt concrete layer by digging up the first two lifts of

HL4 immediately after it was placed to expose the surface of the base layer. The AC was then used to cover up the strain gauge after installation. The cables of the strain gauges were previously buried in the base layer (granular A), and only the head and a small part of the cable were exposed to the asphalt concrete (Figure 4.11 b). The temperature strings were installed as a single unit with the moisture tree; hence no need for further installation. However, care had to be taken with the sensors not to damage them. One temperature sensor was located in the middle of the AC layer for each section at a depth of about 75 mm from the pavement's surface.

A 93% compaction level was achieved for the AC layer. This was checked using the densometer as shown in Figure 4.11 c. The overview of the completed AC layer is shown in Figure 4.11 d.

Figure 4.11: Asphalt concrete paving

4.2.12 Erbsville Construction Summary

In summary, the road was closed to traffic for the construction of this trial section from October 23 until November 7, 2018. This period excluded the closure for the day the bus

pad concrete was finally poured. This happened a couple of days after the site was opened to traffic. The main contractor consistently had at least five crew members on site. This excluded specific equipment operators like the compactor, paver, scraper, and miller. Table 4.4 summarizes the construction duration of activities.

The installation duration for the control section includes truck arrival, filling, and compaction time, while the period for LCC placement includes mixing on-site and QC density check.

Table 4.4: Construction duration summary

Activity	Control	LCC350	LCC250
Excavation of Base and Subbase (min)		130	
Milling Surface Layer time (min)		80	
Milling Surface Layer time (min/m)		2	
Removing Curb (min)		3	
Installation of Base layer (min)		230	
Installation of Surface layer (min)		220	
Installation of Subbase layer (min)	120	28	22

4.2.13 Erbsville Construction Challenges

Because of the small scale of this construction, economies of scale may not be possible; hence the initial cost may be exaggerated. Several other issues arose during construction, some of which may have substantially impacted construction time and expense. Some elements that may have influenced the overall construction time, cost, and pavement performance are as follows:

- Low temperatures and rainy days encountered during construction, especially below 0 °C temperatures, delayed construction activities. This delayed instrumentation installation could have impeded the curing process for the LCC as it was below 4oC.
- Scheduling the activities for the contractor was a challenge. Some of which was because of unfavorable weather conditions, which caused delays in the contractors' other construction sites that had to be completed. Thus, construction activities had to be rescheduled.

- Other construction activities at the location, such as the bus pad, might have caused a slight delay for some road paving activities, thus increasing construction time.
- The weather also impeded the installation of the data logging unit and weather station to retrieve data. Raining conditions made it almost impossible to start obtaining data as soon as construction was over.
- Low temperatures (average of 4 °C) and a lot of rain was present throughout construction. Due to difficulties placing granular A more than 24 hours after the LCC pour increased the project's length. Additionally, rain forced the postponement of construction works, including the asphalt concrete pavement. It should be mentioned that most of the instrumentation was installed while it was raining. This might damage embedded sensors.

4.3 Notre Dame Trial Road

4.3.1 Project site

The Notre Dame Drive project site is located on the Southbound Lane of Notre Dame Drive, in St Agatha, Wilmot township, between stations 1+210 to 1+410. This falls between the intersections of Notre Dame drive at St. Ann Ave North and St. Ann Ave South. The location is shown in the green box in Figure 4.12. The length of the trial section is 200 meters.

4.3.2 Notre Dame Drive pavement design

The road design was completed by an experienced team including members from the Region of Waterloo, CEMATRIX, and the Centre for Pavement and Transportation Technology (CPATT) at the University of Waterloo.

Initial Design AASHTO 93

The AASHTO 93 method was used in designing the pavement sections incorporating the three LCC densities (400, 475 and 600 kg/m^3). Typical parameters from MTO (2013) [182] and ARA (2015) [10] was also adopted in this design. Structural layer coefficient results

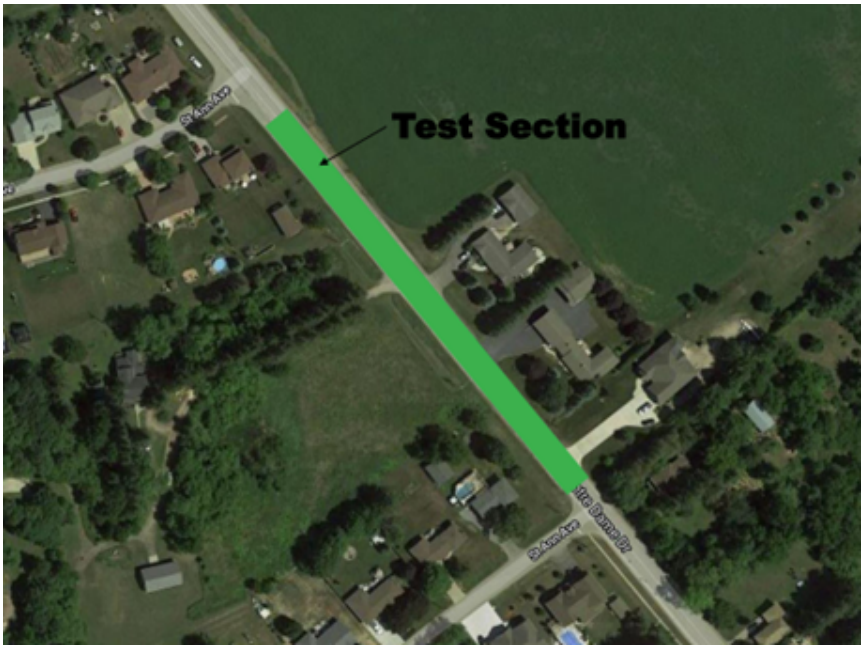

Figure 4.12: Location of trial section (Google, CNES 2021)

based on FWD test analysis performed for the Erbsville (see Chapter 6, section 6.9) were implemented to calculate respective layer coefficients for 400 and 600 kg/m^3 LCC densities.

Table 4.5 outlines the parameters used in the design of the road segment. The operating speed for this road section is 60 km/hr. Based on these parameters, the Equivalent Single Axle Load (ESAL) for the road was estimated with Equation 4.1 and determined to be about 6 million ESALs for 25 years.

$$Total\ ESALs = AADT \times HVP \times HVDF \times TF \times TDY \times \frac{(1+g)^t - 1}{g} \tag{4.1}$$

Total ESALs = $6349 \times 10\% \times 50\% \times 100\% \times 1.6 \times 365 \times 32.03$

Total ESALs = **5,938,067**

Table 4.6 presents the design derived and proposed, compared with the current design for these type of road class in the Region of Waterloo, Ontario, using typical unbound granular material. However, it was noted that the current design of the road was very conservative and would cater to traffic volumes way higher than current traffic levels, as

Table 4.5: Notre Dame Drive AASHTO 93 design parameters

Parameter	Value	Parameter	Value
Traffic (AADT)	6,349	Asphalt layer coefficient (ai)	0.42
Trucks (HVP, %)	10	Granular base layer coefficient (ai)	0.15
Growth rate (g) (%)	2	Granular subbase layer coefficient (ai)	0.11
Truck factor (TF)	1.6	LCC 400 layer coefficient (ai)	0.2
Design life (t, years)	25	LCC 475 layer coefficient (ai)	0.22
Initial serviceability	4.5	LCC 600 layer coefficient (ai)	0.26
Terminal serviceability	2.5	Subgrade Resilient Modulus (MPa)	30
Reliability (%)	90	Drainage coefficient	0.8
Overall standard error	0.49		

presented in the table. The proposed designs represent equivalent performance pavement thickness options compared with the current regional design.

Table 4.6: Recommended layer thickness AASHTO 93 design

Activity	Control	LCC400	LCC475	LCC600
Surface (mm)	150	150	150	150
Base (mm)	150	150	150	150
Subbase (mm)	450	250	250	200/250

The AASHTOWare Pavement ME (MEPDG) was used to evaluate pavement performance. Table 4.7 shows the design parameters' 95% reliability performance evaluation. The findings revealed that all the designs performed similarly, with the LCC sections performing somewhat better. Except for the LCC and granular B subbase layers, default values were used for the MEPDG analysis. For LCC, the results from Ni et al., [175] were used, and for granular B, from ARA [10]. As recommended, LCC was treated as an unbound granular layer with a constant modulus.

Final design

Instead of a granular B subbase, a reviewed design incorporating Granular A was proposed. Table 4.8 presents parameters adopted for the final road design. The parameters were

Table 4.7: MEPDG performance analysis for the designs

Distress type	Target	Control	LCC400	LCC475	LCC600	
					200 mm	250 mm
Terminal IRI (m/km)	3	2.98	2.95	2.94	2.94	2.81
Permanent deformation - total (mm)	10	7.76	6.99	6.83	6.79	6.5
AC bottom-up fatigue cracking (percent)	10	2.34	1.99	1.95	1.93	1.91
AC thermal cracking (m/km)	200	52.53	52.53	52.53	52.53	52.53
Permanent deformation - AC only (mm)	6	2.54	1.84	1.84	1.82	1.86

then applied to design comparative sections with the three LCC densities. The resultant final design is presented in Table 4.9. Although lower LCC thicknesses were derived using the design inputs, it was recommended that the LCC layers should not be less than 200 mm.

Table 4.8: Notre Dame final design parameters

Location	AADT	Trucks	Avg. Truck factor	Directional Distribution	Traffic Growth Rate	Lane distribution	Total Days per Year
		(%)			(%)		
Notre Dame	650	10	1.32	0.5	1	1	365

A detailed section view for the Notre Dame Drive Section is presented in Figure 4.13. The final design consisted of four sections that were each 50 meters long. All sections had similar layer material and thickness for asphalt concrete as the surface layer. The Control section consisted of 300 mm thick granular A material as the base and subbase layers. The other three sections are LCC400, LCC475, and LCC600 for the LCC 400, 475 and 600 kg/m^3 densities, each consisting of 150 mm thick granular A as the base and 200 mm thick lightweight cellular concrete (LCC) as the subbase.

The installation of sensors and the data-logging unit required the help of the main contractor throughout the entire construction process. The installation followed the scheduled placement for each layer. A detailed section view showing the type and location of the sensor is given in Figure 4.14. All sensors were installed along the right wheel path (2.3 meters from the curb's edge) of the southbound lane. The installed instrumentation in-

Table 4.9: Notre Dame Drive final pavement design

Layer	Control	LCC400	LCC475	LCC600
Surface (mm)	190	190	190	190
Base (mm)	300	150	150	150
Subbase (mm)	-	200	200	200

cludes four asphalt strain gauges, four earth pressure cells, twelve moisture sensors, twelve temperature sensors, and six concrete maturity sensors.

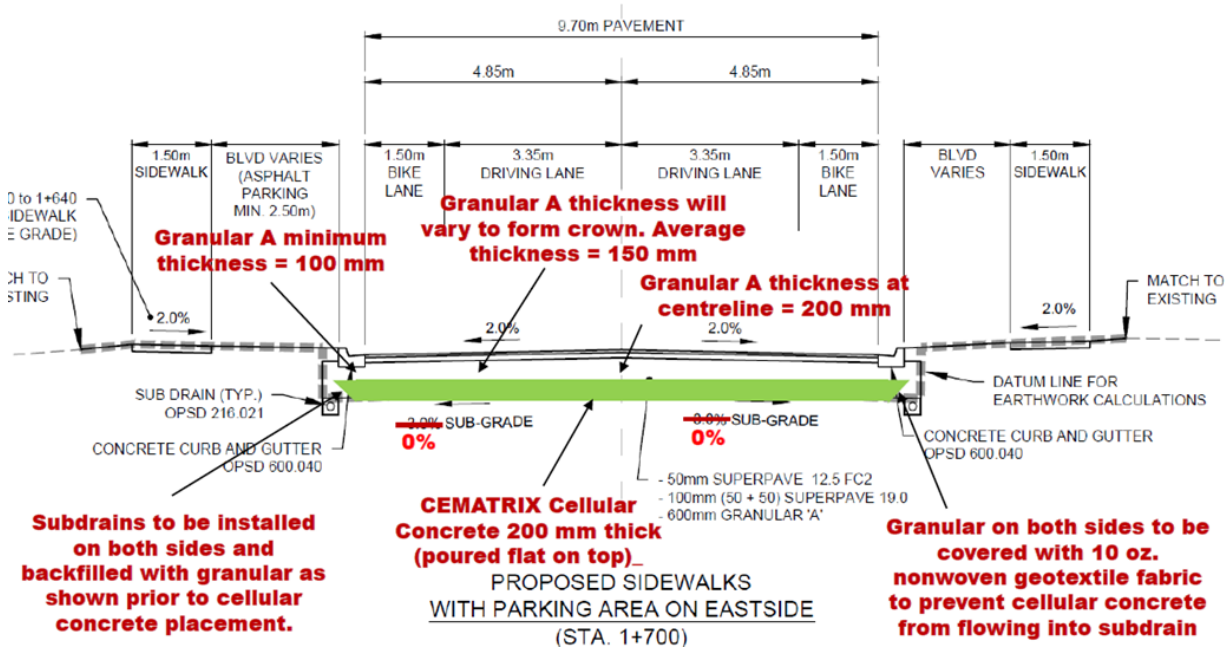

Figure 4.13: Notre Dame Drive typical LCC cross section view

4.3.3 Construction Activities

The construction team included the main contractor (Seegmiller) and representatives from the Region of Waterloo, CEMATRIX (Canada) Inc, and the Centre for Pavement and Transportation Technology (CPATT). The trial road was mainly within the scope of stage one of the entire project contract. Construction commenced on the 31st of May 2021

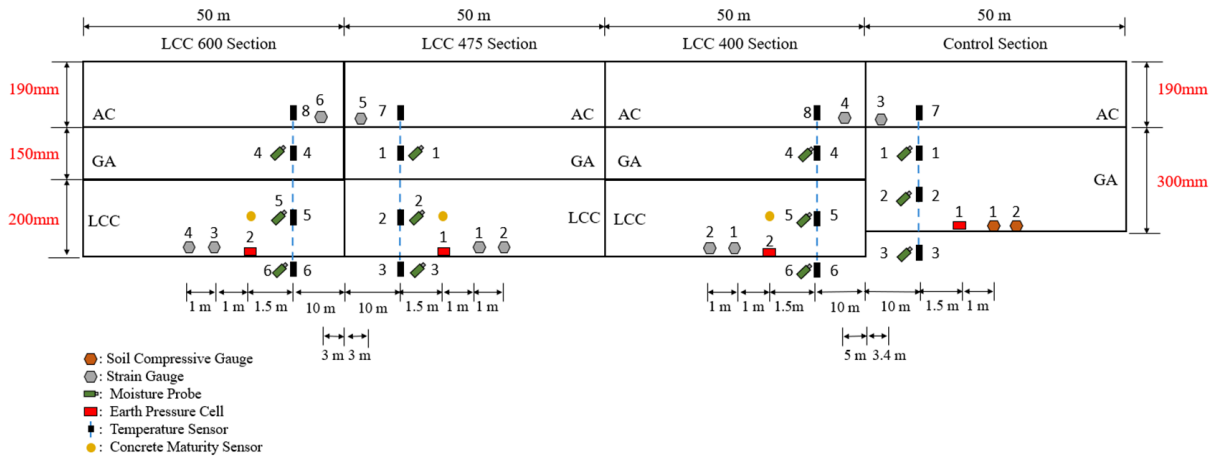

Figure 4.14: Section view of the instrumentation at Notre Dame Drive

and consisted of several activities. Each aspect of the construction of the trial section is discussed subsequently.

4.3.4 Site preparation, excavation, soil sampling, and sensor installation – May 31 to July 14, 2021

Excavation of existing pavement, soil sampling, and preparation of the area to receive the new pavement was performed within this period. Soil samples were collected on July 14, by the CPATT team. Figure 4.15 shows an overview of the subgrade soil that was collected.

Installing baffles and mounting grade stakes for LCC

The placement of baffles for the LCC began on July 13 and was completed on July 15. Grade stakes were installed every five meters throughout the length of the sections, and the proposed LCC surface levels were marked on them. Geotextile fabric and 10 mm diameter reinforcement bars were used to form baffles at five-meter intervals for the LCC400 and LCC475 sections, as presented in Figure 4.15. This was to control LCC flow during the pour due to grades exceeding 1% at these locations.

Overview of subgrade before construction

Installed Baffles for LCC

Figure 4.15: Subgrade overview and installed baffles for LCC

Installing sensors

Most of the sensors that went into the pavement were placed on July 14, a day before the LCC pour, except the asphalt strain gauges. The location for each sensor was marked on the surface of the subgrade.

Pressure cells

One Earth pressure cell was installed in each section. Fine sand obtained offsite was utilized as the base for the circular head of the cell (Figure 4.16 f). The cell was installed at an angle of 45 °C (to the direction of traffic) and held down by metal pegs.

Moisture Probe and Temperature strings

Three moisture and four temperature sensors were attached to a tree made of $\frac{3}{4}$" diameter PVC pipes. These were installed as one unit, as seen in Figure 4.16 e. Before installing on-site, the moisture sensors were soaked overnight in water (Figure 4.16 d) as part of the manufacturer's conditioning process. The location for the top of each layer was also marked on the tree. During installation, a hole was dug in the soil to receive the moisture tree hammered into the subgrade with a mallet to ensure that the moisture sensor was about 150 mm in the subgrade (Figure 4.16 e). Each section installed one temperature sensor and moisture sensor in the subgrade and backfilled with excavated subgrade material. The area around the moisture tree was then hand compacted. The moisture sensor was designed to ensure that the temperature and moisture sensors for each layer above the subgrade were located at the center of the layer. It was also essential to place the moisture

sensors vertically inclined to ensure that they measured correctly. According to specifications, if horizontally placed, error readings could occur. Therefore, before the placement of each layer, the moisture sensor positions were adjusted to fit the specifications. In cases where the layer thickness was just 150 mm (as for the base layer), the sensor was slightly inclined at an angle from the vertical axis.

Concrete Strain Gauge

A total of two concrete strain gauges were placed in each of the LCC sections. Both strain gauges were placed at the bottom of the LCC layer. The gauges were placed on top of the subgrade and slightly raised with wooden props and aggregates to ensure that the gauges were fully coated with the LCC when placed. U-shaped metal pegs were used to fix the strain gauges to the subgrade surface in two locations close to its edges on either side such that they would not move away from their position during LCC pour but still be loose enough to allow for expansion and compression. One gauge was installed longitudinally, while the other was installed in the transverse direction. This concrete strain gauge is presented in Figure 4.16 c. After installation, these gauges were re-calibrated by zeroing them to ensure that they accurately reflected strains induced by the material placed over them.

Soil compression gauges

Two soil compression gauges were installed in the control section to measure the displacement at the bottom of the granular A material installed as the subbase and base layers in this location. U-shaped metal pegs were used to fix the gauges to the top of the subgrade surface. One gauge was installed longitudinally, while the other was installed in the transverse direction Figure 4.16 b.

Concrete Maturity Sensor

Two concrete maturity sensors were placed in the LCC layer for each section. To install the maturity sensor at the middle of the LCC layer, props made with $3/4''$ diameter PVC pipes were utilized. The end of the pipe was shaped in a peg-like manner to allow it to be hammered into the ground. The top of the pipe was smoothened out, and small holes were bored through the top to allow a small metal wire run through and hold down the maturity meter to the pipe and prevent them from falling off during LCC pour (Figure 4.16 a).

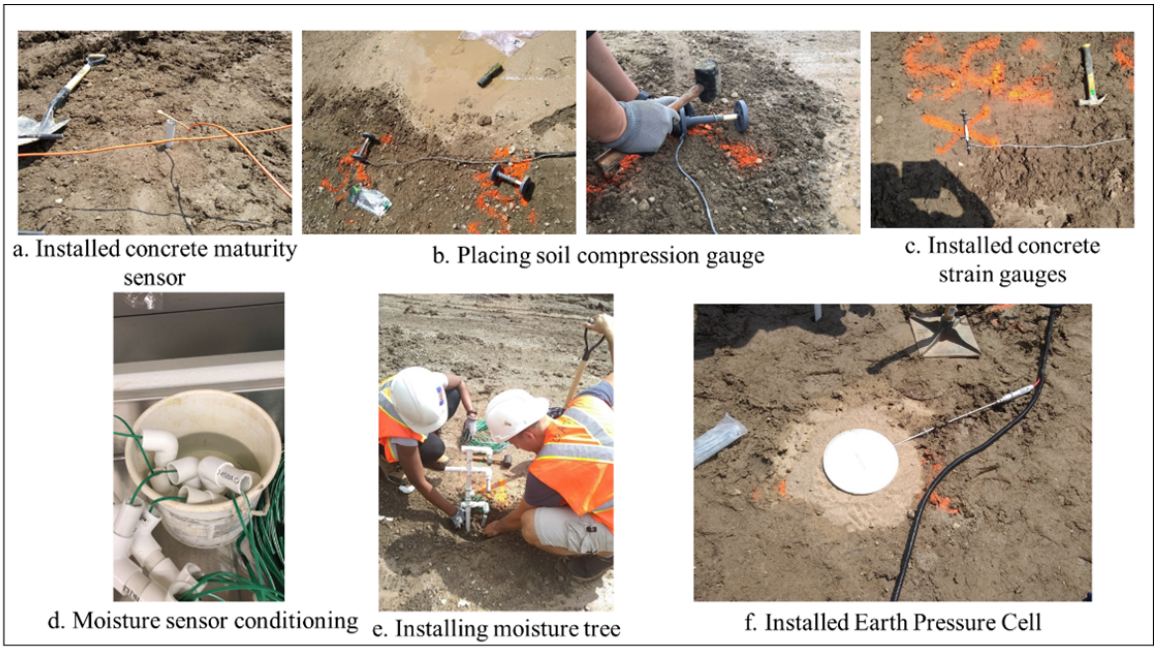

Figure 4.16: Notre Dame Drive instrumentation installation

4.3.5 Placing LCC (July 15, 2021)

LCC pour commenced at 8:00 am with the LCC475, LCC600, and LCC400 sections poured, respectively. Installation of baffles was not completed for the LCC400 section at the time to begin pouring; hence the LCC475 section was poured first. The pour lasted till 5:00 pm the same day, with all sections completed. The temperature for the day during the pour ranged between 20 °C and 27 °C, with no rainfall till after the pour. The wet mix method was employed in placing the LCC layers. (Figure 4.17). Since LCC was free-flowing and self-levelling, no compaction or other activity was required.

A quality control personnel was on-site to monitor LCC density and quality. A quality check was performed to ensure the target LCC density was reached. Samples of LCC were collected from the nozzle of the hose in a cup, then measured on a scale to determine density. The target LCC densities for this project were 400 kg/m^3, 475 kg/m^3 and 600 kg/m^3. All the batches of LCC were placed using 12.4 truckloads (7 m^3 per load) of cement slurry from offsite. The measured density for each batch were between 405 kg/m^3 and 420 kg/m^3 (average of 412.5 kg/m^3) for LCC400, between 475 kg/m^3 and 520 kg/m^3 (average of 492.5 kg/m^3) for LCC475 and between 588 kg/m^3 and 610 kg/m^3 (average of 600.4

kg/m^3) for LCC600. A total of 312 m^3 of LCC was poured. The mix proportion for this project consisted of 100% GU Portland cement, cement/water: 0.51, Foam: unit 78, and In-line mix with Provoton foam (3.3%).

CEMATRIX and the CPATT team collected LCC Samples to perform some material property testing, such as unconfined compressive strength and modulus of elasticity in the laboratory.

Figure 4.17: LCC pour and sampling

4.3.6 Morning after LCC pour

The road was visited the following day (July 16). Pictures in Figure 4.18 show the condition of some parts of the road. Due to heavy rainfall that commenced about three hours after LCC placement, some cracking and water accumulation were observed on the LCC400 section.

Figure 4.18: Water accumulation and cracking close to LCC400 sensor location

4.3.7 Granular A placement - July 19, 2021

Site preparation for placing granular A commenced at 7:00 am on July 19. Placement of Granular A began at 7:30 am. To protect the installed sensors in the control section after installation and LCC pour, the sensors in the control were buried with granular A material on July 15, while protection boxes and paint for visibility were used around the sensors in the LCC sections. Granular A was placed and spread over all the sections. Protection boxes were utilized around the sensors during granular A spread. The material around the sensors was manually evened out and compacted afterward. This was to avoid damage to the sensors by the mechanically operated vehicles.

The CPATT team collected granular A samples during spreading before compaction (Figure 4.19). This layer achieved a 93 to 99% compaction level across the road segment. The smooth drum roller was first used in compacting the layer by moving back and forth in the same path until the entire layer was compacted. Later a rubber tire roller was used following the same procedure to get a smooth surface of the Granular A layer. No vibration was involved during the compaction process for the LCC sections.

Figure 4.19: Sensor protection, granular A sampling, and placement

4.3.8 Settlement on Granular A

Settlement (Figure 4.20) was observed on some parts of the LCC400 section two days after placing the granular A. This may have resulted from the heavy rainfall after the placement of LCC, causing water saturation around the area. A proof rolling test was performed in the presence of Englobe on July 27 with a front-end loader. Minimal deflections corresponding to low areas or former potholes were observed around the curb line of the road. The recommendation was to proceed with grading the granular A road base since this had not been completed. The road base was considered suitable in its current condition, with hopes that warm weather and winds would help dry any damp locations.

4.3.9 Sensor Protection, Cabling, and Data station

Wooden boxes and cones were used to protect the sensors during construction. This was also to help improve the visibility of sensor locations for equipment operators and further avoid damage when no one was on site. All cabling for the sensors was run through flexible conduit pipes to the side of the excavation. A trench was excavated from the side of the road to the data station location. A 100 mm diameter PVC pipe was installed in the trench to receive the cabling from the sides of the excavation to the data station, where they would be connected to the data logging units (Figure 4.21).

Figure 4.20: Settlement on granular A at LCC400 section

Two data logging units were provided by the side of the trial road to collect data from the installed sensors. These units were prepared in the laboratory, and each was composed of one traffic cabinet, two multiplexers, one data logger, one vibrating wire analyzer, and a battery. The multiplexers, data logger, and vibrating wire analyzers were mounted on a perforated laminate board and held with bolts to the back of the traffic cabinet. The units were moved to the trial road location on July 14. One unit was for the control and LCC400 section, while the other was for the LCC475 and LCC600. The logging station was positioned at the intersection point for each section.

All the sensors were connected to the data logging unit and tested to see if the sensors were working. Strain gauges and pressure cells were all calibrated to reflect actual field conditions. Sensors were again zeroed before granular A placement to reflect the strain and stress induced by the material. During construction activities, the data logger was set to read and record sensor data every minute; afterward, its frequency was increased to every five minutes. A 800 $\times$ 800 $\times$ 200 mm plain concrete base was cast for the data logging unit on July 28. The station was mounted on July 30. On this same day, the curb casting for the trial road was completed. A weather station similar to Erbsville's was installed at this location and recorded data hourly.

Figure 4.21: Notre Dame Drive cabling and data logging station

4.3.10 Asphalt Concrete (AC) Base Paving –September 2, 2021

The road was paved with two base lifts of SP 19.0 (15% RAP) asphalt concrete on September 2 and 3. The first lift was placed on the first day and the second lift the next day. The final asphalt lift (SP 12.5FC) was placed nine months after the base lift on May 24, 2022.

Instrumentation installation

Strain gauges and temperature sensors were installed beneath the asphalt layer. The temperature sensor had been previously installed with the moisture tree, and the asphalt strain gauge cabling was run to the data station alongside the others. The strain gauges were sealed in bubble wraps and placed in a well-marked box to provide protection and visibility at the side of the road (Figure 4.22). The gauges also placed construction cones to cordon the area and enhance visibility for coming vehicles.

One asphalt strain gauge was installed in the longitudinal direction per section. The strain gauges were laid beneath the asphalt layer by first, holding them in position with

pegs and embedding the cables within the granular A material (Figure 4.22). Some asphalt concrete was placed beneath, around, and over the sensor to fully embed it before the asphalt base lift was placed. Since the temperature sensors were already exposed above the granular A material, such that it would be located at the center of the asphalt layer, asphalt concrete was also applied to embed it before the final placement of the asphalt.

Asphalt concrete paving

The overall asphalt base paving operation lasted about one and a half days for the entire road segment. Figure 4.22 shows the paving process. During paving, to avoid damage to the temperature sensor and strain gauges, the head of the paver was slightly raised when going over sensor locations. Asphalt concrete samples were obtained during paving to be tested at the CPATT laboratory. A 92% and 91% compaction level was specified for the surface, and base AC lifts, respectively. This was achieved using a smooth drum roller first, then a rubber tire roller.

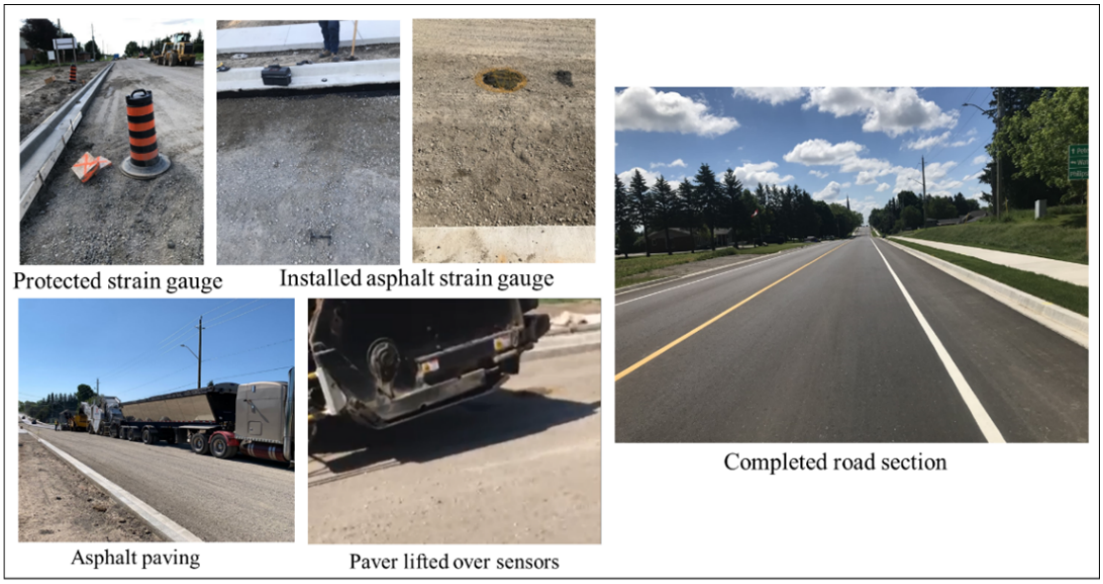

Figure 4.22: Notre Dame Drive asphalt concrete paving

4.3.11 Cracking on the asphalt layer

Some cracking was observed on the base asphalt layer in the southbound lane of the LCC400 section in October of 2021 (Figure 4.23). No action was required at the time, and the cracking was monitored till June of 2022. No further deterioration was noted, and the final lift of asphalt concrete was placed.

Rutting (3mm) Cracking and depression (LCC400 section)

Figure 4.23: Cracking in LCC400 section asphalt layer

4.3.12 Construction Challenges

Few challenges were encountered during construction at Notre Dame Drive.

- Heavy rainfall on the morning of sensor installation affected the already graded sub-grade. Instrumentation was laid on muddy surfaces though care was taken as much as possible to level and smoothen the surfaces before placing the sensors.
- Heavy rainfall immediately after the LCC pour led to cracking of the LCC in the LCC400 section and accumulation of water beneath the LCC400. This could have also damaged the pressure cell in this location which stopped reading after a couple of weeks.
- There was a long-time from the LCC pour to the paving of the asphalt layer. During this time, heavy vehicle traffic was on the road section. Although the LCC layer can

Table 4.10: Construction schedule

Activity	Date
Instrumentation Placement	July 14, 2021
Lightweight Cellular Concrete pour	July 15, 2021
Granular A placement	July 19, 2021
Curb and gutter/Sidewalk construction	July 29 - 30, 2021
Asphalt paving and Asphalt Strain gauge installation	September 2 - 3, 2021
Traffic opening	September 4, 2021

handle vehicular traffic 24 hours after placement, it is recommended to avoid this as much as possible.

- Although the CPATT team started collecting data a day before the LCC pour, the initial data collected over three days was lost due to technical challenges.
- Unfavorable weather conditions caused delays to several construction activities, which could have impacted the time for asphalt paving.
- The availability of subcontractors for various construction activities also added to the construction duration.

4.4 Constructability Analysis- Effect of construction activities on LCC pavements

Constructability analysis has been performed on the Notre Dame Drive trial sections to compare the behavior of LCC pavements under construction loads and activities to that of standard granular subbase materials. This will aid future LCC applications, particularly in guiding construction decisions. Findings from this analysis will serve as a foundation for ensuring that the best possible performance is achieved when LCC is used as a subbase layer in the pavement structure. This section describes the subsurface instrumentation and gives pressure, strain, moisture, and temperature data for these pavement sections during construction. This knowledge will additionally aid in explaining future performance and contribute to developing guidelines for LCC use.

The subsequent sections discuss the installed instrumentation results concerning construction activities occurring within this period. Table 4.10 provides a summary of the

construction schedule. Most sensors were installed in position on July 14, a day before the LCC pour, except the asphalt strain gauges on the pavement the day of the asphalt paving, although the wiring was completed the same day as the other sensors.

4.4.1 Pressure

The dynamic pressure experienced at the surface of the subgrade during the construction period is presented in Figure 4.24. The analyses signify the change in pressure per time and do not reflect the change in pressure due to the subbase material itself. The dynamic pressure from the placement of the granular A material (for LCC475 and LCC600) and some days after granular A placement (For Control and LCC400) up until the asphalt paving operation are presented.

Dynamic pressure as high as 7 kPa was noted at the LCC475 and LCC600 sections during the Granular A placement. Significant pressure change was observed during the curb /gutter and sidewalk construction. During this period, the Control experienced the highest recorded dynamic pressure throughout the construction period of 97 kPa, whereas the LCC600 saw a 31 kPa pressure increase which was the highest increase in this section throughout the construction period. LCC475 dynamic pressure this time was 18 kPa. The high-pressure amplitude at this time was likely due to heavy trucks carrying precast concrete blocks for the gutters. Also, the presence of concrete mixers during the casting of the curbs. The LCC400 pressure cell stopped working during the curb operation, but the most pressure change noted in this section prior to this was 38 kPa at the start of the curb construction operation. A lower pressure reading at the LCC475 compared with LCC600 during curb construction could result from some heavy vehicles not going over the sensor location during this activity. On September 2 and 3, significant pressure changes were also observed due to the asphalt paving operation constituting the asphalt paver and trucks delivering the asphalt concrete. The LCC475 section saw its highest pressure change of 31 kPa than any other construction activity. The greatest pressure changes in the control and LCC600 were 28 kPa and 20 kPa during the asphalt paving operation.

In summary, the Control section experienced 78% more pressure than the LCC600 and LCC475 and 61% more than LCC400 for the period the cell at this location was functional during construction. The LCC400 section, most of the time, seemed to experience similar pressure levels as the Control section going by the initial data available for the LCC400. Unfortunately, after roughly a month of use, the sensor became damaged. The asphalt paving operation appeared to cause 10% and 36% more dynamic pressure at the LCC475 section than the control and LCC600, respectively. The subgrade surface pressure decreased with increased LCC density at the different construction stages. When comparing

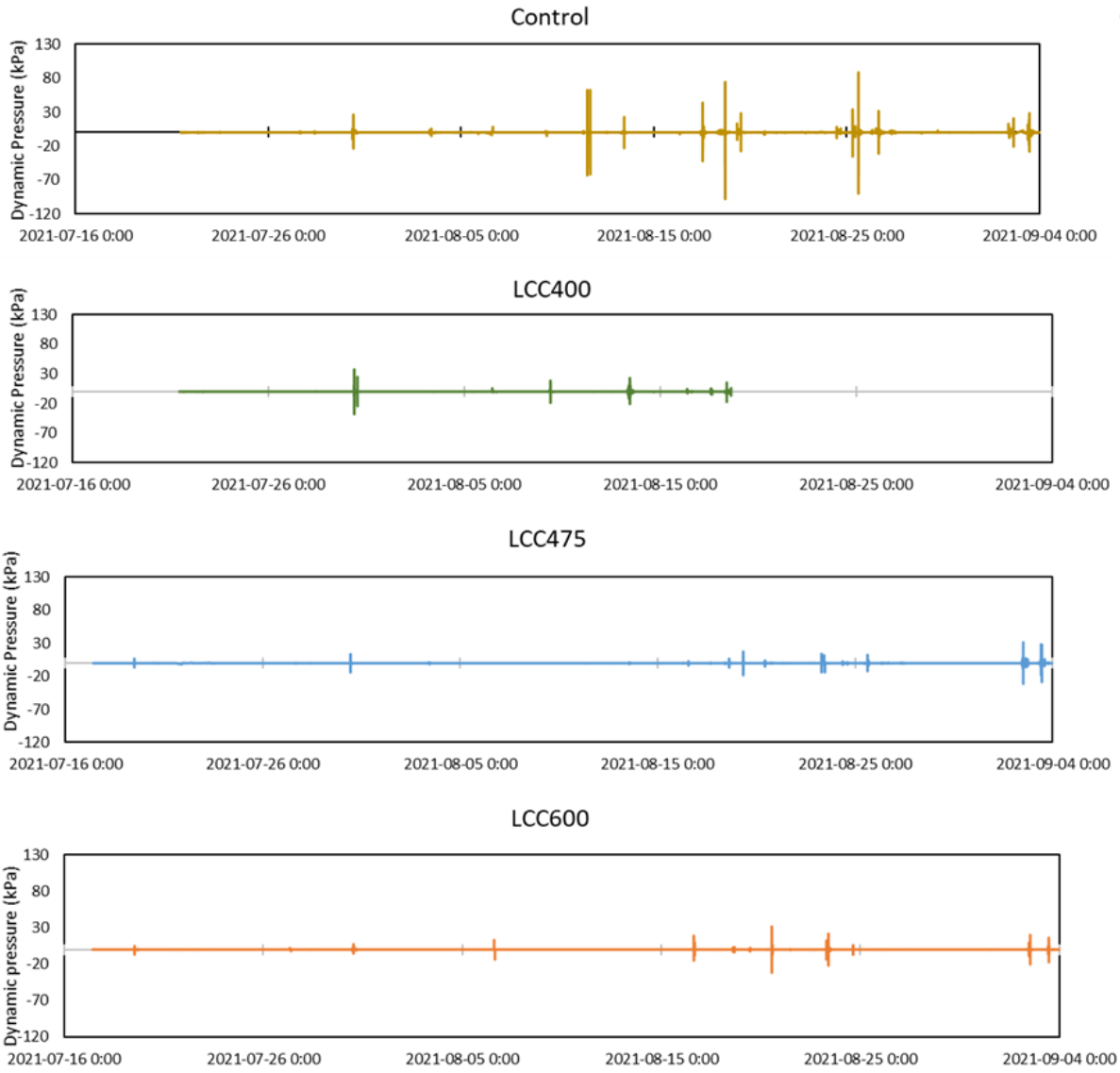

Figure 4.24: Subgrade pressure during construction

the effects of vehicles, a significantly higher effect was observed during the construction of the sidewalk, and curbs than the actual placement of the pavement layers for all the sections

Overall, construction equipment apparently causes a large amount of stress on the

pavement subgrade and structure. There is also a significant time interval between the LCC pour and the placing of the AC layer. During this period, the LCC pavement saw a substantial amount of truck traffic, as seen by the pressure readings at the top of the subgrade, which were pretty high. It might be beneficial to have additional roadside works carried out before pouring the LCC layer to avoid significant damage to the pavement even before opening to traffic.

4.4.2 Moisture

Pavement moisture for all sections is illustrated in Figures 4.25 to 4.27. The layer is said to be fully saturated when the Soil Water Potential (SWP) is zero. The further away from zero the SWP, the drier the pavement layer. The direction of SWP is unimportant; only the absolute value is considered.

The moisture profile of all the sections' base layer appears to follow the precipitation trend in the area. Rainfall times correspond with when most layers reflect SWP 0 or close to zero (Figures 4.28). The control sections' base appears to be constantly more saturated with water than the LCC sections. Although some draining is observed after rainfall events, the highest SWP value attained in the Control section during the study period was 18 kPa. The LCC section base layer drained water faster and more after rainfall events. This was indicated by the peaks and troughs observed in the LCC sections. This drain was particularly higher and noticeable in the LCC400 sections that show SWP as high as 148 kPa within the study period. The LCC475 and LCC 600 have shown SWP of 64 kPa and 25 kPa, respectively.

A similar trend was noted in the subbase like the base layer, where the Control section subbase layer depicted more saturated conditions than the LCC sections. Fluctuations with rainfall events were also observed. The LCC400 values appeared to be mostly drier throughout the study period, with values close to 194 kPa observed. The LCC475/LCC600 station experienced technical problems during data collection, leading to some void readings. This is the reason for the blank spaces in the graph. However, when it read, the data indicated that the LCC475 sections sometimes contained less or no moisture than the LCC400 section. The LCC600 section, in some instances, appeared less saturated than the LCC 400 sections. Generally, the LCC475 and LCC400 subbase most times indicated lower moisture content than the LCC600 subbase.

The Control sections' subgrade seemed to retain less water over time during the study period. However, the control subgrade still appeared to have an average of 57% more moisture than the LCC400 subgrade. Similarly, on average, the LCC475 and LCC 600

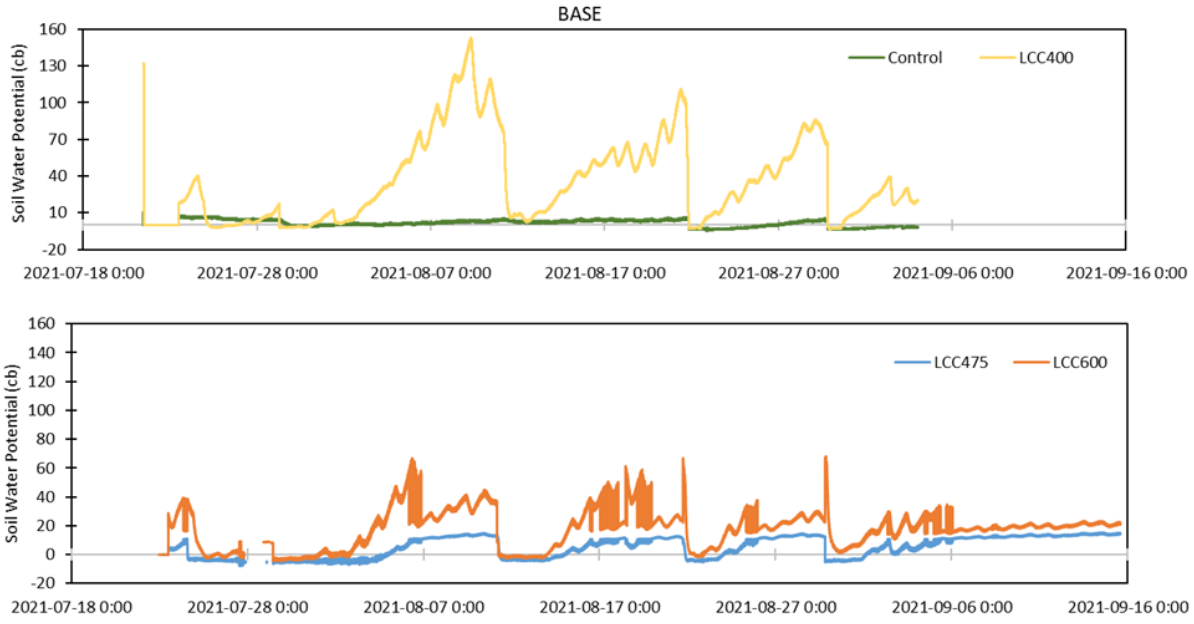

Figure 4.25: Base moisture during construction

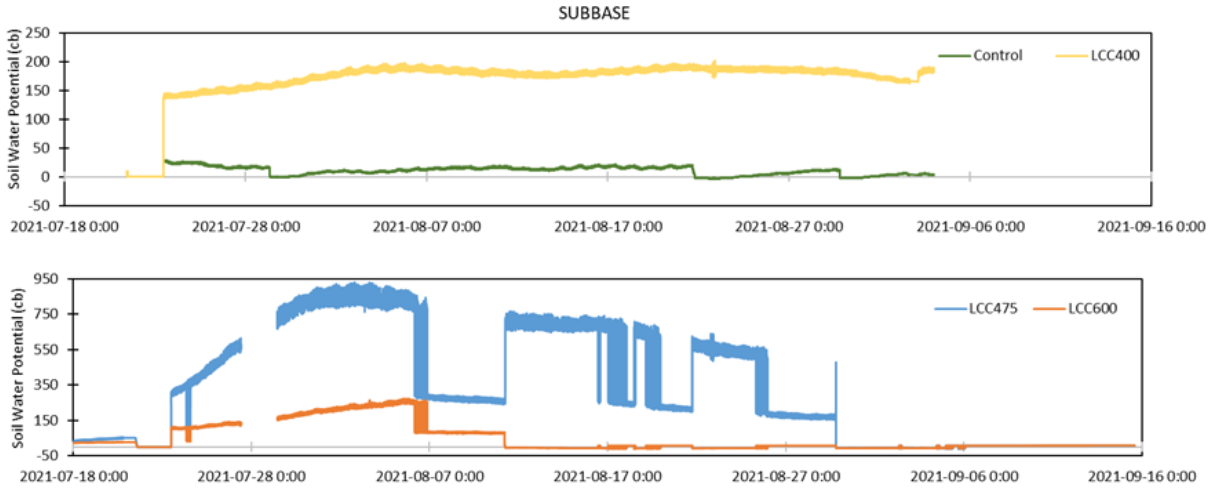

Figure 4.26: Subbase moisture during construction

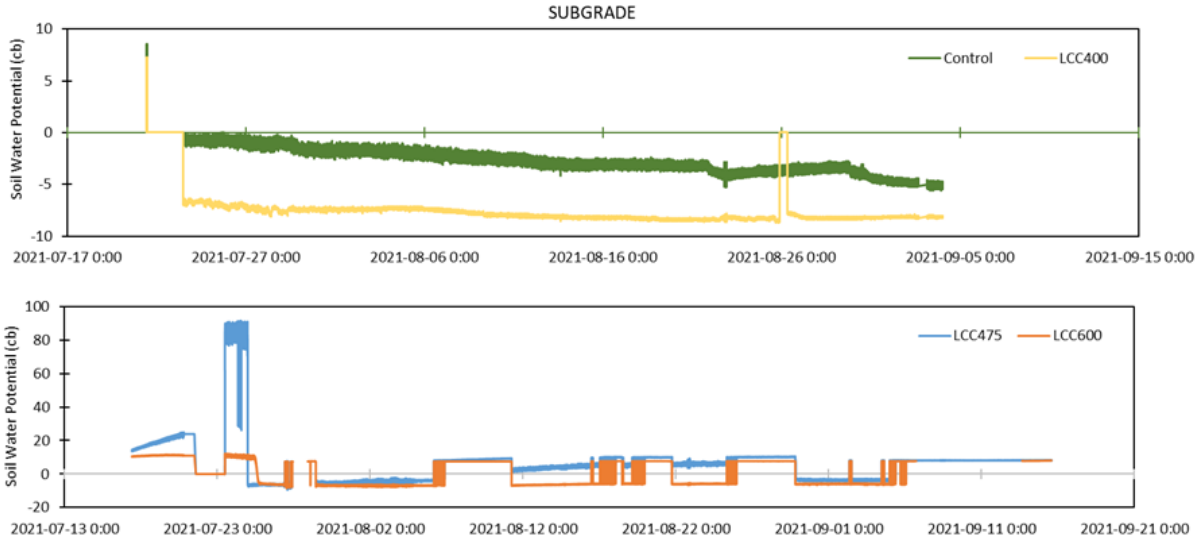

Figure 4.27: Subgrade moisture during construction

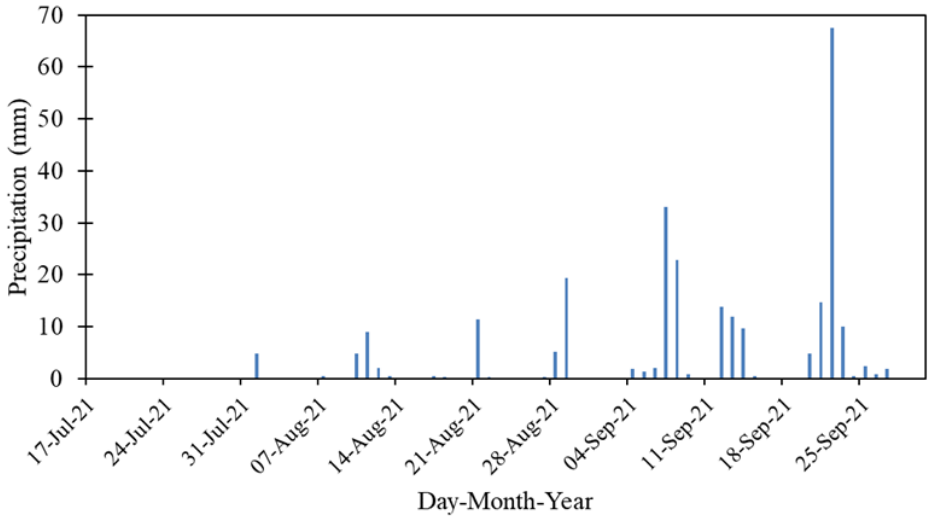

Figure 4.28: Precipitation during construction

subgrades had lower moisture content than the control section, although more fluctuation was noted in these layers than in the others.

Primarily, in the initial construction phases, more water draining from the pavement was noted, but a decrease was recorded over time, and more water was retained within the layers. This could indicate that further compaction of the pavement layers due to numerous truck traffic over extended periods of time without the asphalt concrete being placed, the drainage ability of the pavement layers could decrease, hence the potential for more water retention within the layers. This could yield challenges over time within the pavement structure. In addition, moisture content retention was seen to reduce with a decrease in LCC density. It might be essential to optimize the LCC density to give a balance between strength, moisture retention, and other properties.

4.4.3 Temperature

Figures 4.29, 4.30, and 4.31 present the temperature profile data for all sections and pavement layers during construction. The temperature trend was seen to correspond with ambient temperature in the location. The main temperature variation observed between the LCC sections and Control asides from the initial placement of the LCC material, and the effect of the heat of hydration (not noted in the figures) was 24 hours after the placement of asphalt concrete. The impact was greater on the base and subbase layers in each section. The LCC layers appear to experience a 12% greater temperature increase in the base layers than the control. However, at the subbase, LCC400 experienced a comparable temperature increase to the Control, but the LCC475 and LCC600 sections experienced 35% and 27% lower temperatures. While only a minimal temperature increase of about 3 °C was noted in the subgrade of LCC 475 and LCC600, 24% more temperature was observed in the Control and 39% more in the LCC400. After AC paving operation, the LCC400 layers were subjected to greater temperature fluctuations and a more significant temperature increase in its subgrade. Because of the different trend at this time compared to the other LCC sections, this could indicate a potential problem at this location when compared with results from other parameters such as moisture and pressure; a closer look needs to be taken to see if there is damage within the sections' layer.

Generally, the temperature profile for all layers in all the sections appears to follow a similar trend, especially for the base and subbase layers, and have a quite similar magnitude during the construction period except after asphalt paving. The control sections' subgrade experiences slightly higher temperatures than the LCC sections except for LCC400. Comparing LCC475 and LCC600, it appears that at ambient temperatures between 13 °C and 33 °C, the lower the LCC density, the lower the layer temperature. In addition, with an increase in pavement depth, a decrease in temperature is noted.

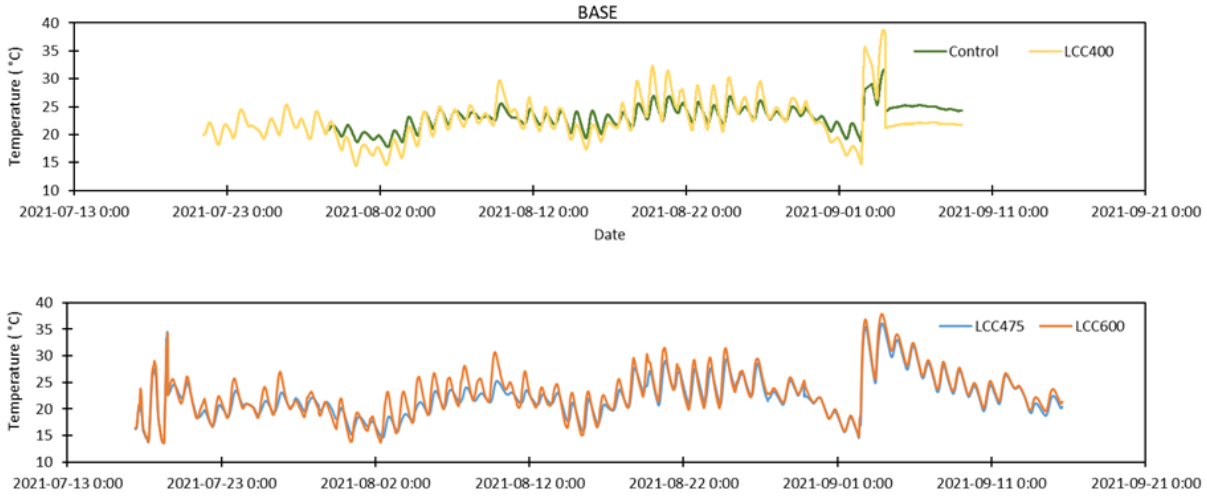

Figure 4.29: Base temperature during construction

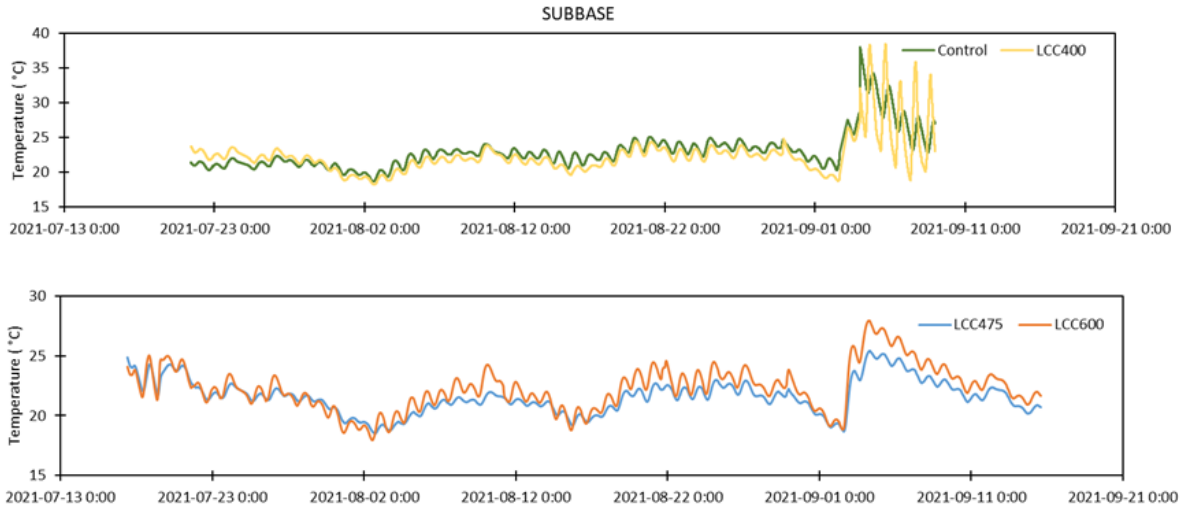

Figure 4.30: Subbase temperature during construction

4.4.4 Strain Gauges

Dynamic longitudinal strain experienced beneath the asphalt layer is presented in Figure 4.32, while Figures 4.33 and 4.34 show the dynamic transverse and longitudinal strains

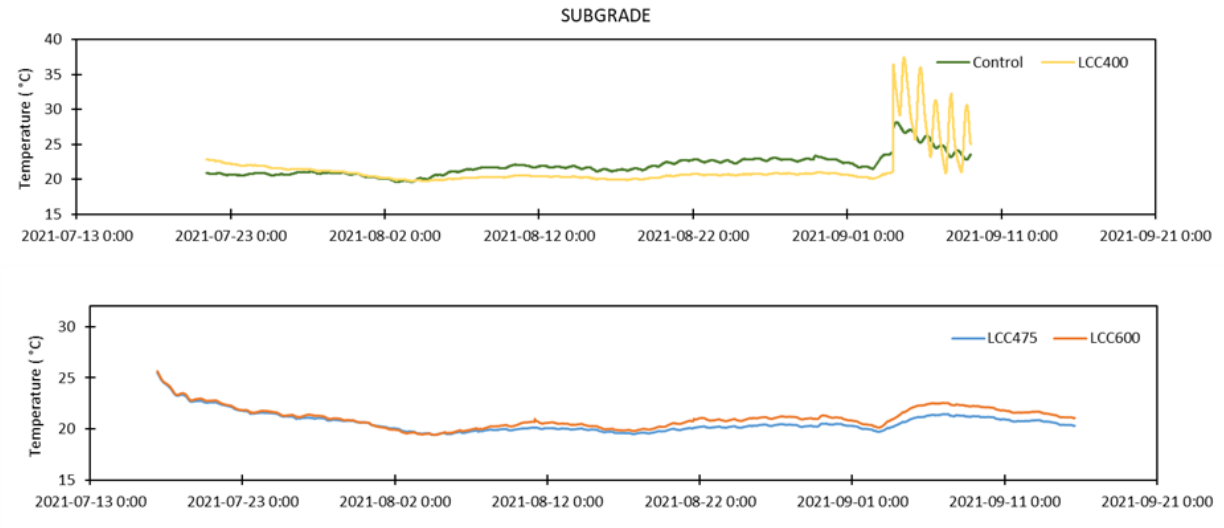

Figure 4.31: Subgrade temperature during construction

beneath the subbase layers accordingly. During the asphalt paving operation, the LCC600 section was noted to experience nine times more strain than the control and three times more than the LCC400 and LCC475 sections beneath the asphalt layer. The LCC 475 and LCC600 saw three times more strain change than the Control. The strain on the LCC400 was 15% more than LCC475. The magnitude of the strains at this location could be because of the concentration of truck traffic within the LCC475 and LCC600 sections at this time. The paver also had a waiting period at this location during the paving operation.

During the granular A placement, a dynamic transverse strain of 287 $\mu\varepsilon$ was seen at the bottom of the subbase for the LCC475 portion, while LCC600 experienced 42 $\mu\varepsilon$. No strain value was available for Control and LCC400 during granular A placement. During the curb and gutter installation, the LCC475 and LCC600 sections appeared to experience higher dynamic strains than the Control and LCC400. The strain values were noted to increase with LCC density during this time. The maximum strain in the LCC600 section was 25% more than LCC475, 70% more than LCC400, and 83% more than the control. Likewise, during asphalt paving, the dynamic strain magnitude was minimal (Between 1 and 4 $\mu\varepsilon$) for control and LCC400; however, significant in LCC600 with a peak value of 181 $\mu\varepsilon$ and LCC475 234 $\mu\varepsilon$. The asphalt paver stayed at the location for a while and wasn't moving; it was moving at the other location. A reduction in transverse strain magnitude of 78%, 46%, and 84% was seen with increased pavement depth from beneath the surface layer to the subbase layer at the control, LCC475, and LCC600 sections, respectively.

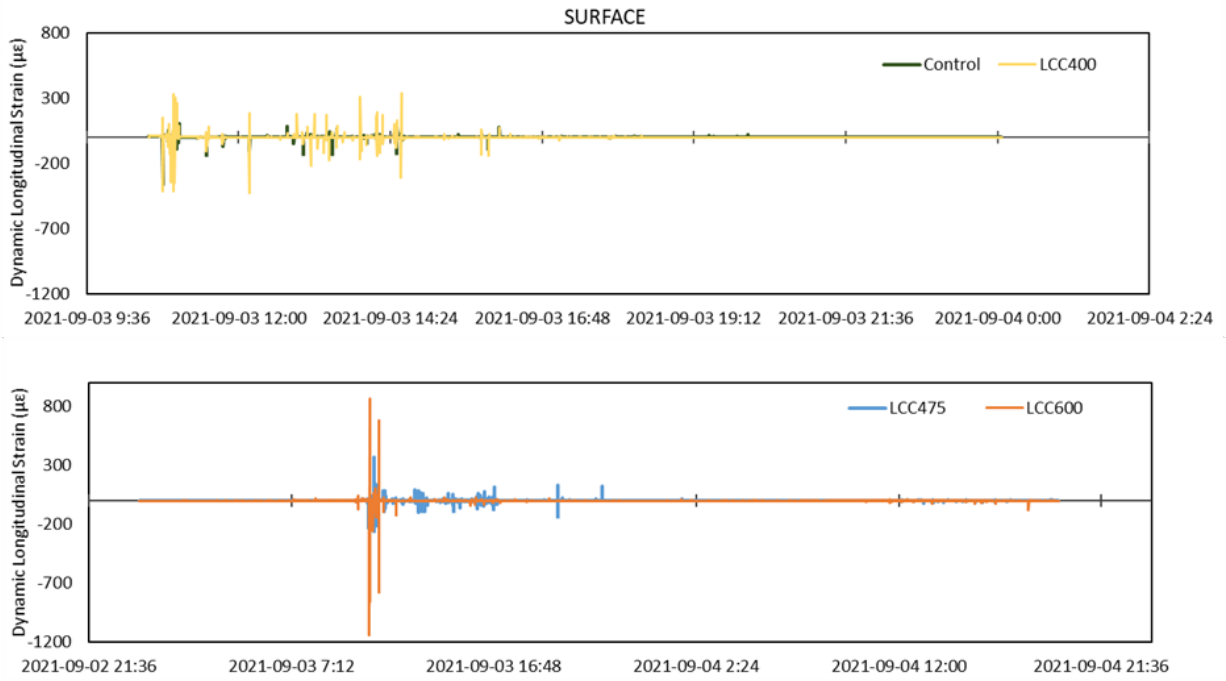

Figure 4.32: Dynamic strain beneath surface layer

Conversely, longitudinal dynamic strains at the bottom of the LCC475 and LCC600 were three and two times less in LCC475 and LCC600 than the transverse strains, respectively. The magnitude for all the LCC sections appeared to be within a similar range of 0 - 50 $\mu\varepsilon$ most of the time. However, at some point, the LCC475 section appeared to have 74% more strain change than LCC400 and LCC600 sections. Unfortunately, the longitudinal strain in the Control section was not responding to changes during this period. Also, strain gauges in LCC475 and LCC600 were faulty between July 27 and 29.

Mostly, construction activities seem to impact greater strains on the LCC pavements than the unbound granular pavement. This is especially true beneath the asphalt layer during paving operations and placement of granular A material. The magnitude of the strain change beneath the asphalt layer during paving increased with increased density. The impact of the asphalt paving operation is not really noticed beneath the subbase layers in the control and LCC400 sections. Strain magnitude reduced with pavement depth, and the LCC600 density seemed to reduce strains at the bottom of the subbase layer the most. There was also a lot of rain during the construction period. This might have also contributed to the high strain readings during this time.

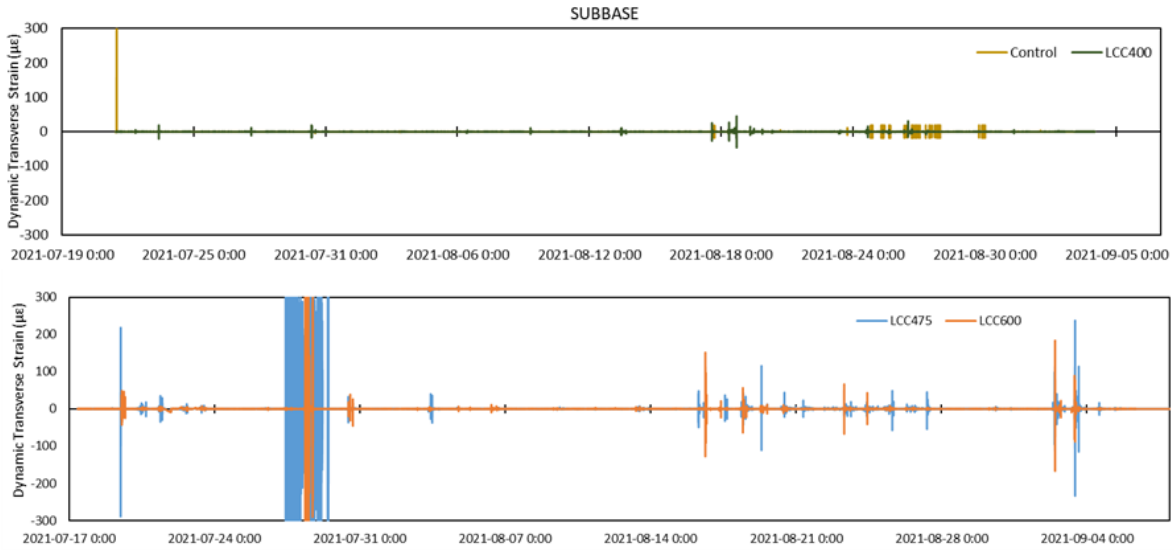

Figure 4.33: Dynamic transverse strain beneath subbase layer

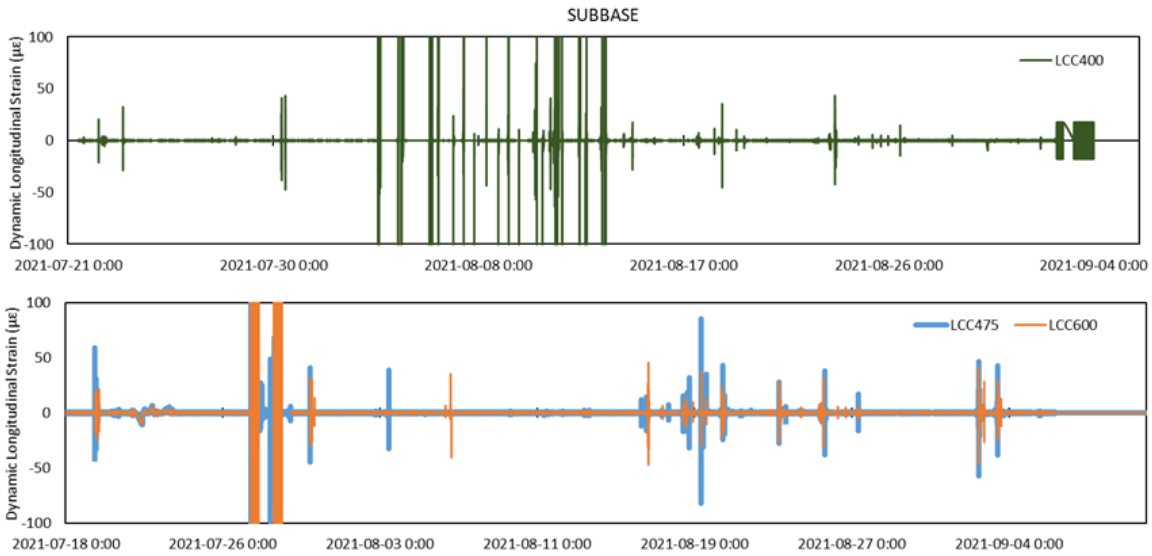

Figure 4.34: Dynamic longitudinal strain beneath subbase layer

4.5 Construction Findings

The practicality of adding three different densities of Lightweight Cellular Concrete in the subbase of flexible pavements was investigated in this section. The construction process, activities, and challenges were discussed. In-situ pressure, strain, moisture temperature, and concrete performance during construction were compared to that of a typical pavement system with a subbase layer of unbound granular material. The results revealed that 400 kg/m^3, 475 kg/m^3, and 600 kg/m^3 density LCC incorporated as a subbase layer could reduce subgrade pressures by up to 78% compared with granular material during construction. Also, all three LCC densities were noted to have a setting time between 5 to 9 hours. The temperature within the LCC pavements became cooler over time with increased density during construction. When pouring LCC in lower temperatures ($\leq$ 4 °C), and construction might need to commence immediately, it might be necessary to insulate LCC layers (e.g., with insulation blankets), to enhance curing.

LCC subbase has also been seen not to hinder the drainage ability of the pavement structure. It causes the base layer to drain water more than the granular alternative during construction. Before asphalt paving, high dynamic strain responses could be present at the surface and subbase of LCC pavements compared with unbound granular material. The dynamic strain was reduced during construction with increased pavement depth for all the sections. This strain reduction was most when a 600 kg/m^3 density LCC layer was applied as pavement subbase. Considering only the subbase layer placement, unbound granular material placement could take over four times longer than an LCC pour of the same thickness. This implies more labor and equipment time usage, therefore higher costs.

Construction method, construction scale, and contractors' experience with similar works have been identified as factors that could affect the performance of LCC pavements. Erbsville section contractors appeared to have been involved with more research-based trial section construction. Also, Erbsville was on a smaller scale, so variables could be controlled more stringently than the Notre Dame section, which involved many more activities; therefore, different crews were involved with the construction. This indicated that communication was essential. When this was absent, it occasionally happened that the personnel involved were unaware of the research being conducted in this area. Furthermore, precipitation coupled with vehicular traffic during construction could weaken the LCC pavements causing them to experience higher strain.

Before asphalt paving, excessive traffic over LCC pavement sections could negatively impact how well the LCC layer performs by increasing stresses, causing early cracking, and weakening the LCC layer. Limiting the amount of truck and vehicle traffic in LCC areas

could be helpful. Alternatively, the roadway construction could be changed to accommodate the projected vehicular loads before placing the asphalt. When changing the design, the site-specific subgrade conditions must be considered to allow for construction and other vehicular traffic. This could require thickening the LCC and/or granular base course. Additionally, shortening the period between LCC pours and asphalt paving operations may significantly lessen the issues now caused by vehicular traffic.

Chapter 5

Laboratory Testing and Performance Prediction

5.1 Introduction

This chapter details the results of several tests on materials received during the construction of the Erbsville and Notre Dame Drive test sections for each pavement layer. It further utilizes the results from these tests in predicting pavement performance using the MEPDG and WELSEA. Moisture–density and CBR tests were performed on the subgrade, subbase, and base materials. The LCC was tested for unconfined compressive strength, installed concrete maturity, water absorption, modulus of elasticity, and Poisson's ratio. The asphalt layer's Bulk relative density and void content were calculated, and specimens were prepared and tested to determine the asphalt concrete's Dynamic (Complex) modulus.

5.2 Asphalt Concrete

Figures 5.1 and 5.2 present the Dynamic (Complex) Modulus results for the Erbsville surface, base, and Notre Dame base asphalt layers. Material samples for the surface asphalt layer could not be retrieved and tested. This layer was placed about nine months following initial construction, which ended with the placement of the base asphalt course. At Erbsville, the HL3 and HL4 class asphalt concrete with PG 64-28 was used as surface and base asphalt, respectively. While at Notre Dame Drive, the same PG 64-28 was used

but with a different class of SP12.5FC and SP19.0 for surface and base asphalt, respectively. These mixes followed the typical Ontario Marshall and SuperPave mix properties [185, 234]. The testing procedure has been outlined in Chapter 3.

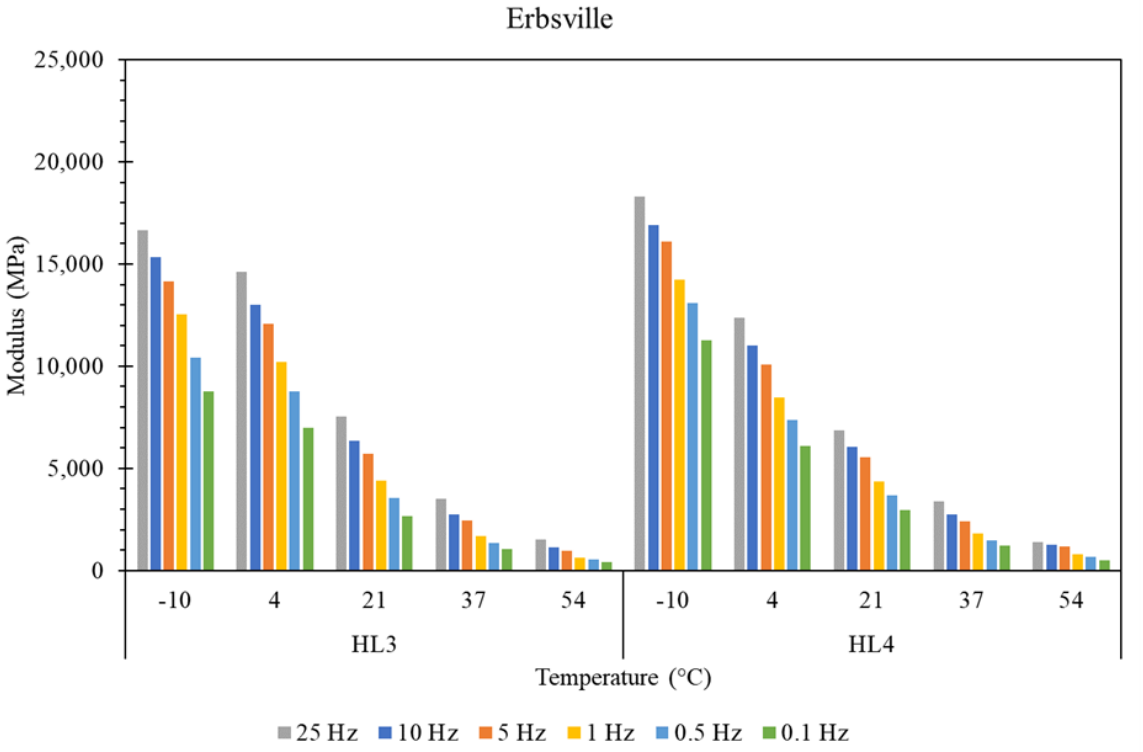

Figure 5.1: Erbsville asphalt concrete modulus

The dynamic modulus for Erbsville surface HL3 for frequencies of 0.1, 0.5, 1, 5, 10, and 25 H_z at -10 °C ranged between 8,760 and 16,655 MPa. At 4°C between 6,967 and 14,618 MPa, at 21 °C between 2,669 and 7,548 MPa, at 37 °C ranged between 1,058 and 3,497 MPa, and at 54 °C between 403 and 1,516 MPa. The lower range value represents the dynamic modulus at the lower frequency of 0.1 Hz, and the higher range represents the dynamic modulus at 25 H_z.

For the Erbsville base layer, the Dynamic modulus for similar frequencies between 0.1 to 25 H_z as stated above were, at -10 °C the Dynamic modulus ranged between 11,285 to 18,330 MPa. At 4 °C between 6,111 and 12,369 MPa, at 21 °C between 2,957 and 6,866 MPa, at 37 °C ranged between 1,210 and 3,390 MPa and at 54 °C between 510 and 1,367 MPa.

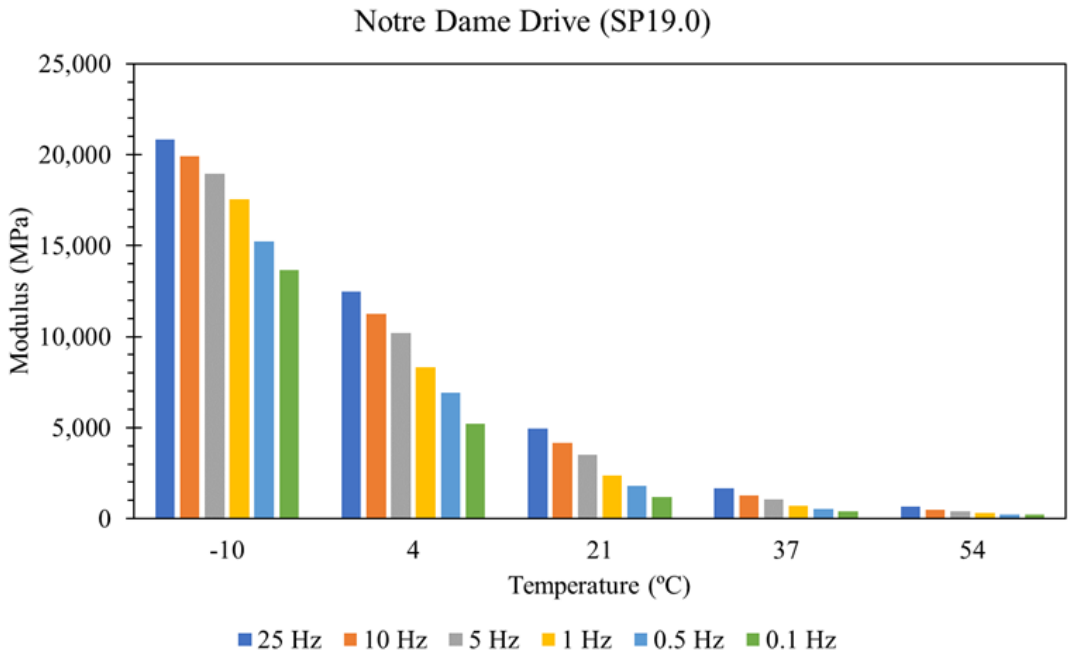

Figure 5.2: Notre Dame Drive asphalt concrete modulus

For Notre Dame Drive, for frequencies between 0.1 to 25 H_z, at -10 °C, the Dynamic Modulus ranged between 13,669 to 20,846 MPa. At 4 °C between 5,214 and 12,460 MPa, at 21 °C between 1200 and 4,956 MPa, at 37 °C ranged between 417 and 1,682 MPa, and at 54 °C between 216 and 653 MPa.

Results indicated that, as expected, the SP19.0 asphalt concrete at Notre Dame was stiffer at lower temperatures across all frequencies than both HL3 and HL4 installed at Erbsville. However, at higher temperatures especially above 21 °C, HL3 and HL4 were stiffer, with HL3 having the most stiffness at 4 °C and 21 °C.

The raw test data was modified for each temperature and frequency combination to produce modulus and phase angle values. The Sigmoidal model used in MEPDG fits the experimental data to create dynamic modulus master curves using Equation 5.1 [148].

$$Log \mid G^*(f,T) \mid = \delta \times \frac{\alpha}{(1+\lambda \times e^{(\beta+\gamma(log f_r))})^{\frac{1}{\lambda}}} \tag{5.1}$$

where |G*(*f*,*T*)| is complex modulus as a function of frequency and temperature, (log

f_r) is the log reduced frequency, δ is the lower asymptotes, α is the difference between the values of the upper and lower asymptotes, β and γ are the shape coefficients.

Figure 5.3 presents the master curves for Erbsville (surface and base) and Notre Dame (base) asphalt concrete. The sigmoidal parameters at 21 °C are shown in Table 5.1. The sigmoidal model was noted to predict the modulus at all temperatures well. However, it had a better fitting for the dynamic modulus (MNE E*) than the phase angle (MNE PA), as evidenced by the minimized respective values in Table 5.1.

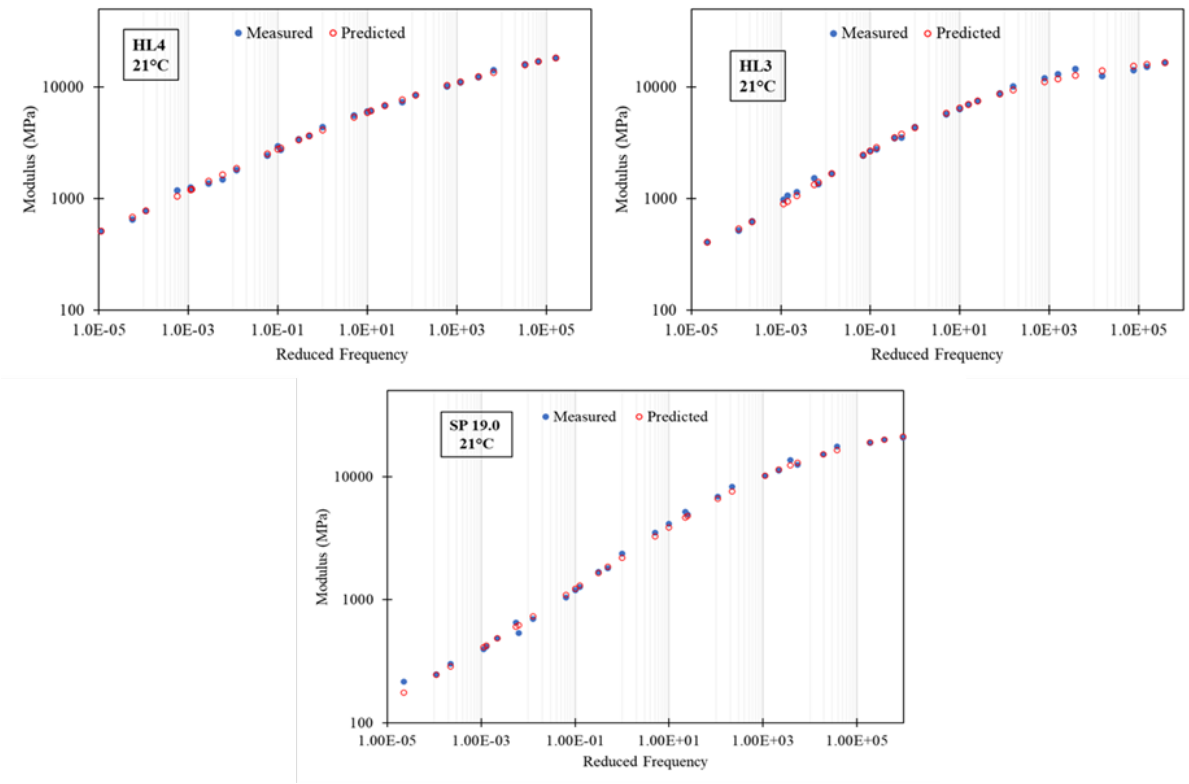

Figure 5.3: Erbsville and Notre Dame surface asphalt master curves at 21 °C

Table 5.1: Sigmoidal Model Parameters

Parameter	Erbsville		Notre Dame
	HL3	HL4	SP 19.0
MNE E*	4.5	2.9	4.9
MNE PA	27.7	16.0	10.9
Minimize	32.2	18.9	15.8

5.3 Unbound Granular Material

5.3.1 Gradation

The gradation properties of the materials are presented in Table 5.2. The values represent the sieve passing percentage. Erbsville and Notre Dame granular A met the specified criteria illustrated by the Ministry of Transportation Ontario, [185], and TAC [234]. The granular B has been determined to be a type B-1. The subgrade gradation correlates with CBR to determine its classification. Figure 5.4 provides some pictures of the sieved material for Notre Dame Drive.

5.3.2 Optimum Moisture Content

The optimum water content (OPC) was determined for the granular A, granular B, and subgrade layers following ASTM D 698 [56], procedure C, and ASTM D1883 [18]. The curve depicting the relationship between maximum dry density (MDD) and OPC for all the unbound materials at both locations is presented in Figure 5.5. Table 5.3 presents the MDD, OPC, and swell values when the materials were soaked in water for four days.

The Erbsville subgrade OPC was 9.9%, with a dry maximum unit weight of 2.30 g/cm^3. The Liquid limit of the soil was 18.3; the Plasticity limit was 15.38, and Plasticity Index was 3. No swelling occurred in the granular A and B layers with OPC of 6.2% and 7.7%, respectively. A 1% swell was observed after soaking the Notre Dame specimen in water for four days. The OPC was 9.4%. The granular A OPC was determined to be 10.6%, with an optimum dry unit weight of about 2.08 g/cm^3.

Table 5.2: Sieve analysis result-percentage (%) passing

Sieve Size	**Erbsville (%)**			**Notre Dame (%)**	
	Granular A	**Granular B**	**Subgrade**	**Granular A**	**Subgrade**
150 mm	-	-	6.31	-	-
106 mm	-	-	-	-	-
37.5 mm	-	-	-	100	-
26.5 mm	100	100	-	99.4	100
19 mm	94.9	90.1	10.08	90.1	96.2
13.2 mm	83.3	-	-	74.3	89.8
9.5 mm	74.6	90.8	-	60.6	82.8
4.75 mm	61.5	73.7	83.61	42.1	67.4
2.36 mm	-	-	-	30.5	53.0
1.18 mm	31.8	55.2	-	22.2	41.1
300 μm	5.8	13.2	-	13.0	-
150 μm	-	-	-	8.0	-
75 μm	1.2	0.7	-	4.0	-

Table 5.3: Optimum moisture content, Max Dry Density (MDD) and swell

Material	**Erbsville**			**Notre Dame**		
	OPC (%)	**MDD (g/cm^3)**	**Swell (%)**	**OPC (%)**	**MDD (g/cm^3)**	**Swell (%)**
Subgrade	9.0	2.30	11.9	9.4	2.19	1
Granular A	6.2	2.29	-	10.6	2.08	-
Granular B	7.7	2.09	-	-	-	-

Figure 5.4: Sieved granular (a & b), subgrade (c-f) material (Notre Dame Drive)

5.3.3 California Bearing Ratio (CBR)

The California Bearing Ratio test indicates the soil's strength as an indirect measure. The test method has been described in section 3.3.1 of this study. CBR values are often used for highways, airports, parking lot, and other pavement designs. The test is relatively simple and inexpensive, which makes it a suitable option. Also, engineering soil parameters such as resilient modulus have been empirically connected with CBR. However, because this value is not a core property of materials, it cannot be applied directly in mechanistic or mechanistic-empirical design techniques [79] .

The test specimens were prepared using the optimum moisture content determined for the respective materials. Because the specimen used for the CBR test were soaked for four days before testing, the moisture content during the CBR test was also determined by taking samples from the top 24.5 mm of the tested specimen [18]. The average moisture content during CBR testing for the Erbsville subgrade was 14%, for granular A was 6%, and 8.2% for granular B. While for Notre Dame Drive, these values were 8.9% for granular A and 10% for the subgrade. The CBR testing was performed on two specimens per material because the values determined at 2.5 mm penetration were less than those obtained at 5.08

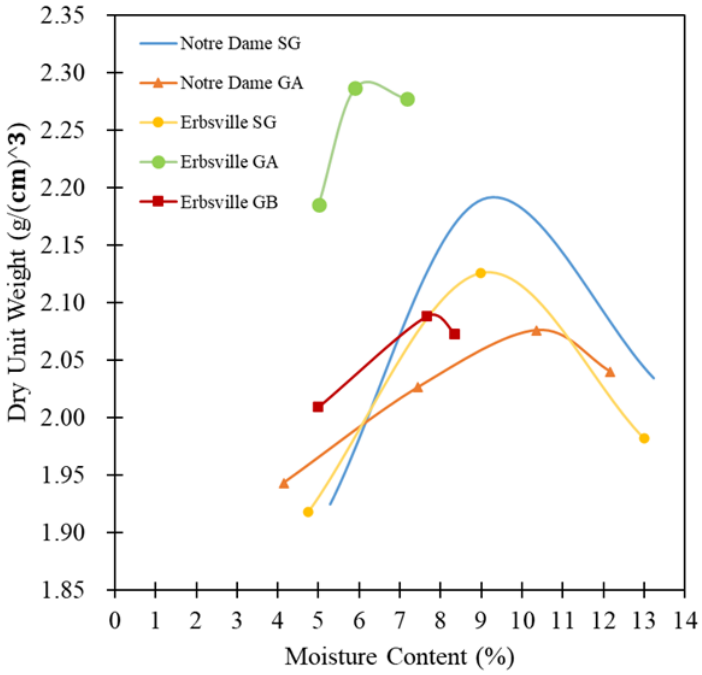

Figure 5.5: Moisture - Maximum Density relationship for unbound layers

mm penetration. The CBR results for the Erbsville and Notre Dame Drive materials are presented in Table 5.4.

Erbsville achieved a CBR value of 9 during testing for two different subgrade specimens. The UCSC soil class was determined to be CL based on measured properties and corresponding with the US. Army Corps of Engineers, 1953, typical CBR values [79]. At Notre Dame, the CBR value was 4, much lower than Erbsville's. The Notre Dame subgrade could be classified as CH - OH based on this and other properties. Erbsville Granular A material was CBR of 54. The Notre Dame granular A had over twice the CBR value than Erbsville. This means it is a stiffer and better-quality material. A CBR value of 27 was derived for granular B.

The AASHTOWare Pavement ME method (MEPDG) correlates CBR with the resilient modulus (MR) by Equation 5.2.

$$M_R = 2555 \times CBR^{0.64} \tag{5.2}$$

Table 5.4: California Bearing Ratio results

Material	Penetration (mm)	Erbsville			Notre Dame		
		CBR 1	CBR 2	CBR Aver.	CBR 1	CBR 2	CBR Aver.
Subgrade	2.5	7.9	9.2	9	3.2	3	3
	5.08	8.4	9.5	**9**	4	4.1	**4**
Granular A	2.5	27	24	26	57	66	62
	5.08	56	52	**54**	121	129	**125**
Granular B	2.5	21.6	23.58	23	-	-	-
	5.08	28.8	24.33	**27**	-	-	-

This equation calculates the resilient modulus of a material with a known CBR value by creating an indirect relationship between the material attribute and CBR, then linking CBR to the resilient modulus [178].

5.4 Lightweight Cellular Concrete

This section presents and discusses the results of Lightweight Cellular concrete material testing.

5.4.1 Compressive Strength

Erbsville

Figure 5.6 shows the Erbville values for unconfined compressive strength. One standard deviation from the mean is shown by the error bars. Over time, the compressive strength increased while specimen compressive strength variability also increased. 1.67 MPa was recorded as the maximum 28-day compressive strength. This is greater than the average values for the 475 kg/m^3 LCC given in BCA (1994) [32], which ranged between 1 and 1.5 MPa. This may be the result of the LCC mix using 20% blast furnace slag in partial cement replacement.

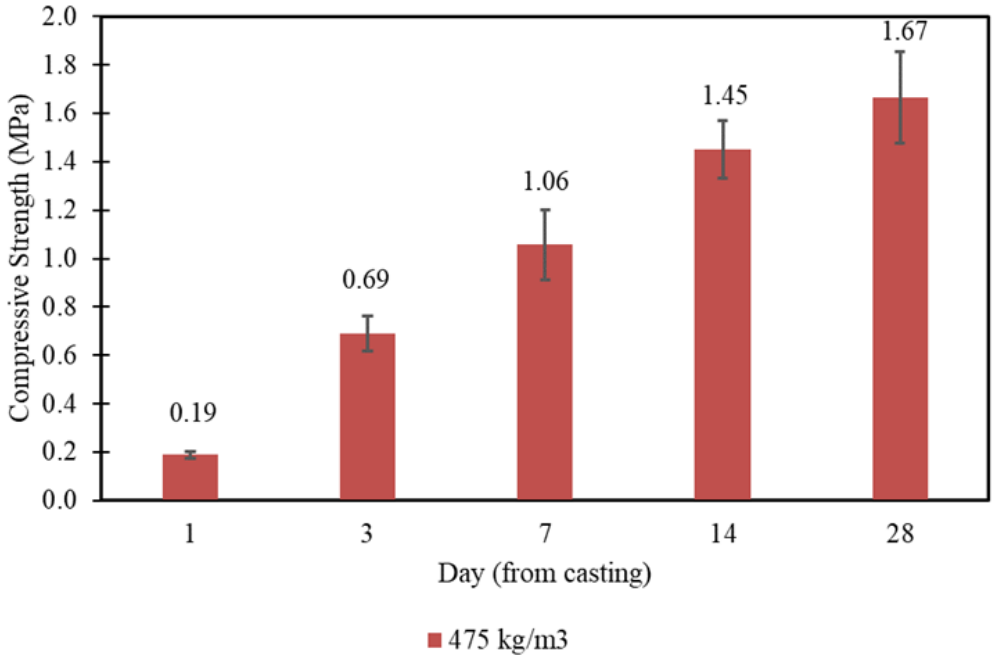

Figure 5.6: Unconfined compressive strength results for Erbsville

Notre Dame Drive

The unconfined compressive strength (UCS) results from over 56 days are presented in Figure 5.7. The error bars indicate one standard deviation from the mean. Table 5.5 also shows the average values for compressive strength over time. The 28-day average values of 0.81, 1.18 and 1.74 MPa for 400 kg/m^3, 475 kg/m^3 and 600 kg/m^3 are consistent with values obtained in previous research where compressive strength of LCC was noted to range between 0.5 and 1.0 for 400 kg/m^3, 1.0 to 1.5 for 475 kg/m^3 and 1.5 to 2.3 for 600 kg/m^3 [32, 174]. Compressive strength was seen to increase over time with an increase in density. However, greater variability in compressive strength was seen as density increased except for day 56, where more variance was observed for the LCC475 specimens. By the third day, the LCC475 and LCC600 sections specimens had surpassed the typical specified minimum 28-day compressive strength of 475 kg/m^3 LCC of 0.5 MPa, according to Maher and Hagan (2016) [153], is sufficient to support the pavement structure as a subbase material. The LCC400 sections surpassed this criterion by day seven.

Comparing day one compressive strength of 475kg/m^3 LCC for both test roads, Notre

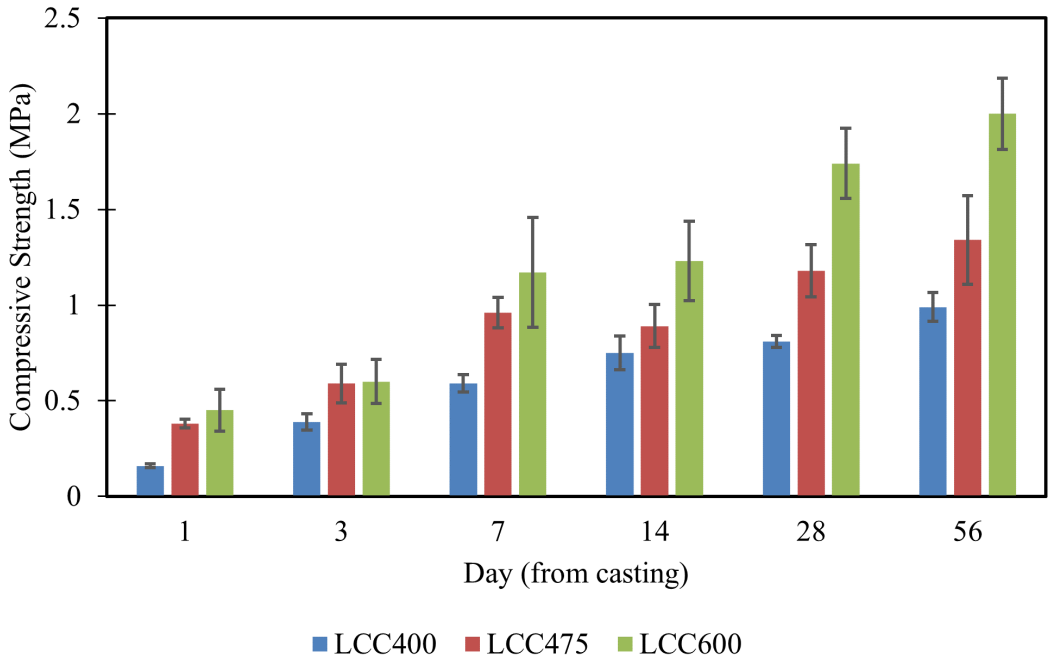

Figure 5.7: Unconfined compressive strength results for Notre Dame

Table 5.5: LCC average compressive strength (MPa) overtime (Notre Dame)

Location	**1**	**3**	**7**	**14**	**28**	**56**
LCC400	0.16	0.39	0.59	0.75	0.81	0.99
LCC475	0.38	0.59	0.96	0.89	1.18	1.34
LCC600	0.45	0.60	1.17	1.23	1.74	2.00

Dame had twice the compressive strength of Erbsville. Likely due to the high early strength concrete utilized at Notre Dame. However, by day three, the compressive strength of the Erbsville mix had surpassed Notre Dame Drives' by 7%. By day 28, Erbsvilles' mix compressive strength was 42% greater than Notre Dame's. Although variations in thickness may result in variances in strength, it is thought that the Erbsville LCC mix's slag component is responsible for a more considerable proportion of these variations. In conclusion, the compressive strength findings for Erbsville and Notre Dame Drive demonstrate that the corresponding LCC layers can sustain the pavement structure as a subbase layer.

5.4.2 Concrete Maturity

Figure 5.8 b presents the resulting interface in the COMMAND software used for analyzing the maturity data and the results for the LCC350 section maturity curve at the Erbsville test section. While Figures 5.8 a, c, and d present the maturity curve for the LCC600, LCC400, and LCC475 for Notre Dame Drive. The maturity curve was determined based on the strength and Temperature-Time Factor (TTF). Compressive strength over 28 days corresponded with the LCC core temperature to determine the concrete maturity for each density. The estimated ultimate strength for the Erbsville LCC350 and LCC250 sections was 2.14 and 2.02 MPa, respectively. The LCC400, LCC475, and LCC600 were determined to have an ultimate strength of 0.93 MPa, 1.25 MPa, and 2.08 MPa, respectively. Compared with laboratory-measured compressive strength results, these maximum strengths are nearly reached or surpassed by day 56 for the Notre Dame section.

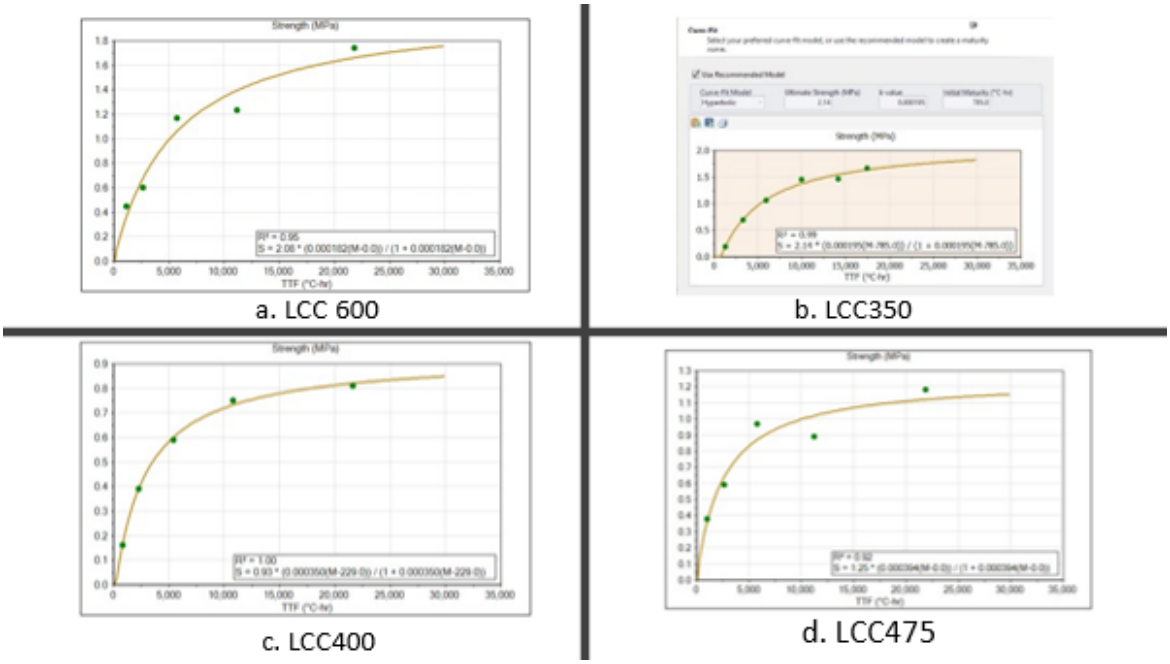

Figure 5.8: LCC Maturity Curve

The findings also reveal that the thickness of LCC plays a role in determining the layers' strength in addition to the slag content already discussed. Regarding the 475 kg/m^3 LCC, a 350 mm thick LCC might have a maximum strength of 6% greater than a 250 mm thick LCC and 71% higher than a 200 mm thick LCC. Although the Erbsville and Notre Dame

475 kg/m^3 LCC had an 11% difference in LCC dry density, there was still a significant difference when LCC thickness was lowered from 250 mm to 200 mm in addition to the inclusion of slag within the mix. LCC strength also increased with density, and the 200 mm thick 600 kg/m^3 LCC was observed to have comparable maximum strength to the 350 mm 475 kg/m^3 LCC density with 20% slag. Therefore, increasing LCC density by about 26% could be beneficial to achieve similar results with minimal thickness.

The temperature change during the first few hours of the casted LCC on Erbsville and Notre Dame Drive test roads is shown in Figure 5.9. The temperature within all the LCC layers at Notre Dame reached their maximums within 5 to 9 hours from casting, with the time to peak temperature decreasing with increased density. Peak temperatures were reached faster than 12 hours which is the typical time LCC could reach its peak temperature according to past studies, as seen in Figure 5.10 [236]. However, Tarasov et al., (2010) [236] also noted that lower density LCC in thinner samples reached peak temperatures faster. The 12-hour phenomenon, however, was evident at Erbsville. The peak temperature for both LCC250 and LCC350 was reached at about the 12-hour mark.

There was also about a 20 °C difference in peak temperature when LCC thickness was increased by 40% at Erbsville. At Notre Dame, the peak temperature within the LCC475 section was the highest and was 21% greater than the LCC400 section and 7% more than the LCC600. The LCC600 temperature surpassed the LCC400 by 13%. According to Jones and McCarthy (2006) [122], peak cellular concrete temperature was found to drop by 40% when cement quantity was reduced from 600 to 300 kg/m^3, as reflected by these results. Although the LCC350 section had a higher LCC 475 kg/m^3 thickness of 350 mm, its peak temperature was lower than the 200 mm thick LCC of the same density. This could be attributed to the fact that the LCC at this location constituted 20% slag, a pozzolanic material replacement for cement. Past studies have proven that replacing parts of cement with pozzolans like fly ash could be beneficial in reducing LCC core temperatures [130, 121]. Furthermore, the effect of lower ambient temperatures at Erbsville (4 °C) compared with Notre Dame (24 °C on average) during LCC pour could have also been a factor.

Generally, the volume of the pour, cement content, concrete density, and the amount, kind, and properties of the cement/filler/aggregate used are all factors that influence the hydration of LCC [36, 122, 236]. The big temperature jump at the onset of the Erbsville sections could be attributed to the considerable difference in ambient temperature (4 °C) during LCC pour and resultant temperature due to heat of hydration from the LCC. Furthermore, the time it takes for LCC to set is critical since it affects the construction schedule. Although there is no standard test technique for assessing the setting time of LCC, Brady et al. (2001) [36] found that the ASTM C266 test method for cement could be used to determine the setting time of cellular concrete. The stiffening of cellular concrete

has been seen after 5 hours of casting at 20 °C [136]. Results in this study reflect similar findings.

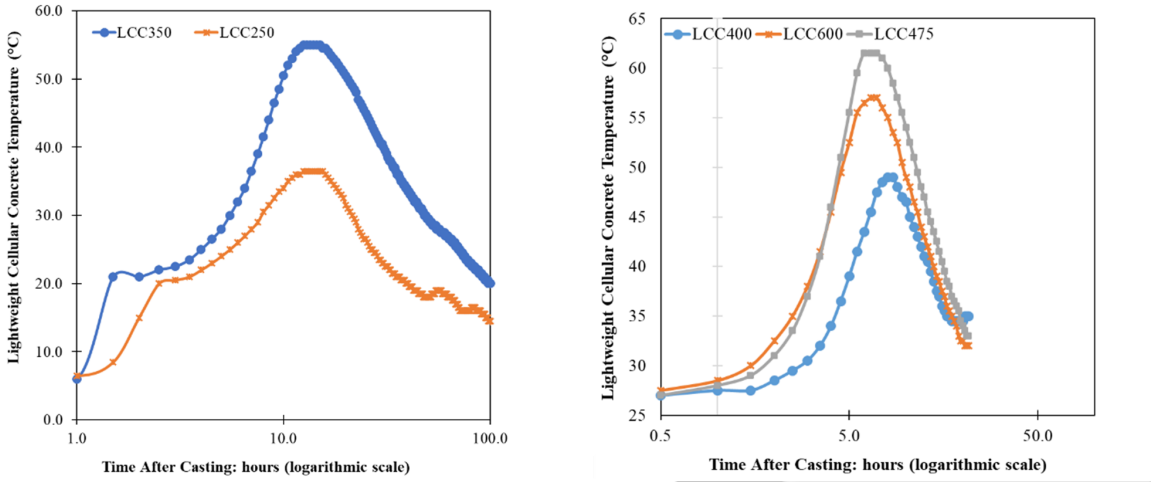

Figure 5.9: Temperature profile of lightweight cellular concrete curing in the field

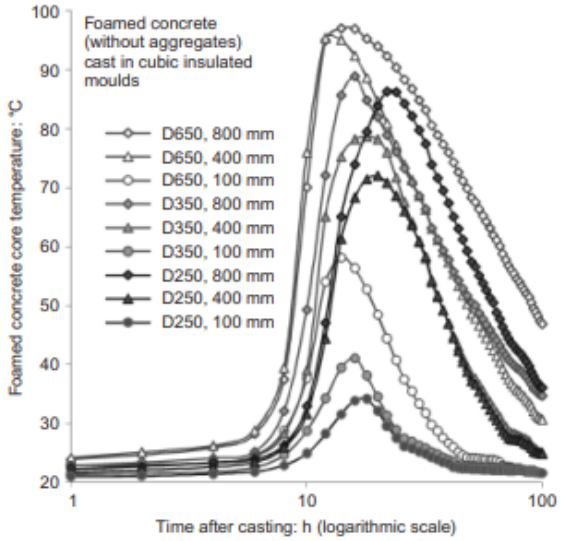

Figure 5.10: Temperature profiles of foamed concrete curing in sealed boxes with different cement contents [236]

The rate of temperature development at the centers of the LCC layers was obtained

and is presented in Figure 5.11. At the centers of the LCC layers, the peaks of the curves represent the maximum rate of temperature rise and the time it occurs. All the peaks lie in the time interval between 3.5 and 4.5h after casting for Notre Dame and earlier between 1.0 and 2.5 h for Erbsville. This demonstrates that because the core of the material is more insulated by itself, the acceleration of heat development starts earlier with increasing LCC thicknesses. Also, this rate of heat development was earlier for the LCC with slag content (LCC350 and LCC250) than the mix without slag. This is in line with research by Tarasov et al. (2010) [236], which showed that larger foamed concrete cubes heated up more quickly and earlier than smaller cubes. Additionally, their study demonstrated that lighter lightweight cellular concrete always exhibited faster rates of temperature rise due to having a lower heat capacity than heavier lightweight cellular concrete. This can be seen between the LCC475 and LCC600 sections. However, the LCC400 reflected the least rate of temperature rise in this study.

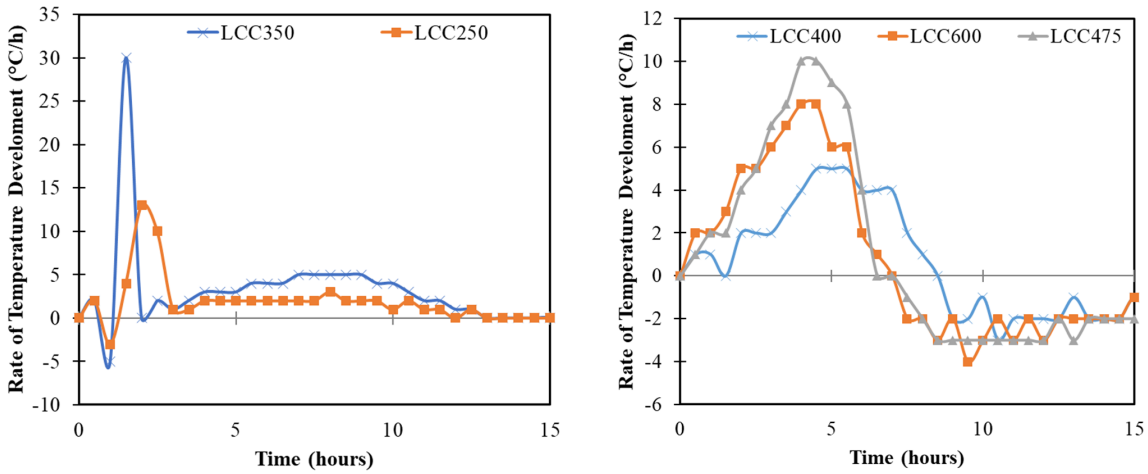

Figure 5.11: Rate of temperature development in lightweight cellular concrete on the field

Concrete maturity testing is beneficial as it could assist in monitoring LCC temperature and can be used to compare not only how LCC is curing but also to gauge the quality control of LCC. Results can be used to compare in-place concrete and cast cylinders. If the maturity estimates differ significantly from the cylinder samples, there may be a problem with the ready mix LCC. Knowledge of this aspect of the LCC material could help save construction time by determining how construction can progress following LCC pour [115].

5.4.3 Modulus of Elasticity

Typical pavement design and prediction tools use the Modulus of elasticity (MOE) and Poisson's ratio (P) of materials as key input parameters. Therefore, this study performed laboratory testing to obtain these parameters. Table 5.6 summarizes the results obtained for both tests.

The MOE values for the densities ranged from 780 to 1,450 MPa. With an increase in LCC density, MOE was observed to increase. The MOE values are comparable with prior research that found an average MOE of 729 MPa for 400 kg/m^3, 1,002 MPa for 475 kg/m^3, and 1,490 MPa for 600 kg/m^3 [174], with a range of 500 to 1,500 MPa in general [32]. These values are comparatively higher than unbound granular typically used in pavement applications material (MOE ranging between 200 – 250 MPa on average as reported in [10]. The Erbsville MOE was more significant than the Notre Dame value for 475 LCC density because the test densities were higher by 11%.

Poisson's ratio for all densities ranged between 0.21 and 0.30. The 475 kg/m^3 density displayed the highest Poisson ratio with an average result of 0.30. These results are greater than those found in other research, which revealed that typical values for these densities range between 0.14 and 0.08 for LCC densities of 300 and 600 kg/m^3, respectively [189]. However, except for the 475 kg/m^3, which was reported to fluctuate from 0.21 to 0.27 in their investigation, Ni (2021) [174] gave comparable findings for densities between 475 and 600 kg/m^3. Nonetheless, the 475 kg/m^3 LCC exhibited the highest Poisson ratio compared to the other densities.

Table 5.6: Modulus of Elasticity results

Location	**Plastic Density**	**Test Density**		**Elastic Modulus**		**Poisson's Ratio**	
	(kg/m^3)	**Aver. (kg/m^3)**	**Std. Dev.**	**Aver. (kg/m^3)**	**Std. Dev.**	**Aver.**	**Std. Dev.**
Erbsville	475	538	9	1,207	117	0.24	0
Notre Dame	400	412	5	888	107	0.21	5
	475	485	14	1,188	241	0.30	14
	600	599	24	1,391	44	0.26	24

Table 5.7: Erbsville Water Absorption results

Number of Days after Casting	Water Absorption (475 kg/m^3)	
	Average	Std.Dev
7	16	4
28	13	3

5.4.4 Water Absorption

Table 5.7 shows the water absorption of specimens from Erbsville. The results suggest that a 475 kg/m^3 LCC absorbs roughly 16% of the water on day seven, but it absorbs less (13%) after 28 days of curing. Although LCC densities of 400 and 600 kg/m^3 were not examined in this work, Ni (2021) [174] found that water absorption for LCC densities of 400 to 600 kg/m^3 ranged between 7% and 12% on day 28 and increased when immersed in water over time. Water absorption reduced as LCC density increased, according to Ni's 2021 [174] research. Kearsley and Wainwright conducted a similar investigation (2001) [131]. This value ranged between 10% and 12% at a density of 475 kg/m^3. However, when compared to Ni (2021) [174], the results of this investigation revealed that absorption was 16% but only 6% in Ni (2021) [174]. The specimens in the Ni (2021) [174] study were immersed in water continuously over time, but the specimens in this investigation were only immersed in water for 24 hours at the designated age. Regardless, the results for day 28 are similar and fall within the same range. The findings show that as LCC ages, its water absorption characteristics decline. Furthermore, on day 28, the test method utilized in Ni (2021) [174] and the one used in this study can yield comparable results.

5.5 Performance Prediction

Some performance analysis was done with the MEPDG and WESLEA to see how the test sections would perform in the future. This would help to influence future maintenance and rehabilitation planning and decision-making. This will also aid in evaluating the life cycle cost and environmental impact of LCC pavements and comparing them to other options. The performance of all pavement sections in the field sites has been considered in this section.

5.5.1 Mechanistic Empirical Pavement Design Guide

The AASHTOWare Pavement ME modeling tool, which employs the Pavement Mechanistic and Empirical Pavement Design Guide (MEPDG) method, was used to evaluate and predict the designed pavement performance over its design life. It included using different levels of data, where level 1 data is the most accurate [69]. The data at this level are obtained from field and laboratory testing. Level 2 data is of medium accuracy, where limited testing is used to determine the material's properties within the pavement layers. Finally, Level 3 inputs represent the least accuracy and involve the use of values from local agencies since actual testing for the pavement materials utilized in a project has not been performed or were not available during the analysis period. For this study, the input parameters used and their respective levels are provided in Table 5.8 for Erbsville and Table 5.9 for Notre Dame Drive.

Field calibrated mathematical equation for flexible pavements used in calculating plastic vertical deformation within all unbound pavement sublayers, and the subgrade is given in Equation 5.3 and for IRI in Equation 5.4 [178].

$$\delta_a(N) = \beta_{s1} k_1 \varepsilon_v h \frac{\varepsilon_0}{\varepsilon_r} \mid e^{-(\frac{\rho}{N})^{\beta}} \mid \tag{5.3}$$

where, δ_a is permanent deformation, N is the number of repetitions, ε, β, ρ, are material properties, ε_r is resilient strain (in/in) and ε_v is the vertical strain (in/in).

$$IRI = IRI_0 + 0.0150(SF) + 0.400(FC_{total}) + 0.0080(TC) + 40.0(RD) \tag{5.4}$$

where, IRI_0 is the initial IRI (in/mi), SF is the site factor, FC_{Total} is the area of fatigue cracking, TC is the length of transverse cracking (ft/mi), and RD is the average rut depth (in).

The prediction was performed for the pavement design traffic of 2,500 AADTT for Erbsville while two different traffic magnitudes (650 and 1,000 AADTT), where 650 AADTT represents the actual design traffic level, and 1,000 simulated a higher traffic level in case of exponential traffic growth. The results for the analysis for Erbsville and both traffic levels on Notre Dame Drive are presented in Tables 5.10, 5.11, and 5.12. Reliability levels and calibration factors used to perform this analysis were those specified for Ontario by the Ministry of Transportation, Ontario [185].

The results show that all the pavement section designs passed for each distress types at the end of the 25 years service life except AC top-down fatigue cracking at Erbsville.

Table 5.8: Erbsville MEPDG input parameters

Parameter (MEPDG Level)	**Level 3**	**Level 1&2**	**Level 3**	**Level 1&2**
Layer	**AC (HL3)**		**AC (HL4)**	
Passing 19mm sieve (%)				98.9
Passing 9.5mm sieve (%)		87.8		78.2
Passing 4.75mm sieve (%)		58.7		57.8
Passing 0.075mm sieve (%)		4.1		4.2
Asphalt Cement Content - by Volume (%)		5		5
Asphalt Cement Grade (PG)		64-28		64-28
Density (kg/m3)		2,403		2,402
Thermal conductivity (watt/meter-Kelvin)	1.16		1.16	
Specific Heat (Joule/kg-Kevin)	963		963	
Reference Temperature	21.1		21.1	
Thickness (mm)		50		100
Layer	**Granular Base**		**Granular Subbase**	
Material Class	A-1-a		A-1-b	
Liquid Limit	6		11	
Plasticity Index	0		0	
Water content (%)		6.2		7.8
Passing 0.075mm sieve (%)		1.2		0.7
Passing 0.30mm sieve (%)		5.8		13.2
Passing 1.18mm sieve (%)		31.8		55.2
Passing 4.75mm sieve (%)		61.5		73.7
Passing 9.5 mm sieve (%)		74.6		90.8
Passing 13.2 mm sieve (%)		83.3		90.8
Passing 19 mm sieve (%)		94.9		90.1
Passing 26.5 mm sieve (%)		100		100
CBR/Modulus (MPa)		54/226		26.5/143
Poisson's ratio		0.35		0.35
Thickness (mm)		150		450
Layer	**LCC Subbase**			
Modulus (MPa)		1206		
Poisson's ratio		0.24		
Thickness (mm)		250/350		
Layer	**Subgrade**			
Material Class				
Liquid Limit		18.3		
Plasticity Index		3		
CBR/Modulus (MPa)		9/72		
Poisson's ratio		0.45		
Passing 0.002mm sieve (%)	8			
Passing 0.075mm sieve (%)	29			
Passing 0.425mm sieve (%)				
Passing 4.75mm sieve (%)		83.61		
Passing 19mm sieve (%)		89.92		
Passing 150mm sieve (%)		93.87		

Table 5.9: Notre Dame Drive MEPDG input parameters

Parameter (MEPDG Level)	**Level 3**	**Level 1&2**	**Level 3**	**Level 1&2**
Layer	**AC (SP12.5FC)**		**AC (SP19.0)**	
Passing 19mm sieve (%)	100			99.5
Passing 9.5mm sieve (%)	77			75.4
Passing 4.75mm sieve (%)	60			56.4
Passing 0.075mm sieve (%)	6			4
Asphalt Cement Content - by Volume (%)	11.8			5
Asphalt Cement Grade (PG)	64-28			64-28
Density (kg/m3)	2,390			2,430
Thermal conductivity (watt/meter-Kelvin)	1.16		1.16	
Specific Heat (Joule/kg-Kevin)	963		963	
Reference Temperature	21.1		21.1	
Thickness (mm)		90		100
Layer	**Granular Base**		**Granular Subbase**	
Material Class	A-1-a		A-1-b	
Liquid Limit	6		26	
Plasticity Index	0		12	
Water content (%)		10.6		9.4
Passing 0.075mm sieve (%)		5		40
Passing 1.18mm sieve (%)		22.2		41.1
Passing 2.36 mm sieve (%)		30.5		53
Passing 4.75mm sieve (%)		42.1		67.4
Passing 9.5 mm sieve (%)		60.6		82.8
Passing 12.5 mm sieve (%)				89.8
Passing 19 mm sieve (%)		90.1		96.2
Passing 25.0 mm sieve (%)		99.4		100
Passing 37.5 mm sieve (%)		100		
CBR/Modulus (MPa)		125/387		4/143
Poisson's ratio		0.35		0.40
Thickness (mm)		300		semi-infinite
Layer	**LCC400 Subbase**		**LCC475 Subbase**	
Modulus (MPa)		844		1,188
Poisson's ratio		0.21		0.30
Thickness (mm)		200		200
Layer	**LCC600 Subbase**			
CBR/Modulus (MPa)		1,391		
Poisson's ratio		0.26		
Thickness (mm)		200		

Table 5.10: Erbsville MEPDG predicted performance

Distress type	Target Reliability	Target	Control	LCC250	LCC350
Terminal IRI (m/km)	95.00	3.00	2.66	2.62	2.61
Permanent deformation - total pavement (mm)	95.00	10.00	4.71	4.20	3.95
AC bottom-up fatigue cracking (percent)	95.00	10.00	7.34	2.10	2.02
AC thermal cracking (m/km)	95.00	200.00	55.49	55.58	55.67
AC Top-down fatigue cracking (percent)	95.00	378.80	833.34	363.15	334.03
Permanent deformation - AC only (mm)	95.00	6.00	6.00	1.09	1.12

Table 5.11: Notre Dame Drive MEPDG predicted performance for 650 AADTT

Distress type	Target Reliability	Target	Control	LCC400	LCC475	LCC600
Terminal IRI (m/km)	50.00	2.30	1.86	1.86	1.86	1.86
Permanent deformation - total pavement (mm)	85.00	13.00	3.17	3.13	3.08	3.05
AC bottom-up fatigue cracking (percent)	85.00	20.00	1.17	1.17	1.17	1.17
AC thermal cracking (m/km)	85.00	190.00	33.17	33.2	33.17	33.17
AC Top-down fatigue cracking (percent)	85.00	40.00	12.89	12.9	12.89	12.89
Permanent deformation - AC only (mm)	85.00	13.00	1.14	1.15	1.16	1.17

Slight increases were noted when traffic increased from 650 to 1,000 AADTT, although not very significant. The Control AC-top-down fatigue cracking was 2.3 times more than the LCC350 section and 2.5 times more than LCC250. AC-top-down cracking for Notre Dame and Thermal cracking for both test sections seemed uninfluenced by a change in subbase type; therefore, they have been excluded from further discussions. The growth in roughness for the pavement sections over 25 years was similar irrespective of subbase material type, as seen in Figures 5.12, 5.13, and 5.14; however, slight differences were noted in the Erbsville thicker 250 mm and 350 mm sections, compared with the respective Control section. It appears that thicker LCC layers could provide smoother pavements over time. Nevertheless, the effect of placing the LCC subbase was noted mostly with

Table 5.12: Notre Dame Drive MEPDG predicted performance for 1,000 AADTT

Distress type	**Target Reliability**	**Target**	**Control**	**LCC400**	**LCC475**	**LCC600**
Terminal IRI (m/km)	50.00	2.30	1.87	1.87	1.87	1.87
Permanent deformation - total pavement (mm)	85.00	13.00	3.39	3.35	3.30	3.27
AC bottom-up fatigue cracking (percent)	85.00	20.00	1.18	1.18	1.17	1.17
AC thermal cracking (m/km)	85.00	190.00	33.17	33.17	33.17	33.17
AC Top-down fatigue cracking (percent)	85.00	40.00	13.18	13.18	13.18	13.18
Permanent deformation - AC only (mm)	85.00	13.00	1.28	1.29	1.31	1.32

permanent deformation for both field sections. As shown in Figures 5.15 and 5.16, the anticipated total permanent deformation was slightly affected by the subbase type. This is expected as the LCC layer serves as protection over the subgrade, thereby minimizing the impact of applied loads at the surface on the subgrade. Generally, the insensitivity of performance indicator results to changes in subbase type could be attributed to the fact that the tool has not been calibrated for the LCC material. Therefore, the layer is still being treated as an unbound layer but with a constant elastic modulus

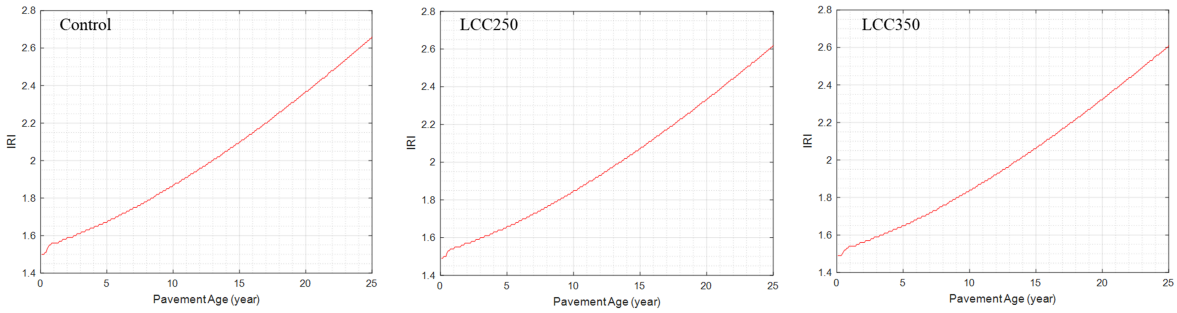

Figure 5.12: Erbsville IRI Prediction

The Pavement Condition Index (PCI) of the road sections was computed using the results obtained from the MEPDG predicted pavement distress data over 25 years. The calculations were based on the formulae provided in MTO's Pavement Design and Rehabilitation Manual [182]. Equation 5.5 gives the PCI formula, while Equation 5.6 provides

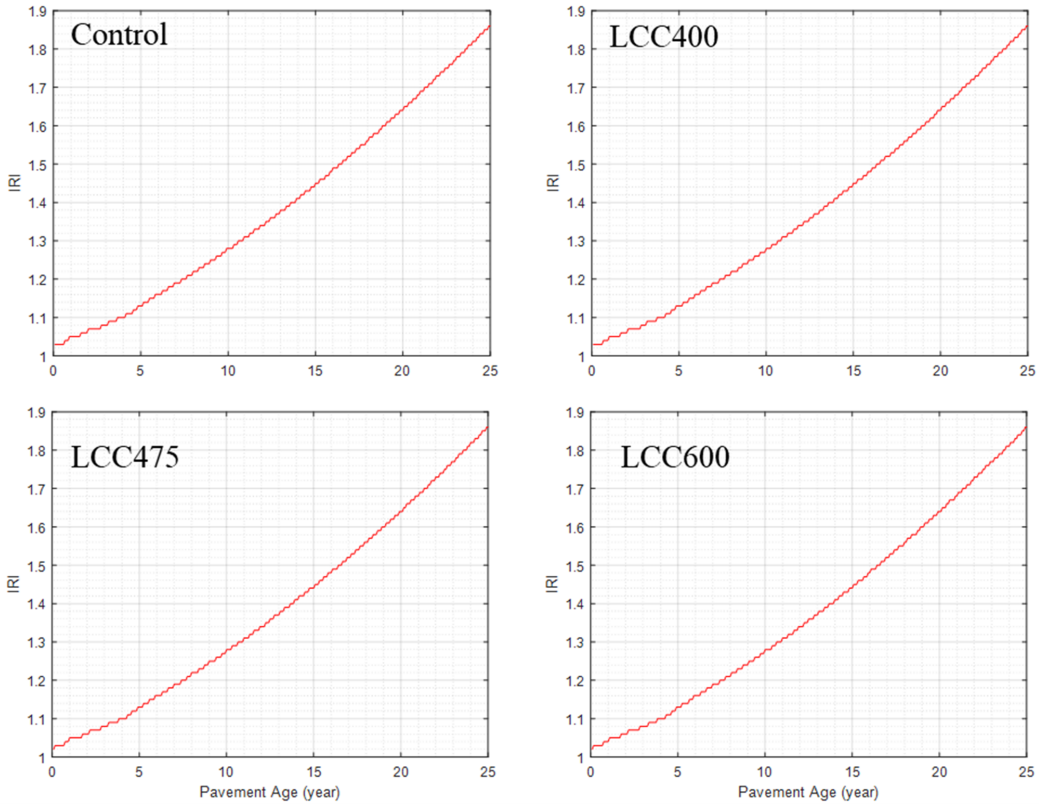

Figure 5.13: Notre Dame Drive IRI Prediction for 650 AADTT

the Distress Manifestation Index (DMI).

$$PCI = Max(0, Min(100, 13.75 + 9 \times DMI - 7.5 \times IRI)) \tag{5.5}$$

$$DMI = 10 \times \frac{(208 - \sum_{k}^{N}(S_k + D_k) \times W_k)}{208} \tag{5.6}$$

where N is the number of distresses related to a given pavement type, S_k is the severity rate of distress k, D_k is the density rate of distress k, and W_k is the weighting factor of distress k.

Performance deterioration curves were generated for all sections using the PCI as a primary pavement performance measure. The performance deterioration curves in the

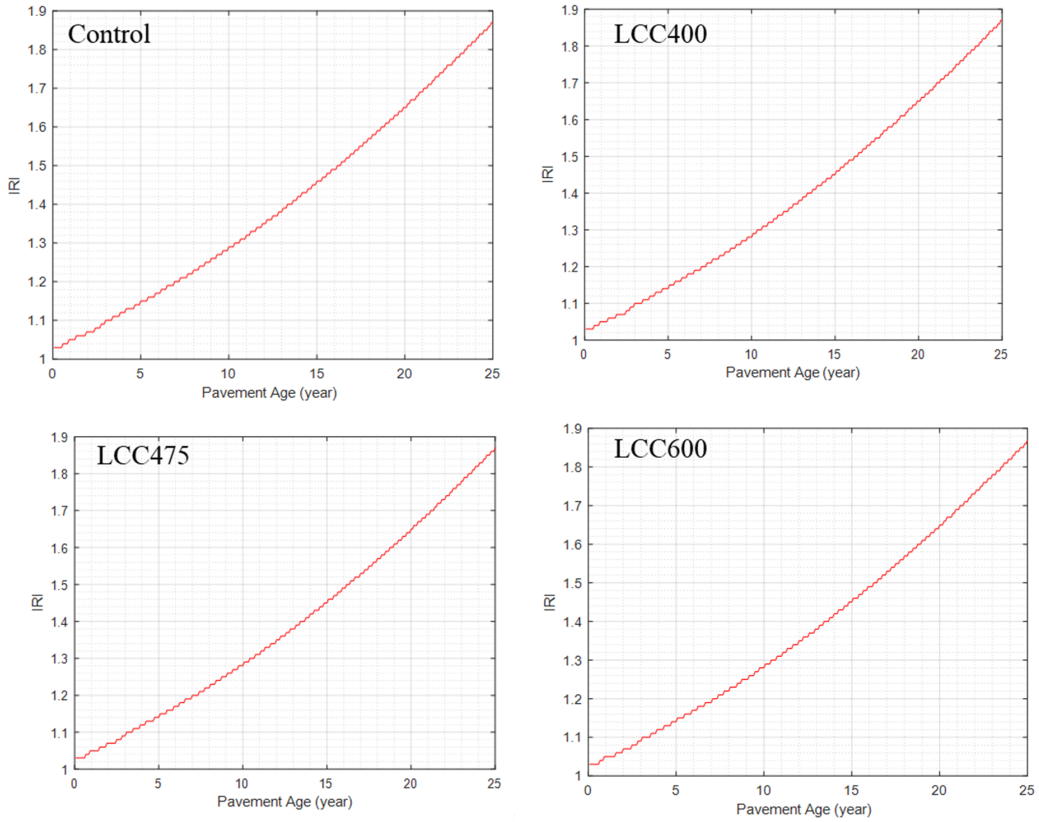

Figure 5.14: Notre Dame Drive IRI Prediction for 1000 AADTT

Notre Dame section were similarly not very sensitive to substituting unbound granular A with LCC as pavement subbase, as shown in Figures 5.17 and 5.18. Nonetheless, we see improved PCI values in the LCC sections for Erbsville, which was even better with increased LCC thickness (Figure 5.19).

5.5.2 WESLEA

Another approach was used to evaluate the pavement's future performance. To anticipate performance, the Waterways Experiment Station Linear Elastic Analysis for Windows tool (WESLEA) was utilized. WESLEA is a Multi-Layer Elastic Analysis (MLEA) program for calculating traffic-induced pavement reactions like stress, strain, and displacement. The software assumes that the pavement layer is linearly elastic and isotropic [69]. This method

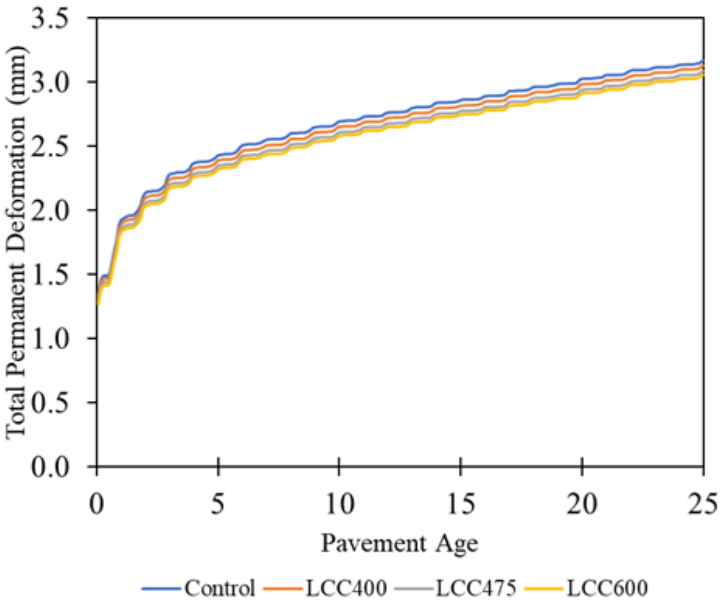

Figure 5.15: Notre Dame Total Permanent Deformation prediction over 25 years (650 AADTT)

was chosen because it provided stress and strain responses that could be compared to real-world performance. This could be very useful in predicting the pavement sections' future performance and giving an idea of any discrepancies that may occur.

This analysis typically generates two critical performance criteria (fatigue and rutting). Fatigue cracking is calculated using Equation 5.7 and rutting Equation 5.8.

$$N_{fc} = 2.83 \times 10^{-6}(\frac{10^6}{\varepsilon_t})^{3.148} \tag{5.7}$$

where, N_{fc} is the allowable number of load repetitions before fatigue cracking and ε_t is the tensile strain at the bottom of the surface layer

$$N_{fr} = 1.0 \times 10^{16}(\frac{1}{\varepsilon_v})^{3.87} \tag{5.8}$$

where, N_{fr} is the allowable number of load repetitions before rutting, ε_v is the compressive strain at the top of the subgrade layer.

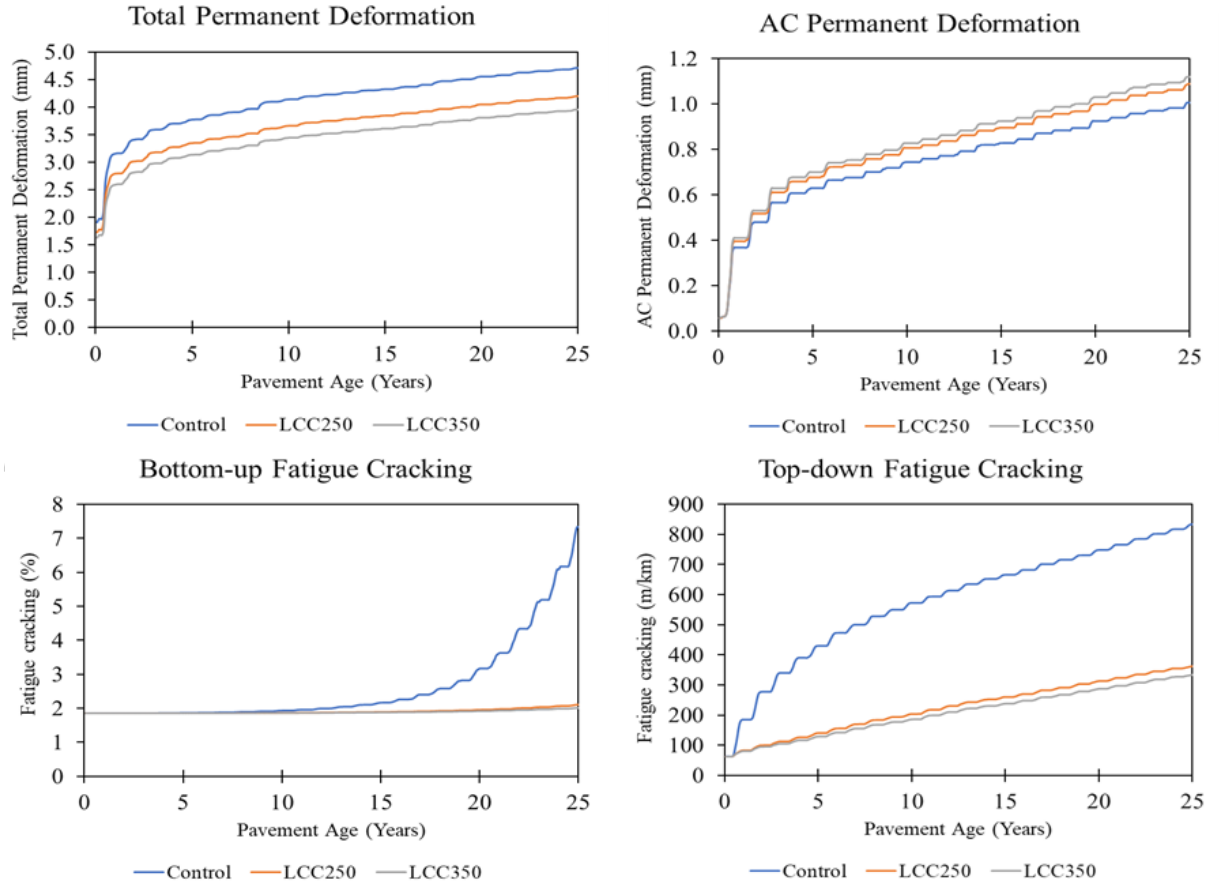

Figure 5.16: Erbsville performance prediction overtime

Table 5.13 lists the material parameters for each layer used in this analysis. Experimental material property data and commonly available data were used once more [10]. The study employed yearly design ESAL values computed from design parameters in Table 4.8. Table 5.14 shows the results for the maximum number of load repetitions allowed before fatigue and rutting set in. It should be emphasized that the tensile strain at the bottom of the asphalt layer is responsible for fatigue, while the compressive stress at the top of the subgrade is responsible for rutting.

In terms of fatigue failure, all LCC sections could handle twice as much traffic as the Control section before failure. When considering rutting, the number of load repetitions increased. Even though the LCC475 and LCC400 have similar densities, the LCC475's rutting performance was much better. The LCC400, LCC475, and LCC600 sections per-

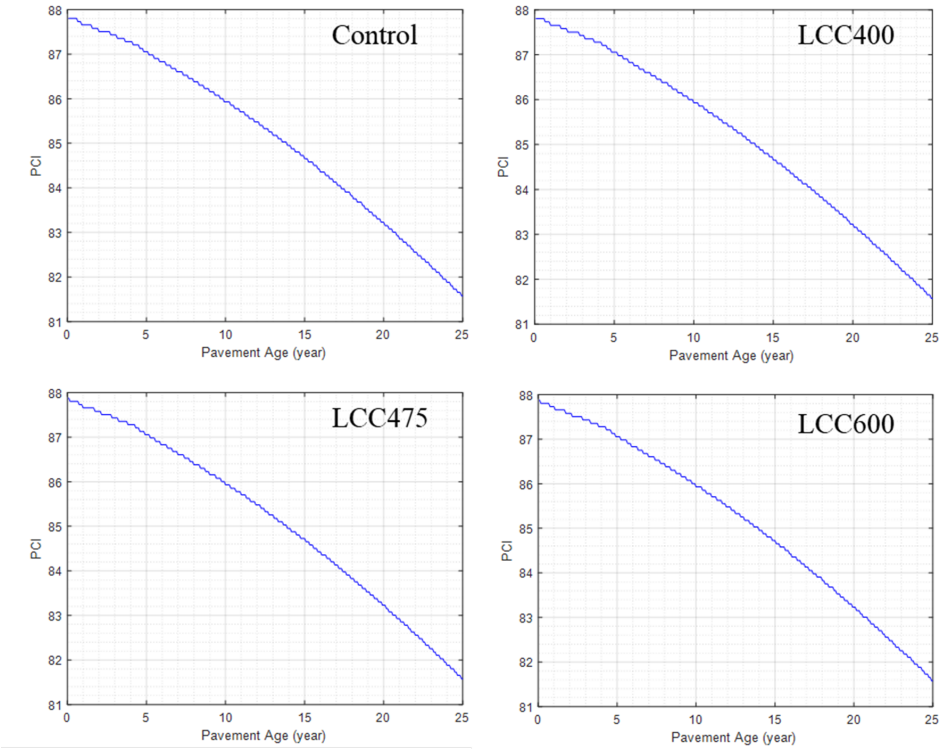

Figure 5.17: Notre Dame Drive PCI prediction for 650 AADTT

Table 5.13: WESLEA Parameters-Notre Dame

Location	**Parameter**	**Control**	**LCC400**	**LCC475**	**LCC600**
Surface	Modulus (MPa)	3,447.20	3,447.20	3,447.20	3,447.20
	Poisson's ratio	0.35	0.35	0.35	0.35
Base	Modulus (MPa)	344.70	344.70	344.70	344.70
	Poisson's ratio	0.35	0.35	0.35	0.35
Subbase	Modulus (MPa)	387	844	1,188	1,391
	Poisson's ratio	0.35	0.21	0.30	0.26
Subgrade	Modulus (MPa)	43	43	43	43
	Poisson's ratio	0.40	0.40	0.40	0.40

formed 3, 6, and 7 times better than the control in terms of allowing more traffic repetitions.

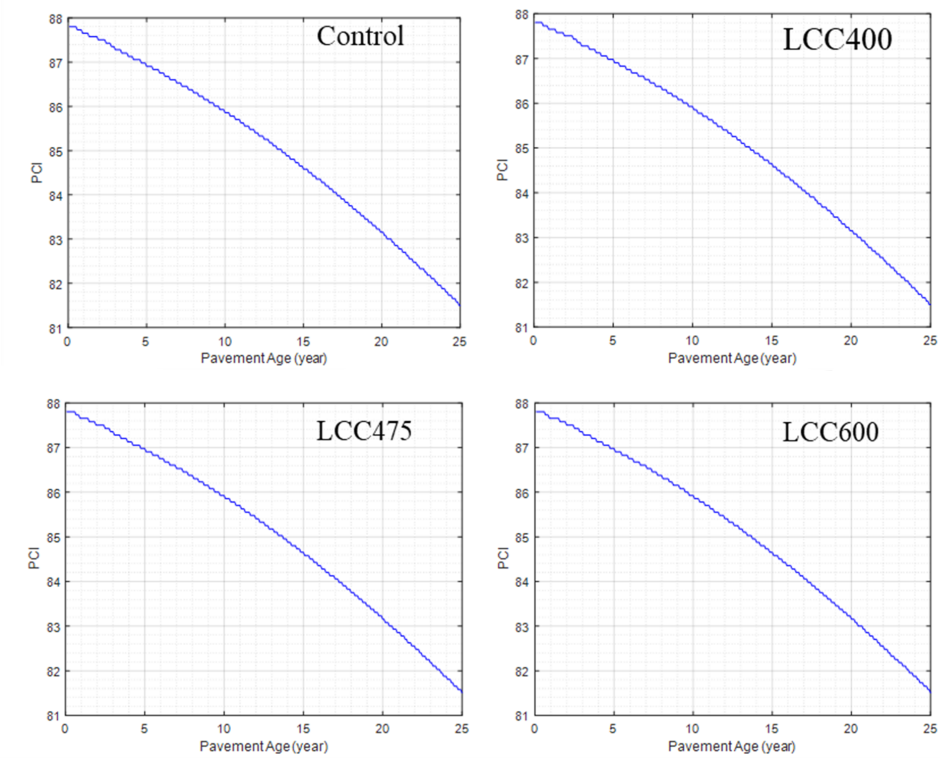

Figure 5.18: Notre Dame Drive PCI prediction for 1000 AADTT

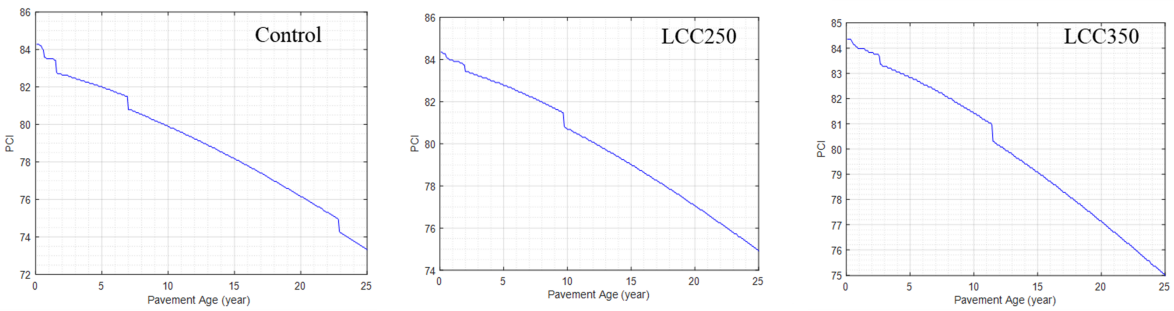

Figure 5.19: Erbsville PCI prediction

Figure 5.20 shows the progression in damage. Failure is deemed to occur when the damage exceeds 1 for both indicators. For fatigue failure, in a do-nothing maintenance scenario, the Control section is expected to fail by year 22, while the LCC sections would not fail

Table 5.14: WESLEA Allowable load repetition results

Section	Allowable load repetition		LCC/Control	
	Fatigue	Rutting	Fatigue	Rutting
Control	2,553,957	390,790		
LCC400	4,446,364	1,361,201	1.7	3
LCC475	5,106,157	2,221,342	2	6
LCC600	5,441,584	2,614,592	2.1	7

within its service life. Rutting could occur by year 15 in the control section and year 22, 23, and 24 for the LCC400, LCC475, and LCC600 sections, respectively.

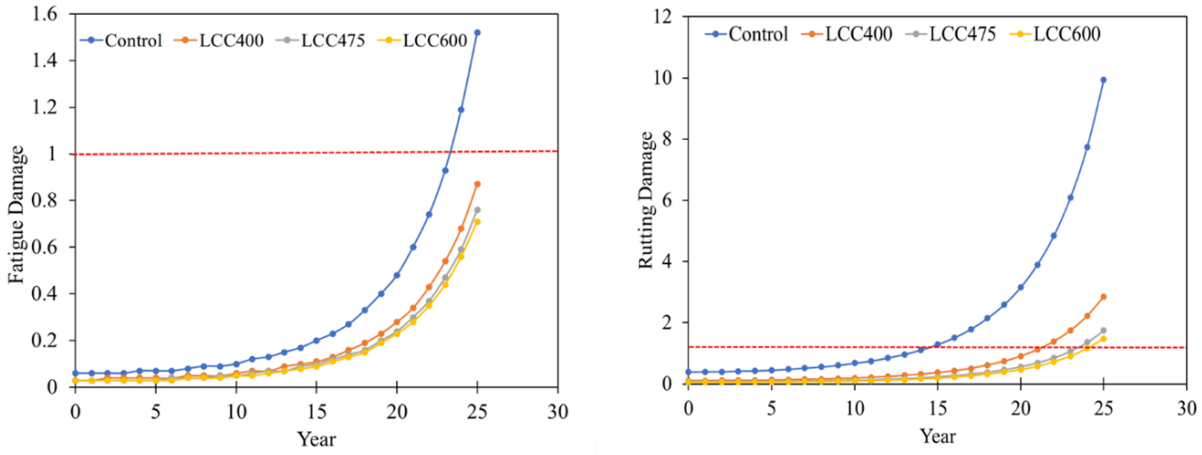

Figure 5.20: WESLEA Fatigue and Rutting failure for 25 years

It can be concluded that the Control section does not fail in terms of rutting and fatigue over the service life by comparing the failure pattern using MEPDG. MEPDG can securely anticipate these sections because layer information has been calibrated. The Control would fail by year 15, according to WESLEA failure standards.

5.6 General Findings

The main findings from laboratory testing of the pavement material properties revealed that the asphalt concrete applied at Notre Dame Drive was stiffer at lower temperatures and less stiff at temperatures above 21 °C than at Erbsville. The subgrade at Erbsville was a CL-type soil and was stiffer (CBR = 9) than that at Notre Dame, which was determined to be within class CL-OH (CBR = 4). A higher quality granular A (CBR = 125) was used at Notre Dame than at Erbsville (CBR = 54). The CBR of the granular B used at Erbsville was 27.

The twenty-eight-day compressive strength for LCC was found on average to be 0.81, 1.18 and 1.74 MPa for 400 kg/m^3, 475 kg/ m^3 and 600 kg/m^3. While for 475 kg/m^3 LCC with 20% slag, it was 1.67 MPa. The 475 kg/m^3 and 600 kg/m^3 LCC layers by day three and 400 kg/m^3 by day seven had surpassed the typical specified minimum 28-day compressive strength of 0.5 MPa, which could be an indication that the layer has sufficient strength to support the pavement structure as a subbase layer. The estimated ultimate strength for the Erbsville LCC350 and LCC250 sections were 2.14 and 2.02 MPa, respectively. The 400 kg/m^3, 475 kg/m^3, and 600 kg/m^3 were determined to have an ultimate strength of 0.93 MPa, 1.25 MPa, and 2.08 MPa, respectively. Adding slag to LCC could be beneficial by improving compressive strength up to 42%. The findings also revealed that the thickness of the LCC plays a role in determining the strength of the layers. A 40% greater thickness could result in a 6% increase in ultimate compressive strength. It could be beneficial to increase LCC density by up to 26% to achieve similar results with minimal thickness. The inclusion of 20% slag was noted to reduce core LCC temperature for the same density and cause the rate of heat evolution to occur earlier. Ambient temperature during LCC pour could also be a factor influencing this phenomenon. 400, 475, and 600 kg/m^3 LCC were determined to be stiffer than granular A and granular B materials by over three times.

LCC with high early strength cement could achieve peak temperatures between 5 to 9 hours during its heat of hydration process. This process takes longer (12 hours) for 25% thicker LCC material of similar density containing 20% slag. The rate of temperature rise for LCC is influenced by cement content, plastic density, and thickness of LCC layer. Lower cement contents would result in lower temperature rise and lower peak temperatures. Higher partial cement replacements with pozzolans like slag could achieve this. Greater LCC thicknesses could also yield lower peak temperatures. Additionally, as 475 kg/m^3 LCC aged, its water absorption characteristic declined.

MEPDG results showed better performance for 250 mm and 350 mm thick LCC than 450 mm unbound granular B. However, it showed a similar pavement condition index at

the end of the 25 years when comparing 150 mm unbound granular A with 200 mm thick 400, 475, and 600 kg/m^3 LCC densities. However, the LCC sections performed relatively better in terms of permanent deformation and IRI. Better performance was also achieved as LCC density increased. Furthermore, WESLEA analysis indicated that 400, 475, and 600 kg/m^3 LCC performed 3, 6, and 7 times better for rutting than the Control, allowing more traffic repetitions. It would allow twice as much traffic as the Control before fatigue failure occurred.

Chapter 6

In-Service Pavement Performance – Instrumentation

6.1 Introduction

This chapter presents and discusses results from the weather station and installed instrumentation at both Erbsville and Notre Dame field sections. It explores the effect of environmental factors such as temperature and precipitation on LCC pavement performance and considers the impact of traffic loads on the performance of LCC pavements. It further compares the results to the performance of the traditional pavement structure with unbound granular subbase material.

6.2 Ambient Temperature and Precipitation

Weather stations were installed at both trial section locations to monitor ambient temperature and precipitation. To ensure that the weather station was reading correctly and validate the readings, temperature and precipitation data obtained were compared with data from nearby weather stations. The first of these was the University of Waterloo (UW Stn) weather station with cartesian coordinates of 43° 28' 25.6" N and 80° 33' 27.5" W and an elevation of 334.4 m. It is about 3.8 km by road from the on-site weather station at Erbsville and 10 km from Notre Dame. The second weather station is owned by Environment Canada (Env. Canada) and is located at the Region of Waterloo International Airport in Breslau, Ontario, with cartesian coordinates of 43° 27' 39.0" N and 80° 22' 43.0"

W and is located 24.5 km away from Erbsville and 27 km from Notre Dame. Erbsville is 5.5 km from Notre Dame Drive. Although the Environment Canada weather station is greater than 8 km from both test field locations, a standard monitoring station must also be used to validate the installed weather station.

The temperature and precipitation trends for Erbsville, Notre Dame Drive, and the Environment (Env.) Canada weather station are compared in Figures 6.1 and 6.2. The temperature and precipitation data trend were similar, with some minor exceptions. Erbsville station and the UW Stn seem to be more correlated. The magnitude differences in the temperature measurements between the weather stations in Erbsville and Notre Dame are also minor. The 2018 precipitation data from Erbsville and the UW station were subjected to a two-sample T-test to ensure the accuracy of the weather station data. The results showed precipitation readings were not significant ($p = 0.99$). In 2022, Notre Dame Drive was compared with Erbsville and Environment Canada. Similar results were observed for the test sections, Notre Dame vs Erbsville ($p = 0.06$), Notre Dame vs Env. Canada ($p = 0.77$), and Erbsville and Env. Canada ($p = 0.10$).

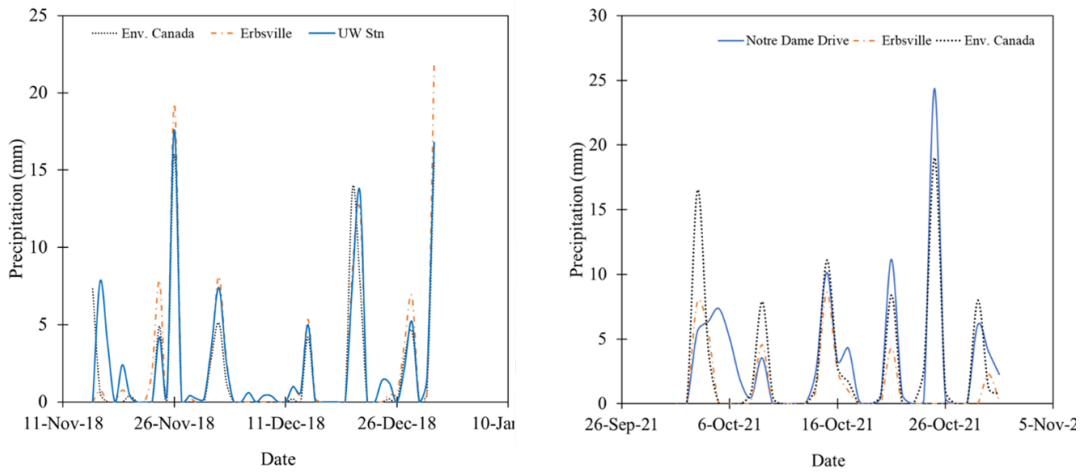

Figure 6.1: Validation of Weather station precipitation

Temperatures from the UW station and the Erbsville weather station were also used in the T-test. The results showed that the readings were statistically equivalent, with a P-value of 0.94 (>0.05) for a 95% confidence level. P-values of 0.15 and 0.19 were obtained between the Environment Canada station and those at Erbsville and Notre Dame. Addi-

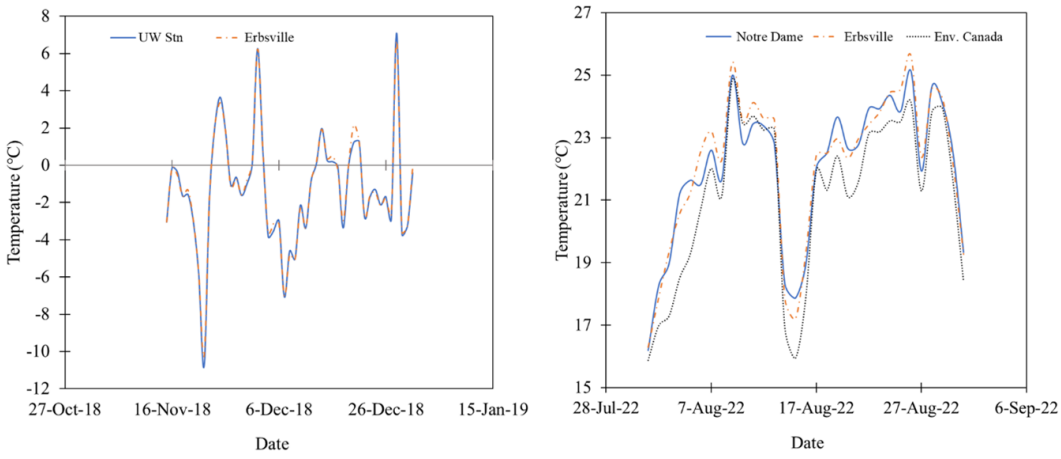

Figure 6.2: Validation of Weather station temperature

tionally, a T-test between Notre Dame Drive and Erbsville revealed, with a P-value of 0.84, that there was no statistically significant difference in the recorded ambient temperature. At each location, the number of wet days was computed. A wet day is defined as a day when precipitation exceeds 0.254 mm. Erbsville data from the first two years of monitoring (between November 15, 2018, and November 14, 2020) indicated that out of the 732 days considered; there were 179 wet days. However, for three months (February, July, and August) in 2019, some technical difficulties were experienced, and there was no data for those months. Considering just the second year (November 15, 2019, to November 14, 2020), within the 365 days studied, 110 days were noted to be wet days. This showed that for at least 30% of the year, precipitation events exceeding 0.254 mm were experienced within the Erbsville study area. The highest daily precipitation of 33.5 mm occurred at the end of March 2019. At Notre Dame, within the study period (August 1, 2021 to June 8, 2022), 158 wet days were recorded out of the 312 days of the study period. This means that 51% of the time, precipitation events over 0.254 mm occurred, and the highest recorded event was on September 22, 2021, with 67.6 mm of precipitation.

The air-freezing index for the study period at each location was estimated. The air-freezing index is a standard metric for gauging wintertime freezing severity and calculating frost depth for mid-latitude regions [34]. This is very beneficial in determining the depths of road pavement structures during design and construction. Soil temperature and maximum

soil frost depth, which may be calculated with the air freezing index, are crucial elements in construction costs, especially below the ground construction [34]. Frost heave is a naturally occurring process that causes soils to exert an outward push on an underground structure, which is caused by how severe the soil frost is [117]. It is possible to reduce pavement construction costs, and make appropriate preparations for upcoming climate conditions [34] and design longer-lasting pavements with an accurate assessment of the maximum soil frost depth.

The air freezing index is calculated with Equation 6.1.

$$F_i = \sum_{i=1}^{N} (T_{ave_i} {}^{\circ}C) \tag{6.1}$$

where, $F_(i)$ is the cumulative total of degree-days during the study period and, T_{ave} is the daily mean temperature calculated with Equation 6.2.

$$T_{ave} = 0.5(T_1 + T_2) \tag{6.2}$$

where, T_1 is the maximum daily air temperature and T_2 is the minimum daily air temperature for a day I, and N is the number of days in the study period considered. For Erbsville, N was 365 days (August 1, 2020 to July 31, 2021), while for Notre Dame Drive, N is 312 days (1 August 1, 2021 to June 8, 2022).

Air freezing index values represent the seasonal magnitude and duration of below-freezing air temperatures. Each August–July cold season accumulates deviations of the daily mean temperature above or below 0 °C known as freezing degree-days; the seasonal air freezing value is defined as the difference between the highest and lowest extrema points of the seasonal time curve plotted [34]. The air freezing index was calculated to be 349 freezing degree days (°C-days) for Erbsville and 459 °C-days for Notre Dame Drive. It should be noted that about three weeks of data were missing for the Erbsville calculation. The frost depth for each location is estimated using Equation 6.3.

$$P = -32.8 + 5.78\sqrt{F} \tag{6.3}$$

where P is the frost penetration in cm and F is the freezing index on °C-days. Erbsville frost depth was estimated to be 75 cm, while Notre Dame Drive's was 92 cm.

6.3 Environmental Effect on Pavement Temperature

For in-situ characteristics of different pavement designs, it is essential to understand the temperature distribution within the pavement cross section [61]. Temperature distribution is a significant factor influencing the mechanical properties and bearing capacity of flexible pavements [12]. To accurately determine in situ performance of flexible pavements, it is vital to predict temperature distribution within layers, especially asphalt concrete. Factors to be considered in determining pavement temperature profile include ambient temperature, seasonal changes (effects of heating and cooling trends), solar radiation, wind speed, and reflectance of the pavement surface [61].

Equation 6.4 was used to calculate each installed LCC density's potential thermal resistance (R) to estimate the insulation characteristic.

$$R = \frac{D}{k} \tag{6.4}$$

where D is the thickness of the layer, and k is the thermal conductivity of the LCC. R is a standard unit of measurement for comparing a material's resistance to heat conductivity ("i.e., a material with a higher R-value shows that material is more effective as insulation [107] p597. Table 6.1 displays the thermal resistances of the investigated LCC densities and layers. Compared to the other layers in this study, the greater or equal to 250 mm thick 475 kg/m^3 density LCC was projected to have the best insulating qualities.

Table 6.1: Thermal resistivity of installed LCC

Density (kg/m^3)	**Thickness** (mm)	**Thermal Conductivity** (W/mK)	**Thermal Resistivity** (m^2 K/W)
400	200	0.08	2.60
475	200	0.09	2.35
475	250	0.09	2.94
475	350	0.09	4.12
600	200	0.10	2.00

Table 6.2 for Erbsville and Notre Dame Drive shows the depths within each pavement section where the temperature has been measured and interpreted in this study.

Table 6.2: Depths of the installed temperature sensor at each location

Layer	Erbsville (mm)		Notre Dame Drive (mm)			
	Control	LCC350	Control	LCC400	LCC475	LCC600
Surface	75	75	50	50	50	50
Base	225	225	175	175	175	175
Subbase	525	475	325	350	350	350
Subgrade	850	750	550	600	600	600

6.3.1 Layer temperature profile over time

The temperature profile within the pavement layers and ambient temperature for the trial roads are presented in Figures 6.3 and 6.4. Readings were taken every five minutes and aggregated to average hourly temperature. Only the surface layer LCC350 sensor was functional at Erbsville. The surface layer followed a similar trend as the ambient temperature and appeared to be the most influenced by it at both locations. The base layer temperature profile and magnitude for all sections were similar, with the T-test revealing no statistical difference (p-value 0.89) for Erbsville. ANOVA for the surface and base layers at Notre Dame produced a p-value of 0.54 and 0.58 for surface and base, showing that there was no difference between these layer temperatures. The temperature sensor at the surface of LCC600 and the control base was not working, therefore excluded from this analysis.

At Erbsville, because the sensor at the surface of the Control was damaged, the LCC350 temperature could not be compared. However, LCC350 surface temperature was observed to follow the trend and magnitude of the ambient temperature closely. This was also the case for all the sections at Notre Dame Drive. At times, especially during warmer months, the pavement surface temperature was noted to be higher than the ambient temperature. This is reasonable because, although pavement layer temperature decreases when air temperature decreases, it takes some time for heat to be released entirely from the pavement surface material. When the ambient temperature rises, the pavement surface absorbs the heat from the sun [134]. The trend also showed that the layers in the control section had more variability in temperature over time compared with the LCC sections. This variability was observed to correspond with ambient temperature variability. The Control's surface layer experienced temperatures 0.24 °C and 1.08 °C higher than the LCC400 and LCC475 sections in the winter, while in the spring, the temperature was 0.5 °C and 0.1 °C higher.

Although there was no statistical difference in the measured base temperatures, at

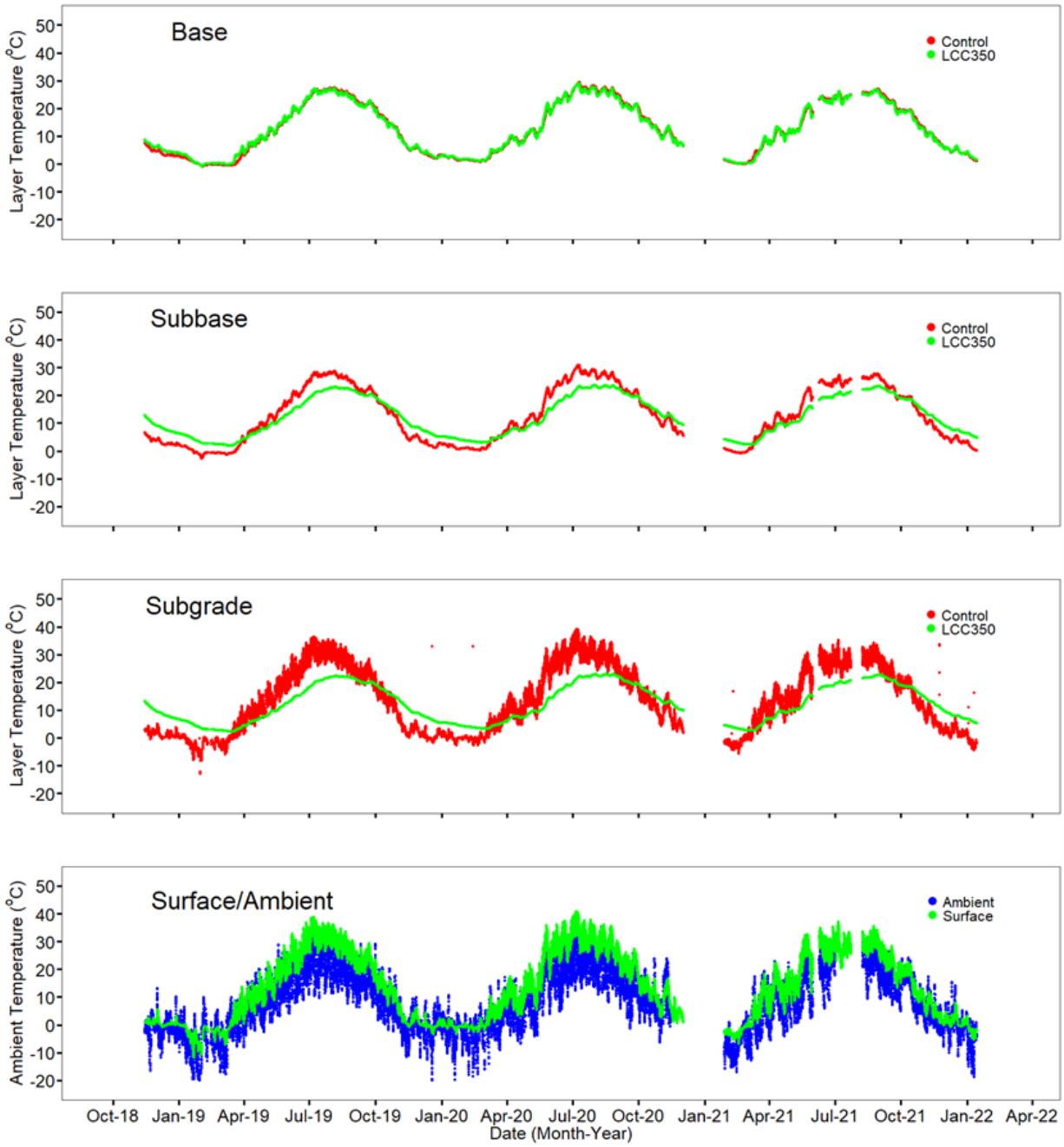

Figure 6.3: Hourly average layer temperature profile for Erbsville

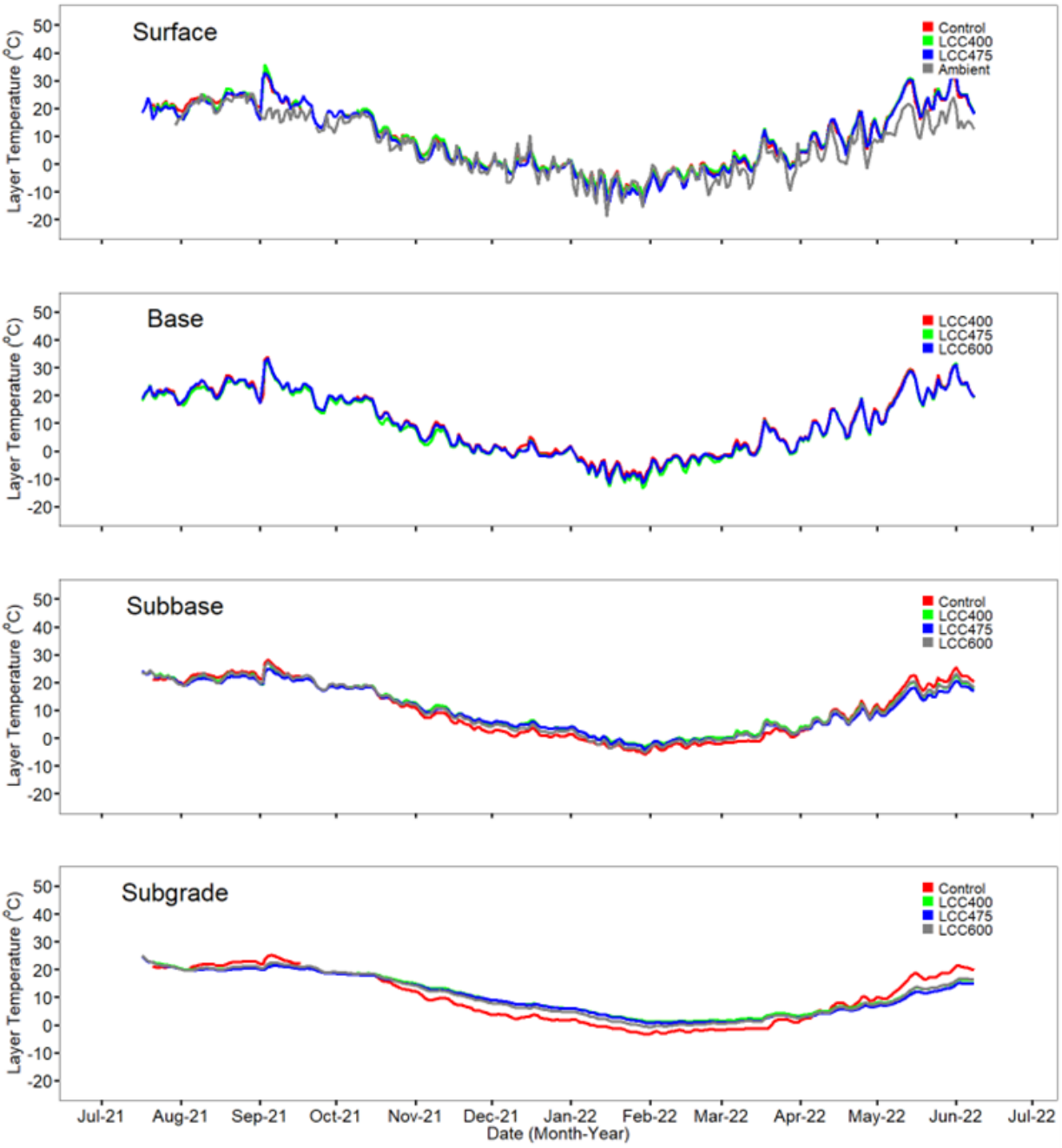

Figure 6.4: Daily average layer temperature profile for Notre Dame Drive

Erbsville, the base layer daily temperature was an average of 0.3 °C higher in the LCC350 than in the control section in the winter and 0.7 °C lower in the summer. At Notre Dame Drive, LCC400 was 0.25 °C higher, and LCC475 was 3.4 °C lower than the control in the winter. During spring (May 2022), both LCC400 and LCC475 remained 0.36 °C and 0.7 lower than the Control. The problem associated with using LCC within pavements is the potential for differential icing on the surface above the LCC layer [272]. This could be a potential concern in these test sections; however, using a granular base layer on top of the LCC could mitigate the effect on the pavement surface. For the base, comparing the LCC layers, the LCC475 base appeared to experience lower temperatures by 3 °C and 2 °C compared to LCC400 and LCC600 during winter. The difference during the springtime temperature was negligible.

During winter, the subbase, and subgrade temperature of the LCC sections remained above zero consistently, but this was not the case in the Control section, whose temperature went below and above 0 °C during the same period at Erbsville. The Control section subgrade remained frozen for most of the winter. Erbsville LCC350 section's subbase and subgrade's average daily temperature remained 3 °C and 4 °C, respectively, higher than the control for the winter and 7 °C and 10 °C lower during summer. A different result is noted at Notre Dame Drive, where the subbase and subgrade temperatures beneath the LCC sections also experienced sub-zero temperatures. During winter, the LCC600 saw the lowest temperature amongst the LCC sections, with an average temperature of 0.7 °C above the Controls'. However, the LCC400 and LCC475 experienced 2 °C and 3 °C above the subgrade subbase temperature. At some point, all the LCC sections in this layer experienced below zero temperature. During Spring, the coolest LCC subbase layer was the LCC475, with an average daily temperature of 5 °C less than the Controls' subbase. The LCC400 and LCC600 section subbase also had lower temperatures of 3 °C and 2 °C than the control subbase.

However, a significant temperature difference was observed at the subgrade. The LCC400, LCC475, and LCC600 had an average daily subgrade temperature of 4.5 °C, 4 °C, and 3 °C higher in the winter than the Control. Amongst the LCC sections, only the LCC600 subgrade saw sub-zero temperatures. LCC400 subgrade layer was the warmest among all four sections. During spring, the Control section experienced higher average daily temperatures of 6 °C, 7 °C, and 5 °C than LCC400, LCC475, and LCC600. The coolest LCC subgrade layer in the spring was in the LCC475 section.

The Control section subgrade temperature at lower ambient temperatures was observed to be lower than its subbase temperature and at higher ambient temperatures to be higher than the subbase temperature at Erbsville. This means that at this location, the ambient temperature had a more significant influence on the subgrade than the subbase layer in the

control section. The LCC350 section displayed a similar trend and magnitude for subgrade and subbase temperatures.

But, at Notre Dame Drive, a reverse case was noted, where the subbase layers experienced lower temperatures than their subgrade for all the sections. This could be attributed to the lower subbase layer thickness at this location compared to Erbsville. It could also be due to environmental factors such as lower ambient temperature at this location with a freezing index of 460 °C-days compared with Erbsville, 349 °C-days at Erbsville, and higher wet days.

The above findings indicate that LCC has good insulation properties, especially for thicknesses above 200 mm. Results show that a 200 mm thick LCC with densities between 400 and 475 kg/m^3 could protect the subgrade immediately beneath it from freezing during cold winters. LCC thicknesses equal to or greater than 350 mm could be even more beneficial in alleviating the possibility of a frozen subbase and subgrade. This is due to the higher thermal resistivity provided by increasing the LCC thickness.

6.3.2 Freeze-thawing within Pavement Layers

The freezing and thawing in each pavement layer were investigated using the temperature data. The period study for Erbsville was 1,157 days (Nov 15, 2018 to Jan 14, 2022), while for Notre Dame Drive it was 327 days (Jul 17, 2021 to Jun 8, 2022). A day when the ambient temperature fluctuates between less than 0 °C and more than 0 °C is known as a freeze-thaw day. Throughout the research period, 267 freeze-thaw (F-T) days were at Erbsville, and 37 F-T days were at Notre Dame Drive. Also estimated were the freeze-thaw cycles in the pavement layers. A freeze-thaw cycle is defined as when the layer temperature changes from less than 0 °C to greater than 0 °C considering hourly average layer temperatures.

Freeze-thaw cycles in cold climates with seasonal frost could be detrimental to the pavement structure. This could lead to a decrease in the supporting capacity of the pavement subgrade [51]. A phenomenon leading to a reduction in subgrade resilient modulus is frost action which occurs in the presence of frost-susceptible soil, water, and freezing temperatures [195]. The effect of this action can be classified into frost heaving and thaw weakening. Thaw weakening happens when frozen soil thaws and ice lenses melt in the springtime, leading to saturated or near-saturated subgrade soil conditions. In contrast, a frost heave occurs when the subgrade pushes upward because of the soil's accumulated moisture expansion when it freezes [195]. A continuous cycle of frost heaving and thawing could cause a weakened subgrade and cracking, as depicted in Figure 6.5.

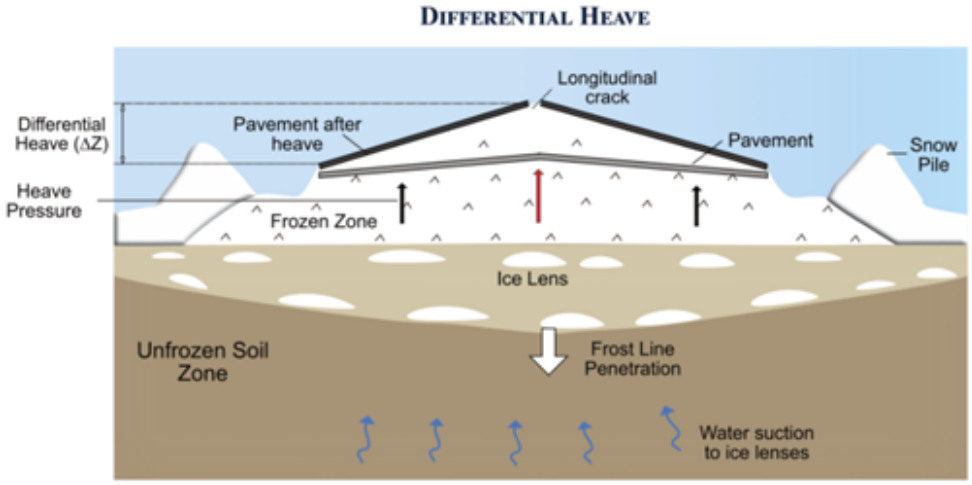

Figure 6.5: Differential Frost Heave [29]

Since water expands by around 9% as it freezes, concrete pores are put under pressure as the water in wet concrete freezes [145]. The cavity will enlarge and rupture if the pressure created exceeds the concrete's tensile strength. Over time, the concrete's expansion, cracking, scaling, and crumbling can result from repeated freeze-thaw cycles and disruption of the paste and aggregate [204]. LCC can be utilized to lessen this problem. The air bubble structure allows water to expand when it freezes without exceeding its tensile strength. It gives the frozen water enough room to expand, limiting the possibility of cracks that could propagate to the pavement surface. This could also prevent water from getting into the subgrade and weakening it. Moisture in the subgrade could lead to rutting failure of the pavement structure. For asphalt concrete, this freeze-thaw cycle could impact its physical and engineering properties making it more prone to distresses such as fatigue cracking and rutting [250].

Typically, the number of freeze-thaw cycles and frost penetration depth depends on the location's air temperature, solar radiation, and wind [234]. Knowing this phenomenon for LCC pavements could help design this type of pavement, especially for cold climates.

Figures 6.6 and 6.7 present the freeze thaw-cycle for each location and the depth at which this parameter was measured. Freeze-thaw cycles were determined based on hourly layer temperature data. At Erbsville, the Control subgrade and subbase experienced 70 and 2 freeze-thaw cycles, while none occurred at the LCC350 sections' subbase and subgrade despite being located within the frost depth zone of 75 cm. This is an indication of its good insulating properties. Contrarily, the Control section's subgrade temperature sensor

was located 100 mm below the frost depth yet experienced several freeze-thaw cycles.

However, at Notre Dame Drive, the LCC600 subbase and subgrade experienced just one freeze-thaw cycle like the Control section at this location. The LCC475 section saw the most (4) in its subbase. This could be attributed to the fact that the whole of this section was located at a slope greater than 1.3 percent meaning that LCC thicknesses within those portions could be smaller than the specified 200 mm. The same (10) freeze-thaw cycles occurred at the base of LCC475 and LCC400, while the LCC600 base saw the most (15) freeze-thaw cycles. The Control subgrade and subbase were mostly frozen throughout the winter; less temperature variability occurred, whereas the LCC section temperatures remained mostly above 0 °C. A different pattern was noticed at the surface of all the sections. The Control saw 1.8 and 1.4 times more freeze-thaw cycles than LCC400 and LCC475. Amongst the LCC sections, the LCC475 surface layer got more freezing and thawing during this period. From Table 6.1, the resistivity for 200 mm, 600 kg/m^3, and 475 kg/m^3 LCC were the lowest, which is evident from the results. This bolsters the assertion that the 475 kg/m^3 with thicknesses equal to or above 250 mm would provide superior insulation properties compared to the others.

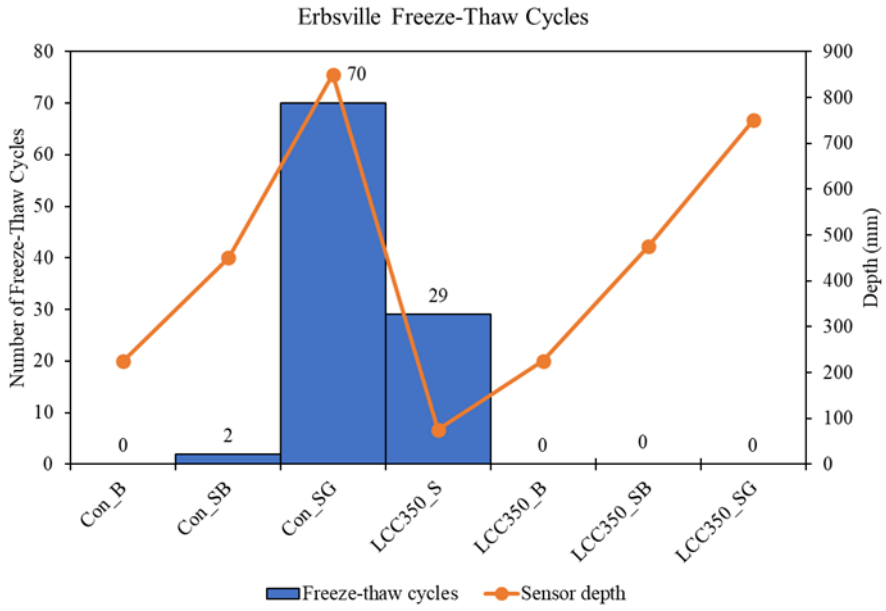

Figure 6.6: Erbsville layer freeze-thaw cycles (Nov 15, 2018 to Jan 14, 2022)

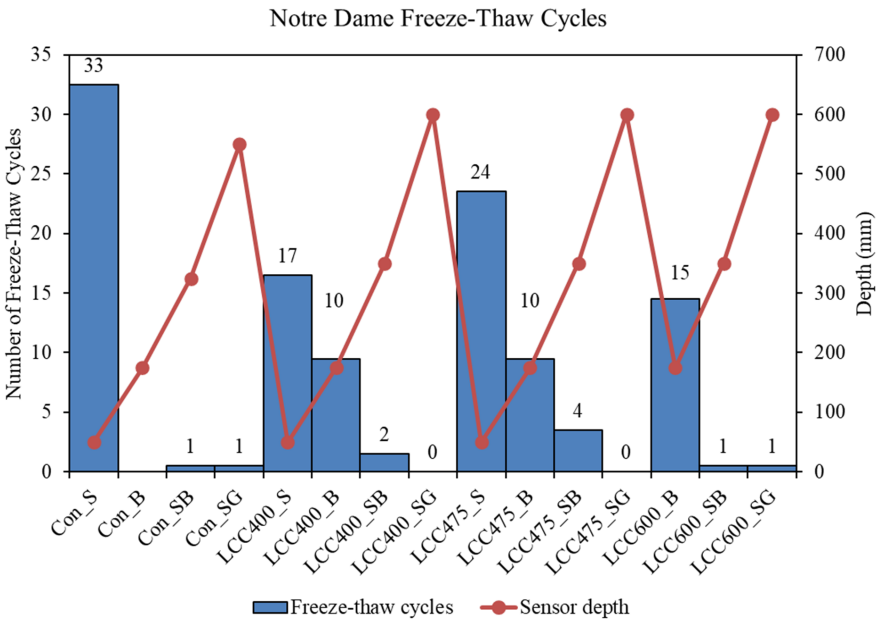

Figure 6.7: Notre Dame Drive layer freeze-thaw cycles (Jul 17, 2021 to Jun 8, 2022)

6.3.3 General Temperature Model

Introduction

Pavement temperature is an important property determining future pavement performance. Although this can be assessed on-site using instrumentation embedded in the pavement layer, doing so is frequently impractical due to the expense [14], labor, and technical constraints. To overcome this challenge, developing theoretical or empirical temperature prediction models may be helpful for quickly and cheaply acquiring information on the actual pavement temperature [164]. Pavement layer temperature determining factors must be considered to do this. Numerous factors influence the temperature of the pavement layer, according to earlier research factors such as ambient temperature, seasonal fluctuations (heating and cooling trends effect), solar radiation, wind speed, pavement surface reflectivity, relative air humidity, heat convection, and heat diffusion [61, 5, 114].

Rumney and Jimenez [213] created a pavement surface and 50 mm depths nomograph in 1969 to establish pavement layer temperature. They used pavement and hourly solar radiation data from desert areas to forecast temperature. Using these data, heat transmission, and energy balance at the pavement surface, a simulation model was created in 1970

by [60]. Furthermore, due to the Strategic Highway Research Program (SHRP) establishing the LTPP program in 1987 and a subset Seasonal Monitoring Program (SMP) in 1994 consisting of 61 LTPP sites to precisely monitor the effects of temperature and moisture variation on pavement performance, several pavement temperature models were developed [35, 151].

Also, analytical approaches using heat transfer models, regression-based models, and computer simulation models have been employed to predict pavement temperature at various times and depths [35, 157, 190]. More research further determined that daily maximum and minimum pavement temperatures can be predicted when given daily maximum and minimum ambient temperature, day of the year, and desired pavement depth for temperature [61]. Their study also verified that temperatures predicted using daily solar radiation could be applied to any location. The study aimed to extend existing models from the Virginia smart road to other places by introducing daily solar radiation that can be calculated for any site to predict asphalt layer temperature. This research considered three depths within the asphalt concrete layer.

A linear regression model was used to determine the pavement's minimum surface temperature from ambient temperature [192]. Using another regression-based equation, they used the estimated parameter further to predict the depth of frost penetration through the pavement. Also, the impact of ambient temperature on the temperature distribution for rigid pavement slabs was examined by [208]. They demonstrated that using a sinusoidal prediction function in their created numerical model to estimate the ambient temperature produced good results.

In Canada, Asefzadeh, Hashemian, and Bayat [14] developed an empirical statistical pavement model to predict the average daily temperature for cold and warm seasons and maximum and minimum pavement temperature at any depth for the surface layer. They used two years of data considering ambient air temperature, solar radiation, wind speed, and relative air humidity as input parameters. They found that the model provided satisfactory results in predicting pavement surface temperature. Segui et al., [223] developed a prediction model for foamed glass aggregate used as an insulating layer in Canada. The design was performed using the Chaussée2 software, with the results from this calibrated with field data to develop the thermal model. They found that FGA could be an effective alternative to extruded polystyrene. However, with limited data in their study, more conclusions could not be drawn.

As established, numerous temperature models have been developed for the typical flexible pavement structure, all of which have their strengths and limitations. Some of these models are very complicated and typically require a lot of input data which could be

impractical in the field. Also, most of these models have focused mainly on predicting pavement surface temperature. Moreover, no model has been developed and validated when lightweight cellular concrete is incorporated as a flexible pavement subbase layer. Knowing LCC layer pavement thermal characteristics could be beneficial in determining in situ LCC pavement performance and further evaluating its insulation properties within the pavement structure. This study seeks to develop temperature models for the typical four flexible pavement layers in Canada and for layers of LCC subbase flexible pavements.

Model Development

A statistical linear regression temperature model was developed using the Erbsville data. Since over three years of data was available for Erbsville, the first two years (November 15, 2018, to November 14, 2020) were used for calibrating the model, while the third plus year (November 15, 2020, to January 14, 2022) was used for validation. Both hourly and daily average temperature data were used for the validation process. Linear regression models were chosen because they combine high accuracy with ease of use [61]. The pavement temperature was measured at four depths: the surface, base, subbase, and subgrade layer. All data processing and analysis were carried out in R v.4.2.1 [240].

The relationship between layer temperature and environmental factors such as moisture and ambient temperature were assessed using a generalized additive model (GAM, Appendix C) with the restricted maximum likelihood smoothing method (n= 156,993, from two years of data). The GAM determined that layer moisture and ambient temperature were significant predictors of layer temperature, accounting for 75.7% of the variability in hourly layer temperature (adj. $R^2 = 0.76$). However, layer moisture has been excluded from the temperature model as the type of moisture sensor used only indicated the moisture level within the layer (Soil Water Potential) and not its volumetric quantity.

Before developing a predictive model, ANOVA was performed to determine if the Control and LCC section's layer temperature differed for the two-year duration calibration data. The result showed that the Control and LCC350 base were statistically the same (p=0.998) at a 95% confidence level. Similarly, the Control base and subbase ($p = 0.964$), LCC350 base and Control subbase ($p = 0.999$), LCC350 surface and Control subgrade ($p = 0.741$), and the LCC350 subgrade and LCC350 subbase ($p = 0.834$) were the same.

Figure 6.8 presents the regression analysis plot between layer and ambient temperature for the calibration period, while Table 6.3 provides the statistical prediction equations and the corresponding parameters. The color for the data points represents the season when it was measured. The regression analysis findings are in line with earlier conclusions that

Table 6.3: Regression parameters for ambient temperature vs. layer temperature

Section	Location	Depth (mm)	Equation	R^2	P_{value}	RMSE
Control	Base	175	y = 6.5 + 0.75x	0.75	0.001	7.14
	Subbase	525	y = 6.1 + 0.81x	0.77	0.001	7.05
	Subgrade	850	y = 5.2 + 0.99x	0.83	0.001	7.62
LCC350	Surface	75	y = 4.9 + x	0.8	0.001	7.52
	Base	175	y = 6.7 + 0.72x	0.76	0.001	7.09
	Subbase	475	y = 8 + 0.52x	0.65	0.001	7.96
	Subgrade	750	y = 8.2 + 0.49x	0.63	0.001	8.15

show the subbase and subgrade of the LCC layers (R^2 of 0.65 and 0.63) are less influenced by ambient temperature compared with the Control section's (R^2 0.77 and 0.83) even though there is a positive relationship between these layers and ambient temperature.

Model Validation

Results from validation with average daily ambient and layer temperature is presented in Figure 6.9. The models showed excellent predictive capacity by accurately predicting temperatures over 80% (Root Mean Square Error (RMSE) 3.64 °C to 4 °C) of the time for all the layers except the LCC350 subbase and subgrade, where an R^2 value of 0.72 and 0.68 and RMSE 3.79 °C and 3.81 °C of were achieved. This is expected as the effect of ambient temperature on the LCC subbase and subgrade was not as strong as in the other layers.

Further validation was also performed using hourly temperature (Appendix A). The linear regression models accurately predicted hourly temperature for the Control's surface, base and subbase layers, and the surface of the LCC350 over 70% of the time ($R^2 > 0.70$, RMSE; 4.03 °C – 5.31 °C). Although less predictive ability was noted for the subbase and subgrade of the LCC350, over 60% of the time, hourly predictions were accurate. Overall, the regression model was more effective in predicting average daily temperature than hourly temperature, which includes another layer of detail going into a micro-scale. This linear regression model can also be beneficial in predicting layer minimum and maximum temperature, as calibration was done using data collected every five minutes aggregated to hourly temperatures.

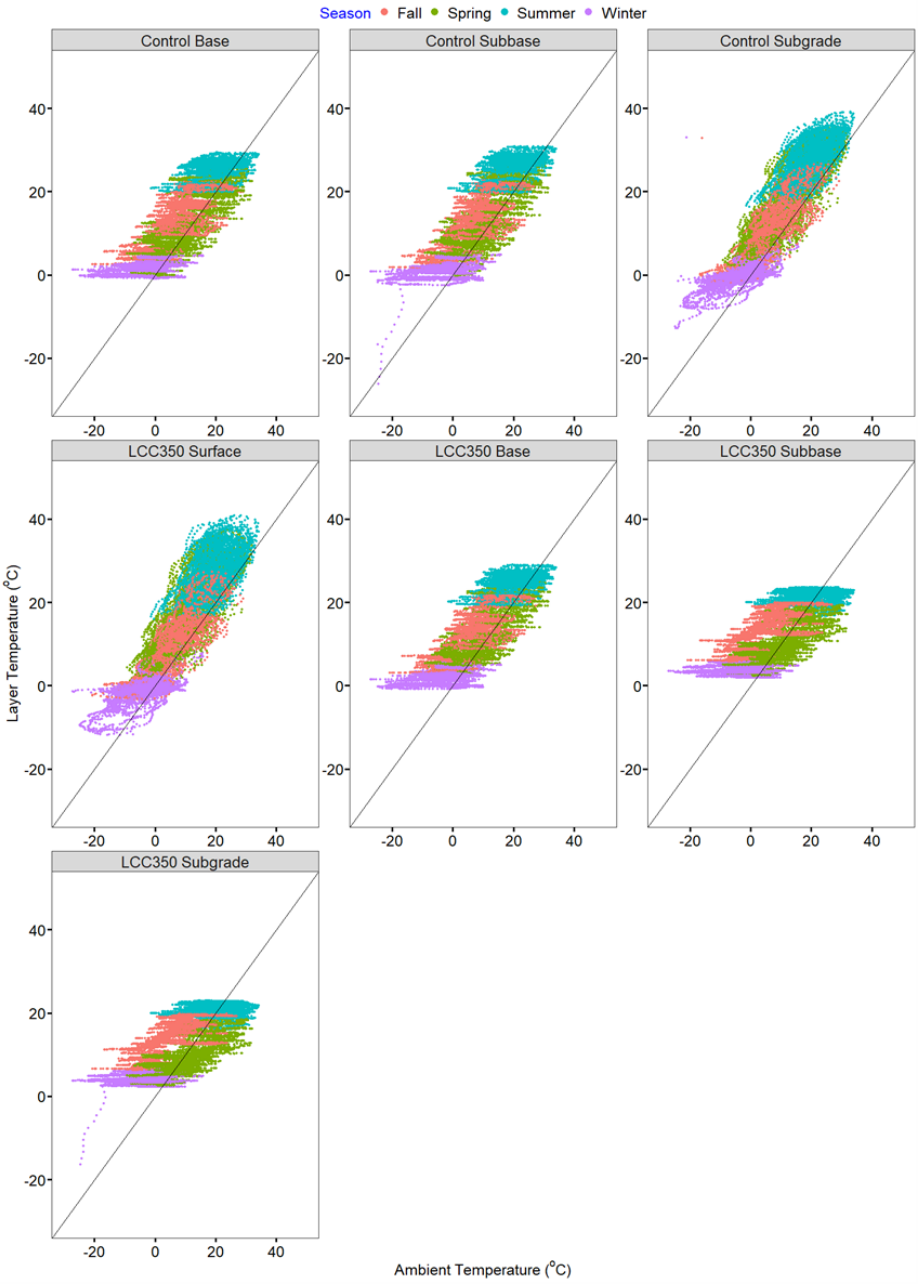

Figure 6.8: Relationship between ambient temperature and layer temperature

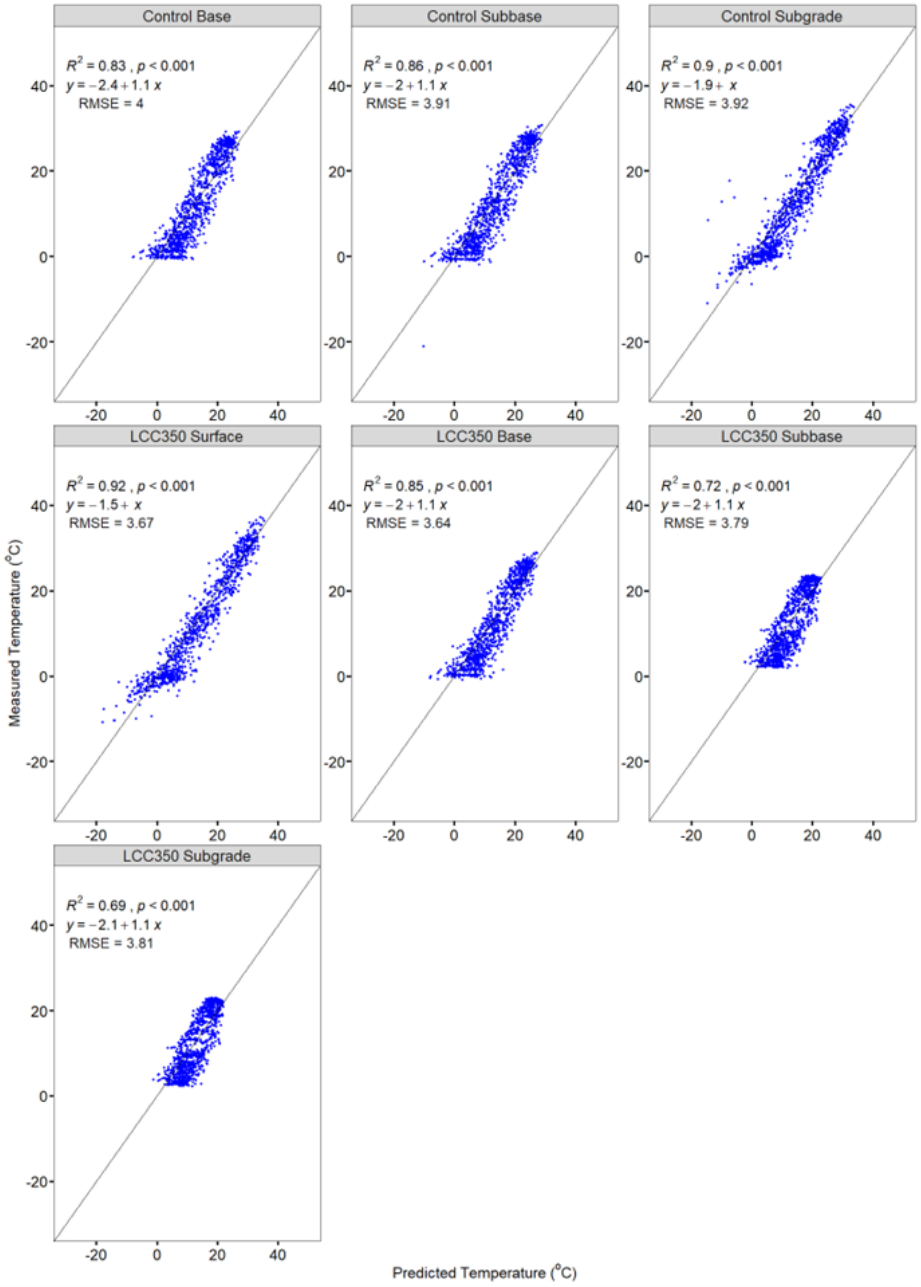

Figure 6.9: Validation for layer temperature using ambient vs. daily average layer temperature

In assessing predictability for other locations and depths, the model was used in predicting the Notre Dame Drive Control and LCC475 section layer temperatures. The outcome is presented in Figure 6.10, including the respective R^2 and Root Mean Square Error (RMSE) values. The certainty was very good, with most layer temperatures predicted accurately over 80% of the time except for the LCC475 subgrade temperature, which was predicted 66% of the time.

The model also predicted the temperature within the other LCC density layers. The results are presented in Table 6.4. The outcome revealed similar findings to the LCC475, with most layers accurately predicted over 80% of the time except the subgrade. This means this equation could be used to predict temperature within LCC pavements with densities between 400 and 600 kg/m^3.

Table 6.4: Validation of LCC400 and LCC600 layer temperature

Layer	**LCC400**		**LCC600**	
	R^2	**RMSE (°C)**	**R^2**	**RMSE (°C)**
Surface	0.90	4.57	-	-
Base	0.89	5.30	0.90	5.54
Subbase	0.85	4.45	0.86	5.03
Subgrade	0.69	6.74	0.72	7.33

In conclusion, the developed equations could determine temperatures within pavement layers for the typical unbound granular and LCC flexible pavements. It is envisaged that utilizing the pavement temperature profile, the models presented would help calculate in situ pavement engineering characteristics. Additionally, by projecting future pavement temperatures using ambient temperature trends from past data, these models can be employed to predict pavement service life and performance (via critical temperature exposure durations).

6.3.4 Seasonal Effect on Layer Temperature

The extent to which ambient temperature influenced pavement temperature during various seasons was also studied. The season was classified based on the typical classification in Canada and followed this order. Winter from December 22 to March 20, Spring from

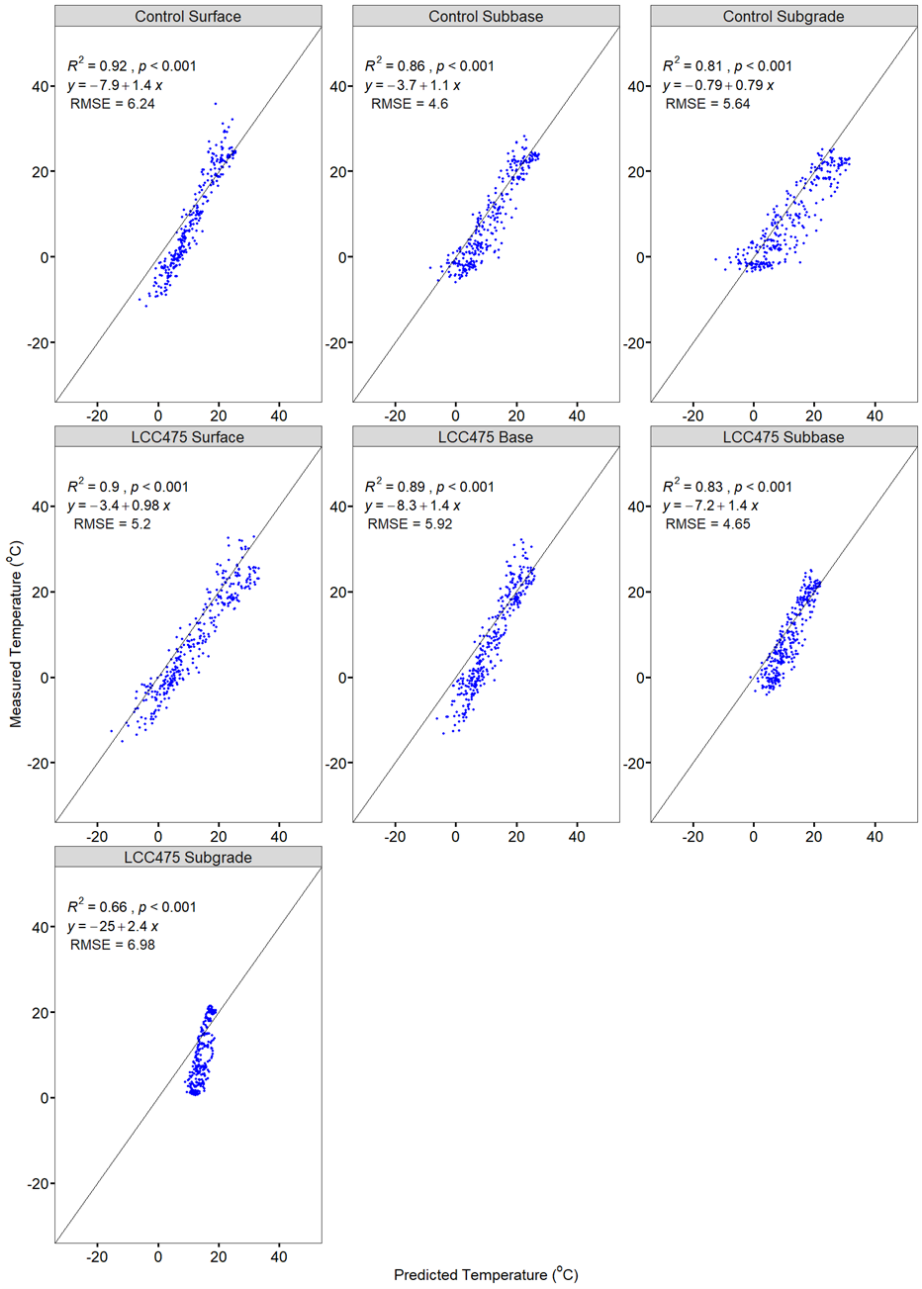

Figure 6.10: Validation for Notre Dame Drive average daily layer temperature using temperature model

March 21 to June 21, Summer from June 23 to September 23, and Fall from September 24 to December 21. The two-year calibration data from Erbsville was used in this analysis.

ANOVA showed a significant difference (P-value = 0.000) between layer temperature for different seasons at a 95% confidence level. To examine which seasons were significantly different, the Tukey ANOVA was performed. Tukey ANOVA analysis showed that the measured temperature for all the sections differed for all seasons.

The results of the seasonal relationship utilizing hourly temperature data are shown in Table 6.5. The findings show that in the fall and spring, there is a higher correlation between the ambient temperature and pavement layer temperature. The link between ambient and layer temperature is weaker when winter and summer are considered. This is remarkably accurate for the LCC's subbase and subgrade, where a weak relationship was found. As a result, higher ambient temperatures may significantly affect LCC subgrade temperatures more than lower ambient temperatures, which is a sign of the material's insulating capabilities. This could also mean that the LCC layer's insulating characteristics are primarily seen in the winter and summer.

Table 6.5: Seasonal relationship between ambient and layer temperature

Section	**Layer**	**Fall**		**Winter**		**Spring**		**Summer**	
		R^2	**RMSE (°C)**	**R^2**	**RMSE (°C)**	**R^2**	**RMSE (°C)**	**R^2**	**RMSE (°C)**
Control	Base	0.60	7.89	0.11	7.52	0.53	5.83	0.17	7.20
	Subbase	0.61	7.35	0.16	7.04	0.55	6.04	0.19	7.67
	Subgrade	0.73	6.74	0.46	7.25	0.67	6.92	0.33	9.23
LCC350	Surface	0.71	5.27	0.41	5.36	0.61	8.02	0.19	10.10
	Base	0.61	7.91	0.12	7.75	0.56	5.76	0.19	6.77
	Subbase	0.55	9.90	0.03	9.52	0.51	5.79	0.02	5.86
	Subgrade	0.55	10.20	0.04	9.77	0.50	5.90	0.00	5.87

6.3.5 Heating and Cooling Effect on Layer Temperature

Daily and Nightly temperature assessments were also performed. This illustrates the daily periods of heating and cooling. In contrast to the summer, spring, and fall, when pavement heating occurs from 10 a.m. to 9 p.m. and cooling from 10 p.m. to 9 a.m., in the winter, the pavement experiences heating from 1 p.m. to 6 p.m. and cooling from 7 p.m. to 12

noon. The heating and cooling time were established by observing the daily temperature trend for the LCC350 surface layer during each season and getting points for the onset of daily increases and decreases in pavement temperature (Figure 6.11). The maximum and minimum layer temperatures might also be simulated with this. This was also done to comprehend how the ambient temperature affected LCC pavements during the day and at night. This investigation utilized the hourly calibration data for the previous two years.

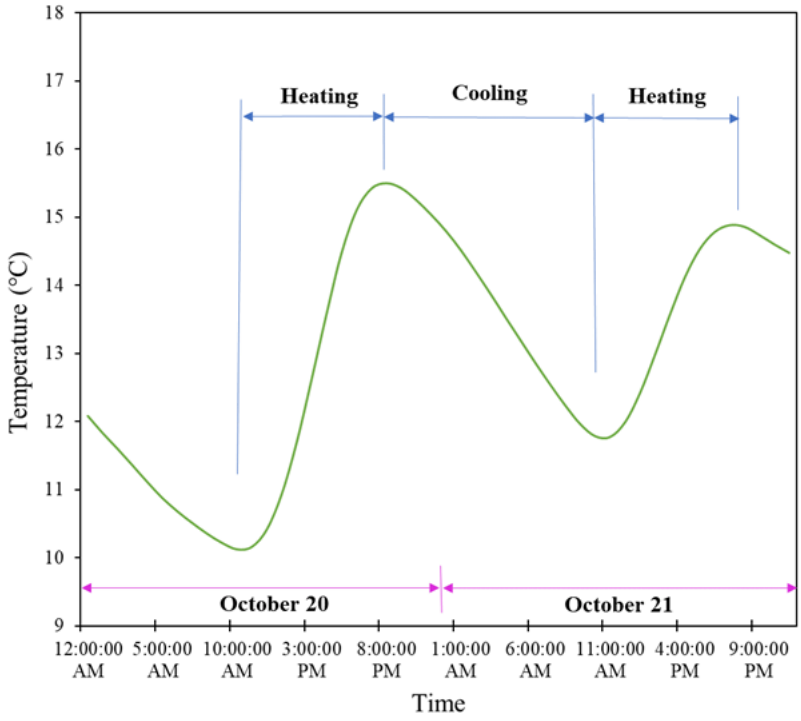

Figure 6.11: Pavement fall season daily surface layer heating and cooling profile

Table 6.6 presents the regression results for the heating period evaluation and Table 6.7. shows the cooling period regression results. The results show that over 70% of the time, in both cases, the Control pavement layers and LCC350 surface and base layer heating and cooling temperatures could be determined by ambient temperature. However, the relationship was weaker in both cases for the LCC350 subbase and subgrade. Nevertheless, based on R^2 values, the cooling period temperatures had a more substantial relationship for these LCC350 layers than the heating period. This was also the case for all the other LCC350 and Control layers. Compared to the heating, a stronger correlation was seen between ambient and layer temperatures during the cooling period.

Table 6.6: Hourly heating period regression results

Section	Location	Heating Period Equation	R^2	P_{value}	RMSE
Control	Base	y = 7.2 + 0.76x	0.72	0.001	7.42
	Subbase	y = 6.8 + 0.81x	0.74	0.001	7.37
	Subgrade	y = 6.3 + x	0.83	0.001	8.16
LCC350	Surface	y = 5.3 +1.1 x	0.86	0.001	7.66
	Base	y = 7.4 + 0.73x	0.74	0.001	7.20
	Subbase	y = 8.7 + 0.52x	0.62	0.001	7.83
	Subgrade	y = 8.9 + 0.48x	0.58	0.001	7.99

Table 6.7: Hourly cooling period regression results

Section	Location	Cooling Period Equation	R^2	P_{value}	RMSE
Control	Base	y = 5.9 + 0.52x	0.77	0.001	6.77
	Subbase	y = 5.6 + 0.81x	0.79	0.001	6.68
	Subgrade	y = 4.1 + 0.97x	0.88	0.001	6.70
LCC350	Surface	y = 3.9 +1.1 x	0.89	0.001	6.05
	Base	y = 6.2 + 0.73x	0.78	0.001	6.73
	Subbase	y = 7.6 + 0.52x	0.67	0.001	7.86
	Subgrade	y = 7.8 + 0.49x	0.65	0.001	8.11

6.4 Environmental Effect on Pavement Moisture

Precipitation is one of the most crucial factors determining moisture content fluctuation in warm, humid areas, with its impact decreasing with depth [97]. In contrast, temperature variation rather than precipitation determines how much moisture is present in cold, dry places [107]. Huang et al.'s [107] study found that according to the observed trend, the moisture content dropped in the fall, remained low throughout the winter, and then increased in the spring, while all summer long, there was a lot of moisture present. Barbi et al., [30] also showed that while a pavement structure's design was not greatly impacted by temperature alone, it was significantly impacted by a rise in moisture levels brought on by climate change. However, the effects of temperature alone may be much more pronounced in areas where permafrost was thawing.

A study by Hedayati and Hossain [97] in assessing subgrade moisture variation due

to rainfall events found that moisture variation occurred due to a combined seasonal and temporal variation. Seasonal variation accounted for ±5% moisture variation, while temporal, which was a result mainly of rainfall events, caused a 12% variation in soil moisture. They suggested that this abrupt rise in volumetric moisture content might result in a large recharacterization of the soil since significant changes in the characteristics of unsaturated soil occur at moisture values near or at saturation. They further developed a real-time-based model using two-year moisture and rainfall events for North Texas and found the model had a good prediction of moisture variability.

Since roadbed materials' resilient modulus, shear strength, permeability, and volume change vary with moisture content [70] [83] [253], moisture within the pavement layers plays a significant role in the deterioration of the pavement structures. Unanticipated changes in soil properties can reduce the useful lifespan of infrastructure and cause severe distress to buried or soil-supported structures such as pavements. A better knowledge of the variations in soil characteristics and the long-term serviceability of pavements can be obtained by estimating patterns of moisture change [97]. Hence a study of moisture variation of LCC subbase and typical unbound subbase flexible pavements is vital to determine its performance over time.

The moisture sensors within the pavements at Erbsville and Notre Dame Drive were installed at the exact location as the corresponding layers' temperature sensor (Table 6.2), at the mid-point of each base and subbase layer, and at a depth $\geq$ 100 mm below the top of the subgrade for each section. At Erbsville, moisture levels within the layers for all the sections throughout the study period indicated saturated or near-saturated conditions (most times, values were close to zero). In contrast, at Notre Dame Drive, more fluctuation in moisture levels was noted. The water table at Erbsville may be relatively high, hence the reason for primarily saturated conditions.

Figure 6.12 illustrates layer moisture and location precipitation details from November 2018 to May 2019 at Erbsville to help understand the impact of precipitation on pavement moisture levels. Moisture levels for the study period are presented in Appendix A. Precipitation events resulted in moisture layer variation. All the sections' moisture levels exhibited a similar pattern until May 2019, albeit the subgrade in the Control section had significantly more variability. After May 2019, it was discovered that the soil water potential (SWP) of the base layer had the same pattern across all sections. While the SWP of the subbase and subgrade in the Control section maintained the same trajectory as its base layer, it deviated from the trend and fell to almost zero in the LCC sections. Average subgrade and subbase moisture levels were lower in the Control section, respectively, by 1.3 and 1.5 times than in the LCC350 section and by 1.4 and 1.6 times than in the LCC250 section. Due to higher temperatures occurring from March in conjunction

with precipitation events, there is the possibility of thawing frozen water in the surface and base layers which could have percolated down to the lower layers for all the sections. Since LCC is less permeable than granular material, this could explain why the SWP in the LCC layer kept decreasing as water could be trapped within the layers. However, the granular B layer's propensity to drain could explain the more significant variability in its SWP, which remained higher than that of the LCC sections. This demonstrates that water was gradually draining from the subbase and subgrade layers in the Control portion. Like Huang et al., (2021) [107] study, the results from Erbsville indicated that temperature variations predominantly influenced moisture levels during the winter.

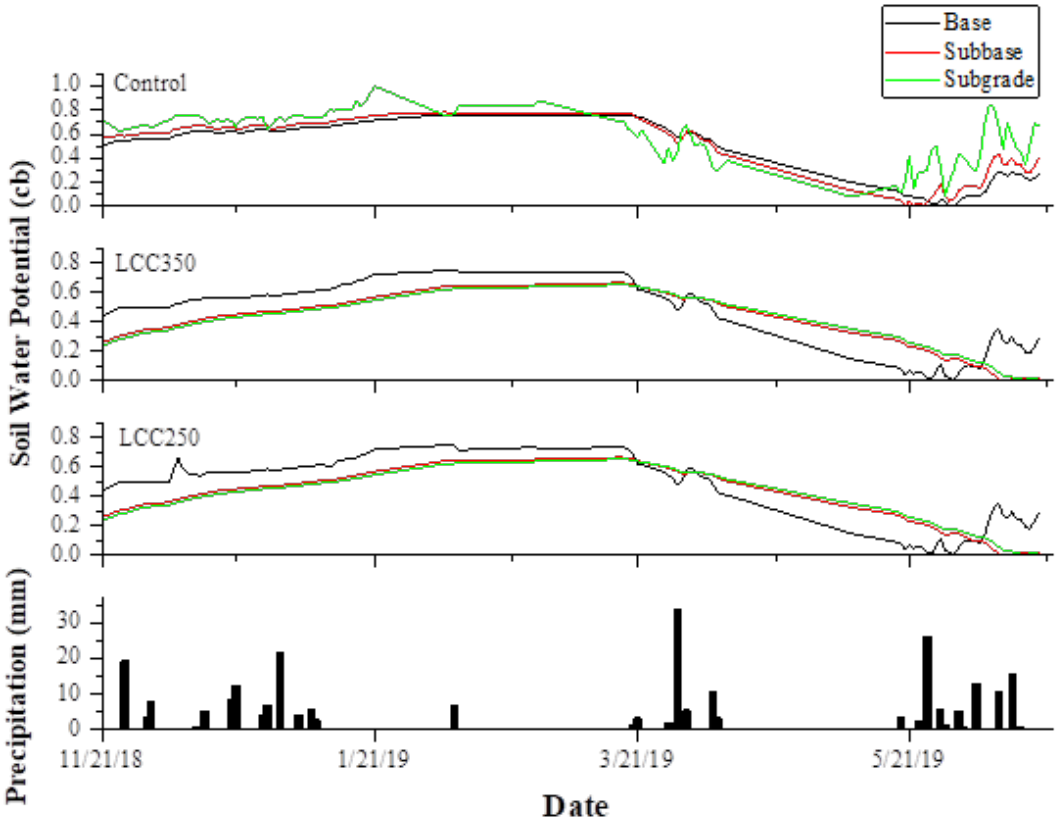

Figure 6.12: Erbsville daily precipitation and moisture profile

A similar trend like Erbsville, where moisture variation was noted after precipitation events, was also observed at Notre Dame. Figure 6.13 provides the general precipitation trend. Most of the time, the base layer for all sections had the least moisture and

experienced greater water drainage away from the layer compared with the subbase and subgrade. The subgrade of the Control was the most saturated compared with the others. The LCC400 subbase also had the least moisture throughout the study period. The Control and other LCC sections subbase alternated moisture variability content from time to time. Overall, the LCC400 base and subbase have the least moisture, and the effect of drain ability after precipitation events was greater in this section compared with the others. Similarly, like Erbsville, in the winter, moisture levels were predominantly determined by the temperature, and it appeared that the material around the sensors was frozen or moisture at this time couldn't be appropriately captured by the sensors due to subzero temperatures.

In further investigating the effect of precipitation on moisture behavior of different LCC densities, two periods of lots of rainfall were selected before and after the winter period at Notre Dame Drive (Figure 6.14). Also, like Erbsville, after the winter into the spring thaw period, the LCC layers had slightly higher moisture content than the Control. The same reasoning is that due to higher temperatures occurring from March in conjunction with precipitation events, there is the possibility of thawing of frozen water in the surface and base layers which could have percolated down to the lower layers for all the sections. Since LCC is less permeable than granular material, this could explain why the SWP in the LCC layer was slightly lower as water could be trapped within the layers.

In October 2021, the Control section's base layer moisture was 49 times, 11 times, and 15 times more than the LCC400, LCC475, and LCC600 sections, while its subbase was ten times more than the LCC400 section and 1.6 and 1.3 times less than LCC475 and LCC600 sections. However, for the subgrade, a reverse case was noted. The moisture content was higher in the LCC400 section by three times than in the Control but twice lower in the LCC475 and LCC600 sections than in the Control. This implies that the LCC475 and LCC600 offered the most protection to the subgrade from moisture than the Control and LCC400 sections at this time.

In May 2022, during the spring, the Control sections' base moisture was slightly lower by 3, 6, and 3 times than the LCC400, LCC475, and LCC600 sections, while its subbase was 2 and 3 times lower than LCC475 and LCC600 sections, but three times higher than LCC400 subbase. In this scenario, the controls' subgrade moisture was like the LCC475 section, yet two times higher than the LCC400 and LCC600 sections.

In conclusion, the LCC400 showed the least moisture content in the base and subbase than the other sections most of the time. However, the LCC475 and LCC600 sections provided more protection for the subgrade than LCC400 and Control sections. In addition, the observed trend showed that moisture content often decreased in the fall, stayed low

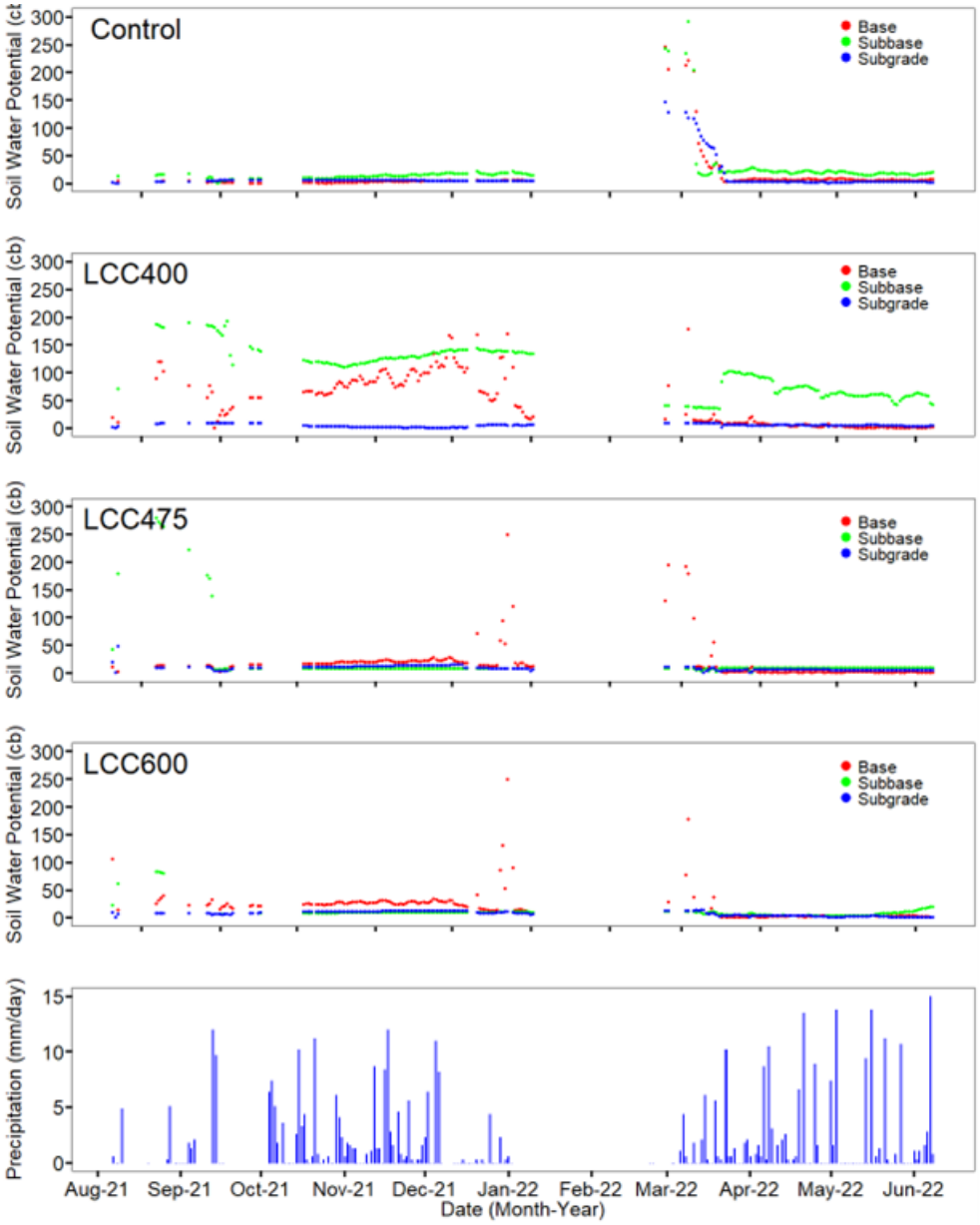

Figure 6.13: Notre Dame Drive daily precipitation and moisture profile

throughout the winter, and then increased in the spring, whereas moisture levels were high throughout the summer. These findings are comparable to the work by Huang et al., [107].

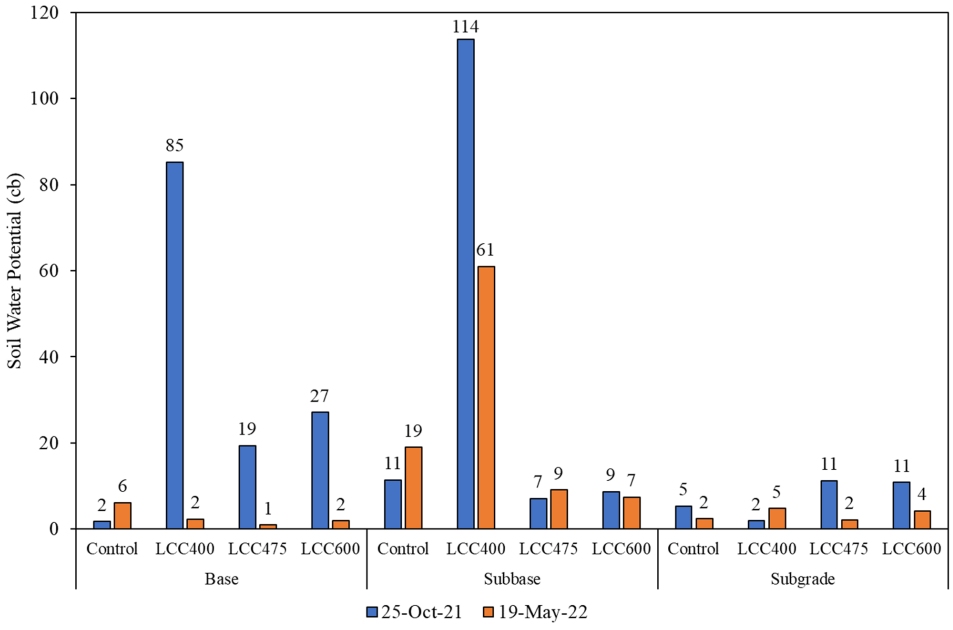

Figure 6.14: Notre Dame layer moisture in October 2021 and May 2022

6.5 Environmental Effect on Pavement Strain

Even though there are a few LCC implementations in road construction, complete post-construction performance test methods and evaluations are still lacking. In addition to questions about how to measure its thermal insulation, freeze-thawing resistance, and stability, it is also essential to understand how LCC contributes to the prevention of rutting, surface cracks, and their elongation and whether the presence of LCC in the subbase influences pavement performance indicators. Factors such as poor subgrade, freeze-thaw cycle fluctuations, inadequate compaction, constructability concerns, and a higher frequency of traffic loads influence rutting and cracking failure mechanisms in flexible pavements [254]. These flaws can endanger people's lives [234]. Critical stresses and strains are considered during design to account for such failures. The tensile strain at the bottom of the surface layer, the deflection at the top of the surface layer, and the vertical compressive stress at the top of the subgrade are all considered for flexible pavements [106].

A critical response that could be utilized to estimate the fatigue life of a pavement is its strain [191]. In colder climates, where pavements frequently become saturated during the spring thaw and the stiffness modulus of the granular layer drops, this strain is a significant

factor [106, 216, 217]. Layer temperature and moisture have been shown to influence the amount of strain experienced within the pavement layers. Salour and Erlingsson (2014) [218] showed that when the groundwater table level was elevated from 2.5 to 1.0 m below the road surface, the estimated strain at the bottom of the AC layer rose by 34%. Likewise, Saevarsdottir and Erlingsson (2013) [214] demonstrated that measured tensile strain at the bituminous base's bottom increased dramatically as the groundwater table ascended from a considerable depth to 30 cm below the subgrade surface. Similar to how changes in the base and subgrade moisture content affect the stiffness of those layers of the pavement system, they can similarly raise strains in the AC layer by lowering the amount of support available [274]. Furthermore, at higher temperatures, asphalt softens and is more susceptible to larger horizontal strains at the base of the asphalt layers [152, 106, 71].

Various models have been employed to determine these critical pavement responses. They have been noted to provide results that could be used to validate the applicability of different pavement design options [248]. For example, KENLAYER and WESLEA calculate these critical structural reactions using the multi-layer linear elastic theory, axle loads, and pavement layer parameters. In addition to axle load distribution and material properties, mechanistic-empirical models, such as the mechanistic-empirical pavement design guide (MEPDG) developed under NCHRP Project 1-37A, use climatic factors to predict pavement performance [207, 7]. On the other hand, the in-situ measuring approach has become a popular way to examine pavement structural dynamic behaviour because it bypasses the limitations of theoretical analysis by revealing the pavement structure's actual stress and strain responses right away [4].

Several full-scale instrumentation field sections have been constructed globally, especially in North America, to monitor the actual response of road pavement layers to various factors influencing their performance. Some of these full-scale instrumented sections include the Penn state test track, National Center for Asphalt Technology (NCAT) Test Track, Minnesota Road Research Project (MnRoad), Virginia Smart Road, Ohio Test Track, the Superpave in situ stress/strain investigation sponsored by the Pennsylvania Department of Transportation, and the Center for Pavement and Transportation Technology (CPATT) test track in Waterloo, Ontario [31, 4]. However, none of these studies have examined instrumented pavement sections with LCC as the subbase layer. Because the specific material qualities of each layer can affect the overall pavement structure's response to varied conditions, it is critical to keep track of how these LCC subbase pavements are performing. These findings will aid pavement design, performance forecasts, and maintenance planning for LCC pavements.

6.5.1 Daily Heating and Cooling Effect on Strain

Notre Dame Drive

Figure 6.15 shows the longitudinal strain and ambient temperature variation beneath the asphalt layer over five days for Notre Dame Drive. The positive strain denotes compression and the negative strain tension within the layers. There is a cyclic change in surface temperature for all sections. The measured strain was noted to begin to move into a compressive state when the heating period starts from about 9 am and peaks at about 5 pm, when it begins to drop into a tensile state till 9 am the next day, which signifies the cooling period. This pattern continues daily over the five days studied, hence a cyclic changing pattern in strain. This heating and cooling effect occurs because the sun's heat is absorbed by the pavement surface and transferred to the cooler material underneath during the day. This process is reversed at night when the heat is transferred to the air via the surface material, which absorbs it from below. Precipitation within this period was 2.54 mm on October 15 and 10.16 mm on 16. Between October 4 and 11, there was rainfall almost every day to a total of 30.27 mm.

On October 11, the longitudinal strain beneath the asphalt layer of the Control section decreased to 1,027 $\mu\varepsilon$ (in compression) when the temperature increased to 24 °C. In contrast, the longitudinal strain increased to 2,203 $\mu\varepsilon$ (in tension) when the temperature decreased to 15 °C. A similar trend was noted for the LCC sections, but with lower magnitudes compared with the Control. The Control at lower daily temperature experienced 93%, 53%, and 55% more strain than the LCC400, LCC475, and LCC600 sections. While at the highest daily temperature, it saw 40%, 64%, and 31% higher longitudinal strains than the LCC400, LCC475, and LCC600 sections. Overall, longitudinal strain increased (towards tension) when layer temperature decreased and decreased (towards compression) when layer temperature increased.

The LCC475 section experienced the least daily longitudinal strain variation at higher temperatures. It had 39% and 47% lower longitudinal strain at high temperatures than LCC400 and LCC600. While at lower temperatures, the LCC400 section had 84% lower longitudinal strain than the LCC475 and LCC600 sections. Since the LCC400 sections' asphalt layer had lower moisture (SWP $>$ 100 cb) in its base and subbase layers at this time, it is possible that at lower temperatures, there was more moisture in the asphalt layers of the LCC475, LCC600, and Control sections (SWP $<$ 10 cb) base and subbase, which could have resulted in higher strain levels within the layers. During cooler periods, suction effects would cause moisture content to rise; hence where moisture is existent, weaker layers occur; therefore, higher strains are induced. Whereas, due to higher temperatures in the

middle of the day, evaporation is more and thus lower moisture levels within the layers [137]. Kodippily et al. (2018) [137] also found that at the end of the day (cooling period), when the soil moisture increased, there was a sudden increase in measured longitudinal strain for the base layer. At this time, the Control could be experiencing higher strains because its base layer was mostly saturated (0 cb).

As layer temperature cyclic amplitude decreased between October 12 - 13, the longitudinal strain amplitude (peak to peak strain) for all the sections also reduced. This peak-to-peak strain can be referred to as thermal strain as it develops due to thermal expansion and contraction [134]. The thermal strain reduction corresponded with times of no rainfall, hence a decrease in layer moisture, which could have resulted in temperature and strain behavior change. While the thermal strain change due to heating and cooling were 1,176 $\mu\varepsilon$, 1,398 $\mu\varepsilon$, 1,289 $\mu\varepsilon$, and 1,058 $\mu\varepsilon$, signifying a 53%, 106%, 160%, and 70% change for the Control, LCC400, LCC475 and LCC600 prior and after October 12 and 13, the changes were 31%, 67%,122%, and 47% respectively on these days. The maximum daily thermal strain change was seen in the LCC400 section, then LCC475, Control, and LCC600 accordingly.

While daily strain change in October (fall) was seen to be lower in the morning (9 am) by 2.1, 17.4, 1.7, and 3.3 times for the Control, LCC400, LCC475, and LCC600 than in the afternoon (5 pm), this factor was 1.3, 1.4, 1.5 and 1.4 for the Control, LCC400, LCC475 and LCC600 in the winter (February). In the spring (April), it was 2.3, 5.6, 2.9, and 2.5 for the Control, LCC400, LCC475, and LCC600. A similar daily pattern as described for the fall was noted across other seasons except for the LCC400, which had the most strains for the winter. It can be observed that the factor is greater in spring than in fall and winter, except for LCC400. The winter had the lowest factor.

In the subbase layer, soil water potential for the LCC400 section during this period ranged from 113 to 119 cb; this meant the layer was quite dry. However, wet conditions were noted in the other sections, with the LCC475 SWP remaining around 7 ($\pm$0.2), LCC600 around 8 cb ($\pm$0.5), and the Control SWP between 8 and 10 cb. Figure 6.16 shows the daily longitudinal strain variation beneath the subbase layer for all the sections with the subbase temperature. The Control, LCC475, and LCC600 sections strains were somewhat influenced by temperature; however, the LCC400 does not appear to be. While there was a clear correlation between LCC600 and layer temperature, the influence of layer temperature on LCC475 and the Control is not so pronounced, although the trend variation was observed. The erratic strain response beneath the subbase of these sections appeared to be influenced by the moisture variation within these layers, especially the LCC475 section, where most of the time, an increase in moisture was seen to cause a decrease in strain. However, this phenomenon is not apparent. Traffic could also be another factor influencing

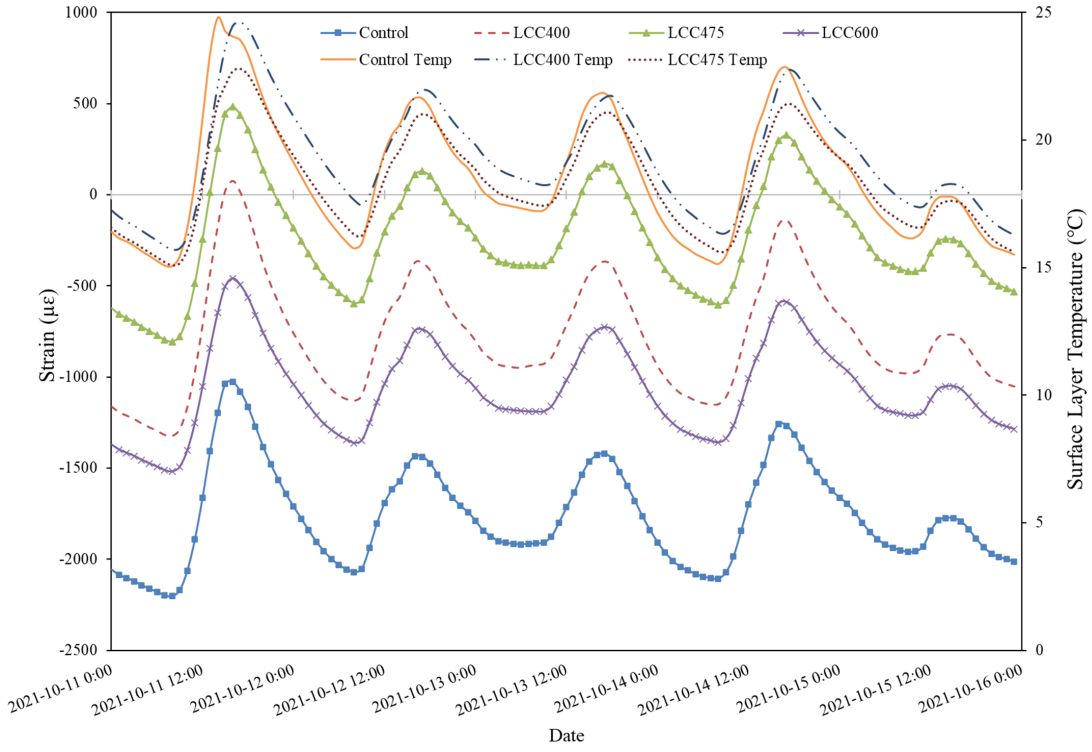

Figure 6.15: Notre Dame Drive daily heating and cooling effect on longitudinal strain beneath asphalt layer

the LCC475 subbase strain. This could explain more variability in the LCC475 section compared with LCC600.

Contrary to what was happening beneath the asphalt layer, longitudinal strain increased (towards tension) beneath the subbase as layer temperature increased. As layer temperature decreased, longitudinal strain decreased (towards compression). On October 11, the peak strain magnitude was lowest in the LCC600, 121 and 69 times lower than the Control and LCC sections. The Control section experienced two times more strain than the LCC475. The magnitude of the strain beneath the subbase layer was smaller by 3, 2, and 500 times compared to beneath the asphalt layer for the Control, LCC475, and LCC600. The strain beneath the subbase of the LCC400 section was two times more and continually increased.

Thermal strain change was 0.5 $\mu\varepsilon$, 69 $\mu\varepsilon$, 11 $\mu\varepsilon$ for the Control, LCC475 and LCC600

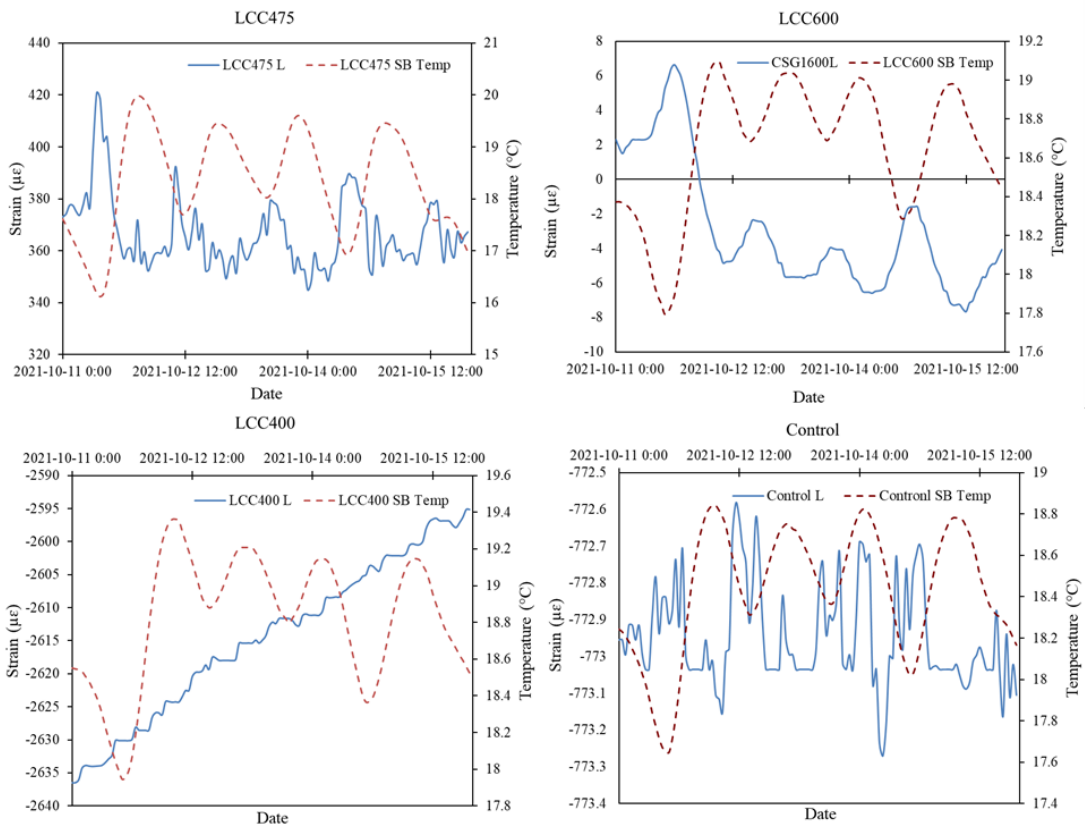

Figure 6.16: Notre Dame Drive daily subbase strain variation

on October 11. Lower thermal strain change was observed like the asphalt layer strains on October 12 and 13. Overall, although longitudinal strain magnitude can be reduced by incorporating 200 mm thick 475 and 600 kg/m^3 LCC material as subbase, this thickness might not effectively limit the daily thermal strains due to contraction and expansion of the subbase material based on these results.

Erbsville

Figure 6.17 presents the daily strain and LCC350 surface layer temperature variation beneath the asphalt layer at Erbsville. There was no strain measurement for the LCC350 section asphalt layer at this time. While a similar trend to the strains at Notre Dame Drive was noted here for the LCC250, where longitudinal strain decreased (towards compression)

as temperature increased, a reverse case was seen in the Control section. In this case, as layer temperature increased, longitudinal strain increased (towards tension). This could be a result of greater thickness which changes the behaviour of the Control section [233]. This could also be a delayed strain response due to the thicker pavement resulting in a slower response. In this case, the pattern like Notre Dame Drive remains but is delayed. Also, SWP was around 0.20 cb for LCC250 and 0.24 to 0.28 cb for the Control.

Like Notre Dame Drive, the measured strain at the LCC250 section began to move into a compressive state when the heating period began from about 9 am and peaked at about 5 pm, when it falls in tension till the next day. The reverse was seen at the Control. Peak-to-peak thermal strain was 5 $\mu\varepsilon$ for LCC250 and 59 $\mu\varepsilon$ for the Control on October 11. Lower thermal strain is also noted on the 12 and 13 due to lower layer temperatures on those days. The daily maximum longitudinal strain for the Control was two times more than the LCC250 section, while the minimum longitudinal strain was 1.5 times more than the LCC250.

Compared to Notre Dame Drive, less longitudinal strain was witnessed at Erbsville's LCC and Control sections. This could be a function of the sections at this location having a thicker pavement structure. Additionally, the subgrade layer at Erbsville is 70% stiffer, providing more support to withstand stresses and strains brought on by traffic and environmental factors.

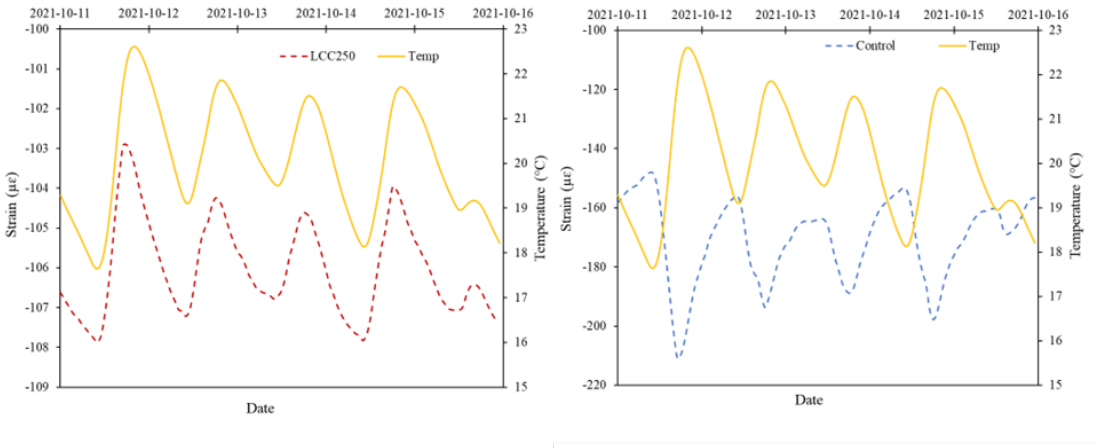

Figure 6.17: Erbsville daily heating and cooling effect on longitudinal strain beneath asphalt layer

The subbase longitudinal daily strain and layer temperature variation for the LCC layers

at Erbsville are shown in Figure 6.18. Temperature variations had a higher impact on strain change closer to the pavement surface. The LCC250 longitudinal strain at the middle (LCC250 LM) and the bottom (LCC250 LB), and LCC350 middle (LCC350 LM) were more influenced by ambient temperature changes than that at the LCC350 LB (bottom). This is because the measured strain depths were 425 mm, 550 mm, and 475 mm for the LCC250 LM, LB, and LCC350 LM respectively, while LCC350 LB was 650 mm beneath the pavement surface.

Unlike Notre Dame Drive, where the LCC layer is 200 mm thick, less impact of ambient temperature on the LCC layer temperature for the LCC350 section (350 mm LCC thickness) is seen. The LCC350 LB longitudinal strain follows its layer temperature trend. Between October 12 and 14, the longitudinal strain was noted to increase as layer temperature constantly increased, although slight daily peak-to-peak variation in longitudinal strain was still noted for longitudinal strain at the middle of both sections and the bottom of LCC250. This thermal strain change was an average of 2 $\mu\varepsilon$, 0.4 $\mu\varepsilon$, 0.6 $\mu\varepsilon$ for the LCC250 LM, LCC250 TB, and LCC350TM. The thermal strain variation at the bottom of LCC350 was minimal. The tensile strain magnitude at the middle of the LCC250 and LCC350 sections were 53% and 5% greater than their respective bottom strains. LCC350 had 66% and 14% lower strains at the middle and bottom than LCC250. This could be attributed to the greater thickness in the LCC350 section.

Figure 6.18 presents the transverse strain and layer temperature variation at the middle and bottom of the LCC sections over five days. While the LCC350 section strain at the middle and bottom of the layer behave similarly to its respective longitudinal strains. However, with higher magnitudes, the LCC250 sections' strain at the middle and bottom of the layer was reversed. In this case, a decreasing trend was noted in the transverse strain as opposed to the increasing trend for its longitudinal strain. Like the longitudinal strain, more variation in strain was found to correspond more closely with ambient temperature than layer temperature. However, this assumes that the LCC250 subbase layer temperature was like that of LCC350.

Thermal strain variation for the middle and bottom of LCC250 was less than 0.5 $\mu\varepsilon$, while minimal variation was found. Although there was no strain measurement in the Control section, following Notre Dame Drive's results, it can be deduced that the 250 and 350 mm thick LCC layer could reduce the tensile strain magnitude at the middle and bottom of the subbase. And limit daily thermal strains due to expansion and contraction of the layer material compared with the traditional unbound granular material.

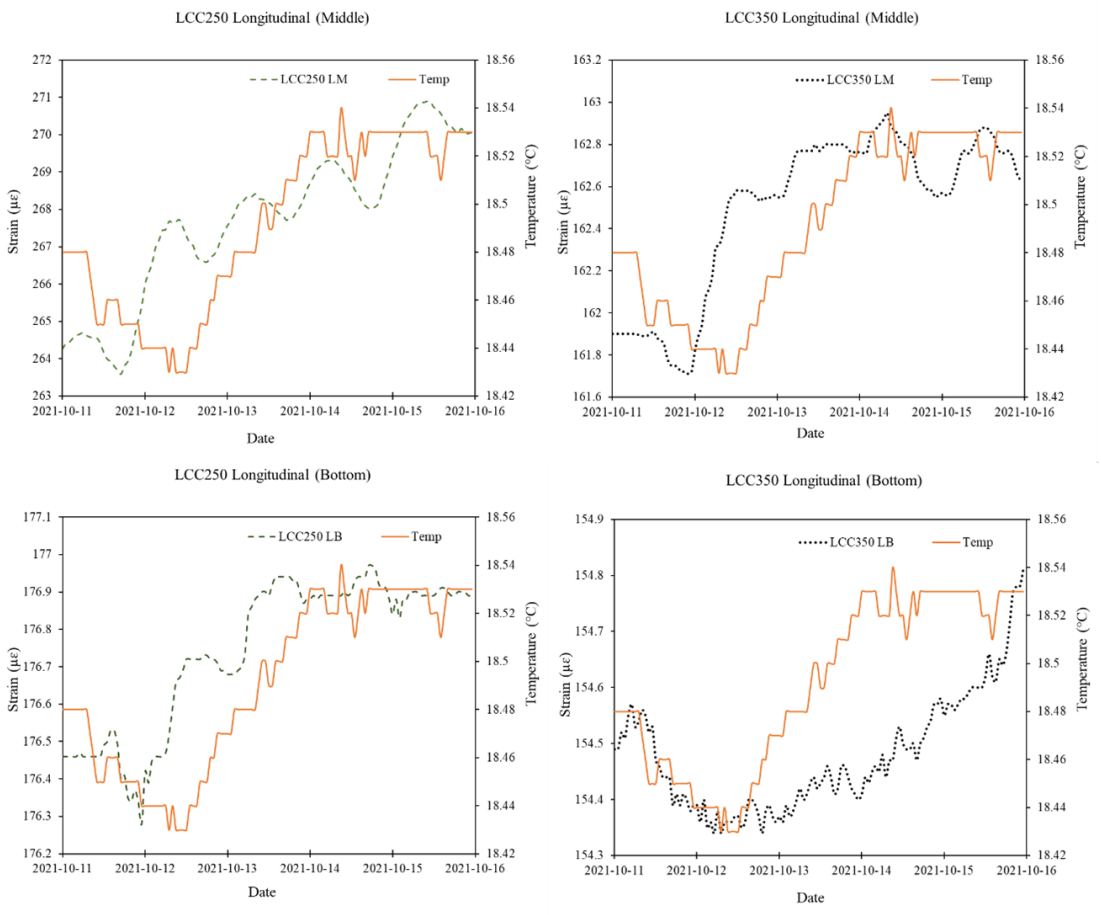

Figure 6.18: Erbsville subbase daily longitudinal strain variation with layer temperature

6.5.2 Seasonal Effect on Strain

The general strain and layer temperature trend over the study period for Erbsville are presented in Figure 6.20, while Figure 6.21 shows the longitudinal strain at the bottom of the asphalt layer and ambient temperature over the study period. In all the sections, the longitudinal strain underneath the asphalt layer seemed irregular over time, but it was more sensitive to traffic loads than temperature changes. The strain gauge for the Control portion was the one that displayed readings throughout the research period.

At the subbase layer, there was a distinct correlation between transverse and longitudinal strain change and seasonal temperature variation at Erbsville. In warmer months,

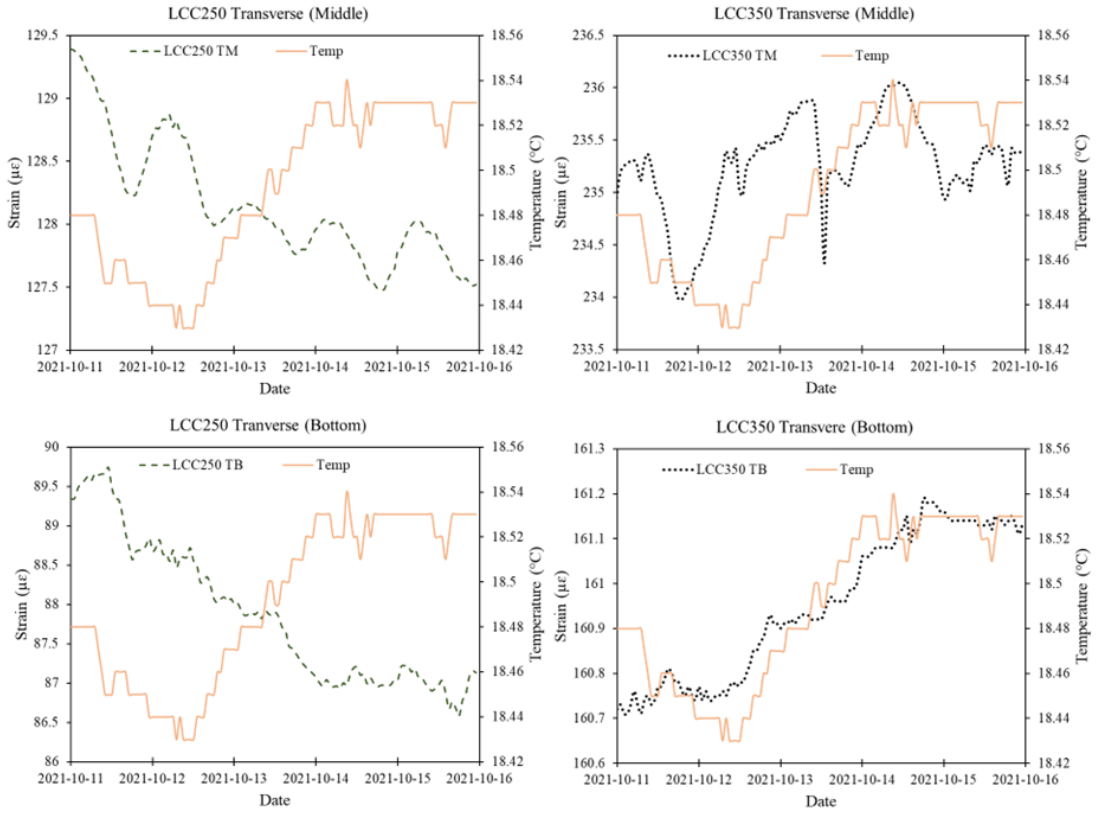

Figure 6.19: Erbsville subbase daily transverse strain variation with layer temperature

strain at the middle and bottom of the subbase layers increased, decreasing during the colder months. This same trend was observed at Notre Dame Drive for strains beneath the asphalt layer. At Notre Dame Drive, the LCC400 section experienced a significant increase in longitudinal strain beneath the asphalt layer between December and March compared with the other sections; however, the strain was reduced afterward. The Control at Notre Dame Drive experienced the most longitudinal strain during the warmer wet months.

The transverse strains at the middle and bottom of the LCC350 subbase layer were greater than the strains at the middle and bottom of the LCC250 layer. Transverse strains in the middle of the LCC layers were higher than the strains at the bottom. A similar trend was noted for the longitudinal strain at the middle and bottom of the subbase layers like the transverse strains. But, at the start of the third year, the strains in the LCC350 subbase middle and bottom became lower than that of the LCC250. For the first two

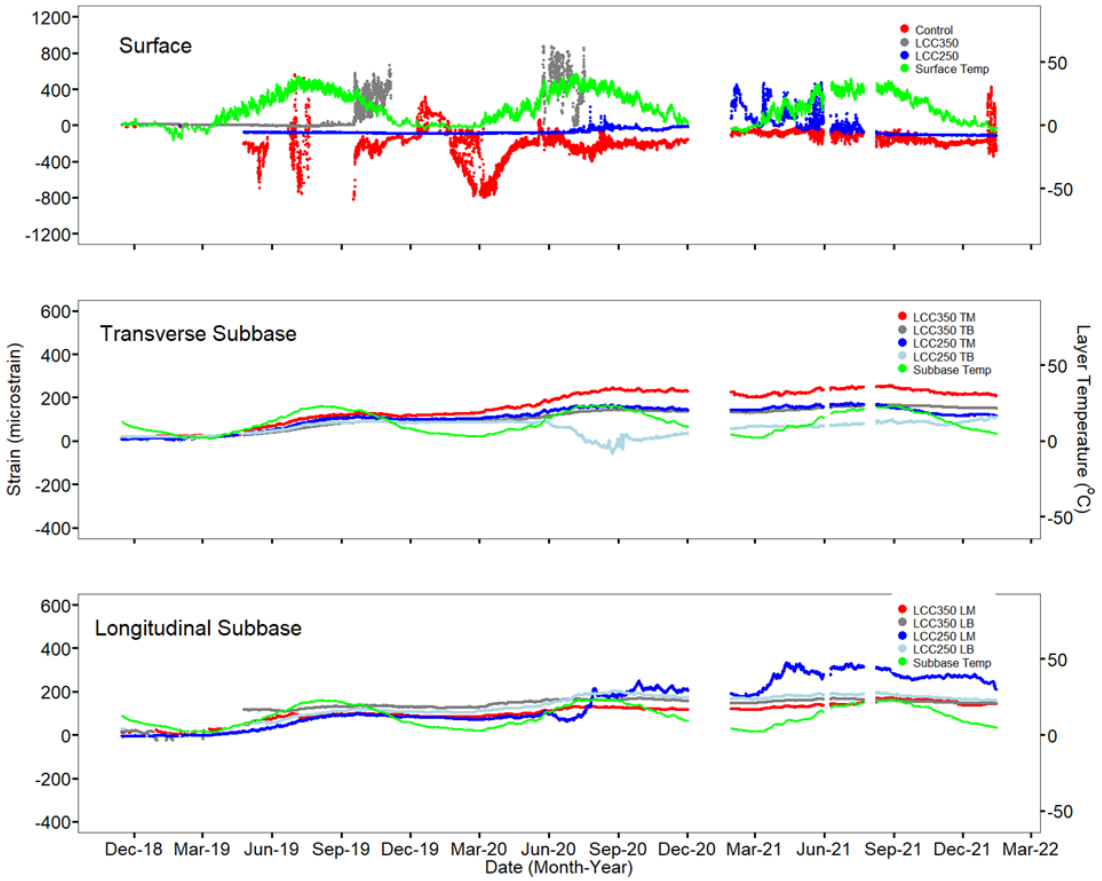

Figure 6.20: Erbsville strain profile over the study period

years, the longitudinal strains in the middle of the LCC layers were lower than those at the bottom. Starting in mid-2020, the strain at the middle of the LCC250 subbase became higher than at the bottom. Beginning in mid-2021, the strain at the middle and bottom of the LCC350 subbase became roughly equivalent. Longitudinal strain in the middle of the LCC250 experienced a significant increase, with more fluctuations noted since the start of 2021. The first year's increase in LCC subbase strain at Erbsville could be the result of cumulative plastic strain over time [112]. Since the second year, there has been a decrease in strain rise. Although their study only mentioned the asphalt layer, this behavior has been observed in previous research [68].

To better understand the seasonal effect of temperature and moisture on strain response, various dates were selected that represented different seasons and corresponded

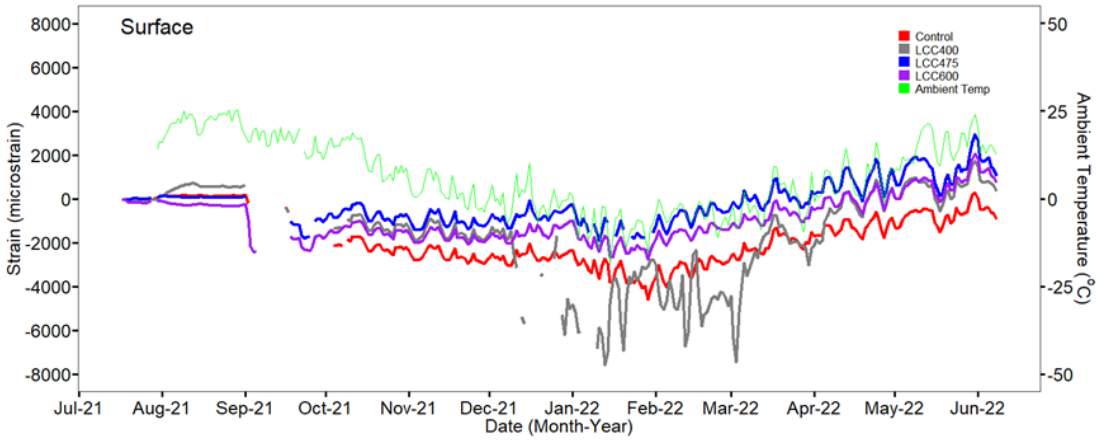

Figure 6.21: Notre Dame Drive strain profile over the study period

to varying temperature and precipitation levels over a year. For Notre Dame Drive, the average daily strain measurement on October 7, 2021, February 4, 2022, March 29, 2022, and May 18, 2022 (presented in this order on the plots represented by the corresponding temperature/moisture at the time) were selected. At Erbsville, February 4, 2019, April 25, 2019, and July 11, 2019, were compared. Figures 6.22 and 6.23 present the longitudinal strain response beneath the asphalt concrete layer.

For all the sections at Erbsville, measured longitudinal strain beneath the asphalt layer increased as pavement temperature increased. Similar findings were seen in a study by Sulejmani et al., (2021) [233]. A change in temperature from 14 °C to 34 °C increased measured strain by 3.2, 6.7, and 1.1 times for the Control, LCC350, and LCC250 sections. The Control section at Erbsville exhibited a more significant strain than the LCC sections, with the peak Control strain recorded at a temperature of 34 °C being 50 times greater than that of the LCC350 and eight times greater than that of the LCC250 sections.

Conversely, for Notre Dame Drive, at lower temperatures, longitudinal strain beneath the asphalt was observed to be the highest for all the sections. It decreased as the temperature increased. For the Control, a change in temperature from 16.6 °C to -6.7 °C increased the measured strain by 1.8 times. For LCC400, a similar change in temperature increased strain by 3.7 times. A shift from 17.9 °C to -7.7 °C resulted in a 2.5 times increase for the LCC475 and 1.5 times increase for LCC600. Like Erbsville, the Control section experienced the most strain across all the periods studied except during the winter, when LCC400 experienced greater strains. At the lowest observed temperature, the Control had 2.5 and 1.8 times more longitudinal strain than the LCC475 and LCC600 sections and 1.3

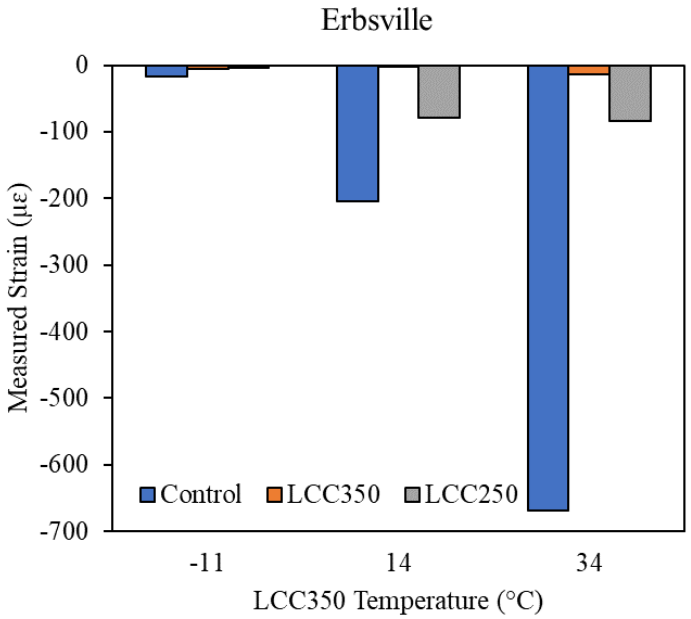

Figure 6.22: Erbsville seasonal change in longitudinal strain beneath asphalt layer

times less strain than the LCC400 section. The LCC475 saw 73% and 30% less strain than LCC400 and LCC600 sections.

The disparity in responses between Erbsville and Notre Dame at lower and higher temperatures may be caused by different material qualities and thicknesses. These results are consistent with Sulejmani et al., (2021) [233]. They discovered that thinner asphalt layers exhibited lower strain at higher temperatures than thicker asphalt layers, which responded differently and showed higher tensile strains at higher layer temperatures. This suggests that their assumption might not be restricted to the asphalt layer alone but that a change in strain response to temperature variation could result from increasing the thickness of the overall pavement structure. Additionally, the behavior of the asphalt material at both locations was different; while the Erbsville AC was stiffer at temperatures $\geq$ 21 °C than the Notre Dame Drive base asphalt, AC at Notre Dame Drive became stiffer at lower temperatures $\leq$ 4 °C. The unbound layer at Notre Dame Drive was also stiffer.

Overall, the results reflect that seasonal fluctuations in temperature and moisture influenced the longitudinal strain response beneath the asphalt layer. It also showed that incorporating an LCC subbase layer could limit the longitudinal strain at the bottom of the asphalt layer compared with the traditional pavement structure.

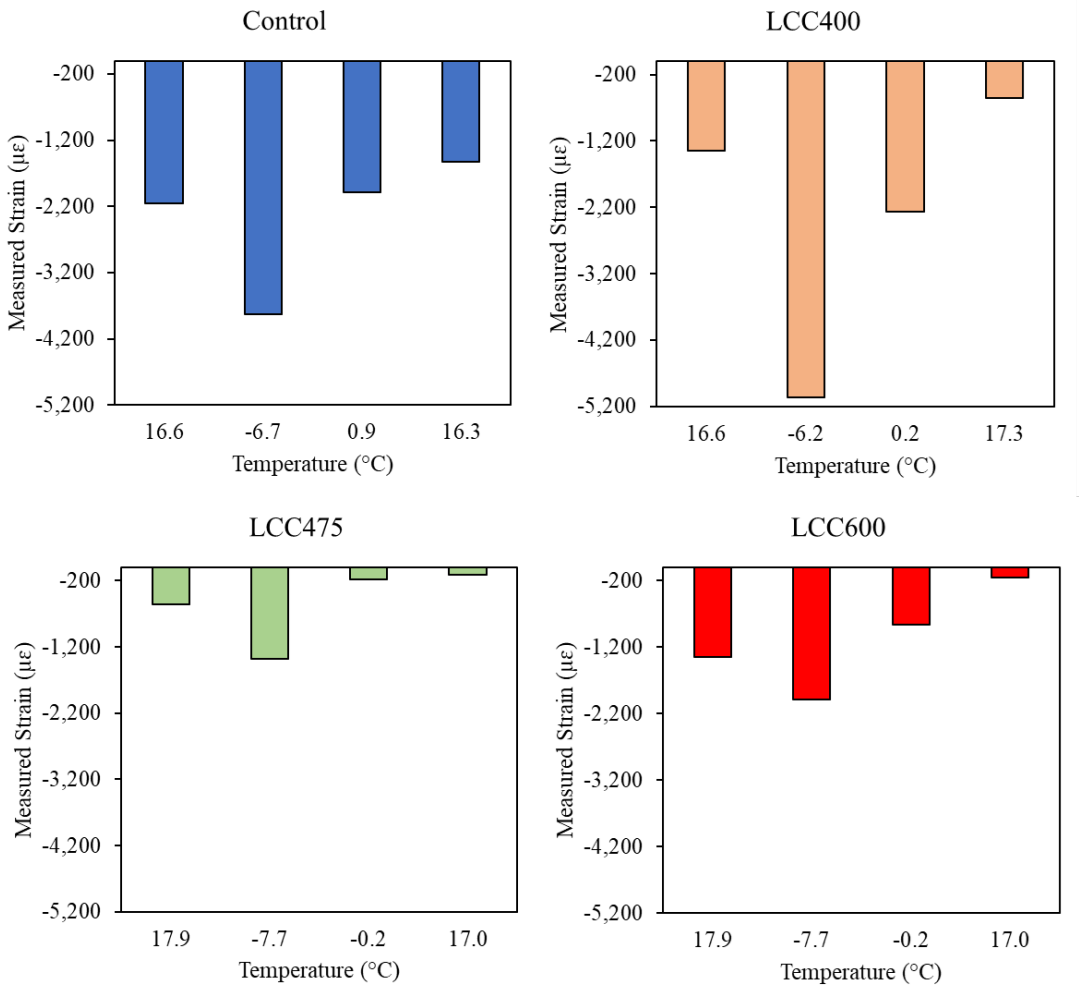

Figure 6.23: Erbsville seasonal change in longitudinal strain beneath asphalt layer

Studying the strain at the middle and bottom of the subbase layer, Figure 6.24 presents the absolute value of strain response across different temperatures for Erbsville and Figure 6.25 for Notre Dame Drive. LM stands for longitudinal strain in the layer's middle, and LB stands for longitudinal strain at its bottom. TM represents transverse strain in the layer's middle and TB at its bottom. At Notre Dame, the strain values are representative of the strain at the bottom of the layer.

At Erbsville, both longitudinal and transverse strains at the middle and bottom of the LCC layers were noted to increase with an increase in temperature and vice versa. An

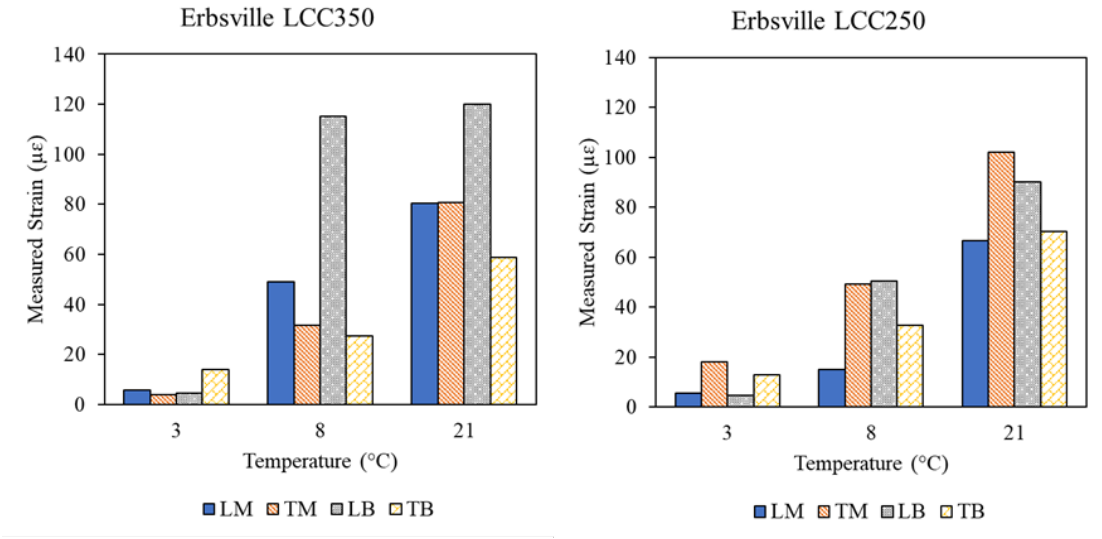

Figure 6.24: Erbsville seasonal change in longitudinal strain middle and bottom of subbase layer

increase in temperature from 8 °C to -21 °C caused longitudinal and transverse strain to increase between 1 to 4 times. The transverse strain at the middle was more than the transverse strain at the bottom, but the longitudinal strain at the middle was less than the longitudinal strain at the bottom. At Notre Dame Drive, higher strains were noted at the bottom of the LCC400 and LCC475 subbase at lower temperatures. Still, the other sections' relationship between temperature variation and strain was unclear. Also, at Erbsville over the study period, the layers were primarily saturated; therefore, no clear-cut connection comparing these days with moisture content was established. Similarly, although there was moisture variation during these times at Notre Dame Drive, no clear relationship was established between moisture and strain for the subbase strain measurements. However, the LCC400 section had soil water potential between 61 and 118 cb and experienced its lowest longitudinal strain when SWP was 61cb and transverse strain at 118 cb. The LCC475 and LCC600 sections saw the least strain responses when the layer was the driest at SWP of 10 cb and 15 cb, respectively. It can be concluded that several factors influence the strains beneath the subbase layers per time, and further investigation is required.

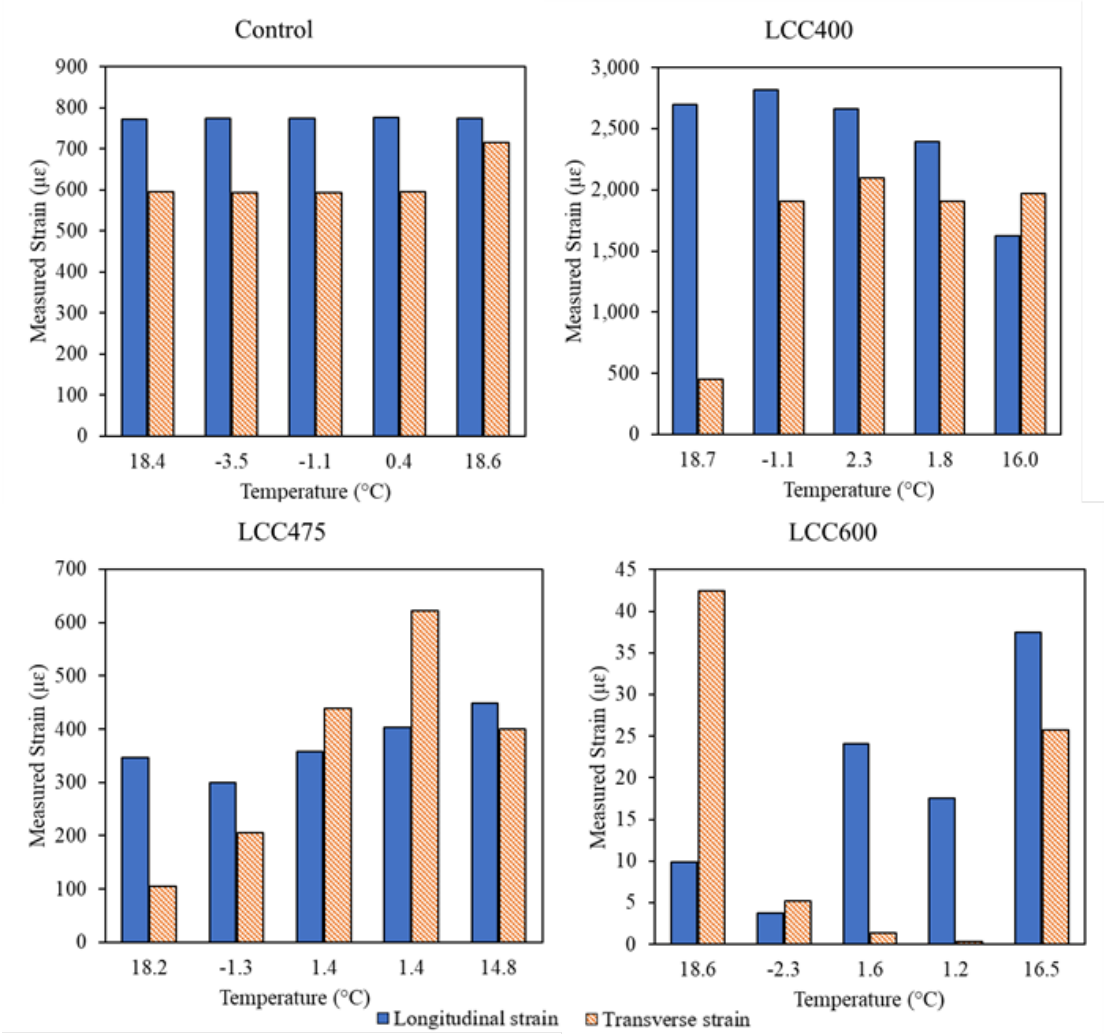

Figure 6.25: Notre Dame Drive seasonal change in longitudinal strain bottom of subbase layer

6.6 Environmental Effect on Pavement Pressure

Regression analysis performed between subgrade layer temperature and pressure at the top of the subgrade at Erbsville revealed a positive relationship between them (p-value < 0.001, over three years of data). Also, results showed a positive relationship between subgrade pressure and ambient temperature. However, R^2 values of 0.32, 0.032, and 0.14

for the Control, LCC250, and LCC350 were obtained for the relationship between subgrade temperature and pressure. On the other hand, R^2 of 0.32, 0.12, and 0.18 were obtained when pressure was correlated with ambient temperature. This showed that a small part of subgrade pressure was influenced by temperature for all sections, and other factors also play an essential role in subgrade pressure response. Regression results also further revealed that the effect of subgrade temperature on subgrade pressure was more pronounced in the Control section than in the LCC sections. The subgrade temperature less likely influenced the LCC250 pressure response. However, the relationship for this section was established with the temperature of the LCC350 subgrade since there was no temperature measurement for LCC250; this could be the reason for this. Furthermore, there was a slightly greater relationship between ambient temperature and LCC subgrade pressure (R^2 = 0.12 and 0.18) than LCC subgrade temperature (R^2= 0.032 and 0.14).

6.6.1 Daily Heating and Cooling Effect on Subgrade Pressure

Figure 6.26 shows the daily subgrade pressure and ambient temperature variation for Erbsville (ERB) and Notre Dame Drive (NDD) for all the sections. There appeared to be a relationship between daily ambient temperature and subgrade pressure. A cyclic pattern variation in pressure corresponded to the daily heating (9 am to 5 pm) and cooling (5 pm to 9 am) periods for the study duration was seen. The negative direction signifies compression and positive direction tension.

At Erbsville, as temperature increased, pressure increased at the Control and LCC350 sections but decreased at the LCC250 section. The difference in behavior could be attributed to the difference in pavement thickness above. The LCC250 thickness was 40% and 80% less than the Control and LCC350. These results concur with Islam and Tarefder [113] , which demonstrated that pavement stress is lowest in the cool early period and highest in the warm afternoon phase. The peak-to-peak change in pressure referred to in this study as thermal stress (due to daily expansion and contraction) on October 11 was 0.04 kPa, 0.01 kPa, and 0.11 kPa for the Control LCC350 and LCC250 sections. The magnitude of thermal stress change corresponded to daily ambient temperature change over the five-day timeline. A sudden increase to 5.1 kPa for the Control and 2.82 kPa for the LCC250 pressure occurred between October 15 and 16, coinciding with rainfall of 2.54 mm on October 15, and 10.16 mm. This did not seem to influence the pressure at LCC350, likely due to greater LCC thickness that could have resulted in a delay for water infiltration. During these days, peak pressure at the Control was an average of 48% and 52% more than the LCC250 and LCC350 sections.

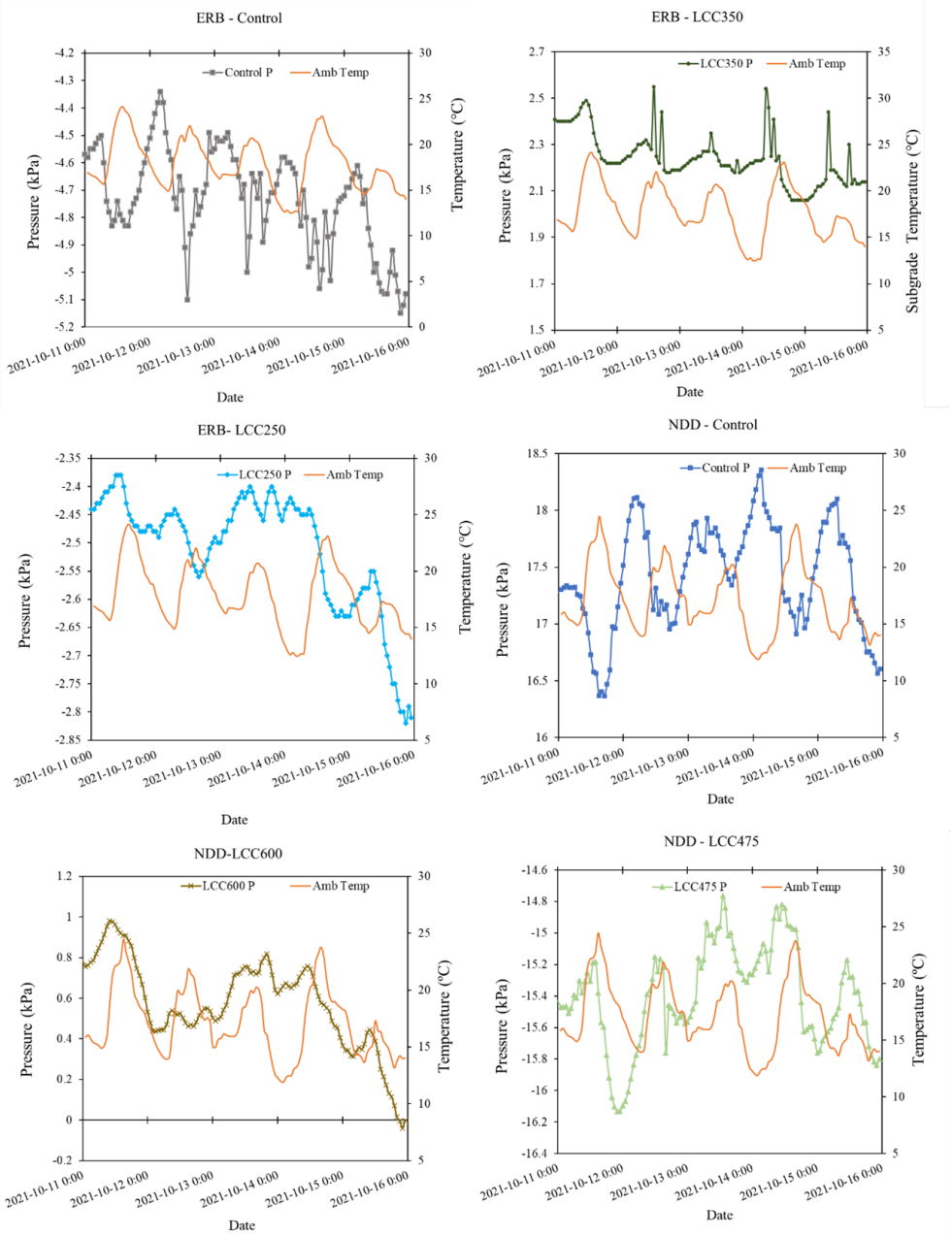

Figure 6.26: Daily temperature and pressure variation

At Notre Dame Drive, as daily ambient temperature increased, subgrade pressure decreased for the Control and LCC475 sections but increased for the LCC600 section. This is likely due to the stiffer subbase at the LCC600 section. Also, the Control section at this location was noted to correspond closely with its layer temperature. As the Control layer temperature increased, pressure increased, so we see this response at the location. Similarly, the LCC475 section corresponded to the changes in its subgrade layer temperature and increased and decreased as layer temperature increased and decreased. The temperature within the LCC600 section followed the same pattern as the ambient temperature, although the relationship was less pronounced. Thermal stress change on October 11 was 1.69 kPa, 0.94 kPa, and 0.54 kPa for the Control, LCC475, and LCC600 sections. The magnitude of thermal stress change corresponded to daily ambient temperature change over the five days studied. During these days, peak pressure at the Control was an average of 48% and 52% more than the LCC475 and LCC600 sections.

In conclusion, daily thermal stress change at the top of the subgrade can be reduced by 44% and 68% when 475 and 600 kg/m^3 of LCC is applied as subbase material. Differences in pavement thickness and material properties could cause subgrade stress responses to differ. Also, thicker pavements could reduce the daily impact of temperature variation on pressure change, thereby limiting the thermal stress change experienced at the top of the subgrade. When the conventional pavement structure thickness was 750 mm, daily thermal stress change was reduced by 24 times compared to a 490 mm pavement structure. Also, when 475 kg/m^3 of LCC as a subbase with pavement structure thickness of 550 mm was used, thermal stress change was reduced by nine times compared to 500 mm pavement structure. A further decrease of 11 times was noted when the LCC thickness was increased to 350 mm from 250 mm.

6.7 Seasonal Effect on Subgrade Pressure

The pressure profile over the study period for Erbsville and Notre Dame Drive are presented in Figures 6.27 and 6.28. The subgrade pressure in the Control fluctuated with changing weather conditions for the first two years; however, a significant drop was noted in the third-year winter period, and it remained less influenced. Whereas, for the LCC sections, there was less variation with changing weather conditions. Similarly, at Notre Dame Drive, seasonal fluctuation was noted for all the sections. Precipitation events also appeared to have more consequences on Control pressure than the other sections. More significant changes in pressure were noted in Control section especially when rainfall exceeding 15 mm occurred.

Different dates covering various temperatures and moisture levels were chosen to examine how temperature influenced pavement subgrade pressure. These dates were January 31, 2019, April 25, 2019, July 11, 2019, and October 26, 2019 for Erbsville, and October 7, 2021, January 31, 2022, March 10, 2022, March 29, 2022, and May 18, 2022, for Notre Dame Drive. The average daily pressure measurements for these days at all the sections have been plotted against the corresponding hourly average noon ambient temperature in the order the dates have been provided (Figure 6.29). Absolute pressure values have been presented in the figure for a clearer comparison of pressure magnitude.

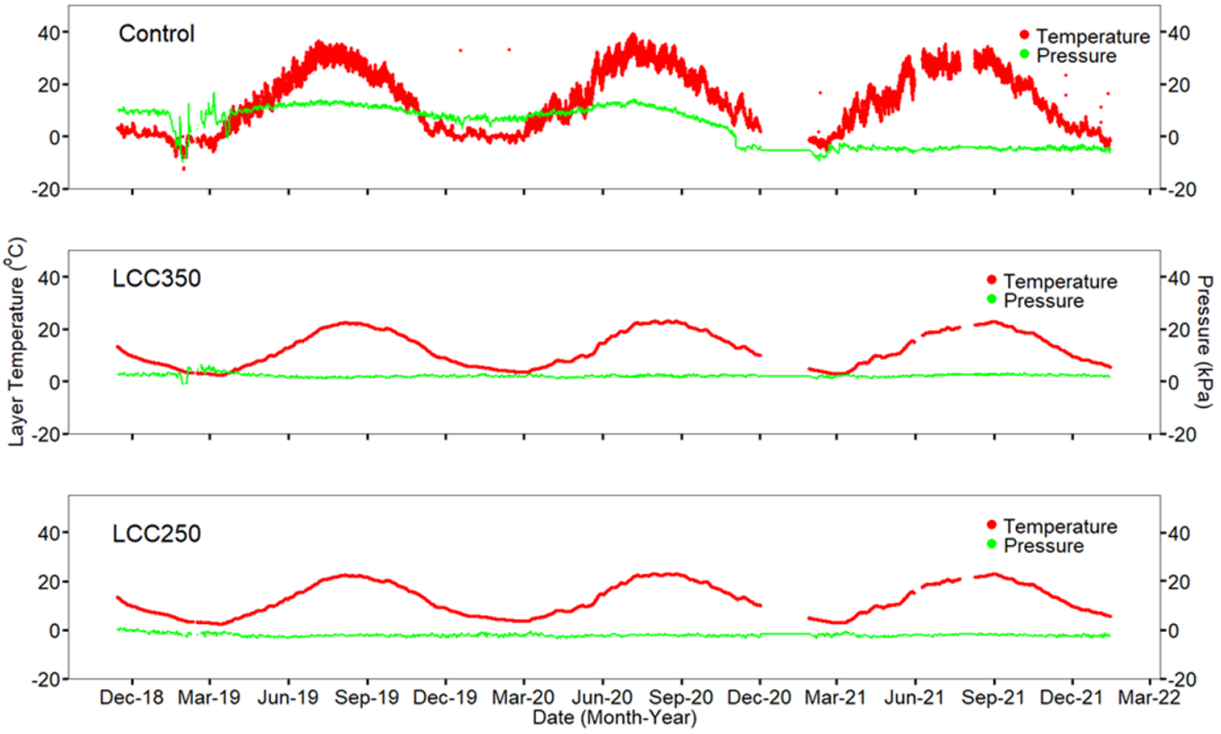

Figure 6.27: Erbsville subgrade pressure profile

At Erbsville, for the LCC sections, the least pressure was noted when the temperature was lowest (-21 °C) in January 2019, while the highest pressure was observed at an intermediate temperature of (8 °C) which was in April. This was likely due to a weaker subgrade during this spring-thaw period. When the temperature increased from -21 °C to 8 °C (January and April), a 1.4 and 2.2 increase in subgrade pressure was observed for the LCC250 and LCC350 sections. However, throughout the study period, the pressure within the LCC sections remained less than 4 kPa at varying temperatures. For the Control sec-

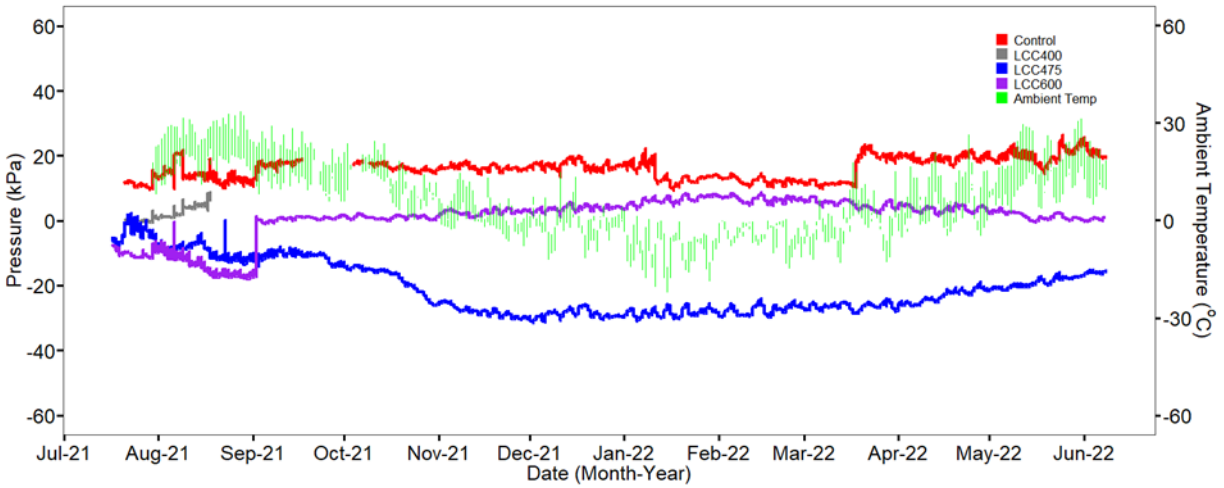

Figure 6.28: Notre Dame Drive subgrade pressure profile

tion, subgrade pressure was the highest at a higher ambient temperature of 25 °C in July. A 1.2 time increase was seen when the temperature increased from 8 °C to 25 °C. Over the period, the Control pressure remained above 10 kPa, with the LCC sections' pressure consistently lower than the Controls'.

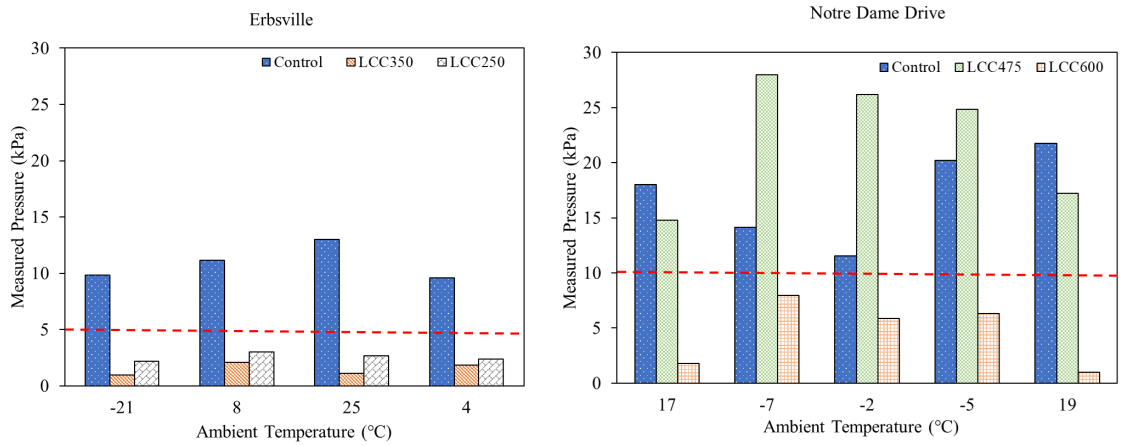

Figure 6.29: Erbsville seasonal subgrade pressure variation

The average subgrade pressure for LCC475 was 15 kPa by mid-October 2021, but by January 2022, it had doubled to 28 kPa, then dropped to 17 kPa by May 2022. A similar

response was noted for LCC600; however, it was of a smaller magnitude. A progression of 1.78 kPa, then 7 kPa, and down to 0.3 kPa by May 2022 was seen. In the Control section, subgrade pressure was 18 kPa in mid-October, reduced to about 13 kPa in January, and then increased to 23 kPa by May 2022. During colder months, we see a decrease in subgrade pressure for the Control but an increase during warmer months. The reverse was noted for the LCC sections, where lower pressure was witnessed during warmer months and higher pressure during the winter. Especially during the spring thaw period, Control pressure increased up to 25 kPa but reduced for LCC sections (to 20 kPa for LCC475 and 3 kPa for LCC600). Subgrade pressure likewise decreased with an increase in LCC density. LCC475 subgrade pressure remained two times more than the Controls' and four times more than the LCC600 section during the winter, while the Control pressure was an average of 1.4 and 46 times greater than the LCC475 and LCC600 during warmer months.

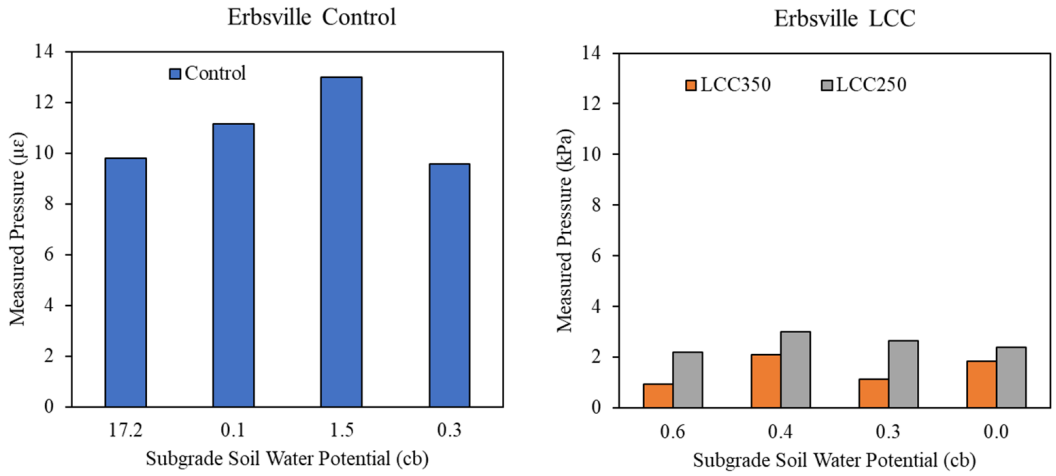

Figure 6.30: Erbsville subgrade moisture and pressure variation

Aside from temperature, layer moisture also influenced subgrade pressure, especially in the Control (Figures 6.30 and 6.31). When the ambient temperature was -7 and -2, the corresponding SWP were 282 cb and 77 cb for the Control at Notre Dame Drive. This meant that the Control subbase layers at these times were drier and corresponded to the times with lower pressure. All the LCC sections for the study period had SWP between 0 and 14 cb, but were drier in January and early March, which were times of their greatest pressure. Less moisture and lower temperatures in the Control subgrade resulted in less pressure, but for the LCC sections, a combination of these factors resulted in more considerable subgrade pressures.

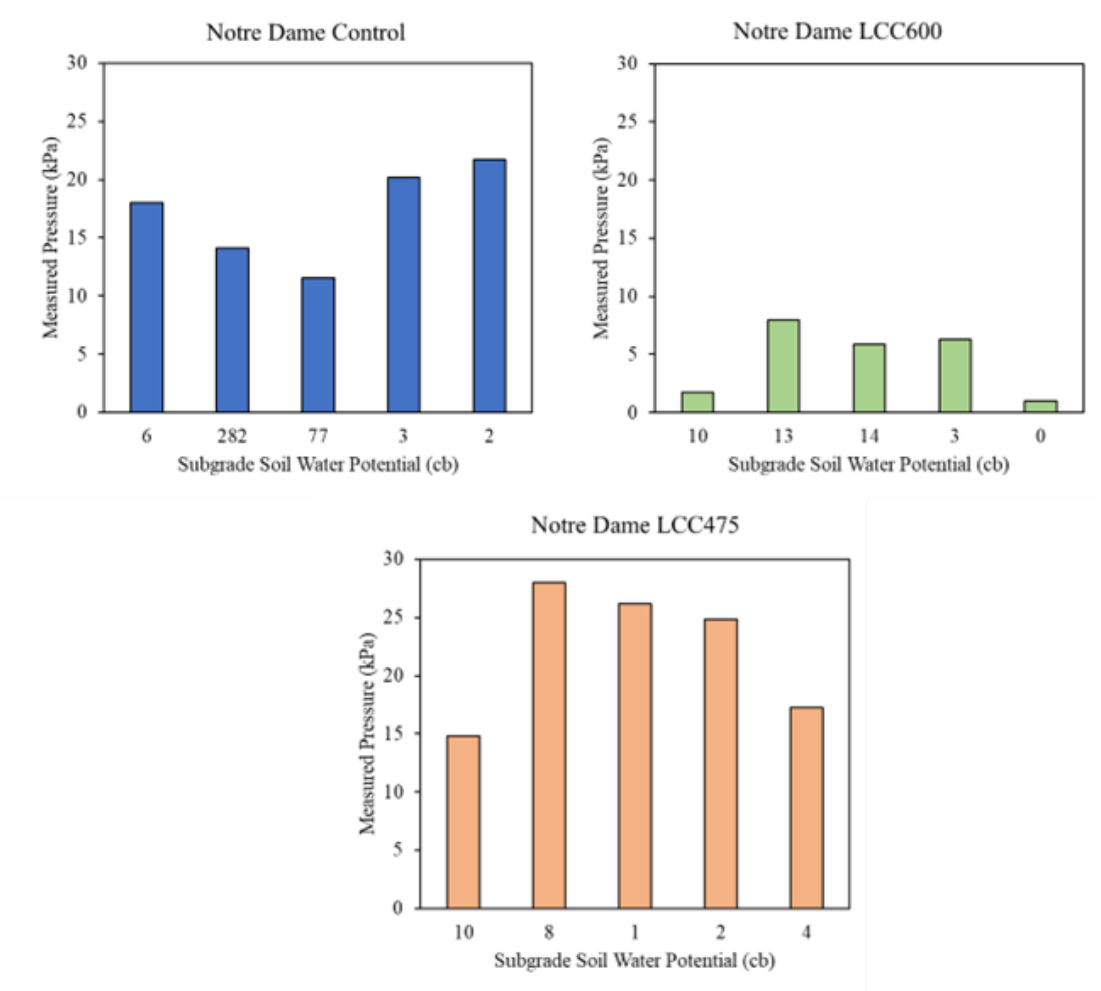

Figure 6.31: Notre Dame Drive subgrade moisture and pressure variation

6.8 Summary of Environmental Effects on Pavements

The environmental impact on LCC and traditional pavement response have been investigated. The findings showed that Lightweight Cellular Concrete had good insulation properties over the pavement subgrade, especially for thicknesses above 200 mm. The results indicated that a 200 mm thick LCC with a density of 400 to 475 kg/m^3 could prevent the subgrade directly beneath it from freezing during harsh winters. Thicknesses equal to or greater than 350 mm could be even more beneficial in alleviating the possibility of a frozen

subbase and subgrade. This is due to the higher thermal resistivity provided by increasing the LCC thickness. LCC insulating characteristics were primarily seen in the winter and summer. While 267 freeze-thaw cycles were noted for ambient temperature, 70 cycles were seen in the subgrade of the 450 mm thick granular B pavement section and none within the 350 mm thick LCC pavement over the study period.

The proposed temperature regression models could be satisfactorily utilized to predict typical unbound granular, flexible pavements and LCC pavements with densities between 400 and 600 kg/m^3 layer temperatures. Superior predictability was achieved when the daily average temperature was used compared with hourly temperature. Better predictability using ambient temperatures could also be obtained in the fall and spring, but the forecast reliability was weaker in the winter and summer.

Although at Erbsville, less change was observed, and the pavement layers in all sections remained saturated or near saturation throughout the study period, pavement moisture was seen to vary with precipitation. The soil water potential, however, appeared to be influenced by the time of year and the permeability properties of the pavement layers. For the base and subbase, the 400 kg/m^3 LCC section offered greater drainage than the other LCC and unbound granular pavements, whereas the 475 and 600 kg/m^3 LCC offered the greatest moisture protection over the subgrade.

Daily, longitudinal strain increased (towards tension) when layer temperature decreased and decreased (towards compression) when layer temperature increased. However, a reverse strain behavior occurred when pavement thickness was increased beyond 550 mm. When daily temperature decreased, longitudinal strain beneath the asphalt layers decreased by 53%, 94%, 40%, and 69% for the control, LCC400, LCC475, and LCC600 sections. However, during the October daily heating and cooling period, the control section had over 52% higher daily maximum longitudinal strain and over 31% minimum strain than the LCC sections. The 475 kg/m^3 LCC had 39% and 47% lower maximum longitudinal strain than 400 kg/m^3 and 600 kg/m^3 and 84% lower daily minimum longitudinal strain than both sections. Daily strain change in the fall was lower in the mornings by 2.1, 17.4, 1.7, and 3.3 times for the Control, 400 kg/m^3, 475 kg/m^3, and 600 kg/m^3 pavement sections than in the afternoon. These factors were 1.3, 1.4, 1.5, and 1.4 in the winter and 2.3, 5.6, 2.9, and 2.5 in the spring. The factor was greater in spring than fall and winter except for 400 kg/m^3 LCC, which also had the greatest daily longitudinal strain change, while 600 kg/m^3 had the least.

Seasonal fluctuations in temperature and moisture influenced the longitudinal strain response beneath the asphalt layer. Compared with the traditional pavement structure, incorporating an LCC subbase layer could limit the longitudinal strain at the bottom of

the asphalt layer. During colder months, 475 to 600 kg/m^3 LCC can potentially reduce the longitudinal strain beneath the asphalt layer by over two times compared to conventional unbound granular pavements. This is also true for 400 kg/m^3 during warmer months, but during winter months, higher strains are induced beneath the asphalt layer by up to 1.3 times more than on conventional pavements. Transverse strains in the middle of the LCC layers were higher than the strains at the bottom.

Daily pressure change at the top of the subgrade can be reduced by 44% and 68% when 475 and 600 kg/m^3 of LCC is applied as a subbase material. However, in the winter, the 475 kg/m^3 LCC pavement tends to experience two and four times more pressure than the Control and 600 kg/m^3 pavements. Differences in pavement thickness and material properties could cause subgrade pressure responses to differ. Also, thicker pavements could reduce the daily impact of temperature variation on pressure change, thereby limiting the thermal stress change experienced at the top of the subgrade. When the conventional pavement structure thickness was 750 mm daily pressure change was reduced by 24 times compared to a 490 mm pavement structure. Also, when 475 kg/m^3 of LCC subbase with pavement thickness of 550 mm was applied, pressure change was reduced by nine times compared to a 500 mm pavement structure. A further decrease of 11 times was noted when the LCC thickness was increased to 350 mm from 250 mm. Less moisture and lower temperatures in the Control subgrade resulted in less pressure, but for the LCC sections, a combination of these factors resulted in greater subgrade pressures.

Greater thickness ($\geq$ 250mm) LCC caused subgrade pressure to be less impacted by seasonal temperature and moisture variation. The conventional unbound granular pavements experienced greater subgrade pressure at higher temperatures whereas LCC pavements had lower pressure. The LCC pavements, however, experienced the greatest subgrade pressures at a lower temperature, which was more pronounced when LCC layer thickness was $\leq$ 200 mm. Pressure decreased with an increase in LCC density.

6.9 Effect of Traffic Loads on LCC Pavement Response

The methodology for this section has been described in section 3.3.3. The loaded and unloaded truck scenarios were performed to simulate traffic loads. The results of this analysis are presented and discussed in this section.

6.9.1 Pressure response

During the experiment, the average ambient and pavement surface temperatures were 25 °C. Figure 6.32 depicts the dynamic pressure indicating the change in subgrade pressure during testing for the loaded scenario and the subgrade temperature. The steering axle was responsible for the first peak and trough in the curves, while the rear tandem axle was accountable for the second set when its first axle was around 50 mm away from and exiting the pressure cell at that point. The truck was seated directly on the sensors as much as feasible. However, because the testing was done on an in-service pavement, with in-service vehicles and a very restricted testing window, it was impossible to ensure that the truck was always directly over each sensor.

The steering axle caused the most significant pressure shift in the Control section of roughly 29 kPa. Lower pressure rises of 8.5 kPa and 10 kPa were seen in the LCC350 and LCC250 portions. The pressure jump followed a similar trend for the unloaded scenario. The recorded values at the Control, LCC350, and LCC250 were 14 kPa, 2 kPa, and 3 kPa, respectively. During testing, a 9 °C warmer subgrade was present in the Control than in the LCC sections. The Control section experienced three times higher pressure fluctuation with a loaded truck than the LCC350 and LCC250 sections. The pressure difference between the control and LCC350, and control with LCC250, was nearly five times larger for the unloaded scenario. Fifteen percent more pressure is noted on the LCC250 than in the LCC350 section. When the pressure imposed by the loaded and unloaded scenario in each section was compared, the Control showed a 52 percent decrease in maximum pressure, a 60 percent reduction was noted in LCC350, and a 73 percent reduction was seen in LCC250.

Accordingly, the average ambient and pavement surface temperatures at Notre Dame were 15 °C and 16 °C. Figure 6.33 represents the dynamic pressure at the top of the subgrade for the loaded scenario with the corresponding subgrade temperature for the control (ConTemp) and LCC (LCCTemp). The middle dual tire single axle induced the first peak and trough, while the others were by the rear tandem axle. In this analysis, the effect of the steering axle was comparable to other smaller vehicles, thereby ignored. The pressure cell in LCC400 was damaged at the time of testing. Therefore, no pressure information is presented. The most significant pressure jump of 35 kPa induced by the front axle of the rear tandem axle was noted in the Control section. The LCC475 and LCC600 sections saw lower pressure increases of 23 kPa and 7 kPa. However, a similar trend was observed for the unloaded scenario at lower pressure magnitudes. The dynamic pressure noted for the Control, LCC475, and LCC600 were about 19 kPa, 9 kPa, and 2 kPa, respectively. In the loaded scenario, the Control section experienced 1.5 times more

pressure than LCC475 and five times more than LCC600.

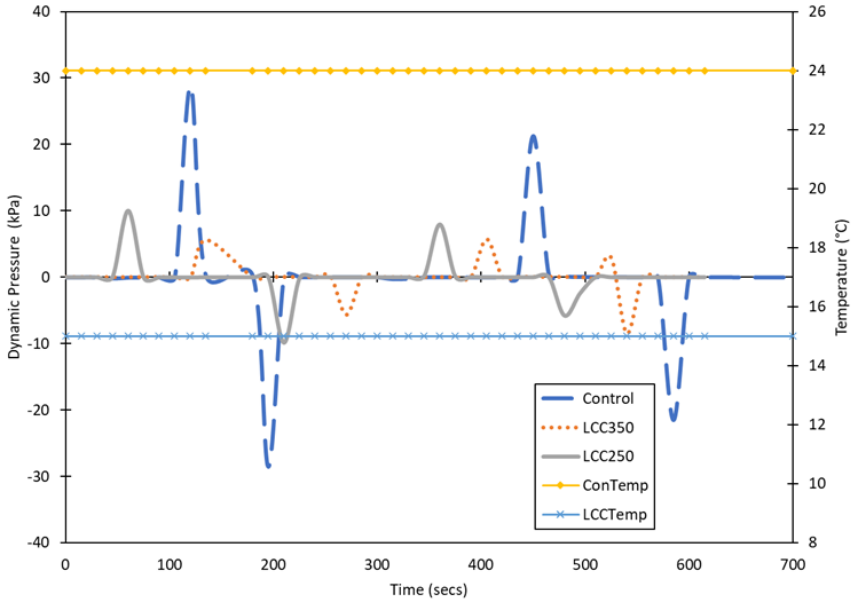

Figure 6.32: Loaded scenario dynamic pressure for Erbsville

Considering the unloaded scenario, this difference was two and ten times more than LCC475 and LCC600. The magnitude of the pressure difference between the Control and LCC350 and the Control and LCC250 was nearly five times larger for the unloaded scenario. As LCC density increased from 475 kg/m^3 to 600 kg/m^3, pressure decreased by 73 percent and 77 percent in the loaded and unloaded scenarios. When comparing the maximum pressure exerted by the loaded and unloaded truck in each area, the Control reveals a 45 percent reduction, whereas 61 percent was found for LCC350 and 75 percent for LCC250.

Figure 6.34 presents the maximum dynamic pressure in the loaded and unloaded scenarios for Erbsville and Notre Dame. It is noticeable that introducing LCC into the pavement structure compared to the traditional unbound materials could significantly reduce subgrade pressures, thereby reducing the stresses generated. Thinner LCC layers showed promising results in reducing the subgrade pressures compared to unbound granular material. This implies savings in overall pavement thickness. Pressure reduction also means lower subgrade compressive stresses, hence a lower rate of total permanent deformation occurrence on the pavement structure [106]. This could delay major rehabilitation works

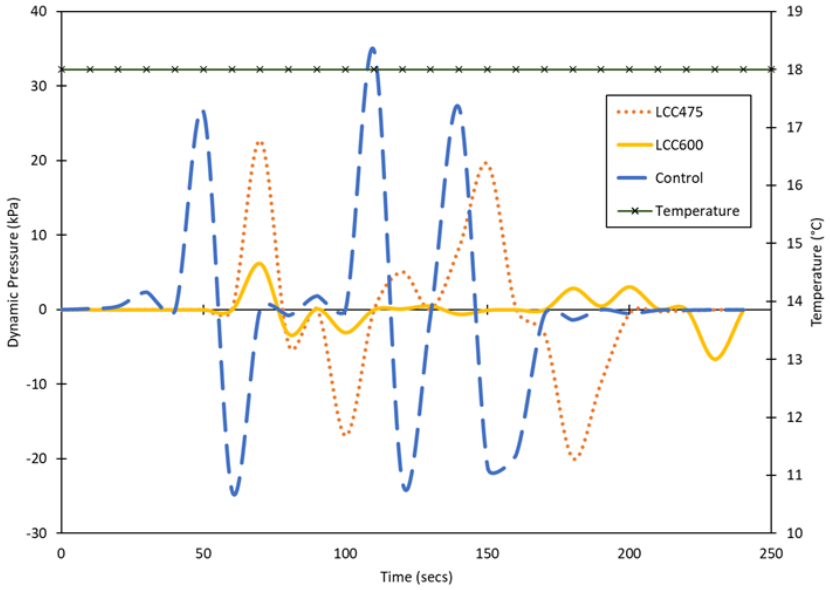

Figure 6.33: Loaded scenario dynamic pressure for Notre Dame Drive

by several years, increasing the pavement's service life, yielding fewer costs, and increasing sustainable benefits in the long run.

Subgrade pressures can be reduced over three times when a 250 mm of 475 kg/m^3 LCC is introduced instead of a 450 mm Granular B subbase. This is also true when looking at Granular A material. Although it could be argued that the Control pavement structure at Notre Dame was 50 mm thinner than its corresponding LCC sections, it should be noted that higher grade granular A material with an elastic modulus of 387 MPa was used compared to 226 MPa at Erbsville. All the sections were seen to have very close Granular Base Equivalency (GBE) factors. Furthermore, increasing LCC density by 26% could further alleviate subgrade pressures by over 70%. This means the LCC pavement could take about eight times more traffic loading before rutting sets in compared to unbound granular materials.

In addition, subbase layer thickness plays a significant role in reducing subgrade stresses. With a 66% reduction in the subbase layer thickness for the Control section from Erbsville to Notre Dame, a 55% increase in pressure was noted. Also, when 475kg/m^3 LCC was applied, a reduction in layer thickness by 29% resulted in a 15% subgrade pressure increase. Translating this to Notre Dame with an even more significant thickness reduction of 43%,

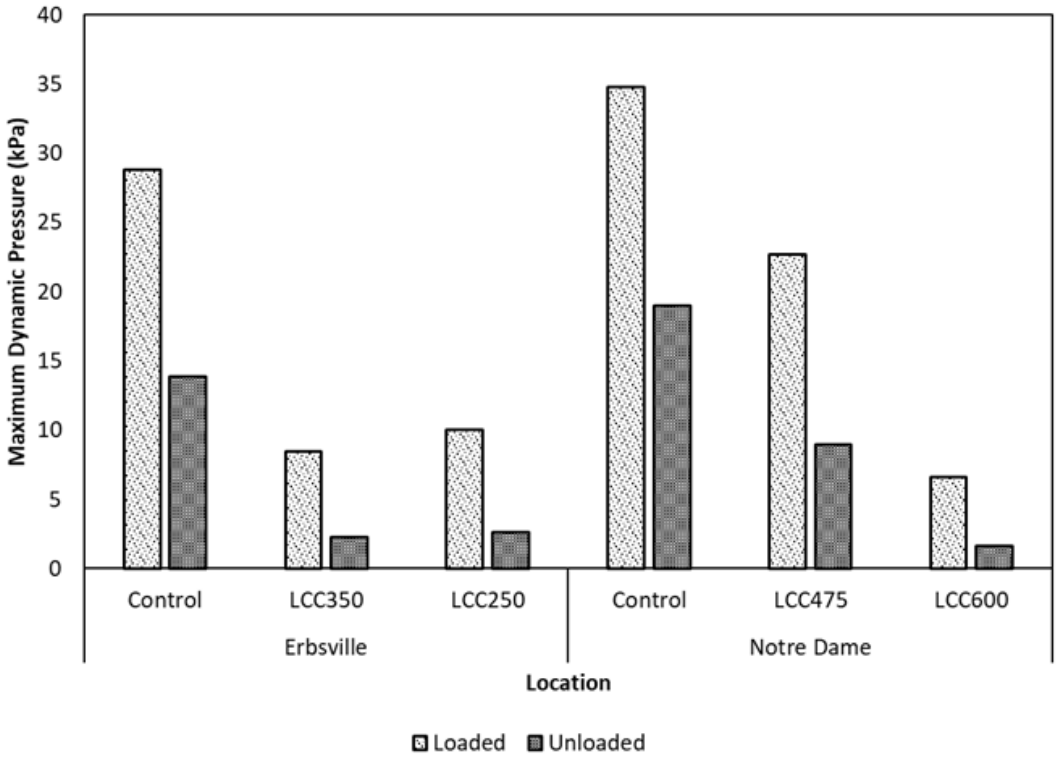

Figure 6.34: Maximum dynamic pressure Notre Dame and Erbsville

a 65% increase in subgrade pressure was seen. However, it is imperative to mention that other factors could play an essential role in this difference, especially when comparing Erbsville to Notre Dame. Firstly, Notre Dame had a thinner pavement. Secondly, the subgrade conditions were different. While the resilient modulus at Erbsville was 72 MPa, a lower subgrade (43 MPa) was encountered at Notre Dame. Thirdly, a slighter higher (2 °C) temperature was noted in the subgrade of Notre Dame than in Erbsville. Fourthly, the tire pressure distribution in both cases was different, and considerations need to be made for differences in the trucks used, although a similar type was used. Again, the speed of loading was different. Although a very slowly moving vehicle was used in Notre Dame, the truck at Erbsville was mostly static from point to point. This could have contributed to the higher-pressure response compared to Erbsville. Lastly, a thicker and better quality of unbound granular material was applied in Notre Dame compared with Erbsville. This could yield differences in pressure response by improving load transfer and decreasing pressure experienced on the subgrade.

Although LCC density applied was stiffer by as high as eight times than granular B and three times than granular A and would have significantly influenced pressure distribution to the subgrade, the subgrade temperature could also be a potential factor to consider as indicated in a study by Immanuel and Timm [109]. For example, in Erbsville, a 9 °C cooler subgrade could mean an even stiffer subgrade below the LCC layers than the unbound granular layer. Therefore, lower stresses are experienced due to loading. This shows the insulation benefit of the LCC layers and their effect on lowering subgrade pressures by reducing significant variations in subgrade temperature and keeping cooler in warmer ambient conditions.

The magnitude of load also yields differences in how the LCC layer reduces subgrade pressures. As load amplitude decreased (unloaded scenario), LCC caused an even more significant decrease (over 15%) on the subgrade pressure than the unbound granular material. This corresponds with An et al., [9] study which showed that increased truck loading would increase subgrade pavement dynamic pressure amplitude. However, for the same density of LCC, as thickness increased, the effect of reducing the magnitude of the pressure due to a decrease in load became smaller. This implies that thinner LCC layers could provide comparable results as thicker layers in reducing subgrade pressure when smaller loads are expected on the pavement structure.

The loaded vehicle's tire pressure distribution could affect vehicle loading characteristics and result in various pressure responses for different axle configurations. When the middle dual tire single axle was elevated in Erbsville, the steering axle exerted a large amount of pressure. However, when the middle axle was in contact with the pavement at Notre Dame, the steering axle exerted less pressure. In addition, a study by An et al., [9] showed that smaller loads increased the amplitude of stresses induced by the front axle than the rear axle.

6.9.2 Strain response

Only the loaded scenario for Notre Dame strain responses is shown in this analysis. The dynamic strain change due to traffic loading was considered in this analysis. Table 6.8 presents the maximum strain readings during the tests. Like the pressure scenario, these strain values were obtained when the first axle of the rear tandem wheels was sitting on the sensors. LCC400 section has been excluded as it appeared there was a problem with the instrumentation cluster at that location. Dynamic longitudinal strain at the bottom of the asphalt layer was highest in the Control section, 45% more than the LCC475 and LCC600 sections. At the bottom of the subbase, the longitudinal strain gauge in the Control section

Table 6.8: Maximum dynamic strain/displacement during loaded scenario (Notre Dame Drive)

Type/Location	**Control**	**LCC475**	**LCC600**
Longitudinal strain bottom AC ($\mu\varepsilon$)	-267	-143	-145
Longitudinal strain bottom of subbase ($\mu\varepsilon$)	-	-41	-24
Transverse strain bottom of subbase ($\mu\varepsilon$)	-186	-41	-12
Displacement at bottom of subbase (mm)	-0.03	-	-

did not change during this test. A 70% larger longitudinal strain was noted in LCC475 than in the LCC600 section, whereas this difference was twice as much in the transverse direction. The transverse dynamic strain in the Control section was 4 and 15 times larger than the LCC475 and LCC600, respectively. The strain value of the control has been calculated using the displacement provided by the soil compression gauge at the bottom of the unbound granular layer. Factors like temperature, load, layer, and overall pavement thickness influence the strain at the bottom of asphalt and subbase layers. According to Ai et al., (2017) [4], strain at the bottom of the surface layer increases with axle load and temperature but decreases with speed.

The maximum dynamic strain decreased by 70% as depth increased from 100 to 300 mm in the LCC475 section and 83% in LCC600. When transverse strain beneath the granular material was compared to the longitudinal strain at the bottom of the asphalt in the Control section, the strain decrease was 30% for a depth increase from 100 to 300 mm, assuming transverse and longitudinal strains were equal at that point.

Lower tensile strains at the bottom of the asphalt layer indicate more allowable load repetition before fatigue cracking occurs [106]. Because the LCC portions were subjected to around half the strains as the Control, these pavement sections could likely handle twice the amount of traffic with the same weight before fatigue cracking develops. This could postpone maintenance and rehabilitation techniques until later in the pavement's life cycle, reducing the overall number of maintenance tasks required by the end of its service life compared to the Control.

6.9.3 WESLEA Analysis

In performing this analysis, the assumption was that the pressure at the top of the subgrade was equivalent to the stresses generated at the exact location. The WESLEA input

parameters are presented in Table 6.9. To simulate the field condition, the elastic modulus for the base, subbase, and subgrade were obtained from laboratory testing performed for the materials obtained from the field. Testing for modulus of Elasticity for the LCC was performed following ASTM C 469 [21], while the CBR values for base and subbase followed ASTM D 698 [56], procedure C, and ASTM D1883 [18]. These values were converted to resilient modulus following the Mechanistic-Empirical Pavement Design Guide (MEPDG) procedure [207, 185]. Typical values for the asphalt layer and Poisson's ratio were obtained from the typical Ontario pavement design manual [10]. Since the FWD back-calculated asphalt modulus was slightly lower than the typical values, it thereby provided a more conservative result. The input parameters are presented in Table 6.9. The measured LCC Modulus obtained was within the range found in the study Ni, Oyeyi and Tighe [176].

Table 6.9: WESLEA input parameters

Layer	**Parameter**	**Erbsville**			**Notre Dame**			
		Control	**LCC350**	**LCC250**	**Control**	**LCC400**	**LCC475**	**LCC600**
Surface	Modulus (MPa)	3,447.20	3,447.20	3,447.20	3,447.20	3,447.20	3,447.20	3,447.20
	Poisson's ratio	0.35	0.35	0.35	0.35	0.35	0.35	0.35
Base	Modulus (MPa)	226	226	226	344.7	344.7	344.7	344.7
	Poisson's ratio	0.35	0.35	0.35	0.35	0.35	0.35	0.35
Subbase	Modulus (MPa)	143	1,089	1,089	387	844	1,188	1,391
	Poisson's ratio	0.35	0.20	0.20	0.35	0.21	0.30	0.26
Subgrade	Modulus (MPa)	72	72	72	43	43	43	43
	Poisson's ratio	0.35	0.35	0.35	0.40	0.40	0.40	0.40

During the analysis, it was discovered that when the traffic loading from Table 3.2 was used, the responses obtained were lower than those found in the field. Therefore, different simulations were performed where tire pressure and load levels were increased. This was because the initial tire pressure in Table 3.2 was an estimate and could have been underestimated. The additional pavement sections were analyzed using the iteration that produced a similar response to that measured in the field for the Control. The Control was picked as a starting point because the program was previously used to replicate typical pavement structures. The findings showed that WESLEA could do so quickly and with comparable results [210]. Figure 6.35 shows the comparison findings for Notre Dame, while Figure 6.36 shows the results for Erbsville.

Weslea Actual represents load (24.4 kN) and tire pressure (405 kPa) from Table 3.2,

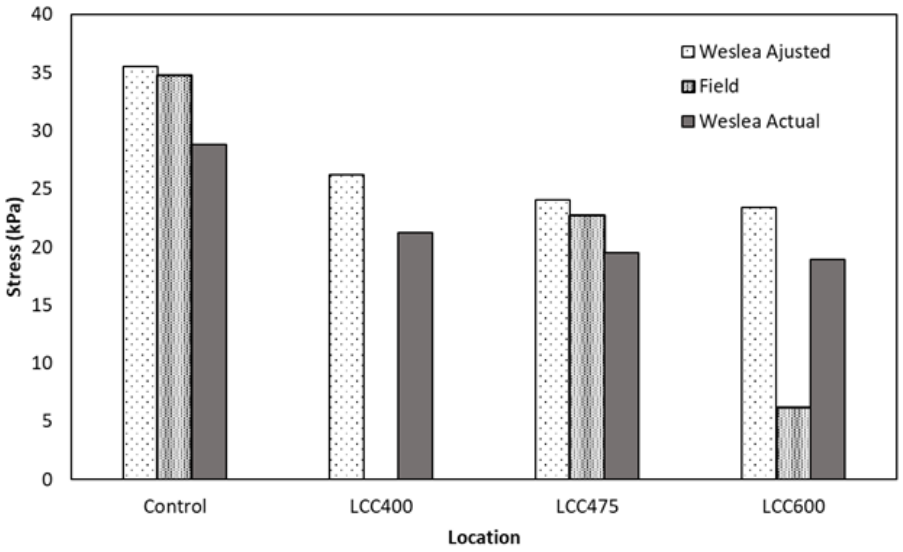

Figure 6.35: WESLEA stress comparison (Notre Dame Drive)

while Weslea Adjusted represents load (30 kN) and tire pressure (499 kPa). The Field is the actual measured response on the field. For Erbsville, these values for load and tire pressure were Actual (34.4 kN, 573 kPa) and Adjusted (38 kN, 633 kPa)

The result showed that, although the Control section when load and tire pressure were adjusted predicted the stresses at the subgrade well compared to the field, the values for the LCC sections were overestimated. This could mean that the multi-layer elastic theory might not be fully applicable, especially for incorporating LCC within the pavement structure, as it is based on the theory of pure elasticity. Also, Weslea has not been calibrated to cater for LCC, a deviation from typical pavement materials used as subbase. Furthermore, study by Loulizi et al., [149] revealed that the layered elastic theory greatly overestimates pavement responses at low and intermediate temperatures while significantly underestimating pavement responses to vehicular loading at high temperatures. Therefore, the testing temperature may have been a significant factor in this discrepancy.

Figures 6.37 and 6.38 compare tensile strain response at the bottom of the asphalt layer and transverse strain at the bottom of the subbase layer for Notre Dame. Although the maximum dynamic strain appears to follow a similar trend in both cases, the measured tensile (longitudinal) strain in the Control section seemed to have been underestimated by WESLEA. However, the actual load and pressure have captured the transverse strain beneath the LCC sections, but the adjusted load overestimated the Control, LCC475,

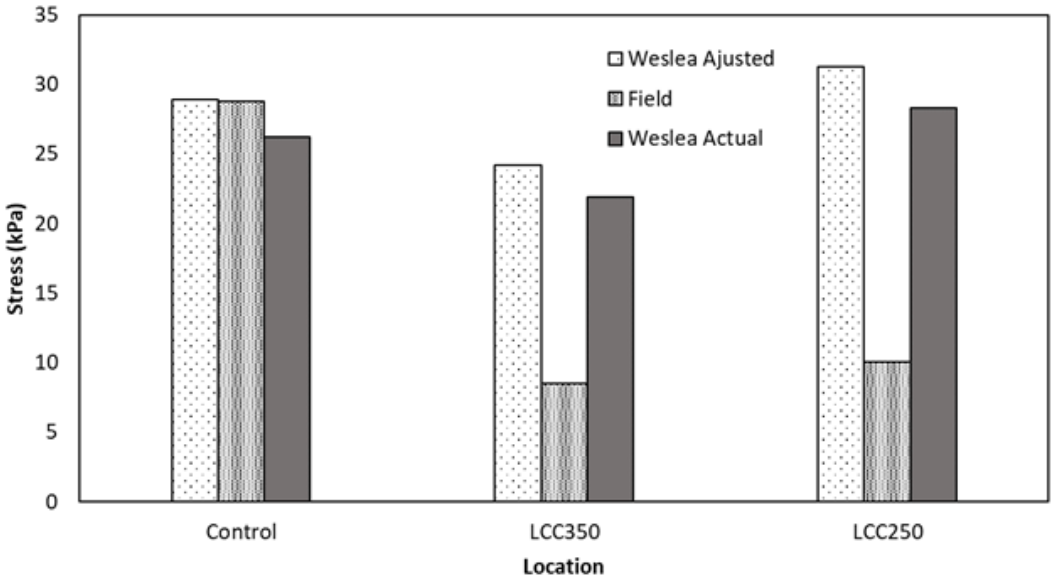

Figure 6.36: WESLEA Stress comparison (Erbsville)

and LCC600 sections strain by 53%, 30%, and 25%, respectively. WESLEA models an increase in strain responses as one moves downward in the pavement structure. In all cases however, the field strain values dropped as the pavement depth increased. This could indicate a limitation in predicting responses as pavement depth increases, especially for LCC pavements.

With this setback, when 1,000 load repetitions were applied to see the damage caused, the LCC sections were seen to allow twice as many loads until fatigue cracking. Up to 8 times more loads for rutting when using the 600 kg/m^3 density. This somewhat validates the theory in the study by Ni, Oyeyi and Tighe, [176] by comparing it with actual measured responses. The potential benefits of LCC could have been under-quantified purely based on the measured field stresses and strain compared with the multi-layer elastic theory by WESLEA software.

Additionally, the variation in loading speed may be responsible for some of the variances seen in the simulated case. The asphalt layer may behave differently depending on the temperature and speed during testing. Therefore, the typical values employed during

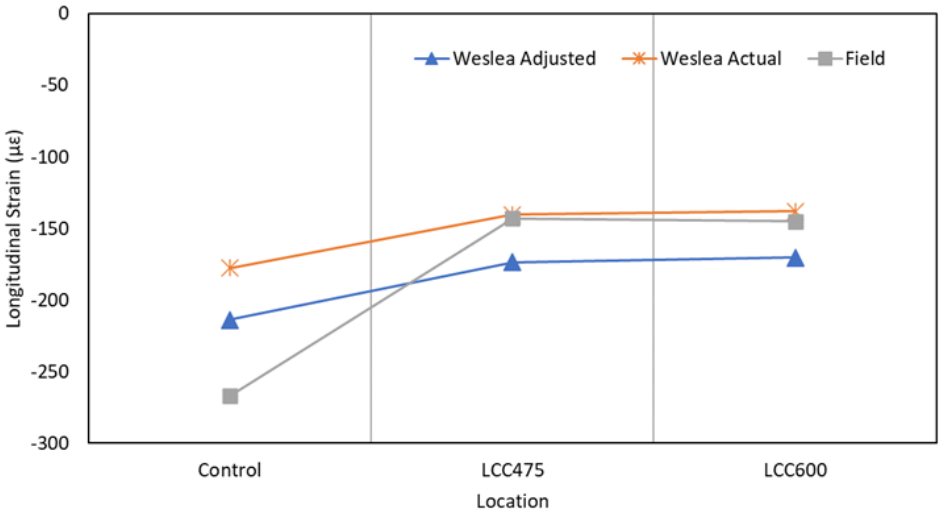

Figure 6.37: WESLEA strain comparison bottom of asphalt layer

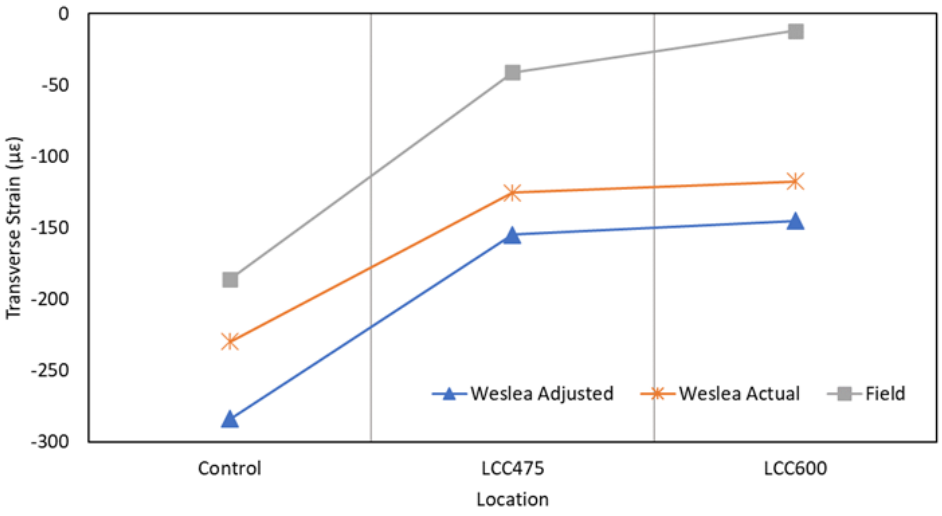

Figure 6.38: WESLEA compared transverse strain bottom of subbase

testing may be underestimating or overestimating the asphalt layer's quality.

6.9.4 Effects of Traffic Load Summary

The field experiment was carried out to investigate the in-situ structural capacity of Lightweight Cellular Concrete subbase pavements and compare them with the traditional unbound materials. This was done by examining the dynamic compressive stress and strain response induced by traffic loads on the pavement structure. In addition, the measured field results were compared with results obtained from WESLEA to determine the applicability of the multi-layer elastic theory in predicting LCC pavement response.

Based on the results, the main findings show that Lightweight Cellular Concrete can potentially reduce subgrade pressure due to traffic by up to three times when compared to unbound granular material. LCC's ability to minimize pressures was influenced by LCC layer thickness, overall pavement thickness, load magnitude, load distribution, tire pressure, and material characteristics. Thinner ($\leq$ 200 mm) LCC 475 kg/m^3 subbase layers could be used where lower traffic volumes and smaller types of vehicles are expected. As pavement depth increased, strain reduction was seen, and incorporating LCC subbase layers could reduce longitudinal and transverse strains even more than unbound granular material.

WESLEA could predict the traditional pavement structure stresses and strains at the bottom of the surface and subbase layers. However, it could overestimate the stresses and strains experienced in LCC subbase pavements. WESLEA calculated stresses could be reduced by 65% and strains by as low as 20% for LCC pavement densities between 475 kg/m^3 to 600 kg/m^3 and layer thicknesses exceeding 200 mm. Moreover, stresses and strains experienced at each layer may be influenced by factors such as layer temperature and moisture, which should be investigated further.

6.10 Chapter Summary

This chapter explored the relationship between environmental and traffic factors on LCC pavement response compared to traditional flexible pavement. Temperature prediction models were developed, and the relationship between environmental factors and moisture, strain, and pressure was established. The influence of traffic load on both pavement structures was also studied.

Chapter 7

In-Service Pavement Performance -Post Construction Testing

The in-service pavement roughness, stiffness and distress performance of LCC and unbound granular subbase flexible pavements were evaluated. Two approaches each were used to assess pavement roughness (SurPro and Dipstick method) and stiffness (Falling weight and Lightweight deflectometer methods). Findings from the visual assessment are also presented and discussed.

7.1 Visual assessment

7.1.1 Erbsville

After construction, a few non-severe distresses were found on the trial road after nine months (June 2019). In the Control section, a few (<10%) centerline cracks at the adjoining connection between the new and old pavements were observed with crack widths ranging between 3 to 12 mm. A slight transverse crack was identified with a width of less than 3 mm. Other types of cracks were found because of extensions from the old pavement cracks. At the LCC350 section, slight centerline and edge cracks were observed, while barely noticeable ravelling was found in the LCC250 section. In June 2022, another visual inspection was performed. Similar distresses like those seen in June 2019 were noted. However, the crack lengths of those extended cracks were slightly greater (Figure 7.1). Also, a small area with alligator cracks was observed in the Control section. Detailed

information regarding the observed distresses can be found in Table 7.1. All the centerline and transverse cracks were reflected from the adjacent pavement, hence were not a result of the failure of the test section (Figure 7.2). In summary, all sections on the trial road appeared to be in good condition with no structural or adverse environmental effects on the pavement surface.

Figure 7.1: Observed distresses at Erbsville

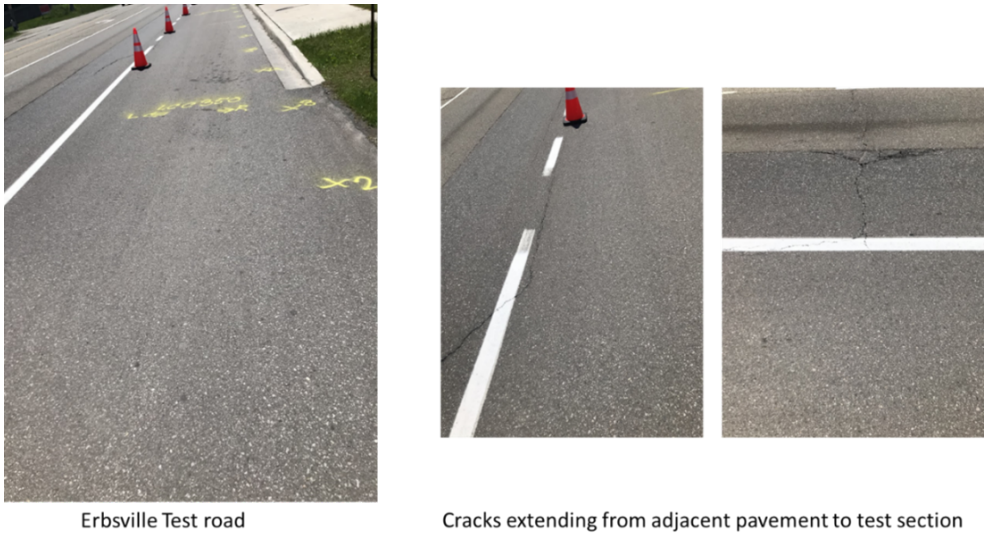

Figure 7.2: Source of distresses at Erbsville

Table 7.1: Summary of Erbsville surface distress survey (June 2022)

Section	Distress type	Severity	Extent	Description
	Centerline crack	1 (Very slight)	<10% (Few)	Width < 3 mm. Single hairline cracks. 5 m long.
Control	Centerline crack	2 (Slight)	<10% (Few)	3 - 12 mm width. Single cracks.
	Alligator Cracks	1 (Very slight)	<10% (Few)	Width < 3 mm. Single crack or single wave formation.
	Transverse crack	1 (Very slight)	< 10%. Cracks are more than 40 m apart	Full width < 3 mm. Single hairline cracks. 45 mm long.
LCC 350	Centerline crack	2 (Slight)	<10% (Few)	3 - 12 mm width. Single cracks.
	Edge crack	1 (Very slight)	<10% (Few)	Width < 3mm. Single crack or single wave formation.
LCC 250	Transverse crack	1 (Very slight)	< 10%. Cracks are more than 40m apart	Full width < 3mm. Single hairline cracks. 1 m long.
	Raveling	1 (Very slight)	<10% (Few)	Barely noticeable loss.

7.1.2 Notre Dame Drive

At Notre Dame Drive, no noticeable distress was seen in June 2022 after the placement of the final surface lift of the asphalt layer.

7.2 Roughness Evaluation

Roughness is an important characteristic of a pavement's longitudinal profile. Environmental conditions, subgrade quality, and traffic loading all play a role in determining the roughness of flexible pavements, according to a study by FHWA [202]. A study by Von Quintus, Eltahan and Yau [255] concluded that the initial smoothness of new AC pavements strongly influenced roughness advancement, while transverse cracks affected roughness over time for AC and AC overlaid pavements. Pavement roughness can be attributed to more pavement-related parameters such as surface material type, application methods, pavement design, the transition between sections, and pavement deterioration type over time, in terms of frequency, severity, and density [200]. Roughness, in turn, has a substantial impact on fuel consumption, vehicle maintenance costs, and the health of pavement users and their vehicles; hence it is a critical pavement measure.

Figure 7.3 shows a method devised by Sayers et al., [220] to determine approximate ranges of pavement roughness (IRI) in relation to road class and speed feature [70, 270, 142, 141]. The influence of pavement roughness is more significant at higher speeds. As IRI rises, the speed at which vehicles may safely utilize the roadway falls [200]. While an IRI value of 0 m/km denotes absolute smoothness, an IRI value of 8 m/km denotes a rough unpaved road surface [221].

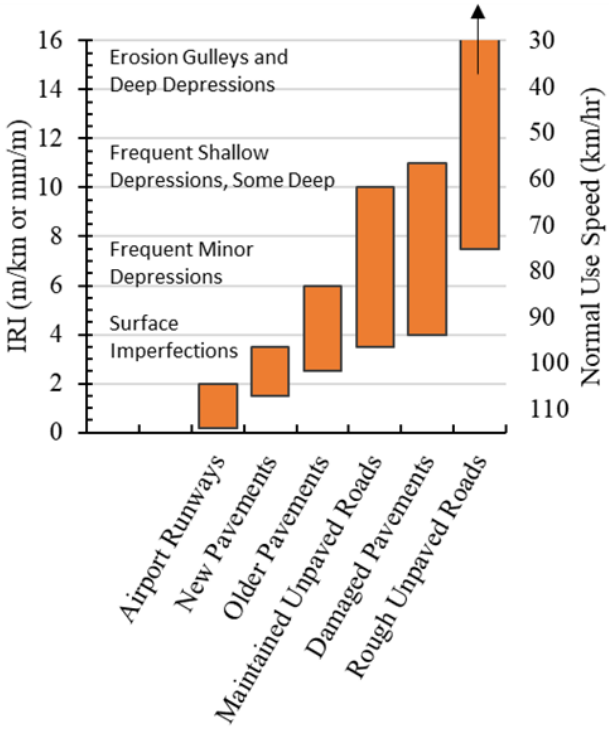

Figure 7.3: The IRI Roughness Scale [221]

In Ontario, the recommended initial IRI values based on treatment while designing for new or reconstruction AC flexible pavements are 0.8 m/km, 1 m/km, and 1 m/km for Freeways, Arterial, and Collector roads, respectively [185]. Local roads have no specified initial IRI; however, the closer to 1 m/km, the better. Similarly, MTO recommends terminal IRI values for freeway, arterial, collector, and local roadways to be 1.9 m/km, 2.3 m/km, 2.7 m/km, and 3.3 m/km, respectively. However, according to Sayers and Karamihas, (1998) [221], newly constructed pavements should range between 1.5 and 3.5 m/km [220].

7.2.1 Pavement Layer Temperature and Moisture during Testing

Tables 7.2, 7.3, and 7.4 show both sections' testing temperature and layer moisture. The pavement layers at Erbsville were generally saturated throughout all testing periods since the soil water potential ranged between 0 and 1, which is why the numbers are not shown here. The temperature and moisture information could enhance the interpretation of measured stiffness and roughness results.

Table 7.2: Erbsville layer temperature during roughness and stiffness tests

Test Date	**Section**	**Temperature (°C)**				
		Surface	**Base**	**Subbase**	**Subgrade**	**Ambient**
02-Dec-18	Control	-	4.9	3.6	0.6	1.8
	LCC350	-0.2	6.7	10.5	11.0	
21-Jun-19	Control	20.0	20.6	21.0	23.0	11.5
	LCC350	22.0	20.0	17.0	16.0	
11-Oct-19	Control	-	17.3	17.1	16.3	9.5
	LCC350	17.5	17.4	16.7	14.4	
02-Dec-20	Control	-	6.4	5.4	1.9	-
	LCC350	0.9	6.2	9.4	9.8	
10-Feb-22	Control	-	-0.6	-1.1	-0.9	-0.1
	LCC350	-1.8	-0.6	2.0	2.7	
09-Jun-22	Control	-	19.4	19.6	19.8	
	LCC350	19.0	18.3	16.3	15.8	

7.2.2 SurPro

Erbsville

The average IRI on each wheel path for the SurPro was calculated using the readings from all the runs. In most situations, there were at least two runs. The findings of the ANOVA analysis showed that there was statistically no distinction between each run in a wheel path. For instance, all the sections for December 2018 and June 2019 had p values above 0.6 at a 95% confidence level. The mean IRI over the study period is presented in Figures 7.4 and 7.5. The error bars represent the standard deviation for each location. Figure 7.6

Table 7.3: Notre Dame Drive layer temperature during roughness and stiffness tests

Test Date	Section	Temperature (°C)				
		Surface	Base	Subbase	Subgrade	Ambient
03-Sep-22	Control	47.2	28.1	25.7	23.6	22
	LCC400	44.8	34.5	24.6	20.9	
	LCC475	42.7	32.5	23.0	20.2	
	LCC600	46.5	34.5	24.5	21.0	
11-Feb-22	Control	-2.0	-2.0	-2.0	-2.0	-1.91
	LCC400	-1.9	-1.8	-0.6	1.2	
	LCC475	-7.2	-9.4	-2.7	0.7	
	LCC600	-	-7.8	-3.5	-0.5	
06-Apr-22	Control	13.4	6.5	5.8	3.6	12.03
	LCC400	11.9	9.3	6.6	4.1	
	LCC475	12.1	8.8	5.4	3.3	
	LCC600	-	8.9	6.2	3.6	
08-Jun-22	Control	23.6	19.2	19.7	19.6	23.58
	LCC400	21.2	18.7	17.5	15.9	
	LCC475	20.2	18.0	16.6	14.7	
	LCC600	-	18.3	17.9	16.2	

Table 7.4: Notre Dame layer moisture during roughness and stiffness tests

Test Date	Section	Soil Water Potential(cb)		
		Base	Subbase	Subgrade
03-Sep-22	Control	1.7	5.0	5.2
	LCC400	19.6	185.5	8.1
	LCC475	3.8	6.6	3.7
	LCC600	19.6	6.7	5.7
11-Feb-22	Control	303.2	322.3	170.2
	LCC400	227.1	43.5	8.1
	LCC475	91.1	7.3	9.1
	LCC600	321.5	10.3	12.4
06-Apr-22	Control	5.6	20.1	2.0
	LCC400	4.9	86.7	5.0
	LCC475	0.4	8.7	5.5
	LCC600	2.3	3.8	3.6
08-Jun-22	Control	7.2	19.9	1.0
	LCC400	2.1	40.7	3.8
	LCC475	1.2	9.1	4.3
	LCC600	0.5	18.7	1.6

compares the IRI profile difference between June 2019 and June 2022, three years apart, for all sections. While the Least Square Difference (LSD) analysis (Appendix B) between the sections' measured IRI is presented in Table 7.5 and the mean section IRI values in Table 7.6.

Erbsville's Control section consistently had higher IRI than the LCC sections on both wheel paths. For LCC sections, the LCC350 at the earlier months for both wheel paths had a higher IRI, but for some of the tests, especially in 2022, the LCC250 IRI was more on both wheel paths. There was higher variability in pavement roughness on the right wheel path than on the left wheel path. IRI also decreased from 2018 to 2019.

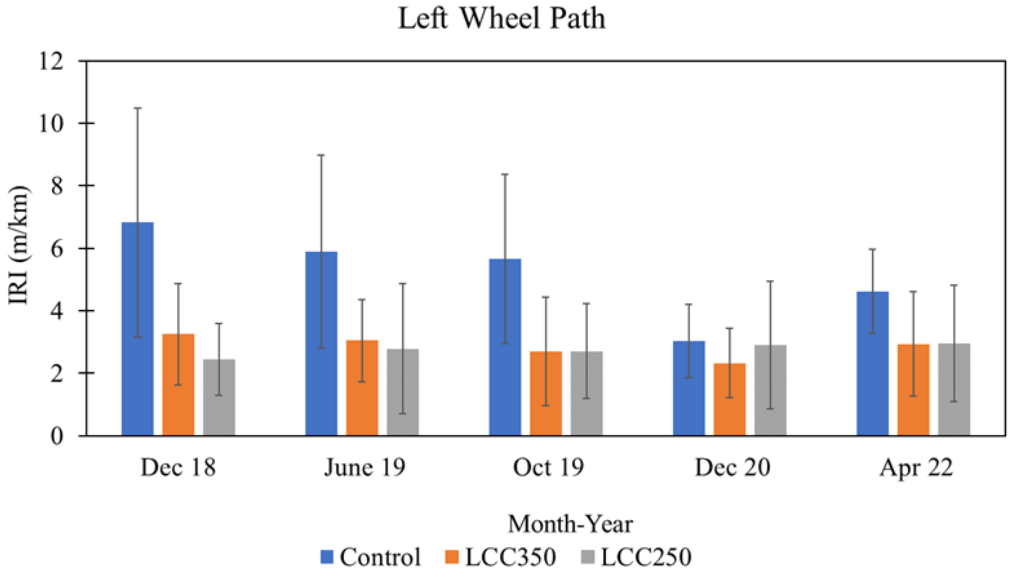

Figure 7.4: Erbsville left wheel path IRI

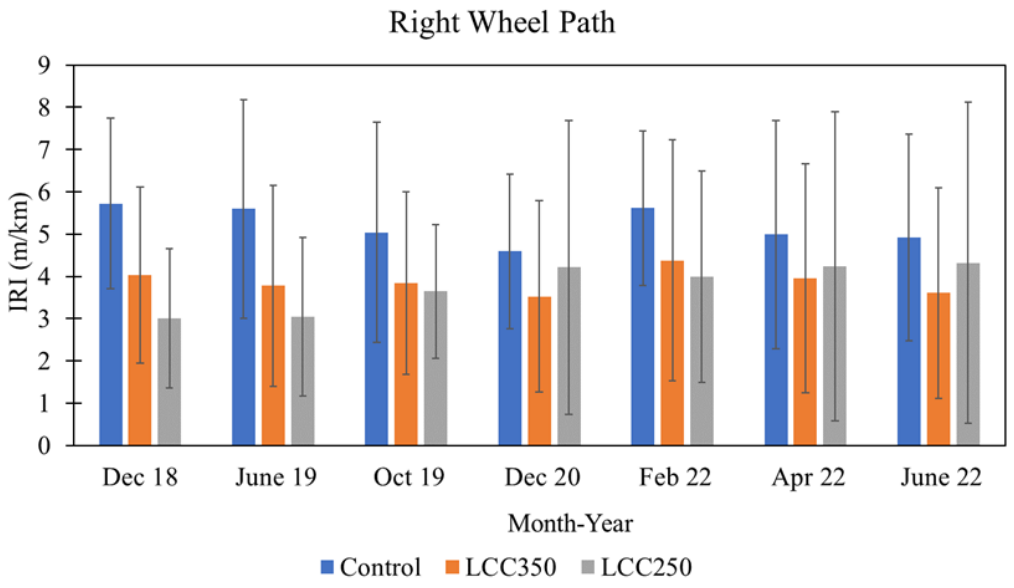

Figure 7.5: Erbsville right wheel path IRI

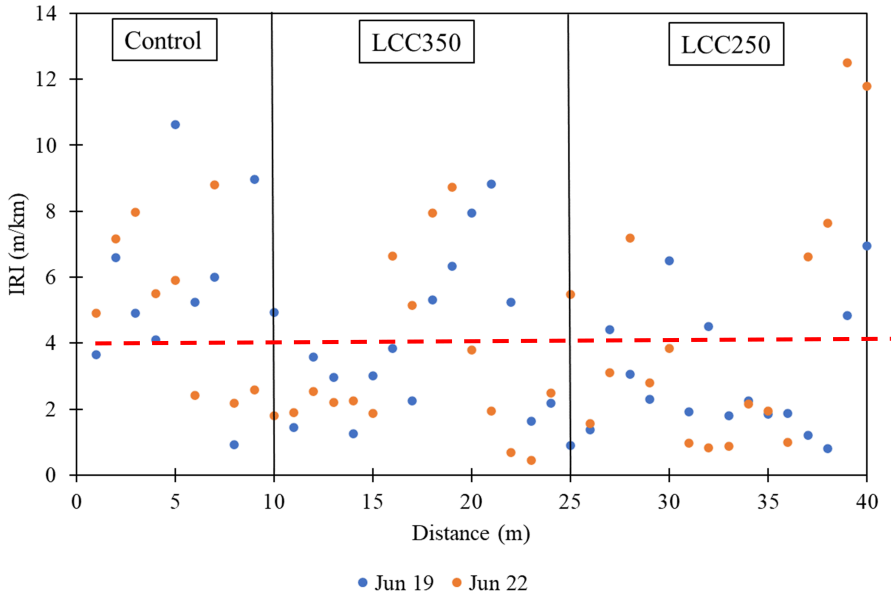

Figure 7.6: Comparison between Erbsville's June 2019 and 2022 IRI profile

Table 7.5: Erbsville's Sections IRI Least Square Difference Analysis

Month -Year	Section Relationship	Left Wheel Path			Right Wheel Path			
		Difference in mean	95% LSD	P-value	Difference in mean	95% LSD	P-value	Comment
Dec-18	Control-LCC350	3.92	2.42	0.001	1.69	1.93	0.008	All LCC different from control
	Control-LCC250	3.95			2.72			
	LCC350-LCC250	0.03			1.02			
Jun-19	Control-LCC350	2.84	2.18	0.004	1.82	2.27	0.037	All LCC different from control
	Control-LCC250	3.10			2.56			
	LCC350-LCC250	0.26			0.74			
Oct-19	Control-LCC350	2.96	2.09	0.003	1.19	NA	0.300	All LCC different in LWP only
	Control-LCC250	2.96			1.39			
	LCC350-LCC250	0.00			0.20			
Dec-20	Control-LCC350	0.71	NA	0.474	1.06	NA	0.629	No difference
	Control-LCC250	0.13			0.38			
	LCC350-LCC250	0.58			0.69			
Feb-22	Control-LCC350				1.24	NA	0.306	No difference for RWP
	Control-LCC250				1.63			
	LCC350-LCC250				0.39			
Apr-22	Control-LCC350	1.68	1.68	0.042	1.03	NA	0.731	All LCC different for RWT
	Control-LCC250	1.66			0.76			
	LCC350-LCC250	0.02			0.27			
Apr-22	Control-LCC350	1.79	NA	0.053	1.32	NA	0.589	No difference
	Control-LCC250	1.54			0.60			
	LCC350-LCC250	0.25			0.72			

Table 7.6: Erbsville section's mean IRI (m/km)

Section	Dec-18	Jun-19	Oct-19	Dec-20	Feb-22	Apr-22	Jun-22
Control	6.27	5.74	5.35	3.81	5.12	4.99	4.70
LCC350	3.64	3.41	3.27	2.93	3.66	3.96	3.15
LCC250	2.72	2.91	3.18	3.56	3.47	4.23	3.63

IRI was observed to fluctuate depending on the testing time. The results also reflect that most Erbsville measured IRI was above 4 m/km. The Control had 44% more points above 4 m/km than LCC350 and 9% more points than LCC250, even though these sections were 50% longer than the Control (Figure 7.6). The highest IRI for the LCC350 section was focused within 15 to 20 m of its length. This was the location of the bus stop; hence this explains why those areas have IRI above 4 m/km. At the LCC250 section, the highest IRI was noted at the edge of the section, which was the location for left-turning traffic. The high IRI values throughout the sections could be due to the fact that the sections are too short and include transitions between the various subbase materials. IRI is typically a better descriptor over longer sections and for roads operating at speeds of 70 km/hr and above.

The Least Square Difference (LSD) result (Table 7.5) revealed that for the first few years, the LCC portions performed noticeably differently from the control section, but by 2022, there didn't seem to be any difference between all the sections. Due to the impact of bus and vehicle traffic on the LCC portions compared to the Control section, the IRI gap between sections may have been closer than in previous years. By June 2022, the Control IRI at Erbsville was an average of 49% more than the LCC350 section and 43% more than the LCC250 section.

Notre Dame Drive

The IRI results for the southbound and northbound left wheel path are presented in Figures 7.7 and 7.8, while the right wheel path IRI is shown in Figures 7.9 and 7.10. The mean IRI values for each direction are provided in Table 7.7. The error bar represents one standard deviation from the mean.

Before the final lift of asphalt was placed on both wheel paths, the most IRI was in April 2022. There was some variation in the IRI measurements along the section profiles, as shown by the error bars. When comparing June 2021 and June 2022, which are represented in the trend for all the other testing times (Figure 7.11), It was observed that the Control

and LCC600 sections performed similarly with data points mostly below 2 m/km. However, LCC475 and LCC400 had a lot of points above 2 m/km. This could be because these locations were situated on slopes greater than 1.3 percent, which could have resulted in lower thicknesses at these locations. Also, before final surface paving, the LCC400 section experienced depressions along its length, which could have contributed to the results. The depressions coincided with former areas of potholes and could also be because of inadequate compaction and the disturbance of the LCC layer due to heavy rainfall a few hours after it was placed. Judging by the 2022 IRI measurements, the LCC400 section appeared to have performed better than prior testing.

After final asphalt lift placement, more consistent IRI was achieved for all the sections on all wheel paths except the northbound right wheel path, where the LCC400 and Control section experienced the most IRI (Table 7.7). Overall, by June 22, the Control exhibited an average of 10% and 13% more roughness than the LCC600 and LCC400 sections and 7% less roughness than the LCC475 on the southbound lane. On the northbound lane, the control had a roughness of 31% and 37% more than LCC600 and LCC475, while the LCC400 had the greatest roughness, 8% more than the control section. LSD analysis revealed that the LCC sections and Control performed differently at various times on the northbound and southbound lanes.

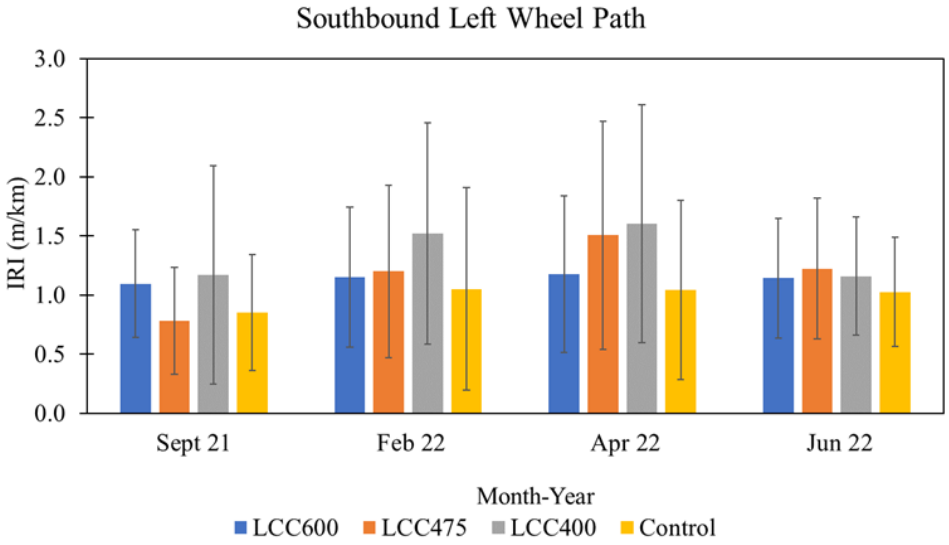

Figure 7.7: Notre Dame southbound left wheel path IRI

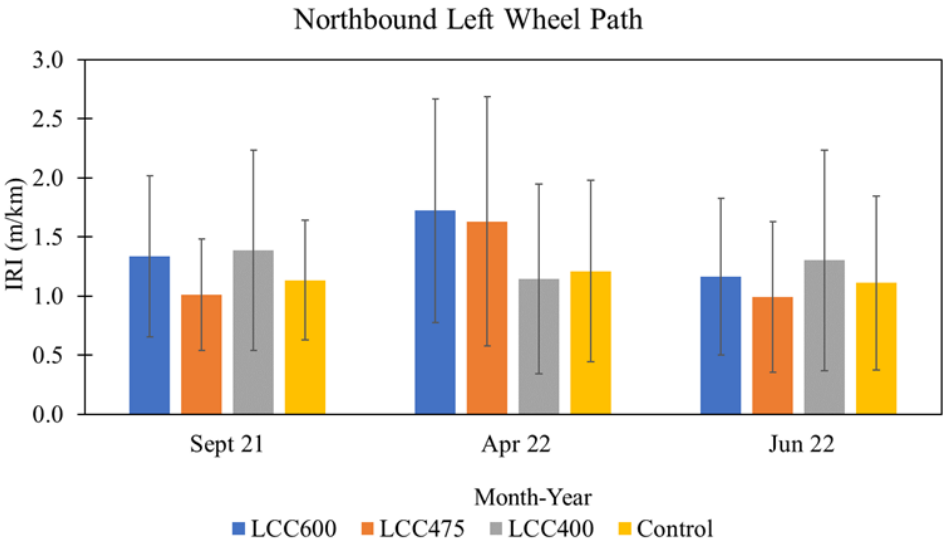

Figure 7.8: Notre Dame northbound left wheel path IRI

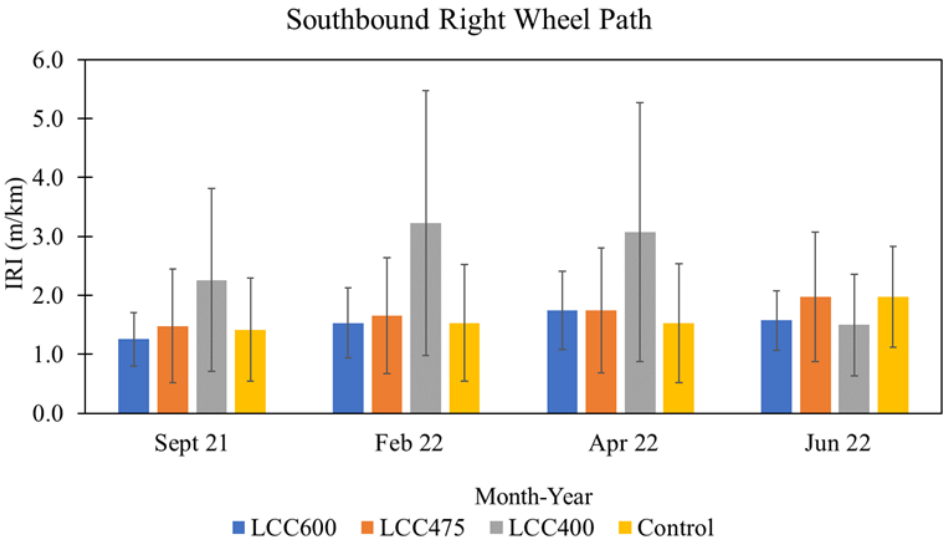

Figure 7.9: Notre Dame southbound right wheel path IRI

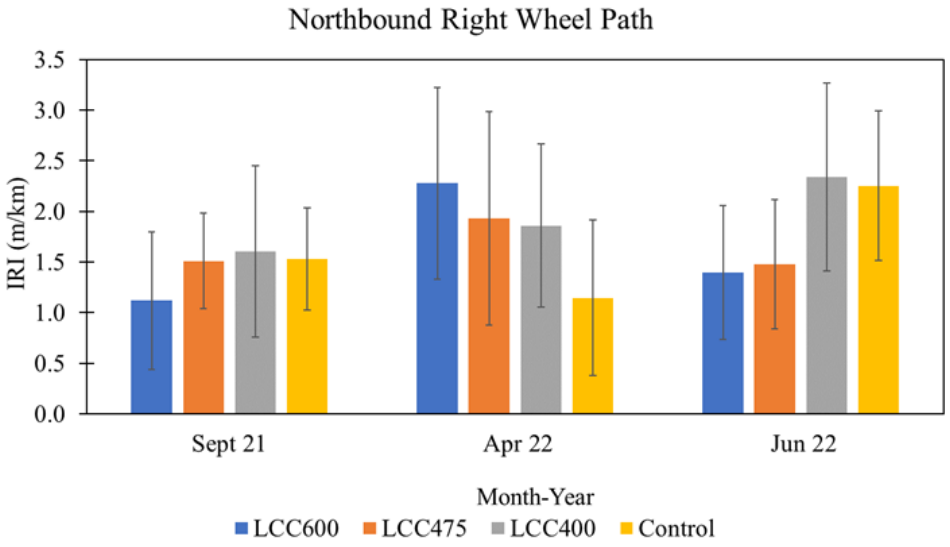

Figure 7.10: Notre Dame northbound right wheel path IRI

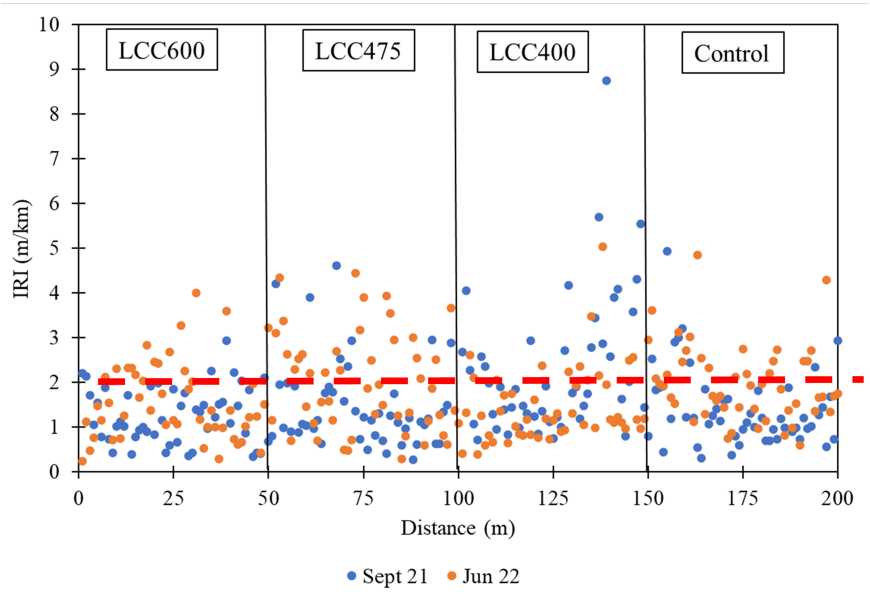

Figure 7.11: Comparison of Notre Dame's September 2021 and June 2022 IRI profile

Table 7.7: Notre Dame Drive mean IRI

Section	Southbound Section Mean IRI(m/km)			
	Sept 21	**Feb 22**	**April 22**	**June 22[A]**
LCC600	1.17	1.34	1.46	1.36
LCC475	1.13	1.43	1.62	1.60
LCC400	1.71	2.37	2.34	1.33
Control	1.13	1.29	1.28	1.50
	Northbound Section Mean IRI(m/km)			
LCC600	1.23		2.00	1.28
LCC475	1.26		1.78	1.23
LCC400	1.50		1.50	1.82
Control	1.33		1.18	1.68

A: Baseline IRI

7.2.3 Dipstick

Figures 7.12 and 7.13 show the measured IRI using this method for the left and right wheel paths at Erbsville, respectively. This method was employed only at the Erbsville location. The dipstick IRI measurements further reflected the same conclusions as the SurPro, signifying that the LCC sections at Erbsville were smoother. However, the magnitude when comparing equipment varied over time. Also, dipstick measured IRI reflected that on the RWP, the LCC350 sections' IRI remained comparatively lower than LCC250 but became similar by April 2022. Measured IRI was most in the control RWP in April 2022, likely due to the spring-thaw effect on the pavement; however, on the LWP, the most IRI was noted in October 2019. Furthermore, the trend in roughness for the sections could also be due to less freeze-thawing and fluctuation in pavement temperature within the LCC sections during the winter compared with the granular B section, as already discussed.

Comparing SurPro and Dipstick IRI, ANOVA analysis indicated that the measurement overtime was statistically different with a p-value over 0.2 (range between 0.21 and 0.98). Table 7.8 shows the percentage differences between dipstick and SurPro IRI values. Negative results indicate that the dipstick measured IRI was higher than the SurPro, while positive values indicate the opposite.

Dipstick was reading about 45% higher than SurPro in June 2019, but by April 2022, the IRI measured by SurPro was 13% more. This demonstrates that employing the two devices resulted in some variability. The outcomes, though, exhibited a comparable pattern.

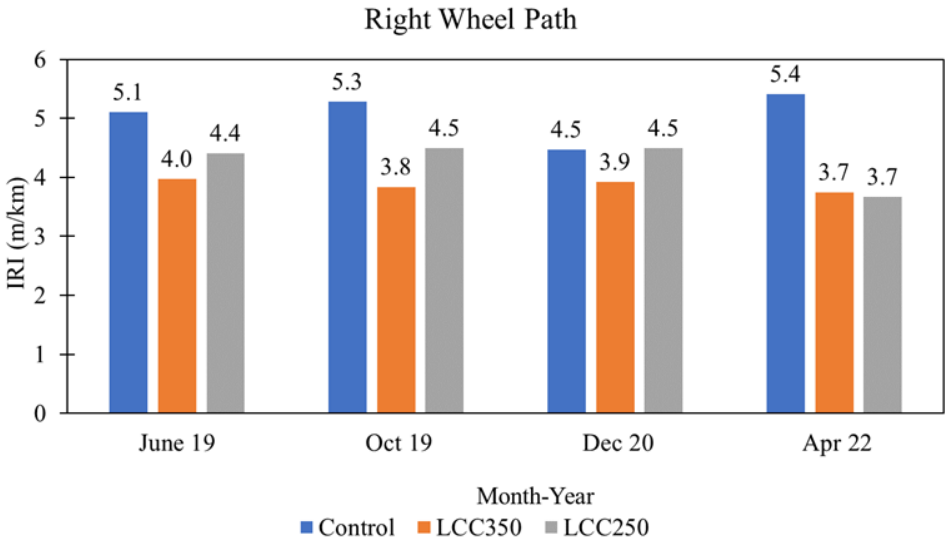

Figure 7.12: Erbsville Dipstick right wheel path IRI

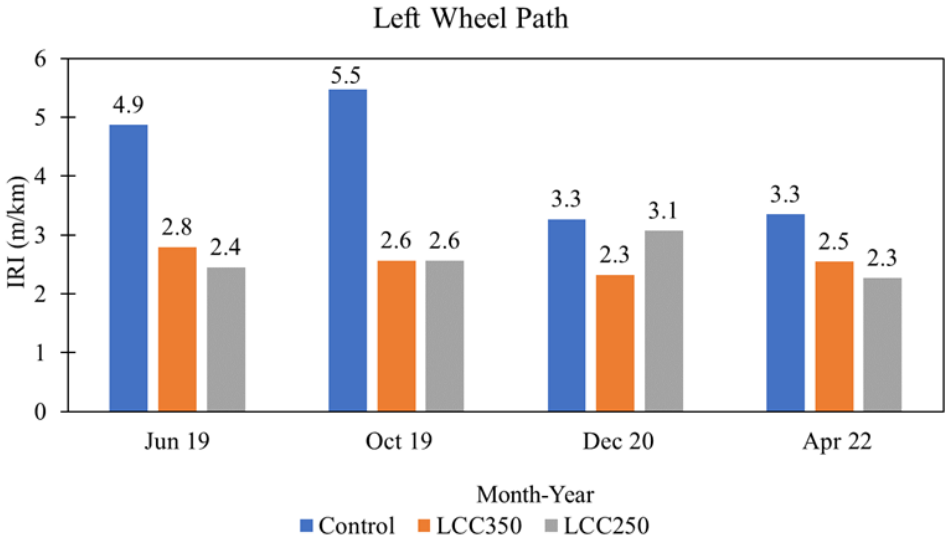

Figure 7.13: Erbsville Dipstick left wheel path IRI

Table 7.8: Percentage difference between SurPro and Dipstick measurements

Month-Year	LWP-IRI (%)			RWP-IRI (%)		
	Control	LCC350	LCC250	Control	LCC350	LCC250
Jun-19	17	8	12	9	-5	-45
Oct-19	3	5	5	-5	0	-23
Dec-20	-8	0	-6	3	-11	-7
Apr-22				8	5	13

LWP: Left Wheel Path and RWP: Right Wheel Path

7.2.4 Summary of Roughness

The roughness progression at the two test sections, Erbsville and Notre Dame Drive were analyzed. The results show that compared to 450 mm thick granular B subbase, 22% and 44% less thick 475 kg/m^3 LCC could provide smoother riding surfaces. Seasonal fluctuation influences pavement roughness and could result from the amount of moisture and temperature within pavement layers. The presence of moisture and temperature variation could cause pavements to contract and expand, therefore altering the pavement profile from time to time. Another significant influencing factor for the advancement of pavement roughness could be road class and function. Due to turning and start and stop movements, road roughness would be increased at intersections. Greater roughness progression would also occur over time on roads near bus stops than on those without this type of traffic that frequently starts and stop in the same area. Additional roughness variables include the initial construction process, which may affect how LCC pavements function over time.

The 200 mm thick 600 kg/m^3 LCC pavement provided an average of 20% smoother pavement for northbound and southbound directions than the control section. While in the northbound direction, the 475 kg/m^3 pavement provided 37% smoother pavement than the control; it was 7% rougher in the other direction. Similarly, an 8% rougher 400 kg/m^3 pavement was encountered in the northbound lane but 13% smoother pavement in the southbound lane. Although conclusions regarding roughness for 200 mm thick LCC pavements for these two densities were not made, it is apparent that they may function similarly to or better than conventional pavements. Current field applications have shown that the incorporation of 200 mm 475 kg/m^3 LCC as subbase over frost susceptible soils would performance significantly better than traditional pavements [64]. This road section at Brentwood Station, in Calgary, has not required repairs for over 20 years of service life, compared to the traditional pavement which required yearly maintenance. It is also evident that several factors play an important role in determining pavement roughness and roughness progression. These factors include the road gradient primarily when the

LCC subbase is being used, construction practices (compaction, early vehicular traffic), environmental conditions, and seasonal variation. IRI progression should be continually monitored to see how these LCC densities perform over time compared with the Control since only limited data is available for these sections.

Furthermore, IRI measurements may vary from testing time to testing time due to various factors, including the testing location not always at the same spot. This causes slightly variable pavement profiles, which in turn causes the IRI measurements to vary. Although care was taken to guarantee that testing occurred consistently at the exact locations, human error cannot be eliminated. Until further data over more extended periods are available, it might be worthwhile to ensure that lower density LCC subbase layers are no thinner than 250 mm. This should be considered when construction activities cannot be controlled or limited after LCC pour before asphalt concrete placement.

SurPro and Dipstick methods produced similar roughness trends for all the sections drawing the same conclusions that the LCC sections provided smoother riding surfaces than the granular B section. However, the magnitude of the measured roughness differed, with the Dipstick results higher at some points and lower at other times.

7.3 Stiffness evaluation

7.3.1 Falling Weight Deflectometer (FWD)

Structural Capacity Evaluation -Erbsville

The ambient temperature was 19 °C, the pavement surface layer 20.8 °C, the Granular A layer 20.5 °C, the Granular B layer 21.7 °C, and the LCC layers 16.6 °C at the time of testing. The section had been in service for nine months at the testing time. Table 7.9 summarizes the findings of the normalized deflection study, which calculated the subgrade resilient modulus (Mr_{des}) and effective structural numbers (SN_{eff}) for the road sections.

The pavement portions appeared to deflect slightly higher than typical. However, the LCC sections showed less deflection than the Control, likely owing to the stiffer subbase material. In addition, the LCC350 section deflected less than the LCC250 section of lower thickness. In all sections, the average normalized area was similar. The effective structural number for Control and LCC350, on the other hand, was similar to and higher than that of the LCC250 section. According to the deflection total thickness calculation, the average subgrade resilient modulus ranged from 42.5 MPa to 56.1 MPa, with effective structural

Table 7.9: Back calculation summary as per AASHTO 1993 pavement design protocol

Location	**Average Normalized d_0 (mm)**	**Average Normalized d_0/d_{200}**	**Average Normalized Area (mm)**	**Average Mr_{des} (MPa)**	**Average SN_{eff} (mm)**
Control	0.513	1.23	512	52.7	118
LCC350	0.311	1.32	500	56.1	120
LCC250	0.366	1.34	499	42.5	96

numbers ranging from 93 to 122 mm. In the analyses, no seasonal reduction factor was employed.

The Elmod software was also used to determine the elastic modulus of individual layers. Figure 7.14 depicts the findings of this investigation. The moduli of hot mix asphalt ranged from 2,500 to 3,483 MPa, with an average of 2,870 MPa. This is comparable to the reported nominal values for new asphalt concrete of around 3,000 MPa [10]. It should be emphasized that the 2,500 MPa low limit was essential to allow accurate back-calculation due to back-calculation limitations, thickness accuracy, and material variability. The section moduli of the LCC350 ranged from 508 to 1047 MPa, with an average of 749 MPa. The moduli of the LCC250 ranged from 547 to 1,292 MPa, with an average of 843 MPa. The LCC layer's overall average moduli from both portions were 796 MPa. Again, the LCC values are comparable to previous studies [63].

Equation 7.1 was used further to determine the structural layer coefficient of the LCC material. The computation is based on the AASHTO layer coefficient published by the Federal Highway Administration of the United States Department of Transportation [50].

$$a = 0.14 \times (\frac{E}{30000})^{0.333} \tag{7.1}$$

where a is the structural layer coefficient, and E is the layer modulus of elasticity in Psi. E was derived using Equation 7.2 to convert the back-calculated average Modulus of Elasticity (796 MPa).

$$E_{psi} = E_{MPa} \times 144.1 \tag{7.2}$$

where E_{psi} is the layer modulus of elasticity in psi and E_{MPa} is the layer modulus of elasticity in MPa. Equation 7.2 with E_{psi} resulted in a layer coefficient (a) of 0.22 for the LCC material. This result corresponded to a past study by Griffths and Popik (2013) [88]

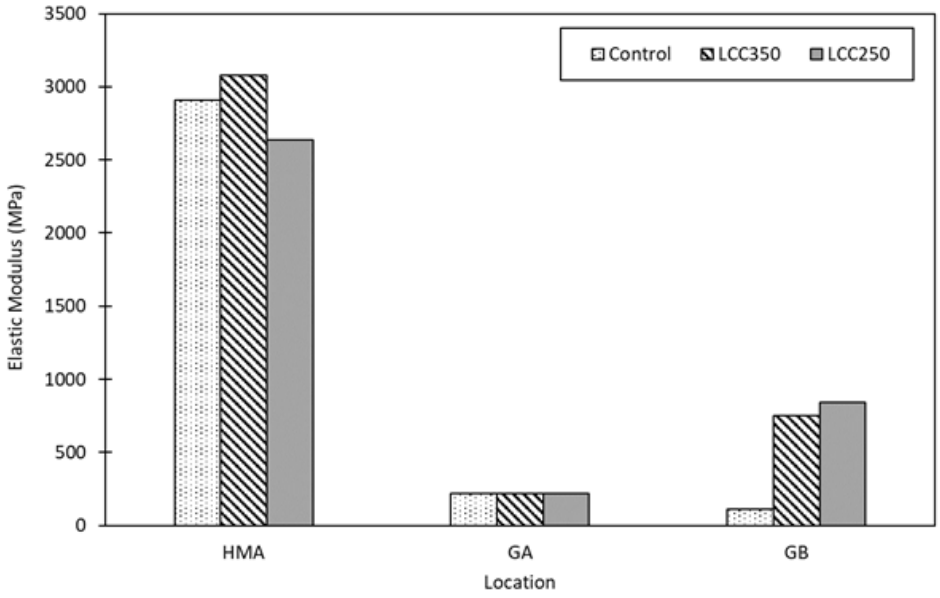

Figure 7.14: Summary of layer thickness and back-calculated elastic moduli

and could provide a reference point when using densities ranging between 400 kg/m^3 and 600 kg/m^3 within the pavement structure. Generally, the variation in the analysis results was likely due to minor variations in material, thicknesses, and data program limitations.

Notre Dame Drive

The FWD test was performed on October 4, 2021. Testing occurred between 10:00 am and noon. The ambient temperature was 15 °C, and the pavement surface layer was 17 °C, 17 °C, and 16.5 °C for the Control, LCC400, and LCC475 at the time of testing. The section had been in service for one month at the testing time. Deflections appeared to be the least on the Control section for all the wheel paths in both directions. The LCC400 southbound right wheel path showed the highest deflection compared to other sections, while the LCC600 section experienced the highest deflection on the northbound right wheel path and left wheel path. The LCC sections also displayed more variation across the sections compared with the Control. These results were different from past FWD tests performed at Erbsville. Also, this outcome could be due to inadequate compaction.

It is believed that less variability and lower deflection outcomes could be obtained over time as traffic continually utilizes these sections. Also, the variability could be due to the stepped and likely lower LCC thickness at specific parts of these LCC sections due to the roadway slope. To further understand the sections' structural behavior, the $AREA_{60}$ method proposed by FHWA was performed. Table 7.10 provides the FHWA (2017) [202] typical interpretation for d_0 and $AREA_{60}$.

Table 7.10: Typical interpretation of d_0 and $AREA_{60}$ values [202]

$AREA_{60}$	**Max. FWD deflection (d_0)**	**Generalised Interpretation**
Low	Low	Weak structure, strong subgrade
Low	High	Weak structure, weak subgrade
High	Low	Strong structure, strong subgrade
High	High	Strong structure, weak subgrade

d_0 and $AREA_{60}$ values are plotted in Figures 7.15 and 7.16. On average, the Control section showed significantly lower d_0 than the LCC400 and LCC475 sections in both directions. It showed comparative deflection in the southbound lane but significantly lower in the northbound lane. Conversely, while the $AREA_{60}$ was mainly within the same range $\pm$50mm for all the sections, the LCC400 and LCC475 had areas of lower $AREA_{60}$. This can be interpreted that the LCC475 and LCC400 sections have a weaker subgrade and a slightly weaker structure compared to the Control and LCC600. By contrast, the LCC600 section had a weaker subgrade, although the structure was as strong as the Control section. These results could be a reflection that there might be something happening within the subgrade of the LCC sections that could be causing higher deflections. It also shows areas of concern with the greatest deflection that requires further investigation. Pavement conditions, loading, pavement structure, and environmental variables all impact FWD testing. For flexible pavements, deflections obtained in deteriorated sections with cracking and rutting are often greater than those in unaffected areas [106].

7.3.2 Light Weight Deflectometer (LWD)

The Lightweight falling deflectometer test was used to evaluate the LCC pavement stiffness over time. Testing was performed at different months to estimate the seasonal effect on the stiffness of the alternative designs. The testing months included February, April, June, October, and December. Test spots at each location were predetermined. As a result, the LWD tests were performed at roughly the same location each time, with a tolerance range

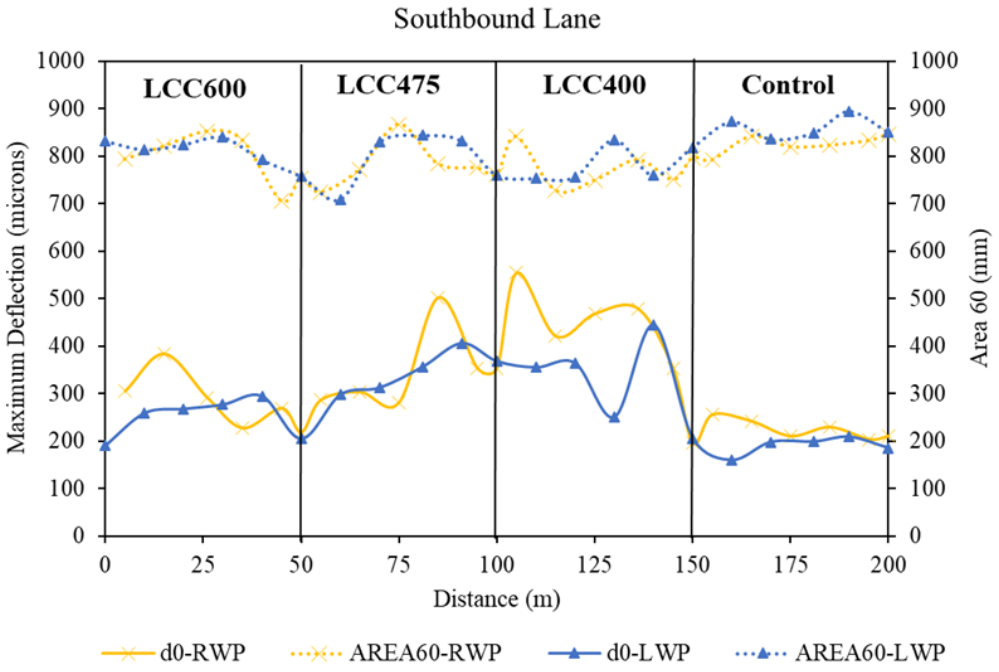

Figure 7.15: Notre Dame Drive southbound lane d_0 and $AREA_{60}$ values

of 1 m^2. The testing location was the same as the FWD test at both places. This section presents and discusses the results for Erbsville and Notre Dame Drive.

Erbsville

Figures 7.17 and 7.18 present the elastic modulus and deflection results for all the testing periods at Erbsville, while Table 7.11 shows the season mean stiffness (average of RWP and LWP). The error bars represent one standard deviation from the mean in the positive and negative directions. A T-test was performed to confirm if the RWP and LWP had different stiffness. The findings suggested that at a 95% confidence level, there was no significant difference in February and April of 2022 (p-value 0.92 and 0.97, respectively). On the contrary, a considerable difference was found between these wheel paths in June 2022 (p-value 0.02). The first pavement testing in December 2018 was completed almost two months after asphalt concrete paving.

The initial measured pavement elastic modulus (indicative of the pavement stiffness) was observed to be the most in the LCC350 (2,506 MPa), followed closely by the LCC250

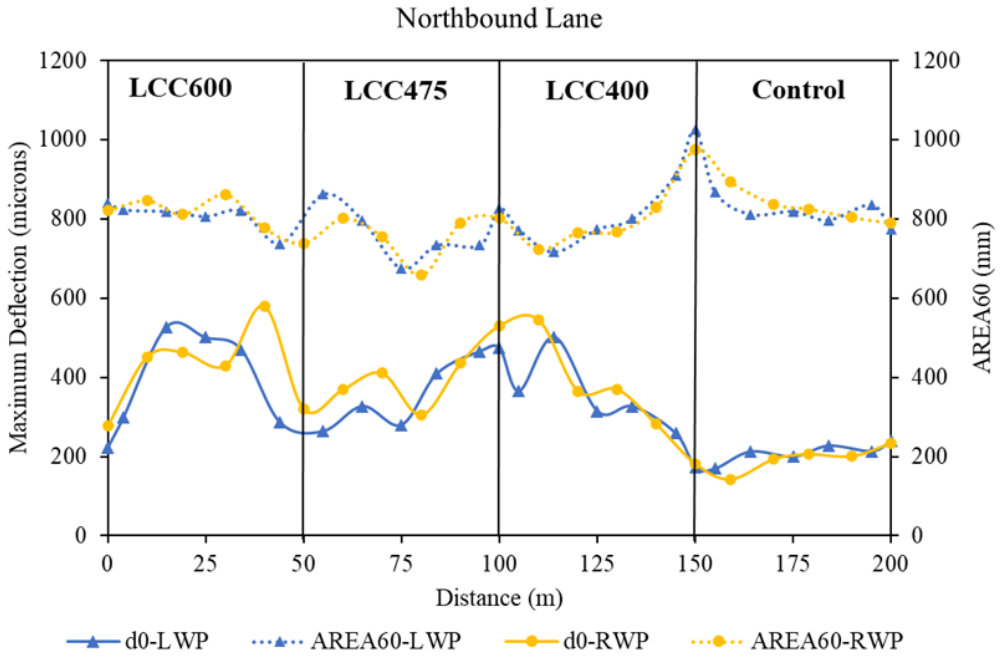

Figure 7.16: Notre Dame Drive nouthbound lane d_0 and $AREA_{60}$ values

section (2,449 MPa) and then the control (1,265 MPa). However, these values only represent near freezing or freezing conditions, producing stiffer pavement layer conditions. Also, only two testing points were completed per section at this time, which could be the reason for the wide gap in stiffness between the LCC and Control section. As can be noted with the error bars and the representative stiffness profile in Figure 7.19, within each section, some variability in stiffness was seen. A similar trend was seen over the analysis period, with the LCC350 section having the stiffest pavement structure and the Control the least. Also, lower deflection values produced higher stiffness, as expected. A study by Apeagyei, (2010) [105] also found spatial variability in pavement subbase and subgrade stiffness when LWD and two other testing equipment were used to assess the pavement stiffness. However, this assessed unbound layers and inferred that the variability could be attributed to soil suction or pore pressure development due to transient loading of the LWD on fine-grained soil.

Stiffness growth (an increase in pavement stiffness) occurred over time. This could be attributed to further compaction of the pavement sections due to traffic over time. Comparing June 2019 and June 2022 (Figure 7.19), a stiffness increase of 25% was found

for the Control, 24% for LCC350, and 23% for LCC250. The slightly lower increase for the LCC sections compared to the Control could be because of these sections' subjection to continuous bus and turning traffic over time. Typically, the bus stops within these two sections, and most of the traffic turning right at the intersection stop and start at the LCC250 section. This could also explain why between December 2018 and February 2022, a stiffness decrease (15%) was observed only in the LCC350 section. Other factors such as moisture content and layer temperature could influence pavement stiffness [105].

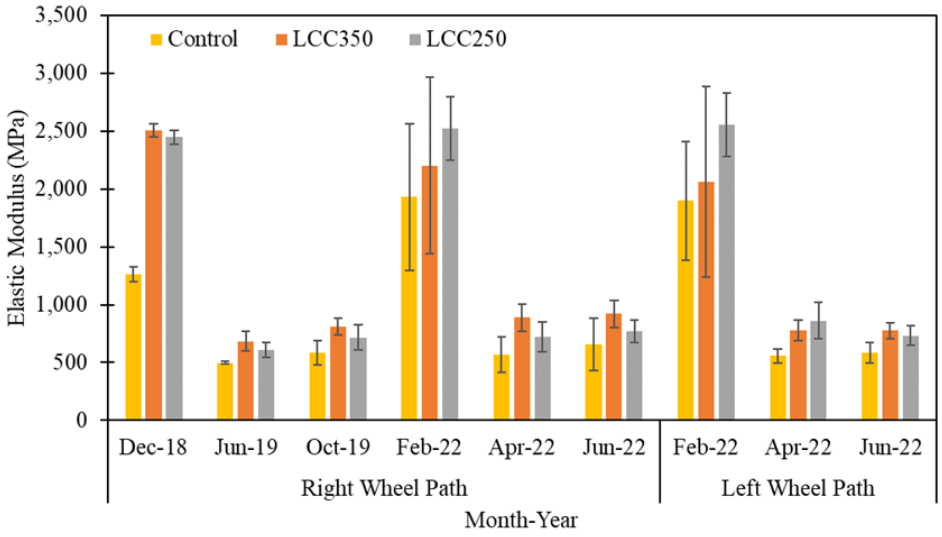

Figure 7.17: Erbsville LWD measured elastic modulus

Table 7.11: Erbsville section LWD measured mean elastic modulus (MPa)

Section	Dec-18	Jun-19	Oct-19	Feb-22	Apr-22	Jun-22
Control	1,265	498	585	1,914	562	621
LCC350	2,506	684	811	2,132	834	849
LCC250	2,449	610	717	2,538	790	751

The significant difference between the measured stiffness for the sections at a 95% confidence level was tested with the least square difference (LSD) analysis. A significant difference existed between the Control and LCC sections, especially in December 2018 and

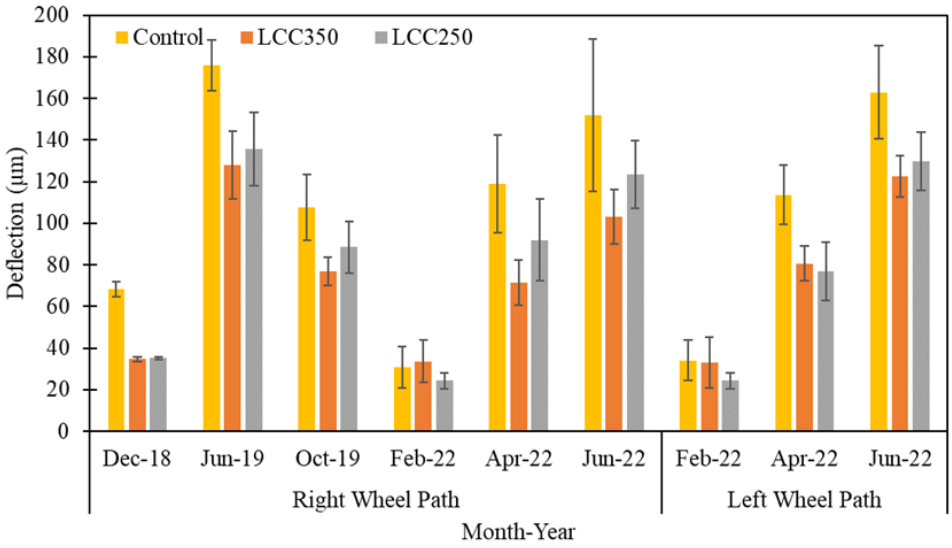

Figure 7.18: Erbsville LWD measured deflection

June 2019 (Table 7.12). But, in October 2019, the Control displayed stiffness not significantly different from LCC250. Also, in 2022, the results showed no significant difference in measured stiffness for all the sections. Only measured stiffness values on the LWP for the LCC sections in April and June 2022 were significantly different from that of the Control. Again, since the LCC sections are the most subjected to vehicular traffic, it is expected that deterioration should occur more rapidly than the Control; this could be why the stiffness values were closer to that of the Control in later years. But the LCC sections still exhibited higher stiffness than the Control.

Table 7.12: Erbsville stiffness least square difference analysis

Section	**Dec-18**	**Jun-19**	**Oct-19**	**Feb-22**		**Apr-22**		**Jun-22**	
Relationship	**RWP**	**RWP**	**RWP**	**RWP**	**LWP**	**RWP**	**LWP**	**RWP**	**LWP**
Control-LCC350	1,241	192	227	216	586	148	314	113	147
Control-LCC250	1,185	112	135	608	836	148	314	113	147
LCC350-LCC250	57	81	91	391	250	163	95	154	43
LSD Criteria	260	97	149	NA	NA	207	173	230	120
P-value	0.000	0.000	0.005	0.515	0.332	0.005	0.001	0.023	0.003

In conclusion, because only the subbase of the pavement structure was altered, it may be argued that the LCC layer enhanced the pavement structure's stiffness compared to the unbound granular B. The stiffness improvement was proportional to the thickness of the LCC.

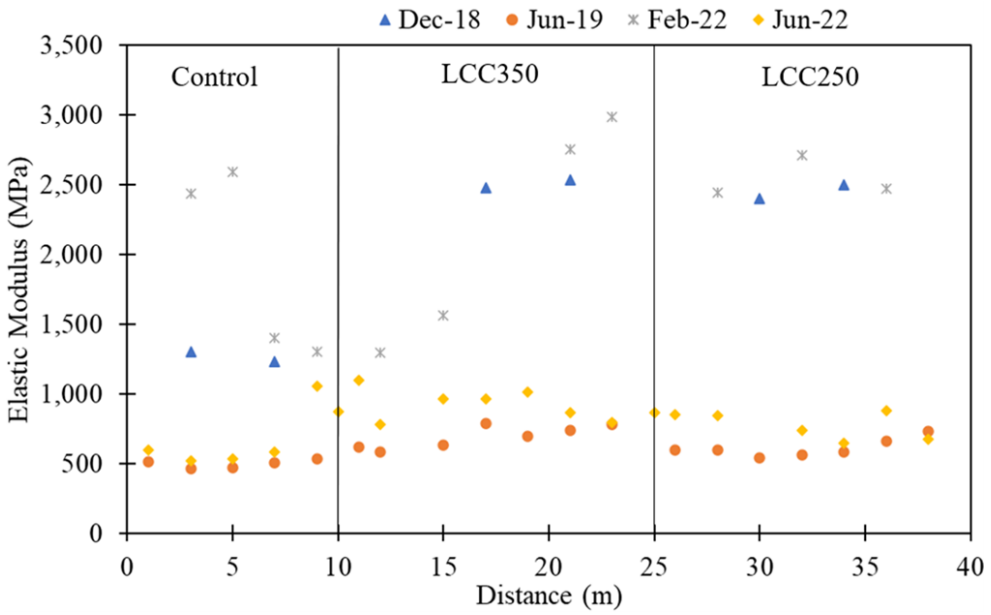

Figure 7.19: Erbsville stiffness comparison overtime

LSD analysis was done on the measured stiffness values between each testing month to determine if there was a seasonal effect on pavement stiffness. Seasonal stiffness analysis showed that the period when the stiffness was performed was a significant factor in determining its magnitude. The 95% LSD criteria were obtained to be 589 MPa for the Control, 504 MPa for LCC350, and 191 MPa for LCC250. No significant difference was recorded in all the sections (at a 95% confidence level) for stiffness measured between April, June, and October when compared with each other. The relationships between these months had mean differences over two times below the 95% LSD criteria. However, when comparing the stiffness between other months such as December/April, December/June, and December/October, the mean difference in stiffness was found to be one time higher for the Control, over three times greater for the LCC350 section, and more than nine times for LCC250 section than the LSD criteria. Similar outcomes were achieved when February stiffness was compared with April, June, and October. A comparison between February and December indicated no difference for the LCC section but noted a significant difference

within the Control. This could further show the insulating properties of the LCC section during the early cold period yielding some difference.

Notre Dame Drive

T-test result for Notre Dame Drive indicated that there was no significant difference between the stiffness measured on the right wheel path (RWP) and left wheel path (LWP) for September 2021 and February, April, and June 2022 (p- values of 0.34, 0.66, 0.09 and 0.10) at 95% confidence level. Figures 7.20 and 7.21 show the mean measured stiffness on each wheel path, while Table 7.13 presents the section mean elastic modulus. The error bars represent one standard deviation from the mean in the positive and negative directions.

In September 2021, the initial elastic modulus for all sections was discovered to be relatively low compared with typical flexible pavements. The stiffness of the Control was 224 MPa, followed by 187 MPa, 146 MPa, and 96 MPa for the LCC600, LCC475, and LCC400. Because the testing was done a few hours after AC was installed, the low stiffness could be attributed to the softer asphalt concrete layer at the time. During testing, the surface layer temperatures were 47 °C, 45 °C, 43 °C, and 47 °C for the Control, LCC400, LCC475, and LCC600, respectively (Table 7-3). The temperatures of the base, subbase, and subgrade were also found to be between 25 °C and 20 °C, with the LCC base layers averaging 5 °C higher than the Controls' and the subbase and subgrade averaging 2 °C lower (Table 7-3).

During the testing period, the Control portion was stiffer than the LCC sections, contrary to the results observed at Erbsville. Construction method, insufficient compaction (no vibratory compaction done during construction) on the LCC sections, excessive truck traffic before AC placement, and the fact that the LCC475 section and a significant portion of the LCC400 were placed on a longitudinal slope greater than 1.3 percent are thought to be factors that contributed to the lower stiffness values. Because LCC is a stiffer material, it is typically projected to provide a stiffer pavement structure, like Erbsvilles' [176]. However, the lower thickness could also be an influencing factor. It is recommended that the pavement sections be monitored to see if improvements in the LCC sections continue as expected.

Comparing stiffness between September 2021 and April 2022, the disparity in stiffness between the Control and LCC sections decreased by 86%, 68%, and 61% for LCC400, LCC475, and LCC600. This could signify that the compaction level within the sections had increased over time due to traffic, and the pavement is gaining strength and stability

to support the pavement structure adequately. Also, the stiffness of the LCC sections was proportional to their density.

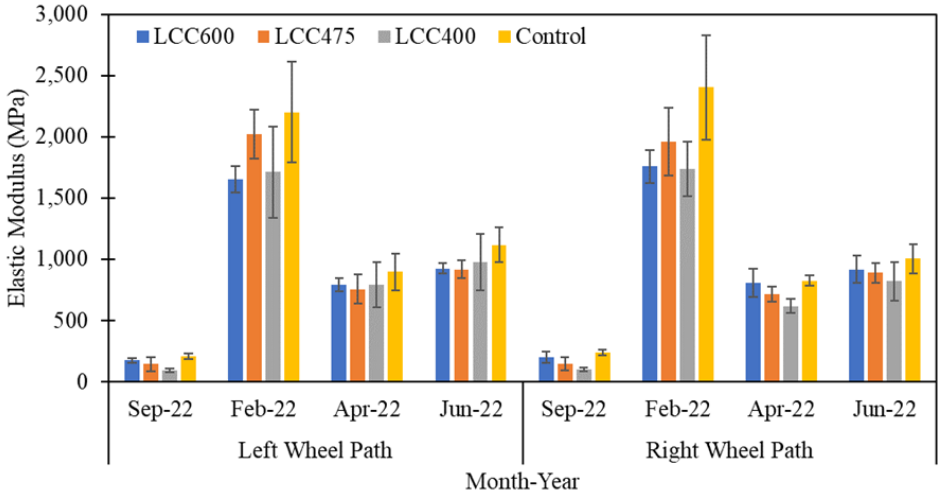

Figure 7.20: Notre Dame Drive elastic modulus on RWP and LWP

Table 7.13: Notre Dame Drive sections mean Elastic Modulus (MPa)

Section	**Sep-21**	**Feb-22**	**Apr-22**	**Jun-22**
LCC600	187	1,706	799	922
LCC475	146	1,993	737	903
LCC400	96	1,726	706	898
Control	224	2,302	861	1,061

Furthermore, the least square difference (LSD) method was applied to assess if there was a difference in measured stiffness between sections. The findings from this analysis are shown in Table 7.14 for the RWP and LWP. The ANOVA analysis first indicated that between September 2021 and April 2022, there was a significant difference between some sections with p values below 0.05 at a 95% confidence level. In Table 7.14, the highlighted portion (bold) indicates the areas with a significant difference in measured stiffness. A significant difference is noted between LCC400 with LCC600 and Control initially. However, after the final AC paving, the measured stiffness indicated no statistical

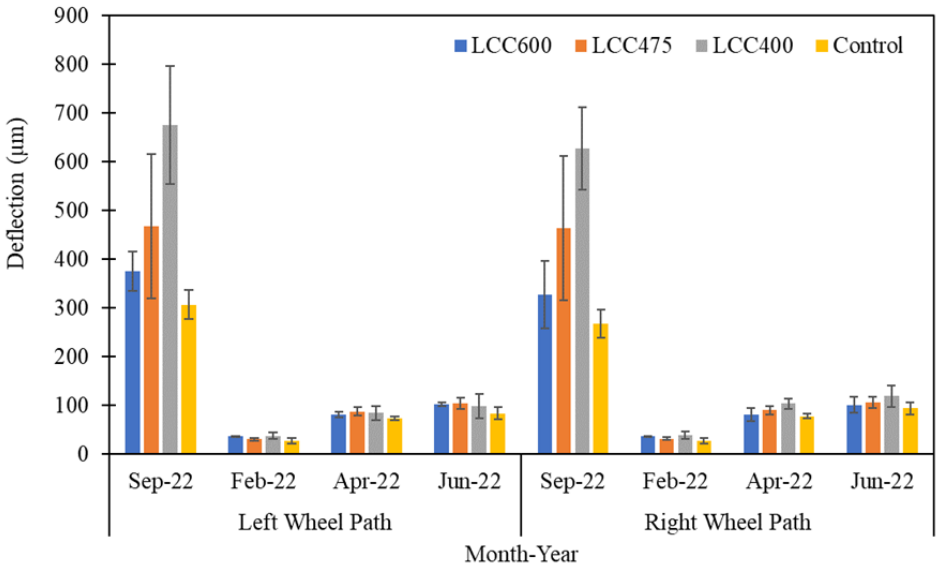

Figure 7.21: Notre Dame Drive deflection on RWP and LWP

Table 7.14: Notre Dame Drive Least Square Difference analysis between sections

Section	**Sep-21**		**Feb-22**		**Apr-22**		**Jun-22**	
Relationship	**RWP**	**LWP**	**RWP**	**LWP**	**RWP**	**LWP**	**RWP**	**LWP**
Control-LCC400	140	109	663	490	209	103	186	141
Control-LCC475	92	58	441	179	108	142	117	199
Control-LCC600	42	26	645	548	20	105	88	191
LCC400-LCC475	48	51	222	311	101	39	69	59
LCC400-LCC600	98	83	18	58	189	2	98	50
LCC475-LCC600	50	32	204	369	88	37	29	8
LSD Criteria	70	54	504	563	133	-	-	-
P-value	0.000	0.000	0.007	0.041	0.002	0.415	0.153	0.134

difference between the sections. This could further show improvement in the stiffness of the LCC sections over time.

The stiffness immediately after the base asphalt was placed in September of 2021 showed a smoother profile along the road section compared with after placement of the surface asphalt concrete layer, where more variability in stiffness within each section was seen (Figure 7.22). The most variability was observed in the Control section, then the LCC400 section. The LCC600 section showed the most constant stiffness along its length. As

expected, the pavements' elastic modulus on average post final AC paving increased by 5, 11, 6, and 5 times for the Control, LCC400, LCC475, and LCC600 sections, respectively. The biggest stiffness jump was noted in the LCC400 section (Figure 7.23).

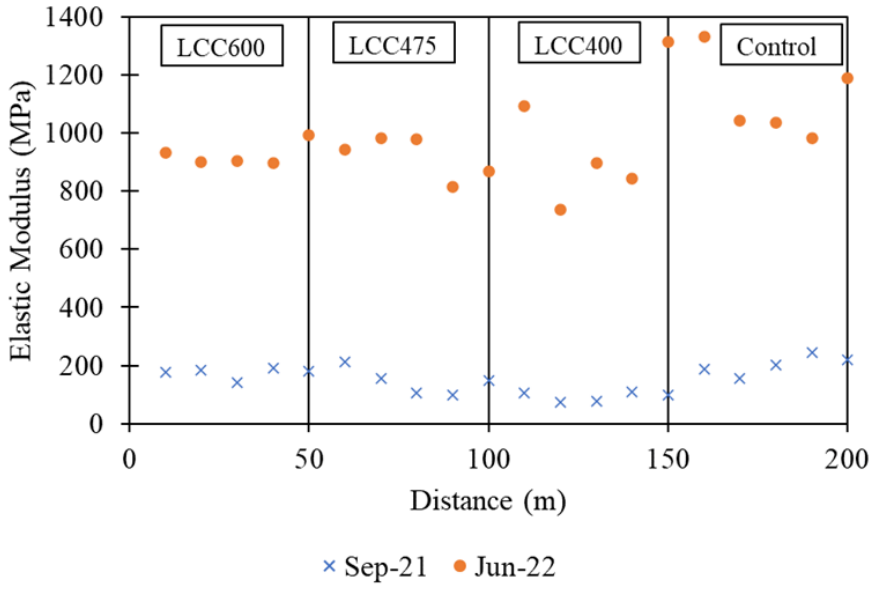

Figure 7.22: Comparison of measured stiffness in Sept 21 and June 22 for Notre Dame

In assessing seasonal effects on each section, LSD results showed that relationships between all the months except April and June (highlighted) were significantly different (Table 7.15). This further proves that temperature and moisture are significant determinants of pavement stiffness, as indicated in other studies [235, 105]. A change in the asphalt concrete surface temperature, which impacts stiffness, could alter the stress condition across the pavement. Due to their typical stress reliance, the underlying unbound layers' performance may be affected by this shift in stress state [274].

Regression analysis was performed between surface temperature for all the sections excluding LCC600 with the respective measured elastic modulus. The result showed a strong relationship ($R^2 > 0.8$) in all the sections (Figure 7.24). When regression was performed with the base, subbase, and subgrade layers, the relationship was less strong and decreased with depth. The ambient temperature over the study period was 22 °C, -2 °C, 12 °C, and 24 °C for September 2021, February, April, and June 2022 (Table 7.4).

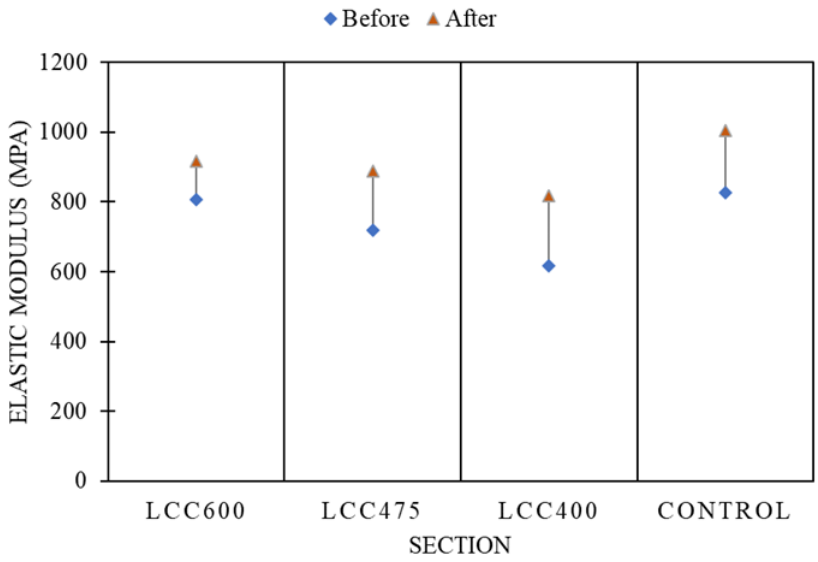

Figure 7.23: Elastic modulus jump before and after surface AC paving

Table 7.15: Notre Dame Drive Seasonal Least Square Difference Analysis

Section	**LWP-IRI (%)**			**LWP-IRI (%)**		
Relationship	**Difference in Mean**	**95% LSD**	**P-value**	**Difference in Mean**	**95% LSD**	**P-value**
Sept-Feb	1738			1794		
Sept-April	656			571		
Sep-June	831	197.32	0.000	737	197.4	0.000
Feb-April	1082			1223		
Feb-June	907			1058		
April-June	175			166		

7.3.3 Summary of Stiffness

The field experiment was carried out to investigate the in-situ structural capacity of Lightweight Cellular Concrete subbase pavements and compare them with traditional unbound materials subbase pavements. This was done by examining the deflections induced by traffic loads on the pavement structure. The findings showed that based on FWD results, the LCC sections with 350 and 250 mm thick 475 kg/m^3 LCC density as subbase provided a four times stiffer subbase layer than the typical 450 mm granular B subbase. The structural layer coefficient for 475 kg/m^3 of Lightweight Cellular Concrete was deter-

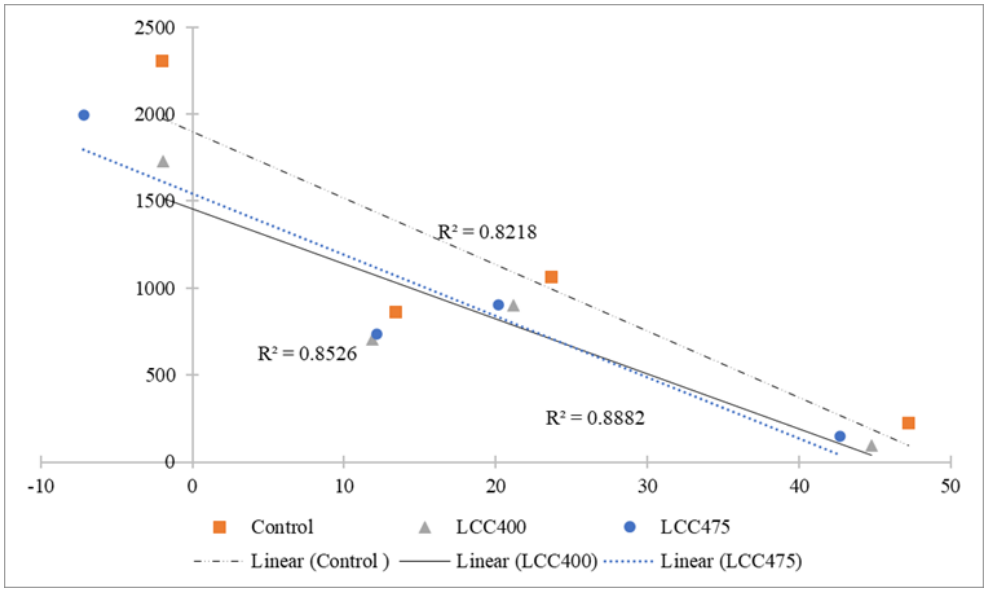

Figure 7.24: Stiffness relationship with surface layer temperature

mined to be 0.22, which can serve as a reference point when designing and installing LCC densities between 400 to 600 kg/m^3 as pavement subbase. The AREA$_{60}$ and d_0 analysis revealed that at Notre Dame Drive, a weaker subgrade existed at the 400, 475, and 600 kg/m^3 lightweight cellular concrete sections compared with the unbound granular material section. Besides, some weak pavement structure spots were noted at the 475 kg/m^3 and 400 kg/m^3. These spots also corresponded with areas that had high IRI. More research is necessary to comprehend what is occurring in these areas entirely.

Lightweight Deflectometer results showed that flexible pavements with 475 kg/m^3 LCC subbase thicknesses of 250 mm produced a 21% stiffer pavement structure compared with twice as thick unbound granular B subbase pavements. The pavement stiffness increased to 36% when LCC thickness was increased by 100 mm. Pavement stiffness was also noted to increase with an increase in LCC layer density and over time for both LCC and unbound granular pavements. Across the road section profiles, variation in stiffness was noted for all the sections, and this variation was evident during the spring thaw period. There was a strong positive relationship between pavement stiffness and pavement surface layer temperature. Pavement stiffness was further seen to be significantly influenced by season, with the winter providing the stiffest pavements and the Spring, the least stiff pavement structure.

Overall, the construction method, insufficient compaction (no vibratory compaction

done during construction) on the LCC sections, excessive truck traffic before AC placement, and the fact that the 475 and 400 kg/m^3 LCC portions were placed on a longitudinal slope greater than 1.3 percent are thought to be factors that contributed to the lower stiffness values at Notre Dame Drive. Because LCC is a stiffer material, it was projected to provide a stiffer pavement structure, like Erbsville.

Chapter 8

Life Cycle Assessment

8.1 Background

Construction's environmental impact is increasingly recognized, as the industry's overall energy consumption accounts for nearly a third of all greenhouse gas (GHG) emissions [273]. Cement concrete is a vital material used in the construction industry for ubiquitous engineering applications. Cement manufacturing accounts for about 5% of global anthropogenic carbon dioxide (CO_2) emissions [58, 99]. The production of 1kg of Portland cement generates 0.81 to 0.87 kg of Carbon dioxide (CO_2) emissions [108, 44, 42]. The cement industry's main source of emissions is the calcination process, which utilizes a lot of fossil fuel and decarbonizes limestone. As a result, methods to reduce the industry's substantial impact are constantly being investigated [143, 271, 210, 261].

Innovative ways to reduce CO_2 emissions connected with cement production have been recommended. One of these is the use of green concrete. Green concrete employs waste material in its mixture, has a low environmental impact production process, or has a high performance and long-life cycle [232]. Given that concrete includes around 12% cement, and the cement sector generates 5% of total global emissions, green concrete presents a chance for the construction industry to adapt [226]. In this situation, the lightweight cellular concrete can be termed green concrete [226].

This chapter examines the economic and environmental impact of LCC produced using the wet and dry mix methods and compares the implications with unbound granular material typically used as pavement subbase. The study explores the environmental impact of producing, transporting, and maintaining pavement sections with three different

LCC densities (400 kg/m^3, 475 kg/m^3, and 600 kg/m^3), granular A and granular B as subbase alternatives. The Life Cycle Assessment (LCA) method was used to estimate the environmental impact of incorporating LCC within the pavement structure.

8.2 Material and Methods

This study was conducted in three stages. The first stage involved the design, instrumentation, and construction of a field section incorporating LCC (see section 4.3). As part of this phase, pavement performance prediction was also performed (see section 5.5). The second stage included obtaining real-time performance data from instrumentation to compare actual and modeled results (see section 6.9). It also included laboratory testing in determining the material properties of existing field layers. The final stage was the life cycle assessment. The LCA methodology specified in the ISO 14020 standard and the framework for pavement LCA provided by the FHWA 2016 [95] report was adopted.

8.2.1 Design and Material Properties

The Notre Dame field section design was adopted for this LCA analysis. The design is presented in Figure 8.1. This design has been adapted from Figure 4.14 in Chapter 4. Applied LCC comprised 100% General Limestone Cement (GUL), a water to cement ratio of 0.51, and preformed foam. Also considered was the effect of substituting 20% pozzolan for the same portion of cement. This field segment is divided into four 50-meter sections, with a Control section using granular A (GA) as a subbase and three LCC sections using 400 kg/m^3, 475 kg/m^3, and 600 kg/m^3 LCC material as subbases, respectively. In this study, these three portions are designated as LCC400, LCC475, and LCC600 based on the densities of the LCC. For all sections, a consistent 90 mm of Superpave 12.5 and 100 mm of Superpave 19.0 (with 15% RAP) asphalt concrete (AC) was laid over 150 mm of granular A material as the base asphalt course. The pavement was built on the same subgrade with a resilient modulus of 43 MPa. However, the LCC400 and LCC475 portions have higher longitudinal slopes ($\geq$ 1.3 percent) compared to the Control and LCC600 portions.

Additionally, an alternate design was completed to obtain a structurally equivalent Control section with granular B in place of granular A (Table 8.1). All the LCC sections remain unchanged for layer thickness. Lifecycle analysis was also performed using this design.

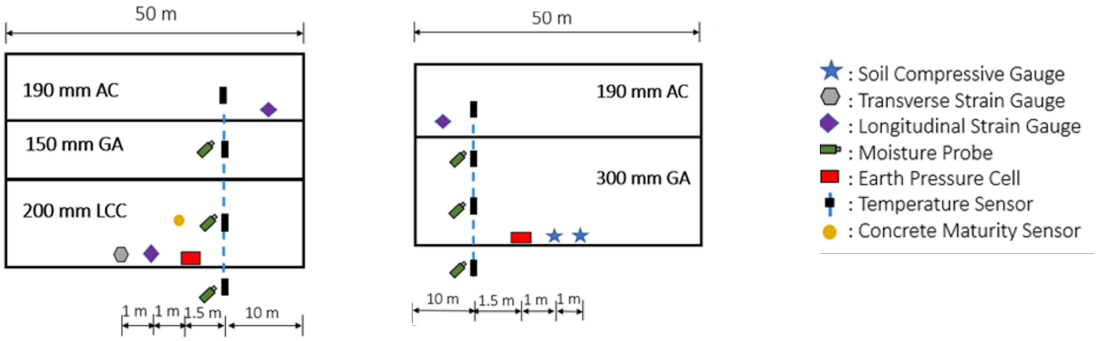

(a) LCC section (b) Control section (c) Legend

Figure 8.1: Cross section for Notre Dame trial road for LCA

Table 8.1: Alternate equivalent design with granular B

Material	**Control**	**LCC400**	**LCC475**	**LCC600**
Superpave 12.5 FC2 (mm)	90	90	90	90
Superpave 19.0 (mm)	100	100	100	100
Granular A (mm)	150	150	150	150
Granular B (mm)	230	-	-	-
Lightweight Cellular Concrete (mm)	-	200	200	200

8.2.2 Production Methods

The wet and dry mix procedures are commonly utilized in applying LCC in the field [63]. A ready-mix company mixes cement and water slurry offsite and brings it to the construction site in the wet mix method. As the material is pumped into place, foam is injected into the slurry in the LCC equipment on-site. In the dry mix method, all material components for LCC manufacture are blended on-site. Cement and water slurry are mixed first in the LCC equipment; then foam is injected into the mixture as it is poured into place. This approach is frequently used for high-volume items.

All material components, methods, equipment employed, and their varied environmental consequences must be examined to generate the LCA for placing LCC. Cement, pozzolanic materials such as fly ash and blast furnace slag, and foam were among the materials considered. The pozzolans are typically provided preblended from the cement supplier. 100% cement mixes could also be used. When using the wet mix method, considerations should be made for the wet mix equipment as well as the ready-mix concrete truck that would transport and mix the concrete. The dry mix equipment, which incorporates all

the processes, was also noted in the dry mix method. Regarding material manufacture and construction, the impact of transportation was considered. The following considerations have been made in performing the life cycle assessment of LCC.

- Source of material
- Production rate/capacity of material at source
- Energy used during material production at source (obtained from CEMATRIX)
- Emissions due to each process
- Waste produced during material production (solid waste and wastewater)
- The properties of raw materials used for M&R, such as virgin aggregate and bitumen, were used for both the mill and overlay baseline.

In assessing the lifecycle of lightweight cellular concrete, Figure 8.2 is a schematic outlining the inputs, processes, and outputs during the operations with required information cradle to gate. Figure 8.3 depicts the flow for the dry mix method and Figure 8.4 for the wet mix method.

8.2.3 Pavement Performance Prediction

MEPDG and WESLEA were used to predict pavement performance (see section 5.5). Input parameters for material properties such as Modulus of Elasticity, Poisson's ratio, and California bearing ratio (CBR) were obtained from laboratory tests performed on field specimens. Other parameters not tested in the laboratory were obtained from recommended AASHTOware Ontario default parameters [185] and typical pavement designs final report by Applied Research Associates, ARA (2015) [10]. Laboratory results found for compressive strength, elastic modulus, and Poisson ratio were like those obtained in the study by Ni, Oyeyi and Tighe (2021) [176] when 80 to 20 cement and slag ratio with similar material characteristics were used. Therefore, this analysis considered comparable performance to using 100% GUL cement for the LCC blend mix.

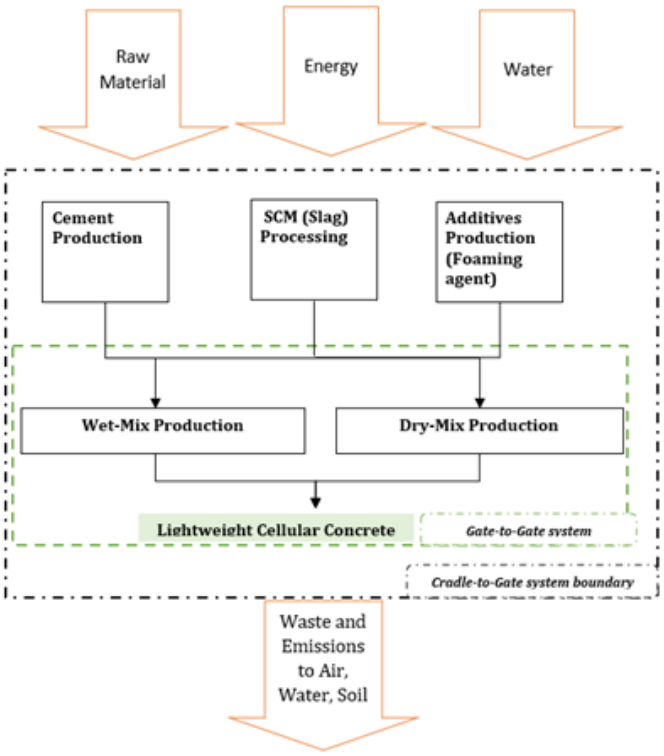

Figure 8.2: Cradle-to-gate production and placement of LCC material for pavements

8.2.4 Maintenance and Rehabilitation Strategies

Maintenance and rehabilitation (M&R) strategies have been developed based on performance prediction results. Following results from predicted pavement performance, the ARA (2015) [10] recommended strategies for minor arterial roads AADTT between 1,000 – 1,500 was adopted. The same M&R strategies for the Control were used to determine the strategy for the LCC sections. The assumption was that the failure pattern would follow a similar trend but slightly delayed for the LCC sections, as indicated in WESLEA performance predictions (see section 5.5.2).

8.2.5 Life Cycle Assessment

Life Cycle Assessment (LCA) is an evaluation technique employed to analyze and quantify the environmental impacts of a product, process, or system by assessing all input and

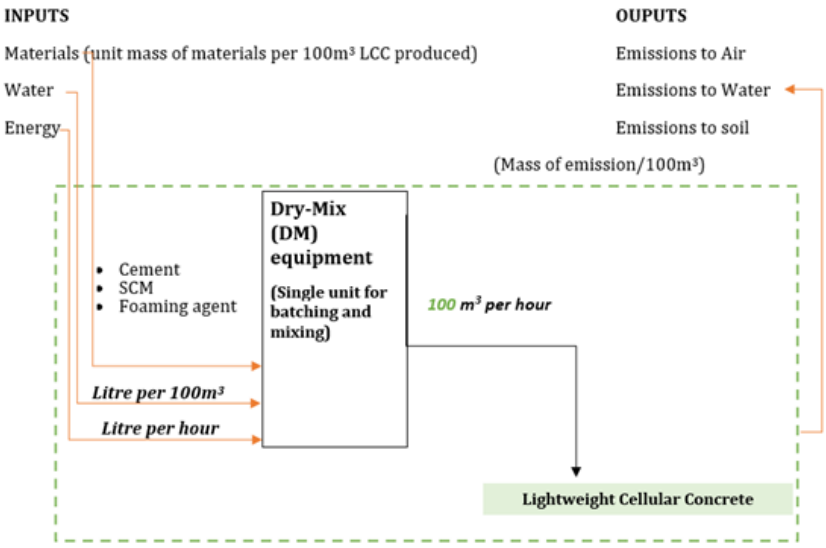

Figure 8.3: Dry mix production and placement of LCC material for pavements

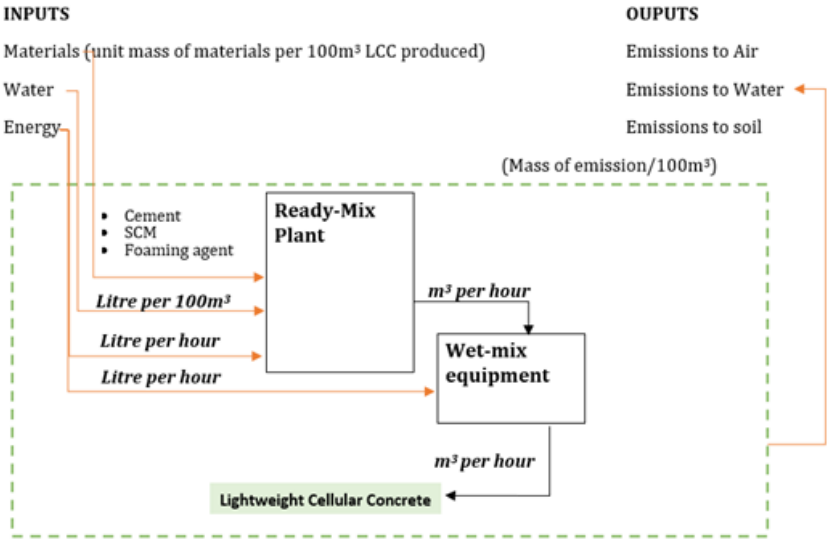

Figure 8.4: Wet mix production and placement of LCC material for pavements

output throughout its lifecycle. Inputs and outputs include but are not limited to materials, energy, emissions, and waste. This study adopted the LCA methodology specified in the

ISO 14020 standard and the framework for pavement LCA provided by the FHWA 2016 [95] report.

1. Goal and Scope: For the purpose of this study, four design alternatives for a minor arterial road section were investigated. The objective was to quantify the environmental performance of subbase materials and design pavement alternatives for potentially weak subgrades. The functional unit of analysis was a one-lane 50 m road section designed for traffic of 650 AADTT and 50-year service life. A lane width of 4.85 m was considered, and the dimensions of pavement layers for each are available in Figure 8.1. The scope of the study is limited to three phases of the pavement lifecycle: material production, initial construction, and maintenance activities. A simplified focus on construction and M&R was adopted here, given that the goal was to show an approach towards a holistic assessment of pavement design sustainability impact. The system boundary considers 50-year service life but not the end of the pavement life; thus end of life environmental impacts were excluded. This study focused on factors impacting GHG emissions and other harmful air pollutants. Water use, for example, though required in every pavement project, was excluded from material production because it does not emit much GHGs. Still, the effect of its transportation has been included. Also, the preformed foam used in LCC production was excluded in this analysis since it constituted less than 0.1% by volume of the total mix.

2. Emissions Inventory: an emission inventory for all phases within the scope was created using an adapted Pavement Lifecycle Assessment Tool for Environmental and Economic Effects (PaLATE) tool initially developed by the Consortium on Green Design and Manufacturing at the University of California, Berkeley [104]. The adapted version was developed by Nasir (2018) [173] as part of a research program to quantify the environmental cost of pavement management. This version includes updated emissions data and emissions factors (EMFs) for Ontario or Canada. An EMF refers to the average rate of emissions associated with an activity. The total emissions of a specific pollutant from a given set of activities can be calculated using Equation 8.1 [84] .

$$TE_j = \sum_i (EMF_{i,j} \times A_i) \tag{8.1}$$

where: TE_j= Total emission for pollutant j in a given geographical area, and time period, units of mass; $EMF_{i,j}$ = Emission factor for pollutant j from source activity i, units of mass/per unit activity; A_i = Total units of activity. The equation and the EMFs in Table 8.2 are used to estimate total emissions for all processes/activities considered within the system boundary of this study.

3. Impact Assessment and Interpretation: The environmental performance was quantified as the environmental cost of emission using the marginal damage cost of five atmospheric emissions: carbon dioxide (CO_2), carbon monoxide (CO), nitrogen oxides (NO_x), sulfur dioxide (SO_2) and particulate matter ($PM_{2.5}$). Because each of the pollutants considered has different effects on human health and the environment, they cannot be directly compared. The environmental impacts of each pollutant were valued using their respective marginal damage (MD) to estimate the total social cost of atmospheric releases. Several models are available to calculate damages from atmospheric releases, but a complete impact assessment can be computationally prohibitive. Thus, MD estimates vary greatly depending on factors such as site and source of emissions, the valuation method used, and the impacts considered [173, 267]. However, this study adapts recently developed marginal damage estimates for 2015 Canadian marginal damage emissions (Table 8.2). These estimates represent the effects of several atmospheric pollutants, so they are used to estimate environmental damage cost (EDC) implications of the pollutants based on their relative social and environmental impacts.

8.2.6 Emission Inventory

Material Production

GHG emissions can arise from the production of the constituent materials used in the composite mixtures in each pavement layer. The materials are listed in Table 8.2 with the emission factors used in the analysis and source of data.

Transportation

GHG emissions can arise when hauling materials ($E_{Material\ Transportation}$) for a specified distance using trucks, rail, or barge. A collection of emission factors (in g CO_2/tonne-km) varying with deadhead percentage and load quantity have been selected for trucks. In contrast, a constant number has been selected for rail and barge, respectively. Given the distance between each location (e.g., plant to site, site to landfill), GHG emissions for transporting aggregate, bitumen, HMA, emulsions, chemicals, and waste can be estimated with Equation 8.2.

Table 8.2: Life Cycle Inventory data

Input parameters	**Input Values**							**Reference**
Emissions	**CO_2**	**SO_2**	**CO**	**NO_x**	**PM_{10}**	**$PM_{2.5}$**	**Total PM**	
Materials EMF								
Cement (kg/t)	8.09E+02	4.10E+00	6.00E-02	3.70E+00	0.00E+00	2.08E-01		[44]; [42]
Asphalt Binder (kg/t)	3.58E+02	1.33E+00	3.85E-01	3.61E-01	2.30E-02	2.30E-03		[156]; [257]; [227]
Coarse Aggregate Crushed Stone (kg/t)	1.42E+00	7.88E-04	1.49E-03	1.23E-04	2.46E-03	1.17E-04	5.81E-02	
Fine Aggregate Crushed Stone (kg/t)	7.30E-02	7.88E-04	1.49E-03	1.60E-02	2.46E-03	1.17E-04	5.81E-02	
Coarse Aggregate Natural (kg/t)	1.42E+00	7.88E-04	1.49E-03	1.23E-04	2.46E-03	1.17E-04	5.81E-02	
Fine Aggregate Natural (kg/t)	7.30E-02	7.88E-04	1.49E-03	1.60E-02	2.46E-03	1.17E-04	5.81E-02	
Mineral Filler Natural (kg/t)	2.24E-02	7.88E-04	1.49E-03	1.60E-02	2.46E-03	1.17E-04	5.81E-02	
Slag (kg/t)	9.86E+00							[111]
Diesel (kg/MJ)	9.67E-02	4.34E-04	3.66E-04	1.38E-03	2.46E-05		3.00E-05	[177]; [230]; [73]
Material production processes								
Hot Mix Asphalt (kg/t)	1.75E+01	1.32E-01	1.30E-02	2.22E-02	1.13E+00	6.96E-02	4.62E-02	[173], [81]
Ready-mix concrete plant (Concrete batching -kg/t)	1.17E+00				3.45E-02	6.12E-02	2.56E-02	
Crack Sealing (One lane -mile)	3.48E+02	1.36E+00	6.81E-01	2.10E+00				[257]
Crack Sealing (One lane -Km)	2.16E+02	8.45E-01	4.23E-01	1.30E+00				
Transportation EMF								
Trucks (kg/tonne-km)	1.08E-01	1.10E-05	1.20E-03	1.43E-03	4.52E-05			[173], [163]
Rail (kg/tonne-km)	1.37E-02	1.01E-07	3.56E-05	2.24E-04	5.10E-06			
Construction EMF								
Non-Road Diesel Equipment (kg/hp-hr)	3.75E-01	2.55E-06	1.51E-03	4.99E-03	3.24E-04			[85]
Emission Unit price ($)								
2010 CAD/Mg	$120	$4,116	$750	$3,050		$27,278		[173]

$$E_{Material\ Transportation}(kg\ CO_2\ e) = \sum(Material\ Quantity_i \times D_i \times EF_{i,j,k} \times 10^{-3}) \quad (8.2)$$

where, Material Quantity$_i$ is the quantity of material i (including basic ingredient, asphalt mixture, and waste) transported, in tonne, D$_i$ is the distance material i was transported, in km, and EF$_{i,j,k}$ is the emission factor for transport mode i corresponds to payload tonnes j and percentage deadhead k, in g CO_2/tonne-km. Distance transported assumptions: Distance for all material transportation was set to be 30 km.

Construction Equipment

Equipment covered by the construction section includes asphalt pavers, compactors, rollers, in-place recyclers, etc. Each piece of equipment has unique values of horsepower and productivity. The emission factors, in this case, are based on the brake-specific fuel consumption value, which is related to the rated horsepower. Equation 8.3 is adapted from the EPA NONROAD [74] and used for quantifying construction emissions.

$$E_{Construction}(kg\ CO_2) = \sum \frac{Material\ Quantity_i}{Productivity_j} \times Power_j \times EF_j \quad (8.3)$$

where, Material Quantity$_i$ is the quantity of material (e.g., hot mix asphalt, recycled material, etc.) in tonne, m^2, or m, Productivity$_j$ is the productivity of the construction equipment j, in corresponding material quantity process per hour, Power$_j$ is the average power of the construction equipment j, in hp, and EF$_j$ is the emission factor for construction equipment j, in kg CO_2/hp-hr. Assumptions for the quantification boundary and default values have been made to maintain the simplicity of the template.

8.2.7 Limitation to LCA Analysis

WESLEA and MEPDG were employed to predict pavement performance over the 50-year period. Although this has been validated with field data, field performance over a more extended period is required to verify results. For the performance analysis, only the mechanical LCC properties were considered. It is possible to obtain even better LCC performance when its insulation properties are added especially when LCC is applied over frost-susceptible subgrades, as seen in the study by Dolton and Mclintosh (2018) [64]. Also, the preformed foam used in LCC production was excluded in this analysis as it constituted

less than 0.1% of the total mix. Due to data availability, not all the environmental impacts were considered for the ready-mix concrete plant, such as SO_2, CO, and NOx. This could cause the emission impacts for these pollutants to be slightly higher in the wet mix method of LCC production. The use and end-of-life phases were excluded in this study; hence emissions accrued to these processes have not been estimated. The approach to be undertaken depended on predicting IRI for 50 years. It was quite challenging to do this for the LCC sections with performance data obtained because MEPDG was not very sensitive for LCC.

8.3 Results

8.3.1 Performance Prediction

As concluded in section 5.5, PCI results from MEPDG indicated similar performance for all four sections. Further analysis with WESLEA showed that in terms of fatigue failure, all LCC sections would handle twice as much traffic as the Control section before failure. And for rutting, the LCC400, LCC475, and LCC600 sections performed 3, 6, and 7 times better than the Control in terms of allowing more traffic repetitions (Table 5.14 and Figure 5.20). For fatigue failure, in a do-nothing maintenance scenario, the Control section was expected to fail by year 22, while the LCC sections would not fail within its service life. Rutting could occur by year 15 in the Control section and year 22, 23, and 24 for the LCC400, LCC475, and LCC600 sections, respectively.

By comparing the WESLEA and MEPDG predicted outcomes, it was found that the suggested maintenance and rehabilitation procedures for typical Ontario pavement designs proposed by ARA (2015) [10] could be employed in the analysis.

8.3.2 Recommended M & R Strategies

Recommended strategies were based on simulation results in WESLEA using results obtained from the number of allowable load repetitions and damage analysis. To remain conservative, avoid overestimating the benefits due to incorporating the LCC subbase, and cater for the scenario where the do-nothing approach is not followed, this study used the number of allowable load repetitions relating to predicted fatigue and rutting damage to determine the time lag between each section. All LCC sections would require similar preventive maintenance about two to three years after it is recommended for the Control.

Significant rehabilitation work would happen in the LCC400, LCC475, and LCC600 sections in three years, six years, and seven years respectively, after similar work has been performed in the Control section.

In verifying that the predicted results corresponded to measured field performance, critical pavement responses from the field were compared with those obtained from the WESLEA simulation. These results were presented in section 6.9.3. The results showed that, given the same load level and loading speed, the responses generated for LCC from WESLEA were overestimated. In fact, lower magnitude responses were achieved on the field as presented in Figures 6.35 and 6.37 for the top of subgrade stress and beneath the asphalt concrete (AC) longitudinal strain. This shows that the predicted damage by the software could be lower. Hence, it was conservative to follow the trend in recommending M&R strategies. It should be noted that the potential benefits could be more significant than presented in this study; however, a more extended data monitoring period would be required to validate this assumption. The recommended M&R strategies for each section are provided in Table 8.3.

Table 8.3: Recommended maintenance and rehabilitation strategies

Activity description	**Quantity per 1 km**	**Expected year**			
		Control	**LCC400**	**LCC475**	**LCC600**
Rout and seal (m)	12.5m	10	12	13	13
Spot repairs, mill 40mm/patch 40mm (m^2)	2%	10	12	13	13
Spot repairs, mill 40mm/patch 40mm (m^2)	10%	15	17	18	18
Mill HMA (t)	40mm	20	22	23	23
Resurface Superpave 12.5FC (t)	40mm	20	22	23	23
Rout and seal (t)	500m	25	27	28	28
Spot repairs, mill 40mm/patch 40mm (m^2)	5%	30	32	33	33
Mill HMA (t)	40 mm	35	41	44	45
Full depth Asphalt base repair (m^2)	10%	35	41	44	45
Resurface Superpave 12.5FC (t)	40mm	35	41	44	45
Rout and seal (m)	500m	40	48		
Spot repairs, mill 40mm/patch 40mm (m^2)	5%	43			
Mill HMA (t)	90 mm	48			
Resurface Superpave 19 (t)	50mm	48			
Resurface Superpave 12.5FC (t)	40mm	48			

8.3.3 Life Cycle Assessment Results

The environmental assessment aimed to see changes in the life-cycle performance of the four different pavement designs. Carbon dioxide (CO_2), Carbon monoxide (CO), Nitrogen

oxides (NOx), Sulphur dioxide (SO_2), and particulate matter 2.5um and 10um ($PM_{2.5}$ and PM_{10}) were the air pollutants studied. The costs of environmental damage were also calculated using the previously described marginal damage estimates. Climate change influence is an important property that this study considered. This is represented as CO_2 emissions, a general metric of GHG emissions in kg CO_2 equivalent. The environmental impact of the two LCC production processes (dry and wet mix) was also investigated.

Original Design

Table 8.4 shows the overall emission data for each section throughout a 50-year analysis period for the dry mix process, and Table 8.5 shows the general emission data for the wet mix process. The Control LCC mix was made with an 80/20 cement to slag ratio in this investigation. This is the suggested mix proportions, which has been studied in previous work extensively [176]. For the dry mix, the LCC400 section produced the least amount of CO_2 emission, followed by the LCC475 section. The Control had 16.2%, 14.8% and 12.4% more than LCC400, LCC475, and LCC600 respectively. Concerning the other pollutants, the Control section produced a larger portion than the LCC sections. SO_2 and NOx emissions were noted to increase with an increase in density of LCC material; however, a negligible emission portion was indicated between the LCC sections for the other pollutants.

Table 8.4: Dry mix total emissions (original design)

Section	**CO_2 (kg)**	**SO_2 (kg)**	**CO (kg)**	**NO_x (kg)**	**PM_{10} (kg)**	**$PM_{2.5}$ (kg)**	**Total PM (kg)**
Control	112,234	679	288	417	5,783	355	274
LCC400	94,088	562	219	355	4,430	274	205
LCC475	95,663	570	219	362	4,430	275	205
LCC600	98,297	583	219	374	4,430	275	205

Table 8.5: Wet mix total emissions (original design)

Section	**CO_2 (kg)**	**SO_2 (kg)**	**CO (kg)**	**NO_x (kg)**	**PM_{10} (kg)**	**$PM_{2.5}$ (kg)**	**Total PM (kg)**
Control	112,234	679	288	417	5,783	355	274
LCC400	94,188	562	219	356	4,431	275	205
LCC475	95,783	570	220	363	4,431	276	206
LCC600	98,448	583	221	376	4,431	277	206

Conversely, the wet mix process caused an increase in CO_2 emission compared with the dry mix approach. In this case, the Control had CO_2 emissions of 16.1%, 14.7%, and 12.3% in the LCC400, LCC475, and LCC600. A similar trend was observed in this case, like the dry mix approach for all the other pollutants with slightly higher emission values.

The environmental damage cost was estimated using the calculated emission data and the related cost for each pollutant to assess the cost implications of environmental pollution from the sections. The result of this evaluation is presented in Figure 8.5. The most environmental damage cost was associated with the CO_2 emissions for all the sections. More environmental cost was incurred when the wet mix approach was used compared with the dry mix process. The Control section resulted in the highest environmental damage cost (EDC, up to $13,468) compared to other sections with the dry and wet mix approaches. The cost for the LCC sections was comparable, with costs remaining less than 3% comparing each LCC section. The Control section had the most EDC considering particulate matter in both LCC mix approaches ($9,691). Overall the sections' lifetime, a minimal cost is associated with CO. Also, in both LCC production approaches, SO_2 and NOx cost less than $3,000. But it should be noted that the Control section had a greater cost implication for the other pollutants in both methods.

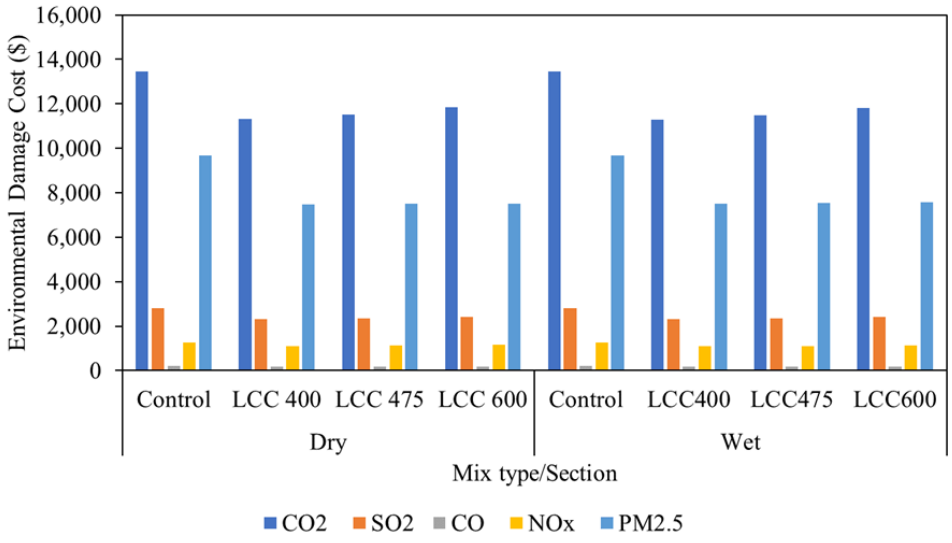

Figure 8.5: Environmental damage cost

The contribution for each lifecycle phase is provided in Table 8.6 for the dry mix and Table 8.7 for the wet mix. Maintenance and rehabilitation (M&R) contributed the

Table 8.6: Dry mix LCA phase percentage contribution

Section	LCA Phases	CO_2 (%)	SO_2 (%)	CO (%)	NO_x (%)	PM_{10} (%)	$PM_{2.5}$ (%)	Total PM (%)
Control	IC	3	2	6	5	2	2	8
	M&R	97	98	94	95	98	98	92
LCC400	IC	12	10	7	16	3	3	8
	M&R	88	90	93	84	97	97	92
LCC475	IC	14	11	7	18	3	4	8
	M&R	86	89	93	82	97	96	92
LCC600	IC	16	13	7	21	3	4	8
	M&R	84	87	93	79	97	96	92

Note: IC is Initial Construction, M&R is Maintenance and Rehabilitation

most to the lifetime emission produced in all sections. The initial construction impacted a very small portion of these emissions, particularly for the Control section, while 92 to 98% of emissions were related to the maintenance phase. However, for the LCC sections, up to 16% of CO_2 emission was linked to the initial construction, while up to 84% was due to M&R. Nevertheless, the contribution of the other pollutants for the LCC sections was mainly related to M&R (up to 97%). Comparing both mix processes, a lower portion was associated with initial construction for the dry mix process than the wet mix for CO_2 emission.

Table 8.7: Wet mix LCA phase percentage contribution

Section	LCA Phases	CO_2 (%)	SO_2 (%)	CO (%)	NO_x (%)	PM_{10} (%)	$PM_{2.5}$ (%)	Total PM (%)
Control	IC	3	2	6	5	2	2	8
	M&R	97	98	94	95	98	98	92
LCC400	IC	12	10	7	16	3	4	8
	M&R	88	90	93	84	97	96	92
LCC475	IC	14	11	7	18	3	4	9
	M&R	86	89	93	82	97	96	91
LCC600	IC	16	13	7	21	3	4	9
	M&R	84	87	93	79	97	96	91

Note: IC is Initial Construction, M&R is Maintenance and Rehabilitation

In summary, Figure 8.6 shows the relative environmental impact for each section compared with the Control. The environmental impact of the Control design over the 50 years was greater than the other sections. CO_2 emissions can be reduced by up to 16% when replacing granular A with LCC material for a 50-meter road length. Furthermore, a

0.1% further reduction can be achieved if the dry mix method is used instead of the wet mix approach. Note that the magnitude of these percentages could quickly increase when considering longer road sections.

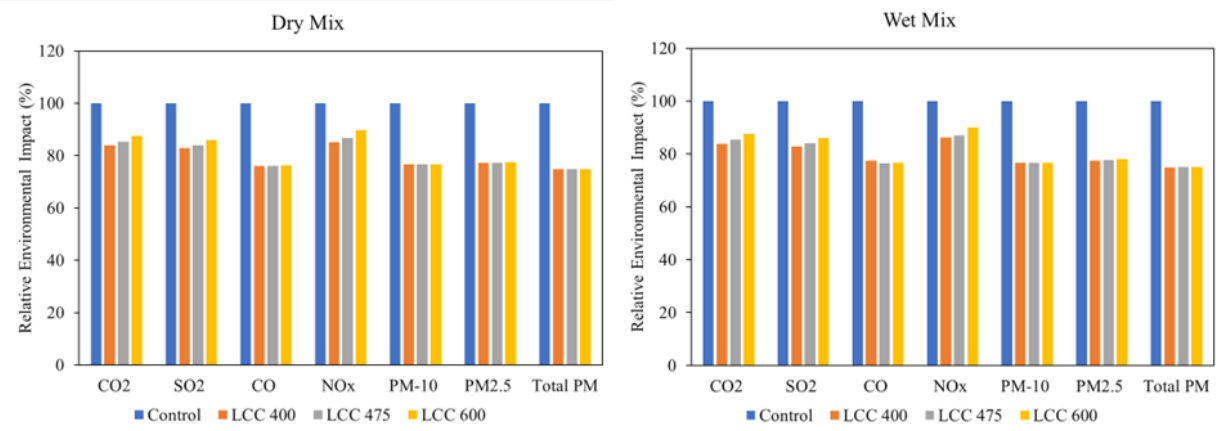

Figure 8.6: Relative environmental impact to the Control section

Subbase Layer Contribution to Emissions

Emission contribution comparison has been performed for just the subbase layer. Figure 8.7 illustrates the overall contribution of all life cycle phases for the subbase from material production to the final M&R with the dry and wet mix methods. The LCC material produced the greatest percentage of CO_2 emission. This is expected because of the cement content, whose production is known to create a large amount of greenhouse gas emissions [273]. This percentage contribution increased with an increase in LCC density.

Similarly, Sulphur dioxide (SO_2) was emitted mainly within the LCC sections, with the higher LCC density contributing more. CO and PM_{10} were more elevated in the Control, with almost all the PM_{10} contribution and about 40% of the CO emission. However, a tiny portion of $PM_{2.5}$ and NOx were related to the Control, with the higher LCC density contributing significantly more to this case.

For the wet mix method, a similar trend to the dry mix was noted except for the PM_{10} where a larger proportion was contributed by the LCC sections, with more contribution attributed as LCC density increased.

The wet and dry mix approaches were compared based on the many processes within the life cycle. Figure 8.8 shows data for CO_2 emission during material production and

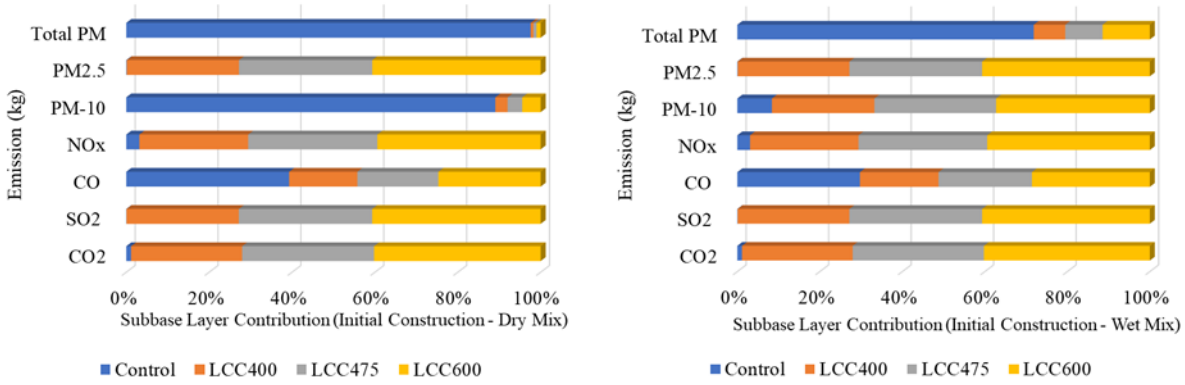

Figure 8.7: Subbase layer emission contribution

initial construction (MPC) and transportation (TP). Compared to transportation in both LCC production methods, material production and construction for LCC portions created the largest percentage of CO_2 emissions. In the Control segment, however, transportation contributed nearly four times as much as material production and construction. The effects due to transportation were also clearly more for the wet mix than the dry mix method.

Regarding other pollutants (Figure 8.9), the wet and dry mix methods for producing LCC produced equivalent levels of SO_2, CO, and NOx. However, the wet mix method had higher PM_{10}, $PM_{2.5}$, and total PM than the dry mix method. Generally, CO and PM contributions were less than 20 kg in all sections for both approaches. In the Control, as in previous results, the biggest proportion of PM occurred when producing the subbase (granular A). Regarding subbase material transportation, the Control subbase (granular A) had the largest impact on all contaminants. This could suggest that travel distance could be an important factor when using unbound granular materials in road pavements. In addition, the larger the density of LCC, the greater the impact on transportation emissions.

Alternate Design (Granular B)

The overall results for the lifecycle analysis performed using the alternate design with granular B in place of granular A are presented in Tables 8.8 and 8.9 for the dry and wet mix. A similar trend like the original design was noted. However, in this case, the LCC400, LCC475, and LCC600 yielded a 16.7%, 15.3%, and 12.9% lower CO_2 emission in the dry mix method. This was a greater decrease compared with when granular A was applied. The wet mix method's CO_2 emissions for all the LCC sections were 16.6%, 15.2%,

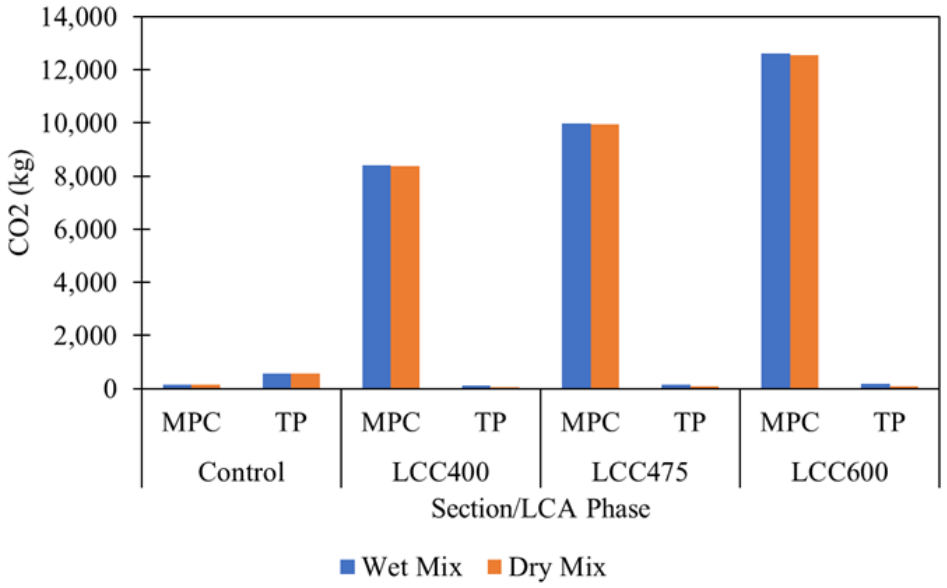

Figure 8.8: Subbase layer contribution (Initial Construction CO_2)

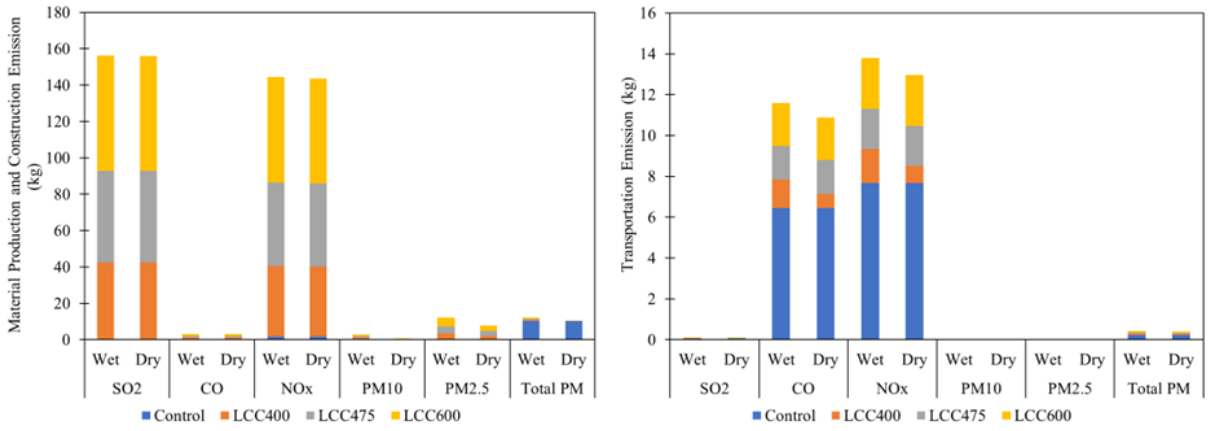

Figure 8.9: Subbase layer contribution to material production, construction and transportation

and 12.8%, accordingly. Slightly higher values for other pollutants were observed in the wet than dry mix method.

Tables 8.10 and 8.11 further show the percentage contribution of the different LCA

Table 8.8: Dry mix alternate design total emission

Section	CO_2 (kg)	SO_2 (kg)	CO (kg)	NO_x (kg)	PM_{10} (kg)	$PM_{2.5}$ (kg)	Total PM (kg)
Control	112,893	679	294	427	5,784	355	285
LCC400	94,088	562	219	355	4,430	274	205
LCC475	95,663	570	219	362	4,430	275	205
LCC600	98,297	583	219	374	4,430	275	205

Table 8.9: Wet mix alternate design total emission

Section	CO_2 (kg)	SO_2 (kg)	CO (kg)	NO_x (kg)	PM_{10} (kg)	$PM_{2.5}$ (kg)	Total PM (kg)
Control	112,893	679	294	427	5,784	355	285
LCC400	94,188	562	219	356	4,431	275	205
LCC475	95,783	570	220	363	4,431	276	206
LCC600	98,448	583	221	376	4,431	277	206

Table 8.10: Alternate design dry mix LCA phase contribution

Section	LCA Phases	CO_2 (%)	SO_2 (%)	CO (%)	NO_x (%)	PM_{10} (%)	$PM_{2.5}$ (%)	Total PM (%)
Control	IC	4	2	8	8	2	2	12
	M&R	96	98	92	92	98	98	88
LCC400	IC	12	10	7	16	3	3	8
	M&R	88	90	93	84	97	97	92
LCC475	IC	14	11	7	18	3	4	8
	M&R	86	89	93	82	97	96	92
LCC600	IC	16	13	7	21	3	4	8
	M&R	84	87	93	79	97	96	92

Note: IC is Initial Construction, M&R is Maintenance and Rehabilitation

phases. Like the initial design, M&R constituted the main emission centers for all sections. Environmental damage cost was slightly higher when the wet mix approach was adopted than the dry mix (Figure 8.10). Generally, less environmental cost occurred in the LCC sections for all the pollutants than in the Control. In terms of relative impact, compared to the Control, LCC caused less pollution in all cases (Figure 8.11).

Figure 8.12 presents the respective subbase layer contributions to emissions. The same trend as the original design was noted; however, greater magnitudes in the Controls' contribution where applicable were witnessed.

Table 8.11: Alternate design wet mix LCA phase contribution

Section	LCA Phases	CO_2 (%)	SO_2 (%)	CO (%)	NO_x (%)	PM_{10} (%)	$PM_{2.5}$ (%)	Total PM (%)
Control	IC	4	2	8	8	2	2	12
	M&R	96	98	92	92	98	98	88
LCC400	IC	12	10	7	16	3	4	8
	M&R	88	90	93	84	97	96	92
LCC475	IC	14	11	7	18	3	4	9
	M&R	86	89	93	82	97	96	91
LCC600	IC	16	13	7	21	3	4	9
	M&R	84	87	93	79	97	96	91

Note: IC is Initial Construction, M&R is Maintenance and Rehabilitation

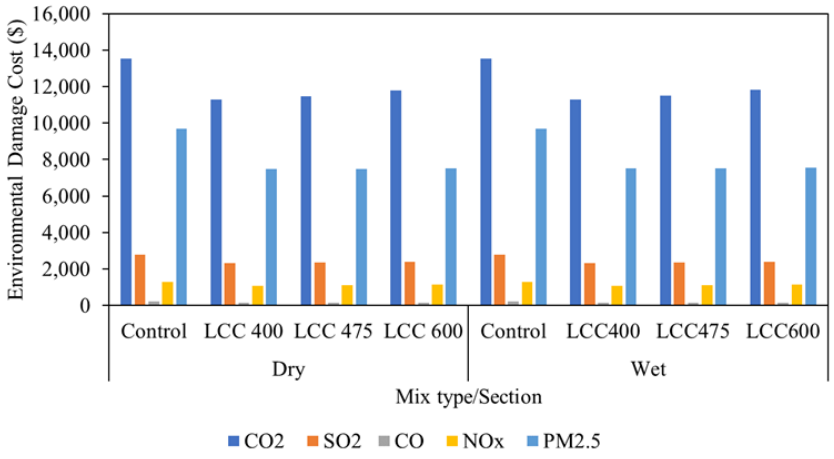

Figure 8.10: Alternate design environmental damage cost

The amount of emission associated with placing one cubic meter of each subbase material was determined (Table 8.12). These estimates include material, production, and placement process. Generally, more pollutants were emitted when an equivalent design of granular B was used in place of granular A. This is likely due to the increase in layer thickness when this occurs and slight differences in material composition. A subbase with granular B is typically used in Ontario, and granular A is predominantly used as the pavement base layer. Therefore, comparing the typical pavement subbase material (granular B) with the LCC layers, one cubic meter produced less CO_2, SO_2, NOx, and $PM_{2.5}$ than the LCC sections. However, more CO, PM_{10}, and total PM were produced when granular

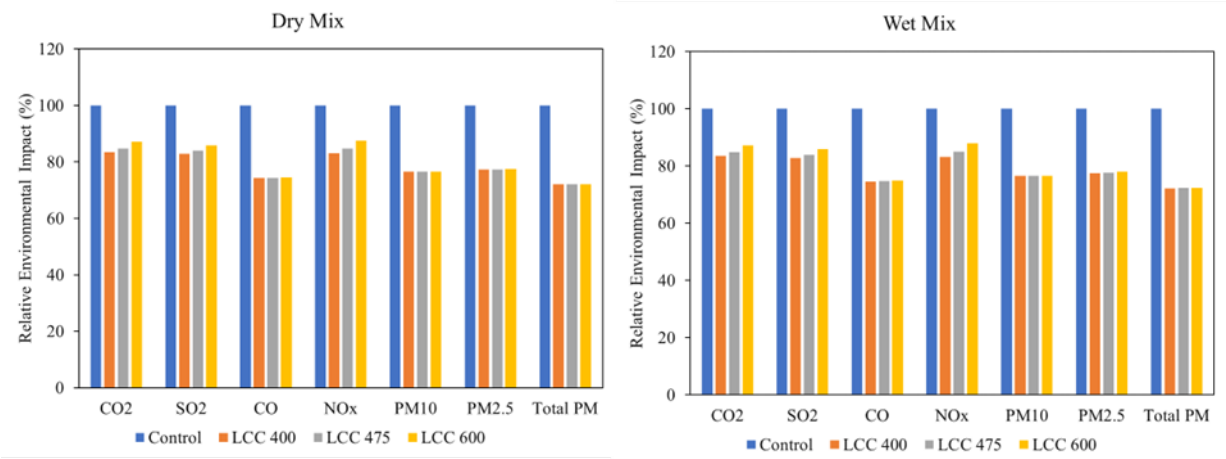

Figure 8.11: Alternate design relative environmental impact to the Control section

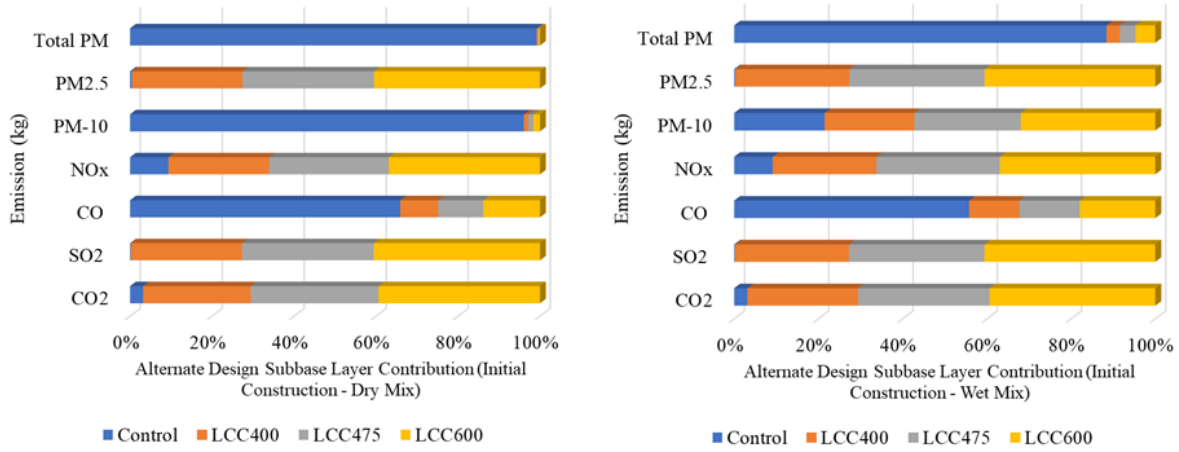

Figure 8.12: Alternative design subbase layer contribution

B was used compared with LCC using the dry mix method. Mostly, the emitted pollutants were more when LCC density increased.

The production and placement of 1 m^3 of 400 to 600 kg/m^3 LCC yielded CO_2 emissions between 174 and 264 kg. Although earlier research discovered that 1 m^3 of 445 kg/m^3 foamed concrete production resulted in 302 kg CO_2 emissions [273], the foamed concrete mix in their study included fly ash, foamed glass granules, silica fume, and metakaolin which could have caused the difference. Hertz and Halding (2022) [101] also found that

Table 8.12: Emissions (kg) in placing 1 m^3 subbase material

Description	Material	CO_2	SO_2	CO	NO_x	PM_{10}	$PM_{2.5}$	Total PM
Control	Granular A	10	0.003	0.094	0.130	0.006	0.000	0.146
	Granular B	18	0.005	0.182	0.268	0.012	0.001	0.284
Dry Mix	LCC400	174	0.872	0.029	0.810	0.000	0.044	0.001
	LCC475	206	1.036	0.035	0.962	0.000	0.052	0.001
	LCC600	261	1.308	0.044	1.215	0.000	0.066	0.001
Wet Mix	LCC400	176	0.874	0.045	0.832	0.014	0.069	0.012
	LCC475	209	1.037	0.053	0.988	0.017	0.081	0.014
	LCC600	264	1.310	0.067	1.248	0.021	0.103	0.017

the production of 1 kg of foamed concrete with a density of 900 kg/m^3 resulted in 0.322 kg of CO_2, whereas 600 kg/m^3 resulted in 0.467 kg of CO_2. Their results are comparable to the findings of this study which showed that per kg of production and placement of 400 to 600 kg/m^3 LCC, there was 0.43 to 0.44 kg of CO_2 generated.

Considering only the production process, the dry mix method of producing 1 m^3 of LCC generated 0.62 kg, 0.74 kg, and 0.93 kg of CO_2 for 400 kg/m^3, 475 kg/m^3, and 600 kg/m^3 LCC, respectively. The wet mix approach yielded 1.39 kg, 1.66 kg, and 2.09 kg of CO_2.

Maintenance and Rehabilitation Contribution

The M&R activities have been categorized within a 10-year time frame. The effect due to the M&R within the 10-year period through the life of the pavement up to 50 years is presented in Figure 8.13. The following M connotations represent every ten years. M1 means year 0 - 10, M2 year 11- 20, M3 year 21 – 30, M4 year 31 – 40, M5 year 41 – 50. The M&R regimes were the same for the wet and dry mix processes. Since there was no M&R in the LCC sections for the first ten years, no environmental damage was caused during this time. However, 9% of its total CO_2 emission was seen for the Control. Aside from CO_2, PM_{10} also shared a large portion of the emissions. The most environmental damage was observed within years 11 to 20 for all sections. At this time, more CO_2 emission was noted in all the LCC sections (similar levels) than in the Control. Between years 21 to 30, comparable levels of emission were observed for all pollutants in all the sections. The Control section caused the least pollution between years 31 and 40 compared to all the other periods and with the LCC sections. While the LCC sections experienced minimal

emissions in the last ten years of service life, the Control section caused the second largest CO_2 emission throughout the 10-year M&R time frames considered for this analysis.

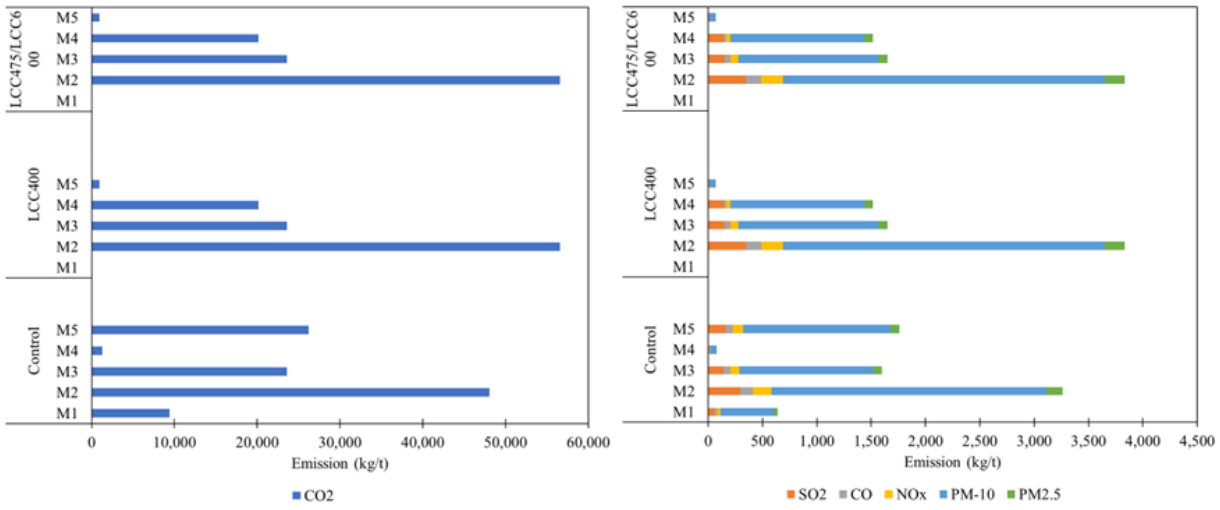

Figure 8.13: Environmental Impact of M&R activities

8.3.4 Sensitivity Analysis

Three different scenarios have been analyzed to determine how environmental impact could be influenced when activities within LCA processes are changed. These scenarios include changing material proportions for the LCC subbase, and varying material transportation distances for all subbase material.

Material Proportion Sensitivity

The sensitivity of the pollutants to changes in LCC slag proportion was analyzed. The slag content in the base case was 20%. The sensitivity analysis investigated the effect of none, smaller and larger proportions of slag within the LCC mix on all the pollutants considered in this study. CO_2, SO_2, and NO_x were the three pollutants most influenced by this change. Generally, the result showed that reducing the slag content led to increased CO_2 emission for both the dry and wet mix methods (Table 8.13 and Appendix D). This is due to an increase in the cement content, whose production yields significant greenhouse gas emissions [108, 44, 42]. LCC mixes with no slag content produced 2.1%, 2.5%, and

3.1% more CO_2 than the base case for LCC400, LCC475 and LCC600, respectively. A similar trend was detected for the other pollutants, where over 2% SO_2 and 3% NO_x were produced for all densities.

Comparing the LCC CO_2 emission with granular A and B material, even when 100% Cement (GU) was used, the LCC sections had 14%, 12%, and 9% lower CO_2 emission than granular A and 15%, 13%, and 10% than granular B for LCC400, LCC475, and LCC600 accordingly. A similar trend was noted for the other pollutants but with a lower percentage change.

Table 8.13: LCC sections' sensitivity to change in slag content

Emissions	**Section**	**Slag content**		
		100% GU	**10% Slag**	**30% Slag**
CO_2	LCC400	2.1%	1.1%	-1.1%
	LCC475	2.5%	1.2%	-1.2%
	LCC600	3.1%	1.5%	-1.5%
SO_2	LCC400	1.8%	0.9%	-0.9%
	LCC475	2.2%	1.1%	-1.1%
	LCC600	2.7%	1.3%	-1.3%
NO_x	LCC400	2.6%	1.3%	-1.3%
	LCC475	3.0%	1.5%	-1.5%
	LCC600	3.7%	1.8%	-1.8%

Distance Sensitivity

Granular A distance

Results from the sensitivity analysis to transportation distance of granular A for the original design are presented in Figure 8.14 for CO_2, CO, and NO_x. These were the pollutants with the most significant changes due to distance variation. The assessment examined the effect of shorter and greater distances than the base case distance of 30 km. The rate of change in emissions due to granular A transportation distance change was slightly lower in the Control section than in the LCC sections. A 100 km distance was noted to cause the most increase in emissions in all cases. At this distance, however, in the dry and wet mix method, actual CO_2 emissions remained 16%, 14%, and 12% less than

the Control for LCC400, LCC475, and LCC600 sections. All the LCC sections' emissions stayed lower for all the distances than the Control.

When granular A distance increased above 30 km, the emission change rate decreased with an increase in LCC density. Still, when transportation distance was smaller than 30 km, the rate of emission change was more significant for lower LCC density.

Granular B distance

In terms of sensitivity to granular B transportation distance, the results are shown in Figure 8.15. The LCC sections remained constant all through as there was no granular B within the sections. Like the granular A distance sensitivity, the three pollutants with the greatest response to the distance change were CO_2, CO, and NO_x. CO emission was the most sensitive to this change. Increasing transportation distance to 100 km resulted in a 2%, 8%, and 6% increase in CO_2, CO, and NO_x emissions, respectively. While reducing the distance triggered lower emission levels.

LCC distance

Similarly, the same emissions were the most sensitive when LCC transportation distance was varied (Figure 8.16). Emission levels increased and decreased with a reduction or addition in LCC transportation distance compared to the base case distance of 30 km. Consistent with the other analysis, the environmental impact was more for higher LCC densities. The percentage increase for all pollutants was greater in the wet mix approach as distance increased compared to the dry mix approach. When transportation distance decreased, however, a more significant decrease was noted for the wet mix than the dry mix method. The wet mix approach was more sensitive to changes in transportation distance than the dry mix. This can be attributed to the additional transportation required for the delivery of the base slurry mix to the construction site in this approach.

8.3.5 Comparison with other Subbase/Insulating layers

Table 8.14 compares the life cycle assessment for unbound granular material, three densities of lightweight cellular concrete, foam glass aggregates, and three types of expanded polystyrene (based on the production methods) blocks as detailed in [266]. Although the system boundaries differed as described. The 400 kg/m^3 LCC density produced the least environmental impact compared to the others.

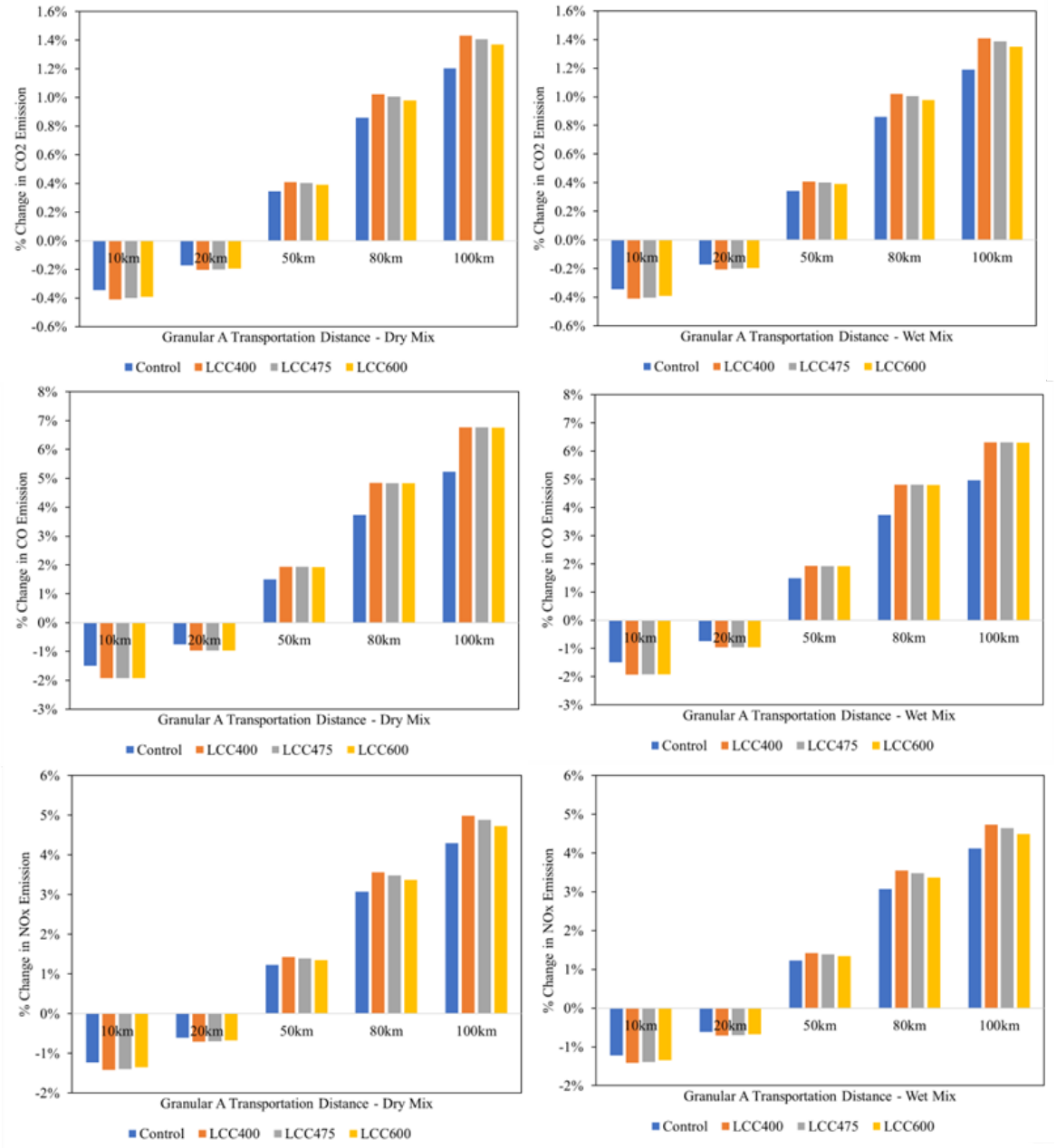

Figure 8.14: Sensitivity to change in granular A transportation distance

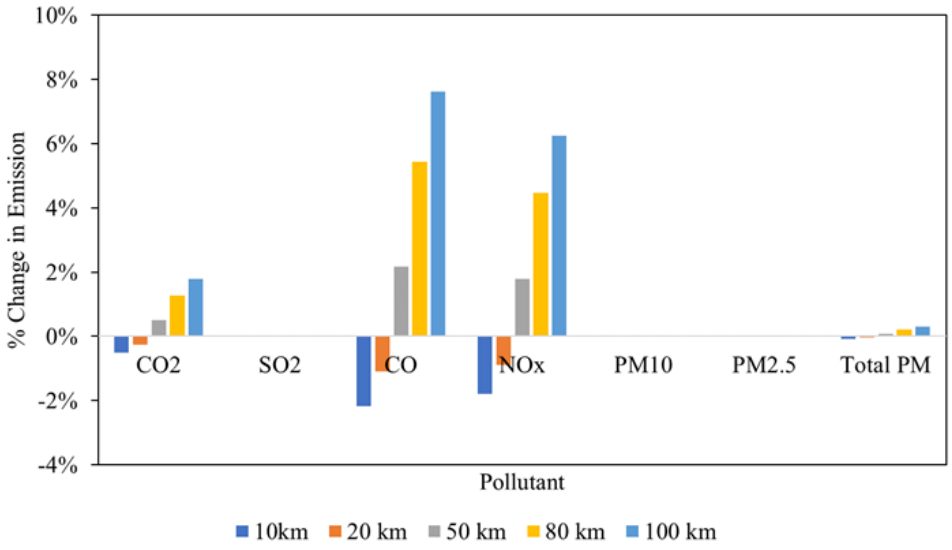

Figure 8.15: Sensitivity to change in granular B transportation distance

8.3.6 LCA Summary and Conclusions

The following are the main findings from the Life Cycle Assessment for unbound granular and LCC subbase flexible pavements.

- CO_2 is the major pollutant produced in the production, construction, maintenance, and rehabilitation of flexible pavement structures with typical material layers (asphalt concrete, granular A, and granular B) and lightweight cellular concrete subbase material.
- Replacing granular A with 400, 475, and 600 kg/m^3 LCC containing 20% slag could reduce total life CO_2 emissions by 16%, 15%, and 12% using the dry and wet mix approach. It can also reduce the environmental impact of SO_2, CO, NO_x, PM_{10}, and total PM, leading to lower environmental costs.
- The dry mix method would produce about 0.1% less CO_2 emissions than the wet mix method. The dry and wet mix approach for densities between 400 to 600 kg/m^3 would cause less environmental damage for all pollutants considered in this study than granular A.
- Using granular B as a subbase instead of granular A would lead to greater environmental damage. 1% more CO_2 emissions occurred.

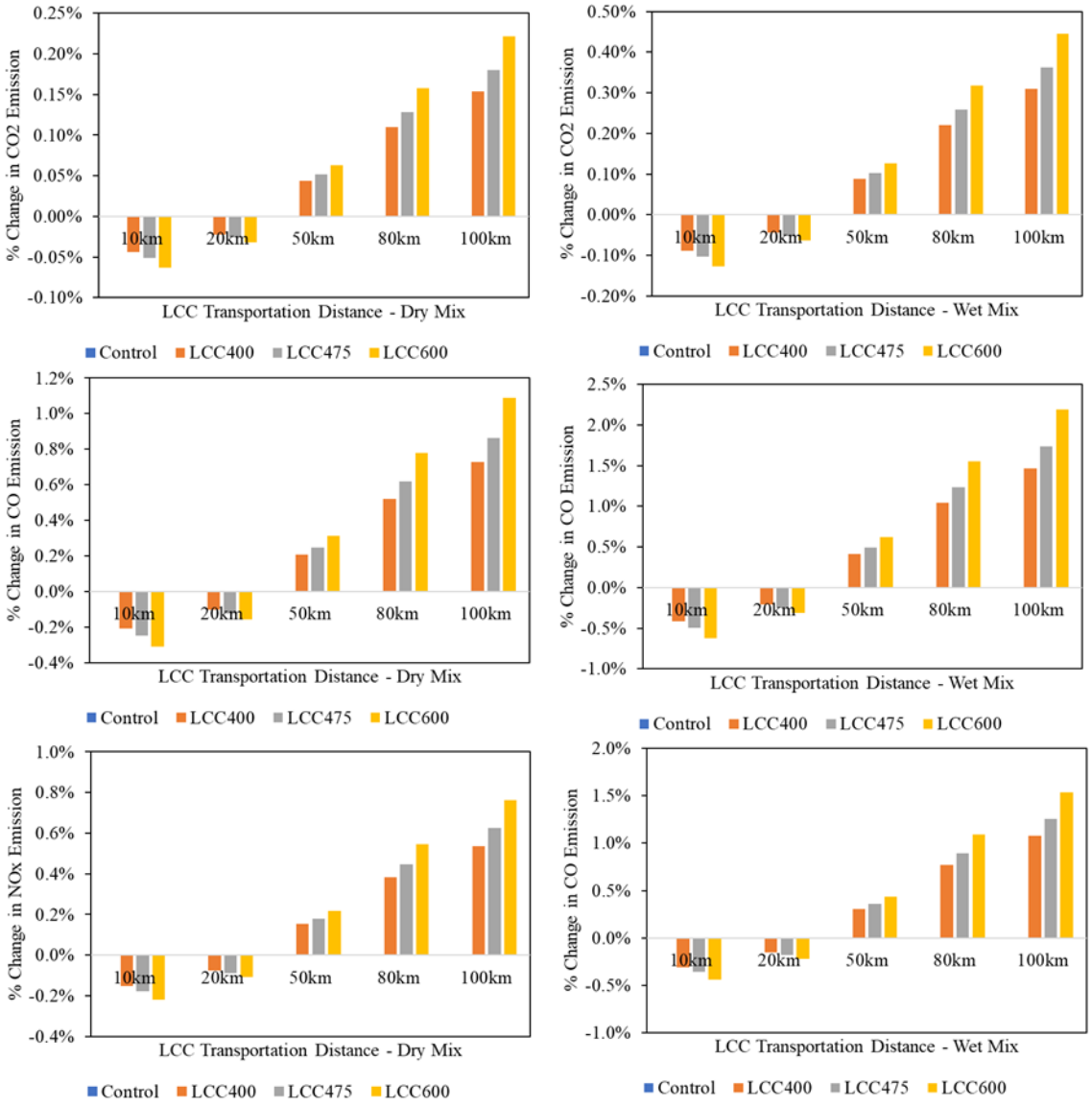

Figure 8.16: Sensitivity to change in LCC transportation distance

- Replacing granular B with LCC densities between 400 and 600 kg/m^3 could reduce CO_2, SO_2, CO, NO_x, PM_{10}, $PM_{2.5}$ and total PM emission by up to 16%, 17%, 24%,15%, 23%, 23%, and 25%, respectively.

Table 8.14: LCA Comparison for other subbase and insulation materials

Material	CO_2 (kg)^A	CO_2 (Kg CO_2 eq)^B	Description	Reference
Foam glass aggregate	0.26	4.72E+11	Study used Open LCA and Simpro, electricity used in production of materials, considered material production, transportation and initial construction	[266]
Expanded Polystyrene (EPS1-3)	1.19 – 4.80	1.18E+12	Study used Open LCA, Simpro and the Khoo et.al (2005) model, considered material production, transportation and initial construction	[266]
Granular A	0.005	1.01E+10	Study used adapted version of PaLATE by Nasir (2018) [173]. Considered material production, transportation, initial construction and maintenance and rehabilitation	Current study
Granular B	0.008	1.02E+10		
Lightweight cellular concrete (400kg/m^3)	0.43 - 0.44	8.51E+09	Study used adapted version of PaLATE by Nasir (2018) [173]. Considered, two methods of material production (wet and dry mix), transportation, initial construction and maintenance and rehabilitation	Current study
Lightweight cellular concrete (475kg/m^3)	0.43 - 0.44	8.65E+09		
Lightweight cellular concrete (600kg/m^3)	0.43 - 0.44	8.89E+09		

Note: A:CO_2 in Production of 1kg of material (kg). B:in 1km X 15m X 6m road construction

- The majority (over 90% for the Control and 80% for the LCC sections) of emissions happened during the M&R activities compared to initial material production and construction.
- Considering just the subbase layers in the dry mix method, the largest portion of CO_2, SO_2, $PM_{2.5}$, and NO_x emissions occurred in the LCC sections with greater LCC densities emitting more. In comparison, the Control contributed almost all PM_{10} and 40% of CO emissions. The wet mix LCC contributed more PM_{10}, and the SO_2 and CO_2 contributions within the LCC sections were mostly even.
- Material production and initial construction with LCC material yielded more emissions, especially CO_2, than granular A, with more emissions for higher density LCC. However, transportation of unbound granular A induced more emissions than LCC.

- Emission levels were sensitive to material transportation distance. The most sensitive pollutant to changes in transportation distance was CO_2, CO, and NO_x. The rate of change in emissions due to granular A transportation distance change was slightly lower in the Control section than in the LCC sections.

- A 100 km distance was noted to cause the most increase in emissions. At this distance, however, actual CO_2 emissions remained 16%, 14%, and 12% less than the Control for LCC400, LCC475, and LCC600 sections. Other pollutants also remained lower in the LCC sections.

- When granular B was applied, an increase in transportation distance resulted in an increase in emission levels up to 8% in some pollutants and vice versa.

- LCC mixes with no slag content had 14%, 12%, and 9% lower CO_2 emission than granular A and 15%, 13%, and 10% than granular B for LCC400, LCC475, and LCC600 accordingly. A similar trend was noted for the other pollutants but with a lower percentage change.

- One cubic meter of producing and placing granular A and B produced 10 kg and 18 kg of CO_2, respectively, while 400 kg/m^3 LCC produced between 174 to 176 kg, 475 kg/m^3 between 206 to 209 kg, and 600 kg/m^3 between 261 to 264 kg of CO_2.

- The dry mix method production process of 1 m^3 of LCC generated 0.62 kg, 0.74 kg, and 0.93 kg of CO_2 for 400 kg/m^3, 475 kg/m^3, and 600 kg/m^3 LCC, respectively. The wet mix approach yielded 1.39 kg, 1.66 kg, and 2.09 kg CO_2.

- Compared with foamed glass aggregate and expanded polystyrene, using LCC between 400 and 600 kg/m^3 as subbase produced less CO_2 emission in road construction.

Chapter 9

Lifecycle Cost Analyses

9.1 Introduction

Life Cycle Cost Analyses (LCCA) is described as an "economic assessment considering all agreed expected major and relevant cost flows across a period of analysis reflected in monetary value," according to the International Organization for Standardization (2008) [82]. The estimated expenses are those required to meet specific performance goals, such as dependability, safety, and availability." The LCCA essentially explains the project's immediate financial impact. It is commonly used as a strategy in public procurement to encourage more environmentally friendly activities [199]. An LCCA analysis often includes parts such as establishing design alternatives, defining the analysis period, determining the discount rate based on the country or state's economic development, estimating the specific cost, and ultimately analyzing the results [241, 258, 263].

The economic implications of lightweight cellular concrete have only been partially studied. According to a 2020 study by Jose, Soman and Evangeline [124], the cost of producing lightweight cellular concrete was 53% lower than that of regular concrete. Zhuo (2021) [272] utilized FEM to predict the performance of four different insulation materials for pavement applications based on comparable thermal and mechanical structures and found that the conventional pavement without insulation was the most expensive to attain the same thermal performance. The most expensive insulated pavement was the LCC pavement, followed by pavements made of tire chips, foamed glass aggregates, and ultimately XPS pavement. However, in their analysis, only the initial construction expenditures were examined. Also, although the study suggested that the LCC section was equivalent to the XPS's from a mechanical perspective, LCC is much stronger. Likewise, very high initial

costs were presented for LCC; conversion equals $335 CDN per cubic meter. Moreover, installation costs necessary for XPS due to precision requirements of placing boards would be higher than LCC's.

Most past research has mainly concentrated on initial construction and manufacturing costs. There is currently no information on the lifecycle cost of LCC as a structural subbase part of pavement construction. This chapter examined the economic impact of lightweight cellular concrete used as a subbase alternative to granular A and B, which are typical unbound layers within the pavement structure. It explores the financial implication of producing, transporting, placing, and maintaining pavement sections with different subbase materials, including three different LCC densities (400 kg/m^3, 475 kg/m^3 and 600 kg/m^3). The lifecycle cost analysis method was adopted to evaluate the economic impacts. The life cycle cost of utilizing LCC in the pavement structure was calculated by adding up the original and future costs.

9.2 Method

The net present value (NPV) method is one of the most used LCCA approach by Canadian agencies, [165]. The unit costs for the initial construction of each layer and the selected treatments were collected from [10], and some were built up using prevailing market prices in the test section location. The unit costs are listed in Table 9.1. The total life cycle cost (LCC_{Total}) was estimated using the net present value approach in Equation 9.1.

$$LCC_{Total} = C_{ini} + [\sum_{i=1}^{n} C_{m,i} \times (\frac{1}{1+r})^n] - SV \times (\frac{1}{1+r})^n \tag{9.1}$$

where, C_{ini} is initial cost of construction in ($); C_m is the cost of maintenance m in the i^{th} year in ($), r is the discount rate (5%), i is the year of implementation, n is the design life, and SV is the salvage value in ($).

Total cost was calculated for the initial construction and maintenance program applied in the scenario with granular A subbase and alternate design with granular B subbase. To bring the cost of M&R treatments to present worth, a discount rate of 5% real rate was used, reflecting common practice in Canada [165, 234]. The salvage value was converted to a present worth considering $n = 50^{th}$ year, as this cost occurs at the end of the period analyzed. Salvage value was calculated using Equation 9.2.

$$SV = \frac{L_{rem}}{L_{exp}} \times C_{pvt} \tag{9.2}$$

where: L_{rem}= remaining service life of the last M&R treatment; L_{exp}= expected service life of the last M&R treatment; C_{pvt} = cost of the last M&R treatment.

Furthermore, a second important indicator, the Equivalent Uniform Annual Cost (EUAC) which is calculated based on the estimate of Net Present Value (NPV) and distributes the cost into the pavement life cycle [264] was estimated with Equation 8.

$$EUAC = LCC_{Total} \times [\frac{i_{discount} \times (1 + i_{discount})^{AP}}{(1 + i_{discount})^{AP} - 1}] \tag{9.3}$$

where EUAC represents the Equivalent Uniform Annual Cost of the maintenance/ rehabilitation activities, LCC_{Total} represents the total life cycle cost (LCC_{Total}) estimated using the net present value approach, $i_{discount}$ represents the discount rate, and AP represents the time period in years being considered.

9.3 Cost items

The unit price used in the analysis of the asphalt concrete surface layer, binder layer and base were adopted [10] and presented in Table 9.1. The unit prices were updated using a growth factor with a discount rate of 5%. The unit price used in the analysis of the LCC subbase with densities of 400 kg/m^3, 475 kg/m^3, and 600 kg/m^3, were estimated to be \$135, \$155, and \$180, respectively, on average. At the same time, the granular A and B subbase was \$25.33 and \$21.11 accordingly. The unit price of M&R activities is likewise provided also in Table 9.1.

LCC unit cost estimates were determined using the Richway Cellular Calculator developed by Richway industries [212]. To use this tool, base slurry estimates were obtained from Lafarge Canada for the specific mix used on the trial road. Furthermore, the cost of skilled and unskilled personnel, equipment, and material costs was included. These were obtained from the prevailing market within the study area. Also, a mark-up percentage was included for the contractor's overhead and profit.

Table 9.1: Unit cost of materials

Item	**Unit Cost 2015** [10]	**Unit Cost 2022**
HMA -Surface SP 12.5	$105	$147.75
HMA -base layers SP 19	$96	$135.08
Granular A	$18	$25.33
Granular B	$15	$21.11
Removal of existing pavement	$65	$91.46
Excavation to required depth	$80	$112.57
LCC 400		$135.00
LCC 475		$155.00
LCC 600		$180.00
Rout and seal, m/km (m)	$5	$7.04
Mill HMA, mm (t)	$15	$21.11
Spot repairs, mill 40 mm/patch 40 mm, % area (m^2)	$35	$49.25
Full depth asphalt base repair, % area (m^2)	$45	$63.32
Resurface with Superpave 12.5, mm (t)	$105	$147.75
Resurface with Superpave 19, mm (t)	$96	$135.08

9.4 Maintenance and Rehabilitation

The M&R strategies recommended in section 8.3.2; Table 8.3 have been adopted in this analysis.

9.5 Limitation to LCCA

- For all portions, the same distance was used for material transportation. Although this was true for the study's trial road construction, it should be noted that the material transportation distance could vary depending on the project and region.
- The costs incurred by users due to the delay and use of the pavement section have not been considered. These factors could point to the advantages of employing LCC, such as fewer construction delays due to fewer M&R activities and smoother pavements over time.
- The use phase was excluded due to limitations in predicting IRI for the LCC sections. This could also reflect a benefit should the LCC pavements perform as anticipated.

- The insulating capabilities of cellular concrete could also contribute to the longevity of the roadway, especially in areas with frost-susceptible soils. However, the insulation property of LCC was not included in the performance prediction.

9.6 Results

9.6.1 LCCA for Original Design with Granular A

The LCCA for the trial road section design is provided in Figure 9.1. This presents the total life cycle cost, the cost for initial construction and M&R activities, and the cost for all the three life cycle phases considered in this analysis. The LCC production method covered in this analysis was the dry mix method. The Control section was noted to have the least life cycle cost, with values 10%, 11%, and 13% lower than LCC400, LCC475, and LCC600 sections, respectively. The greatest cost center for the LCC section was during initial construction due to the cost of the LCC material and the additional excavation requirement for the LCC sections. Also, the salvage value of the Control section at the end of the 50-year analysis period was significantly higher than the LCC sections (over 500 times more than LCC400 and 27 and 26 times more than LCC475 and LCC600). This was due to a maintenance activity performed in year 48 in this section, significantly increasing its value. However, the maintenance cost for the LCC sections was observed to be considerably lower (71%, 75%, and 77% less than the Control for LCC400, LCC475, and LCC600 correspondingly). This is expected as fewer M&R efforts were required in these sections compared with the Control. The lifecycle cost increased with an increase in LCC density with the cost of LCC400 and LCC475 at a comparable level (not more than 0.5% difference in cost).

9.6.2 LCCA for Alternative Design with Granular B

The lifecycle analysis results for the alternate design are presented in Figure 9.2. The alternative design has been seen to reduce the cost difference gap compared with the original design. The Control in this case also had the least life cycle cost, with lower percentages of 4%, 4%, and 6% less than LCC400, LCC475, and LCC600 sections, respectively (Figure 9.3).

The equivalent uniform annual cost was determined for the design options and can be found in Figure 9.4. Both Control sections with granular A and B had the lowest annual

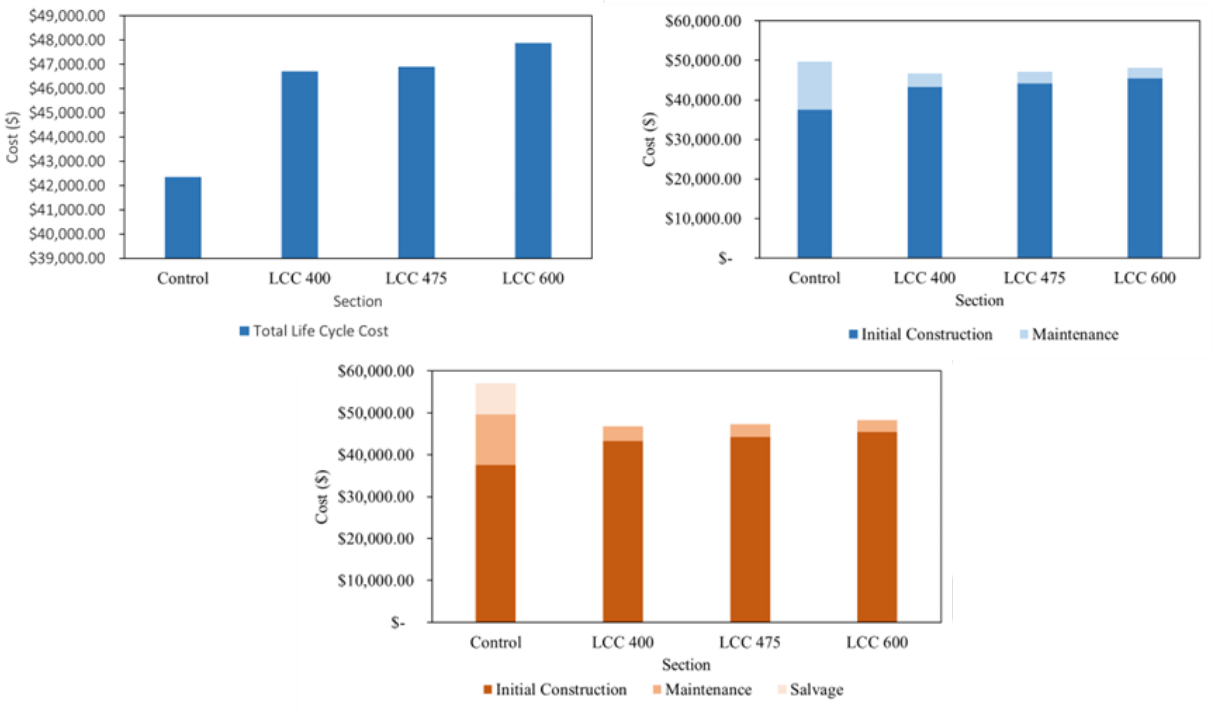

Figure 9.1: LCCA for design with granular A

cost implication, with the pavement consisting of granular A performing better in terms of cost. A negligible difference (0.4%) in cost was observed between the LCC400 and LCC475 sections. The LCC600 segment had the greatest annual cost.

9.7 Sensitivity Analysis

Sensitivity analysis was used to determine the impact of various parameters on the total life cycle cost of the sections. To conduct this analysis, the following aspects were considered.

- Discount rate: Because this value may fluctuate over time, it was prudent to investigate the implications for lifecycle cost.
- LCC cost: LCC costs are determined by several factors, some external to the supplier/contractor and others internal. These costs could also vary based on project specifics (i.e., daily/overall volumes, schedule, location, etc). LCC cost is a crucial

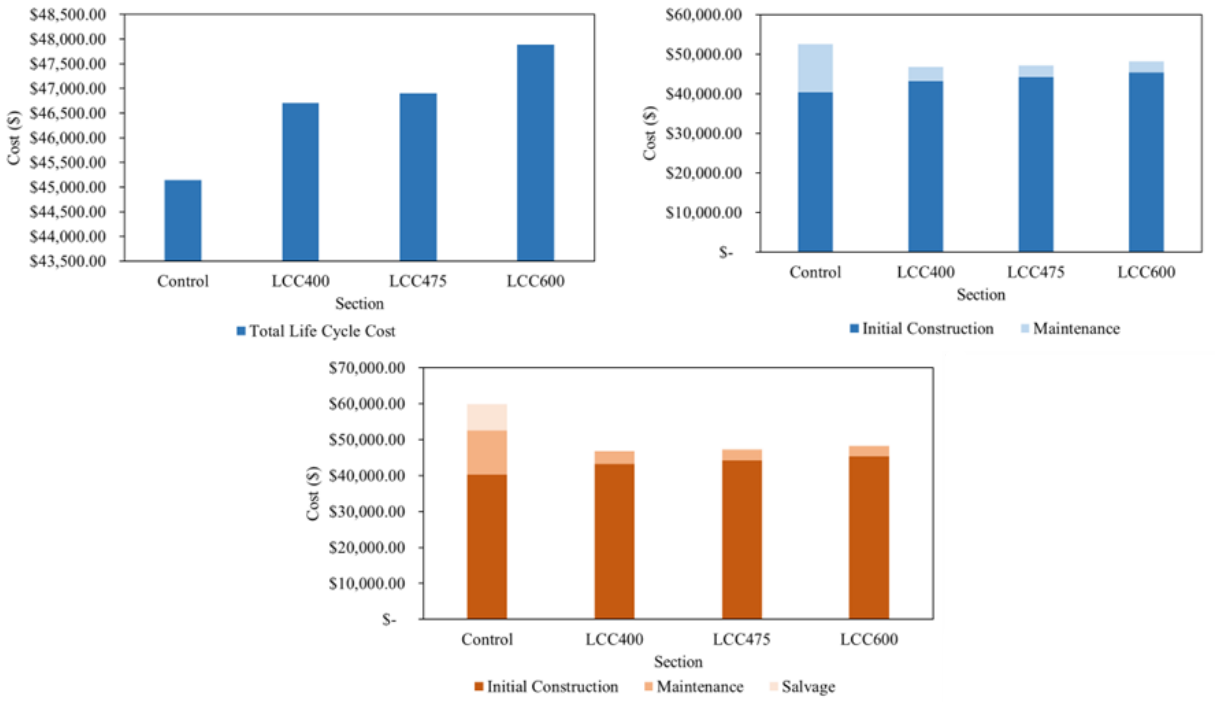

Figure 9.2: LCCA for alternate design with granular B

aspect that could substantially impact the initial construction cost. Costs below and beyond the average baseline cost were studied.

- Unbound granular material cost: The cost for production and supply of unbound granular material could change depending on factors such as the availability of quality aggregates and transportation distance [234].

9.7.1 Change in LCC Cost

Figures 9.5 and 9.6 show the impact of changes in the cost of LCC. A rise or decrease in the cost of LCC resulted in an increase or reduction of total life cycle cost. The cost change was proportionate to the density of LCC. When the LCC cost was increased, the cost changed more in magnitude than when it was decreased. When comparing the actual total costs of granular A and granular B alternatives, reducing LCC costs by up to 40% did not result in LCC portions being cheaper than Granular A; however, when LCC costs were decreased by 40%, granular B costs were over 2% higher than the all the LCC sections.

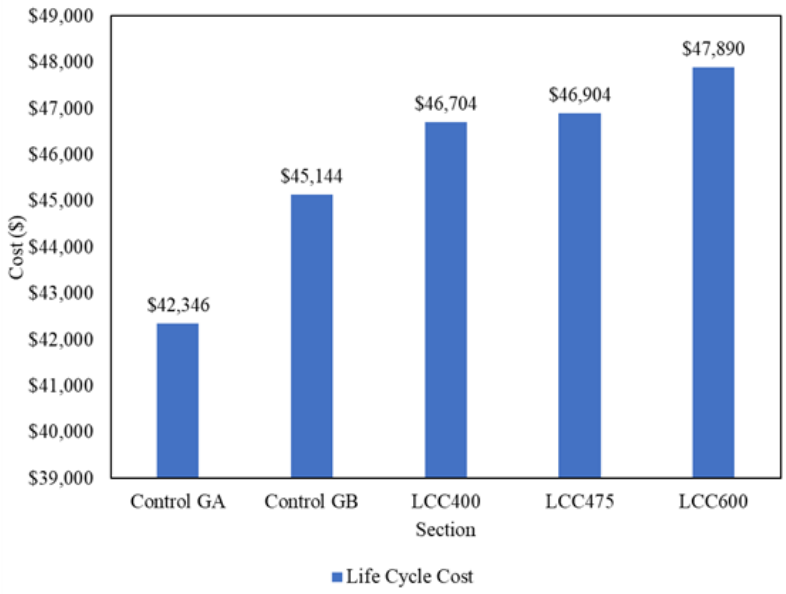

Figure 9.3: Total Life Cycle Cost comparison for designs

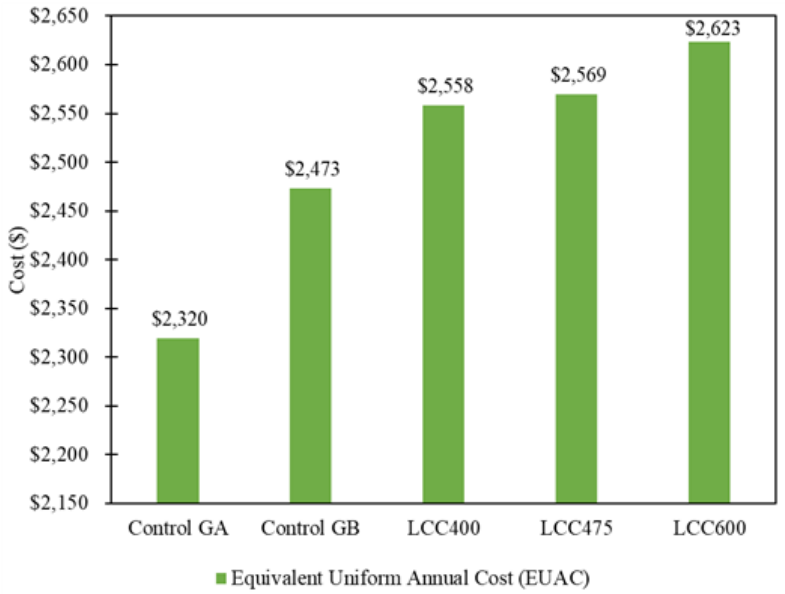

Figure 9.4: Equivalent Uniform Annual Cost for designs

9.7.2 Change in Cost of Granular A

A change in the cost of granular A led to a difference in total cost for all sections (Figure 9.7). The change was more for the Control section than LCC sections because granular A served as both the base and subbase layer. Increasing the granular A cost triggered minimal changes between the LCC sections. When granular A cost increased, LCC percentage change for LCC total lifecycle cost reduced slightly with an increase in density. However, although the actual cost of granular A increased in greater proportions, increasing its cost by up to 35% did not make it more expensive than the LCC sections (Figure 9.8).

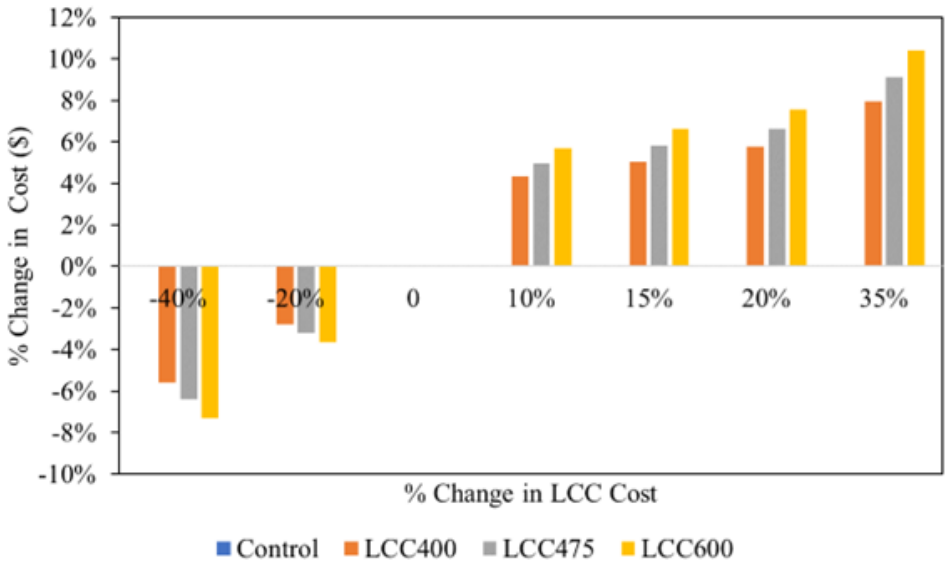

Figure 9.5: Percentage impact of change in LCC cost

9.7.3 Change in Cost of Granular B

The cost of granular B was lowered by up to 40% and increased by up to 35% in this analysis. Figure 9.9 shows that the reduced granular B cost widened the cost gap between the Control and LCC sections, making it even more affordable. Even with a 35% increase in granular B cost, the LCC sections were still more expensive. Nonetheless, as granular B cost increased the cost disparity with the LCC sections decreased.

Using the bank of Canada's interest rates between 1932 and 2022 [262] as a basis, discount rates ranging between 0.5% and 12% were selected for the sensitivity analysis

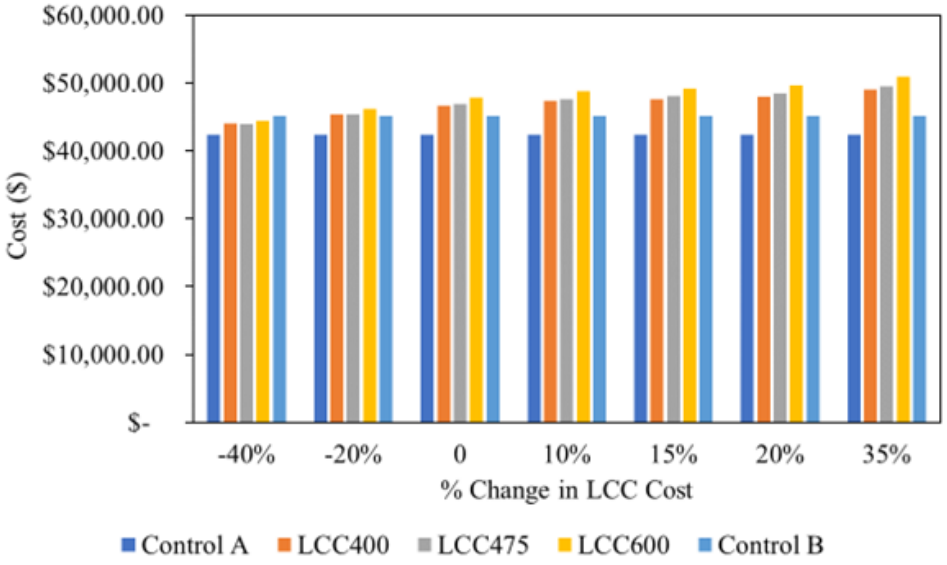

Figure 9.6: Difference in actual cost due to change in LCC cost

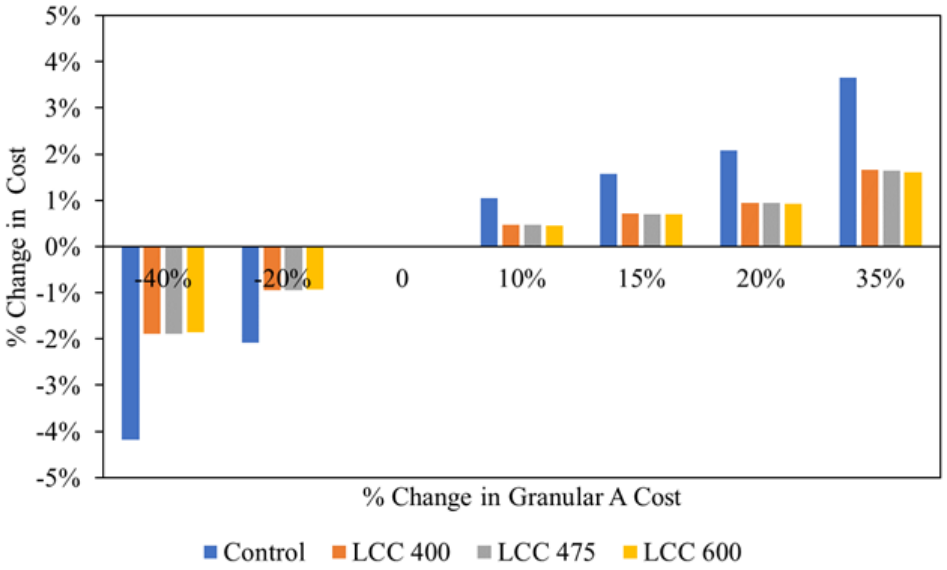

Figure 9.7: Percentage impact of change in granular A cost

(Figures 9.11 and 9.12). Generally, when the discount rate was lower, the total life cycle

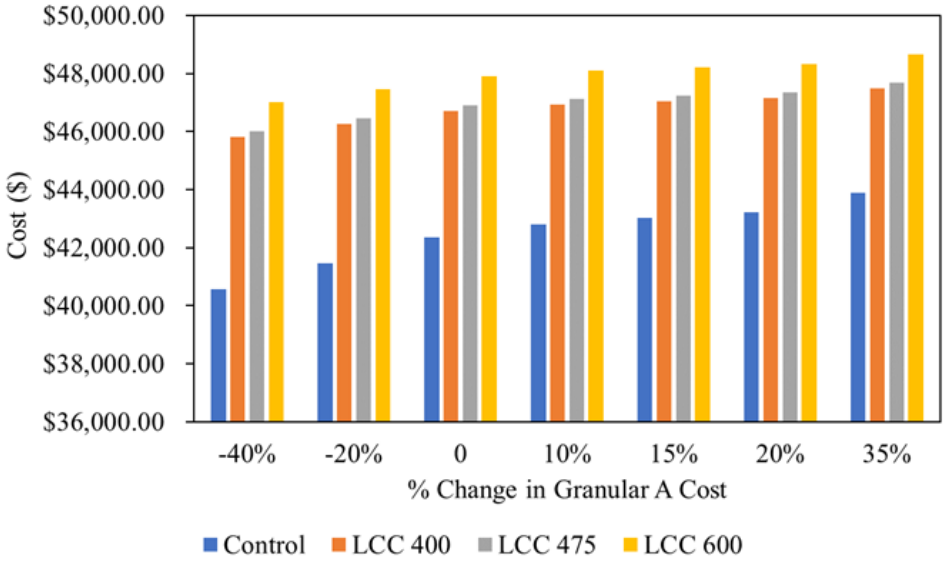

Figure 9.8: Difference in Actual cost due to change in granular A cost

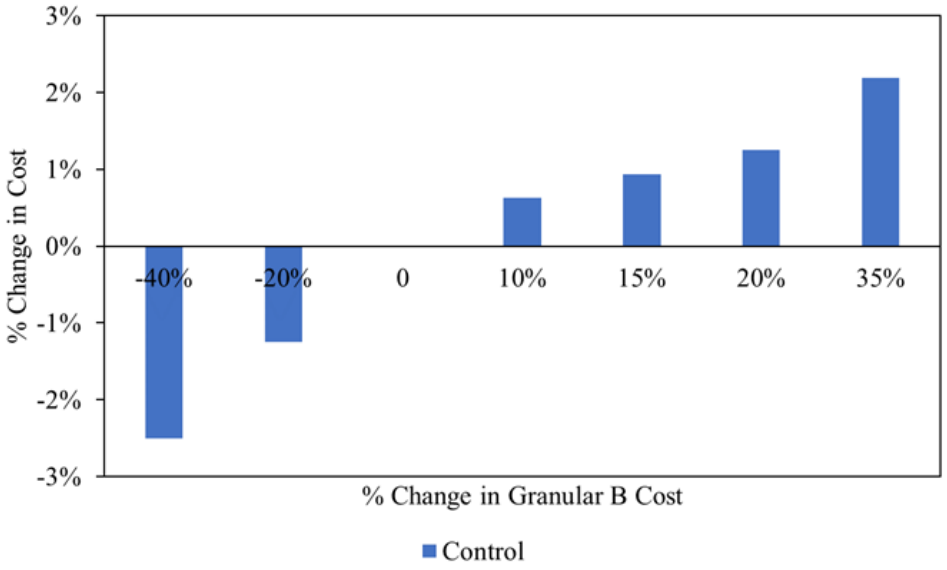

Figure 9.9: Percentage impact of change in granular B cost

costs were higher for all the sections. Interestingly, even though higher costs were noted,

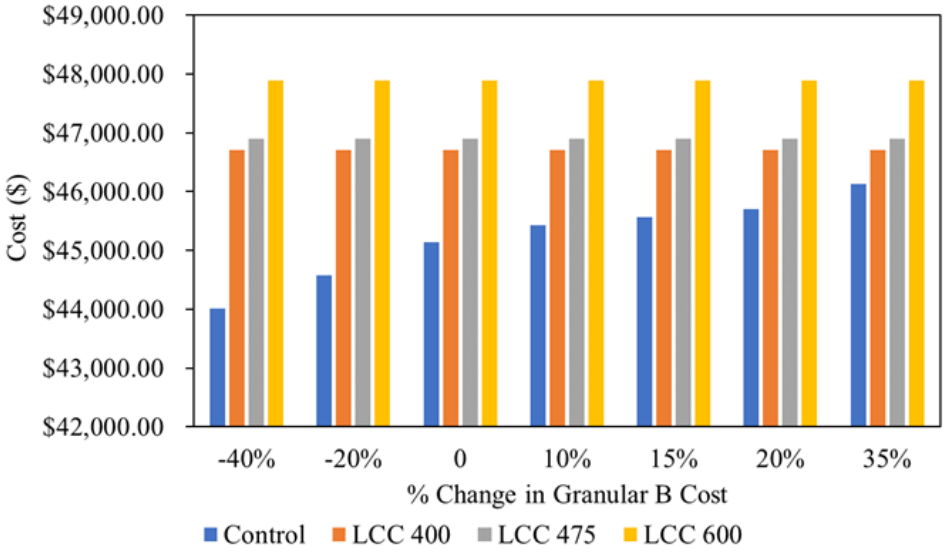

Figure 9.10: Difference in Actual Cost due to change in granular B Cost

the LCC475 and LCC600 sections experienced lower cost increases than the other sections when the discount rate was lower than or equal to 4%. At a 0.5% discount rate, though, the percentage increase in the cost of LCC400 became lower than LCC475. With discount rates above 5%, a more significant decrease in cost is seen for LCC400, granular A, and granular B sections, with the highest reduction, observed in the LCC400 section. The sensitivity analysis suggests that the cost for all the sections had a higher magnitude of sensitivity when discount rates were lower than 5% compared to when the rate was higher. A discount rate of 0.5% could produce an 18% increase in pavement lifecycle cost, while a 12% discount rate yielded just about a 7% decrease in pavement total life cycle cost.

Considering the actual total lifecycle cost for this scenario, Figure 9.12 shows that, at all discount rates used, granular A remained the cheapest option. When the discount rate was below 4%, LCC475 became the more affordable option than the other LCC sections. Likewise, LCC600 was the most expensive option from a 2% discount rate and above, while GB became the cheapest option from a 1.5% up discount rate than the LCC sections.

Therefore, the influence of the discount rate could skew the lifecycle cost of the alternative pavement designs, but in all cases, granular A would remain the cheapest alternative. Amongst the LCC sections, LCC475, most of the time, was the most cost-effective.

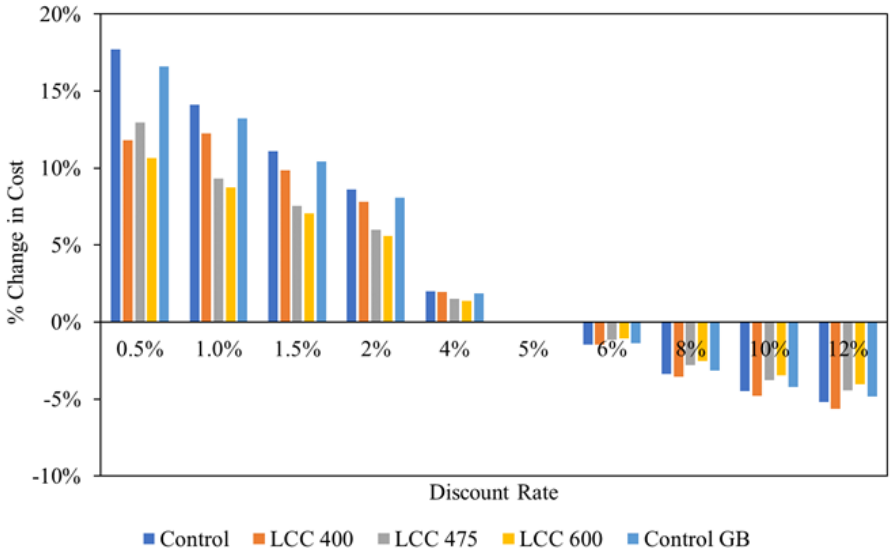

Figure 9.11: Percentage impact of change in discount rate

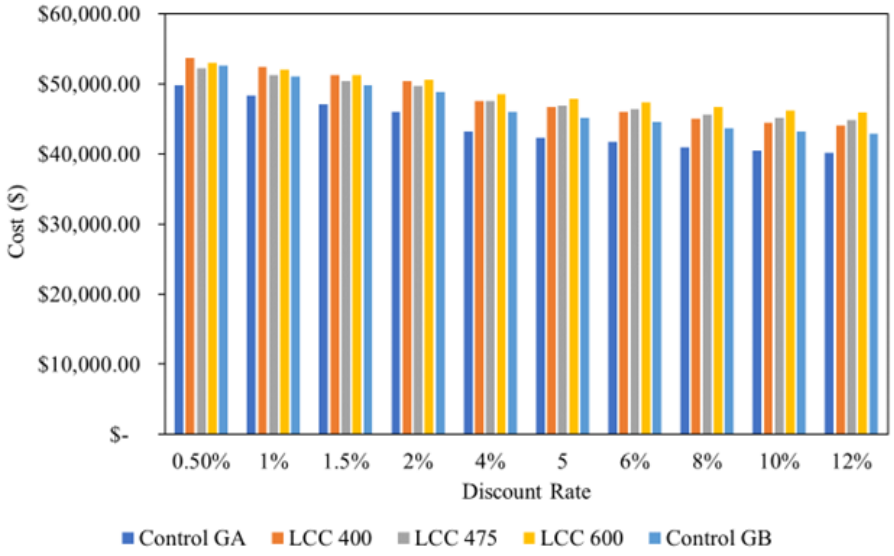

Figure 9.12: Difference in actual cost due to change in discount rate

9.7.4 Summary

The results from the Lifecycle Cost Assessment can be summarized as follows.

- Flexible pavement sections with granular A had between 10 to 13% and granular B, between 4 to 6% lower total life cycle costs at the end of a 50-year analysis period compared with LCC subbases.
- The yearly cost commitment for 400 kg/m^3, 475 kg/m^3, and 600 kg/m^3 LCC subbase was also between 10% to 13% more than when granular A was used and between 3 to 6% more when granular B was used respectively.
- Initial construction contributed the most to all sections' total lifecycle costs. The initial construction costs for the Control with granular A were 15%, 18%, and 21% lower than the sections with 400, 475, and 600 kg/m^3 LCC, respectively. These percentages were 7%, 10%, and 13% lower when granular B was used.
- When only initial construction and maintenance LCCA phase costs were compared, the LCC sections yielded lower total life cycle costs, 400 kg/m^3 (6%), 475 kg/m^3 (5%), and 600 kg/m^3 (3%) than the Control with granular A. Similarly, it was 12%, 11%, and 9%, respectively, less than the Control with granular B. The costs increased with an increase in LCC density LCC.
- Comparative life cycle costs were achieved when 475 kg/m^3 and 400 kg/m^3 LCC density were applied. But 600 kg/m^3 LCC density generated 2% more cost than 475 kg/m^3 and 400 kg/m^3 LCC densities.
- Total lifecycle cost was sensitive to changes in the cost of subbase material. Even with a 40% LCC cost reduction, the granular A Control section remained cheaper. But a decrease in LCC cost by 40% caused the Control with granular B to become more expensive than the LCC sections.
- An increase in granular A and B costs by up to 35% did not make the LCC sections cheaper. However, when granular A or B cost increased, its total lifecycle cost disparity became smaller compared with the LCC sections.
- According to the sensitivity analysis, the cost for all the sections was more sensitive to changes in discount rates below 5% than it was to changes above. A pavement's total life cycle cost may grow up to 18% at a discount rate of 0.5%, while it could reduce by just around 7% at a discount rate of 12%.

- The influence of discount rate could skew the lifecycle cost of the alternative pavement designs, but in all cases studied, granular A remained the cheapest alternative. The section with 475 kg/m^3 LCC was primarily identified as the most economical among the LCC sections.

Chapter 10

Conclusions and Recommendations

10.1 Construction conclusions

The construction process during and after the LCC pour for the trial sections was analyzed. Challenges were identified and documented. Information from this helped interpret subsequent performance. The following conclusions have been reached based on on-site monitoring, testing, and instrumentation monitoring during construction.

- 400 kg/m^3, 475 kg/m^3, and 600 kg/m^3 density LCC incorporated as a subbase layer can reduce subgrade pressures by up to 78% compared with granular material during construction.
- When pouring LCC in lower temperatures ($\leq$ 4 °C), and construction might need to commence immediately, it might be necessary to insulate LCC layers (e.g., with insulation blankets), to enhance curing.
- LCC subbase does not hinder the drainage ability of the pavement structure and causes the base layer to drain water more than the granular alternative during construction.
- High dynamic strain responses could be present at the surface and subbase of LCC pavements before asphalt paving compared with unbound granular material. Dynamic strain reduced with an increase in pavement depth when granular and LCC material were used as subbase, especially for 600 kg/m^3 LCC subbase.

- Placing unbound granular material could take over four times longer than pouring a Lightweight Cellular Concrete subbase of the same thickness. This implies more labor and equipment time usage, therefore greater costs.

- Construction factors that impact LCC pavement performance include; construction method, construction process, construction scale, contractors' experience with similar work, duration between LCC pour and surface layer placement, excessive vehicular traffic on LCC sections before surface layer paving, and environmental factors. A combination of precipitation and vehicular traffic could result in higher strains within the LCC layers.

- Excessive vehicles and trucks over the LCC pavement sections before asphalt paving could be detrimental to LCC pavement performance by inducing higher strains, leading to early cracking and weakening of the LCC layer. Avoiding this traffic on LCC sections before asphalt paving could be helpful. The roadway design structure could be modified to allow for the anticipated vehicular loads before asphalt placement. Design modifications to accommodate construction and other vehicular traffic must consider site-specific subgrade conditions and could involve increasing the LCC and/or granular base course thicknesses.

- In addition, limiting the duration between LCC pour and asphalt paving operations could help reduce the problems present due to vehicular traffic.

- Construction crew training and an open line of communication are essential considerations when the LCC subbase is to be incorporated within the pavement structure. This is because care is required throughout the process up to asphalt concrete placement to ensure good future performance of LCC subbase pavements. When the construction crew's buy-in is obtained, it becomes easier to ensure that measures are adhered to achieve good performance.

10.2 Material Properties

The laboratory testing evaluation for pavement material properties at Erbsville and Notre Dame Drive reflected some differences that could have influenced pavement performance. These findings have been outlined below.

- The asphalt concrete applied at Notre Dame Drive, was stiffer at lower temperatures and less stiff at temperatures equal to or above 21 °C than that at Erbsville. A

lower quality subgrade (CBR 4 < 9 at Erbsville) was present at Notre Dame Drive, and better-quality granular A (CBR 125) was used at Notre Dame than at Erbsville (CBR 54). The CBR of the granular B used at Erbsville was 27.

- Twenty-eight-day compressive strength for LCC was found on average to be 0.81, 1.18 and 1.74 MPa for 400 kg/m^3, 475 kg/m^3 and 600 kg/m^3. While for 475 kg/m^3 LCC with 20% slag, it was 1.67 MPa.

- The 475 kg/m^3 and 600 kg/m^3 density layers by day three and 400 kg/m^3 by day seven had surpassed the typical specified minimum 28-day compressive strength of 0.5 MPa, which could be an indication that the layer has sufficient strength to support the pavement structure as a subbase layer.

- Adding slag to LCC density could be beneficial by improving compressive strength up to 42%. The findings also reveal that the thickness of LCC plays a role in determining the strength of the layers. 40% greater thickness could result in a 6% increase in ultimate compressive strength.

- It could be beneficial to increase LCC density by up to 26% to achieve similar results with minimal thickness.

- LCC with high early strength cement could achieve peak temperatures between 5 to 9 hours during its heat of hydration process. This process takes longer (12 hours) for 25% thicker LCC material of similar density containing 20% slag. This is a vital consideration in determining the construction schedule after LCC pour.

- The rate of temperature rise for LCC is influenced by cement content, plastic density, and thickness of the LCC layer.

- 400, 475, and 600 kg/m^3 LCC were determined to be stiffer than granular A and B materials by over three times.

- As 475 kg/m^3 LCC aged, its water absorption characteristic declined.

- MEPDG results showed better performance for 250 mm and 350 mm thick LCC than 450 mm unbound granular B. However, it showed a similar pavement condition index (PCI) at the end of the 25 years when comparing 150 mm unbound granular A with 200 mm thick 400, 475, and 600 kg/m^3 LCC densities. But, the LCC sections performed relatively better in terms of permanent deformation and IRI. Better performance was also achieved as LCC density increased.

- WESLEA analysis indicated that 400, 475, and 600 kg/m^3 LCC densities performed three, six, and seven times better for rutting than the Control in terms of allowing more traffic repetitions and would allow twice as much traffic than the Control before fatigue failure occurred.

10.3 Instrumentation

10.3.1 Environmental Effects

Monitoring and analyzing over three-year data for Erbsville and over ten months for Notre Dame Drive trial road sections discovered the following environmental characteristics of LCC and traditional subbase flexible pavements.

- LCC subbase thickness $\geq$ 250 mm has greater performance in terms of insulation, reducing subgrade pressures and pavement strains due to environmental factors compared with unbound granular material and lower LCC thickness. The potential to do this also increased with an increase in LCC density except for its insulation capability that increased with decreased density.
- LCC layer's insulating characteristics are primarily seen in the winter and summer as its layers are less influenced by ambient temperature during these seasons.
- 267 freeze-thaw cycles were observed in the air temperature, while 70 cycles were measured in the subgrade of the 450 mm thick granular B pavement section and none within the 350 mm thick LCC pavement over the study period.
- Both conventional and LCC pavement layer temperatures can be estimated using the proposed linear regression temperature models. It is envisaged that utilizing the pavement temperature profile, the models presented would help calculate in situ pavement engineering characteristics. Additionally, these models can be employed to predict pavement service life and performance by projecting future pavement temperatures using ambient temperature trends from past data.
- Pavement moisture was seen to vary with precipitation. Soil water potential depends on the season and pavement layers' permeability characteristics.
- The 400 kg/m^3 LCC provided superior drainage ability than the other LCC and unbound granular pavement for the base and subbase, but the 475 and 600 kg/m^3 LCC density provided the greatest protection from moisture for the subgrade.

- The horizontal strain at any depth in the pavement structure was smaller in the morning (just at the start of the heating period) than in the afternoon (start of the cooling period). The strain was also typically tensile in the morning (before 9 am) and compressive in the afternoon (between 9 am and 5 pm) beneath the asphalt layer. However, when pavement thickness increased beyond 550 mm, a reverse or delayed strain behavior occurred. This is an important design consideration.

- The maximum daily thermal strain change due to contraction and expansion of the asphalt concrete layer was seen in the 400 kg/m^3 pavement, then 475 kg/m^3, Control, and 600 kg/m^3 accordingly.

- Due to daily cooling and heating, when the temperature increased, strain beneath the asphalt layers for the Control and LCC sections decreased by 53%, 94%, 40%, and 69% for the Control, 400 kg/m^3, 475 kg/m^3 and 600 kg/m^3 sections. However, the Control section had higher longitudinal strain magnitudes (over 52%) than the LCC sections at low daily temperatures and over 31% than the LCC sections at peak daily temperatures.

- The magnitude of daily strain change was greater in spring than fall and winter for all pavement sections except for 400 kg/m^3 subbase pavement, which had the most significant change in the fall. The other pavements experienced the lowest daily strain change in the winter.

- Seasonal fluctuations in temperature and moisture influenced the longitudinal strain response beneath the asphalt layer. 475 to 600 kg/m^3 LCC can potentially reduce the longitudinal strain beneath the asphalt layer by over two times compared to conventional pavements. This is also true for 400 kg/m^3 during the warmer months, but during the winter, 400 kg/m^3 experienced 1.3 times higher strains beneath the asphalt layer than on conventional pavements.

- Transverse strains at the middle of the LCC layers were higher than those at the bottom while longitudinal strains at the middle were mostly lower than at the bottom of the layer.

- Daily subgrade pressure change can be reduced by 44% and 68% when 475 and 600 kg/m^3 of LCC is applied as a subbase material.

- Factors influencing subgrade pressure response include ambient and layer temperature, moisture variation, pavement thickness, and material properties. Thicker pavements could reduce the daily impact of temperature variation on pressure change,

thereby limiting the thermal stress change experienced at the top of the subgrade. When the conventional pavement structure's thickness was 750 mm, daily pressure change was reduced by 24 times compared to a 490 mm pavement structure. Also, when 475 kg/m^3 subbase LCC with pavement structure thickness of 550 mm was used, daily pressure change was reduced by nine times compared to 500 mm pavement structure. A further decrease of 11 times was noted when the LCC thickness was increased to 350 mm from 250 mm.

- The Control subgrade experienced less pressure due to lower temperatures and less moisture, whereas the LCC sections experienced higher subgrade pressures due to a combination of these variables.

- Greater thickness ($\geq$250mm) LCC caused subgrade pressure to be less impacted by seasonal temperature and moisture variation. Conventional pavements experienced more subgrade pressure at higher temperatures, whereas LCC pavements have lower pressures. The LCC sections however experienced their greatest subgrade pressures at lower temperatures this was more pronounced with LCC layer thickness $\leq$ 200mm.

10.3.2 Traffic Load Effect

The main findings are summarized below, based on the investigation of dynamic compressive pressure (stress) and strain response induced by traffic loads on the traditional and LCC subbase pavements.

- Lightweight Cellular Concrete reduced subgrade pressure due to traffic by up to three times when compared to unbound granular material.

- LCC's ability to reduce pressures is influenced by LCC layer thickness, overall pavement thickness, load magnitude, load distribution, tire pressure, and material characteristics.

- In areas where lower traffic volumes and smaller types of vehicles are expected, thinner ($\leq$ 200 mm) LCC 475 kg/m^3 subbase layers could be used.

- Strain reduction was seen with increased pavement depth, and incorporating LCC subbase layers could reduce longitudinal and transverse strains even more than unbound granular material.

- WESLEA could predict the traditional pavement structure stresses and strains at the bottom of the surface and subbase layers. However, it could overestimate the stresses and strains experienced in LCC subbase pavements. WESLEA calculated stresses could be reduced by 65% and strains by as low as 20% for LCC pavement densities between 475 kg/m^3 to 600 kg/m^3 and layer thicknesses exceeding 200 mm.
- Stresses and strains experienced at each layer may be influenced by factors such as layer temperature and moisture, which should be investigated further.

10.4 Visual Assessment

Following three and one year of service for Erbsville and Notre Dame Drive, the sections were visually inspected, and the following conclusions were drawn.

- The sections were found to be generally in excellent condition.
- Most of the cracks noted at the Erbsville location resulted from cracking from adjacent pavements that propagated into the trial section, except for very slight alligator cracking noted on the unbound granular section after three years of service life.

10.5 Pavement stiffness

Falling Weight Deflectometer

The outcome of the Falling weight deflectometer tests is summarized below.

- LCC subbase layers with 350 and 250 mm thick 475 kg/m^3 LCC as subbase can provide four times stiffer subbase than the typical pavement structure with 450 mm granular B subbase.
- The structural layer coefficient for 475 kg/m^3 of Lightweight Cellular Concrete is 0.22. This can guide when designing 400 to 600 kg/m^3 LCC subbase pavements.
- According to the AREA$_{60}$ and d_0 study, the 400, 475, and 600 kg/m^3 portions of lightweight cellular concrete at Notre Dame Drive had weaker subgrades than the unbound granular material. There were also some areas of the pavement with a weaker pavement structure at the 475 kg/m^3 and 400 kg/m^3 sections. More research is required to understand what is happening in these locations completely.

Lightweight Deflectometer

Based on the lightweight deflectometer test, the following conclusions have been made.

- Flexible pavements with LCC subbase thicknesses $\geq$ 250 mm could produce a 21% stiffer pavement structure compared with twice as thick unbound granular B subbase pavements. An increase of 36% in stiffness can occur when LCC thickness increases by 100 mm.
- Pavement stiffness increases with LCC layer density and over time for both unbound and LCC pavements.
- There may be discrepancies in pavement stiffness along road sections, particularly following the spring thaw. When determining the structural suitability of pavements, this should be considered. A variety of testing stations should be used to provide an accurate picture of the existing pavement structure.
- Time of testing, pavement temperature during testing, construction method, insufficient compaction, excessive truck traffic on LCC pavements before AC placement, and road gradient could influence LCC pavement stiffness.

10.6 Pavement Roughness

Pavement roughness evaluation revealed the following outcomes.

- LCC subbase thickness 250 mm can produce over 22% smoother riding surfaces than unbound granular pavements.
- Lower LCC thickness equal to 200 mm could yield over 20% smoother pavements for a 600 kg/m^3 LCC subbase. While varying results were seen for 400 and 475 LCC subbase pavements compared to unbound subbase materials due to varying reasons discussed, it was evident that they may function comparably or better than conventional pavements.
- Factors influencing roughness progression in LCC pavements include environmental conditions, seasonal variations, road class, road function, road gradient, subgrade conditions, initial construction process and practices (compaction, early vehicular traffic).
- SurPro and Dipstick methods can provide similar roughness trends for pavement sections; however, the magnitudes in roughness measured could differ by up to 31

10.7 Lifecycle Assessment

Based on the life cycle assessment, the following conclusions have been made.

- CO_2 emissions can be reduced by up to 16% when 400 to 600 kg/m^3 LCC is used, producing less SO_2, CO, NOx, PM_{10}, and total PM environmental impact than granular A.
- Using LCC with densities between 400 and 600 kg/m^3 in place of granular B may result in reductions in CO_2, SO_2, CO, NO_x, PM_{10}, and total PM emission of 16%, 17%, 24%, 15%, 23%, 23% and 25% respectively.
- The dry mix method would produce about 0.1% less CO_2 emissions than the wet mix method and reduce the other emission levels.
- Material production and initial construction with LCC material yielded more emissions, especially CO_2, than unbound granular material, with more emissions for higher density LCC. However, transportation of unbound granular A induced more emissions than LCC.
- Emission levels were sensitive to material transportation distance. The most sensitive pollutant to changes in transportation distance was CO_2, CO, and NO_x.
- LCC emission levels were also sensitive to slag content variation. The most sensitive pollutant to these changes were CO_2, SO_2, and NOx. LCC mixes with no slag content had 14%, 12%, and 9% lower CO_2 emissions than granular A and 15%, 13%, and 10% than granular B for LCC400, LCC475, and LCC600 accordingly.
- One cubic meter of producing and placing granular A and B produced 10 kg and 18 kg of CO_2 respectively, while 400 kg/m^3 LCC produced between 174 to 176 kg, 475 kg/m^3 between 206 to 209 kg and 600 kg/m^3 between 261 to 264 kg of CO_2.
- The dry mix method production process of 1 m^3 of LCC generated 0.62 kg, 0.74 kg, and 0.93 kg of CO_2 for 400 kg/m^3, 475 kg/m^3, and 600 kg/m^3 LCC, respectively. The wet mix approach yielded 1.39 kg, 1.66 kg, and 2.09 kg CO_2.
- Compared with foamed glass aggregate and expanded polystyrene, using 400 and 600 kg/m^3 LCC as insulating subbase produced less CO_2 emission in road construction.

10.8 Life Cycle Cost Analyses

An evaluation of the lifecycle cost of lightweight cellular concrete compared to unbound granular layers influenced the following conclusions.

- Flexible pavement sections with granular A had between 10 to 13% and granular B, between 4 to 6% lower total life cycle costs at the end of a 50-year analysis period compared with LCC subbases.
- The yearly cost commitment for 400 kg/m^3, 475 kg/m^3, and 600 kg/m^3 LCC subbase was also between 10% to 13% more than when granular A was used and between 3 to 6% more when granular B was used respectively.
- Initial construction contributed the most to all sections' total lifecycle costs. The initial construction costs for the Control with granular A were 15%, 18%, and 21% lower than the sections with 400, 475, and 600 kg/m^3 LCC, respectively. These percentages were 7%, 10%, and 13% lower when granular B was used.
- When only initial construction and maintenance LCCA phase costs were compared, the LCC sections yielded lower total life cycle costs, 400 kg/m^3 (6%), 475 kg/m^3 (5%), and 600 kg/m^3 (3%) than the Control with granular A. Similarly, it was 12%, 11%, and 9%, respectively, less than the Control with granular B. The costs increased with an increase in LCC density LCC.
- Comparative life cycle costs were achieved when 475 kg/m^3 and 400 kg/m^3 LCC density were used. But 600 kg/m^3 LCC density generated 2% more cost than 475 kg/m^3 and 400 kg/m^3 LCC densities.
- Total lifecycle cost was sensitive to changes in the cost of subbase material. Even with a 40% LCC cost reduction, the granular A Control section remained cheaper. But a decrease in LCC cost by 40% caused the Control with granular B to become more expensive than the LCC sections.
- An increase in granular A and B costs by up to 35% did not make the LCC sections cheaper. However, when granular A or B cost increased, the disparity in its total lifecycle cost became smaller compared with the LCC sections.
- According to the sensitivity analysis, the cost for all the sections was more sensitive to changes in discount rates below 5% than it was to changes above. A pavement's total life cycle cost may grow by up to 18% at a discount rate of 0.5%, while it could reduce by just around 7% at a discount rate of 12%.

The influence of discount rate could skew the lifecycle cost of the alternative pavement designs, but in all cases studied, granular A remained the cheapest alternative. The section with 475 kg/m^3 LCC was primarily identified as the most economical among the LCC sections.

10.9 Design of Lightweight Cellular Concrete Subbase Pavements

The Granular Base Equivalent method, Mechanistic-Empirical Design guide, and AASHTO 93 methods can be employed in designing LCC subbase pavements. Packages based on the linear elastic theory can also be used to assess critical responses in LCC pavements; however, certain adjustments might be necessary to determine actual performance, especially in cases where design alternatives are being compared. It is recommended that when MEPDG is used, other analysis tools such as WESLEA, KENLAYER, and PAVEXpress should be used to supplement and interpret performance prediction results since MEPDG does not currently have calibration factors for LCC.

Regarding LCC layer thickness design, it could be worthwhile to ensure LCC subbase layers are no thinner than 250 mm when densities below 475 kg/m^3 are to be used over weak subgrades. Especially when construction activities cannot be controlled or limited after LCC pour before asphalt concrete placement. Modifications could be made to this thickness recommendation as more data is available over time.

10.10 Overall Feasibility

The application of Lightweight Cellular Concrete subbase within the pavement structure is a feasible alternative to traditional subbase material, especially when subgrade insulation is required and weak subgrades are encountered. Comparatively, thicknesses equal to or over 250 mm for densities between 400 and 600 kg/m^3 will provide superior field performance compared with unbound granular material subbase with equal or higher thicknesses. Lower critical responses could also be achieved, ensuring that pavement failure is delayed; hence, longer-lasting pavements could be achieved.

Pavement design approaches currently used in designing flexible pavements could be employed in designing LCC subbase pavements; however, proposed adjustments are recommended. For example, WESLEA generated strains and stresses could be reduced by a

factor of 0.2 and 0.65 for LCC between 400 and 600 kg/m^3. Since calibration factors are not currently available in MEPDG for LCC, it could be worthwhile to use other packages like WESLEA to support pavement design analysis. The structural coefficient of 0.22 has also been proposed as a benchmark for designing Lightweight Cellular Concrete pavements with a density between 400 and 600 kg/m^3.

Compared to unbound granular subbase, LCC pavements were determined to have a lower environmental impact through life cycle analysis. Lower density LCC would cause less environmental damage than higher densities. It could be more beneficial to employ the dry mix approach for LCC production, especially when transportation distances are great and the production scale is immense. To further lower the environmental damage of LCC, substituting a portion of cement with slag or comparable pozzolans is recommended.

In terms of Life Cycle Cost Assessment, LCC pavements were found to have a higher life cycle cost than unbound granular pavements; however, 400 and 475 kg/m^3 LCC costs were comparable. The initial high construction cost was the determining factor which depends mainly on LCC cost. Since an average LCC price was employed in the analysis, there is potential that the LCC pavements could be cheaper. Also, sensitivity analysis reflected that a 40% reduction in LCC price made it a more affordable alternative than granular B. Moreover, suppose insulation benefits of LCC are added, LCC performance could be much better, resulting in lower total life costs. In terms of the maintenance cost, the LCC sections were less expensive to maintain, especially the 400 and 475 kg/m^3 LCC pavements. However, future applications and evaluations of the use of LCC will provide further information on performance that can better inform lifecycle costs.

This research provides an understanding of the behavior of lightweight cellular concrete subbase, which is crucial in proposing its use for different pavement applications. When deciding on density for various road conditions and classes, it is vital to consider the strain and stress patterns within the pavement structure. For example, the results from this study showed that 475 kg/m^3 had the greatest resistance to daily strains induced by temperature variation and would perform comparatively better across all seasons compared to the unbound layer. However, when looking at thicknesses of and below 200 mm, it could experience greater subgrade pressures at sub-zero temperatures. This could inform design requirements. Furthermore, the temperature regression models for LCC and unbound granular subbase pavements developed in this study could be used to estimate flexible pavement temperatures incorporating these materials as subbase.

10.11 Recommendation for Future Work

- Further field evaluation for 400 to 600 kg/m^3 Lightweight Cellular Concrete densities over an extended period is necessary.
- Incorporating Lightweight Cellular Concrete insulation and structural properties to assess its performance adequately and overall benefits should be considered.
- Performance prediction models assessing Lightweight Cellular Concrete pavements under varying conditions should be investigated.
- Quantifying construction benefits such as time and cost savings due to the Lightweight Cellular Concrete subbase should be studied.
- An in-depth lifecycle cost analysis could be performed to consider social costs associated with using Lightweight Cellular Concrete compared with unbound materials.
- A study into the development of calibration factors of Lightweight Cellular Concrete for use in MEPDG is necessary.

Chapter 11

Guidelines for Future Applications of Lightweight Cellular Concrete Subbase

This chapter recommends guidelines and specifications for Lightweight Cellular Concrete subbase (LCCS) in flexible pavement applications. These guidelines are a product of laboratory work by Ni (2021) [174] and this study. Other past studies have also been referenced within the guidelines.

Guideline Specification for Lightweight Cellular Concrete Subbase in flexible pavements

This guide provides information on the materials, properties, design, handling, and road pavement subbase applications of cast-in-place Lightweight Cellular Concrete Subbase having wet (cast) densities between 400 to 600 kg/m^3.

TABLE OF CONTENT

1. GENERAL

1.1 Description

Cellular concrete sometimes referred to as foam concrete, is a lightweight, insulating construction material consisting of Portland Cement or Portland Limestone Cement, water, foaming agent, and compressed air. Fly ash and slag are often added to the mix to customize material properties. Cellular concrete usually contains no sand or aggregate. Fresh cellular concrete is highly flowable and can be pumped into place over large distances (up to 1,000 m) through flexible hoses. In most cases, cellular concrete is cast in place.

Cellular concrete can have wet densities from 250 to 1600 kg/m^3; however, most roadway applications are placed at wet densities of 400 to 600 kg/m^3. This specific pavement application of cellular concrete is here forth referred to as Lightweight Cellular Concrete Subbase (LCCS).

Lightweight cellular concrete subbase (LCCS) may be produced using either "wet" or "dry" mix processes. "Wet" mix processes use a cement and water slurry batched by a ready-mix supply company. The slurry is delivered into the LCC equipment, which injects foam into the slurry and pumps the LCCS into place. "Dry" mix refers to the process whereby all the constituents of the LCCS are blended on site, first by mixing the cement and water into a slurry, followed by injecting the foam and pumping the LCCS into place.

LCCS is commonly used to reduce or prevent the settlement of roadways located on soft or compressible soils. Also, roadways constructed over frost-susceptible soils often experience frost action, which is characterized by heave as the subgrade soils freeze during winter months, followed by softening during spring thaw. Due to its insulating qualities, LCCS may be used to limit or prevent frost action.

1.2 Scope

This guide provides data and techniques for designing and applying cast-in-place Lightweight Cellular Concrete Subbase (LCCS) in flexible pavements. The use of this document shall be in accordance with the contract documents.

2. REFERENCED STANDARDS AND REPORTS

The specification refers to the following standards, specifications, and publications: ASTM International with corresponding AASHTO

C 78	Standard Test Method for Flexural Strength of Concrete Using Simple Beam with Third-Point Loading (AASHTO T 97)
C 94	Standard Specification for Ready-Mixed Concrete
C 150	Standard Specification for Portland Cement
C 157	Standard Test Method for Length Change of Hardened Hydraulic-Cement Mortar and Concrete
C 469	Standard Test Method for Static Modulus of Elasticity and Poisson's Ratio of Concrete in Compression
C 494	Standard Specification for Chemical Admixtures for Concrete
C 495	Standard Test Method for Compressive Strength of Lightweight Insulating Concrete (AASHTO T 22)
C 496	Standard Test Method for Splitting Tensile Strength of Cylindrical Concrete Specimens (AASHTO T 198)
C 513	Standard Test Method for Obtaining and Testing Specimens of Hardened

	Lightweight Insulating Concrete for Compressive Strength
C 518	Standard Test Method for Steady-State Thermal Transmission Properties by Means of the Heat Flow Meter Apparatus
C 595	Standard Specification for Blended Hydraulic Cements
C 666	Standard Test Method for Resistance of Concrete to Rapid Freezing and Thawing (AASHTO T 161)
C 796	Standard Test Method for Foaming Agents for Use in Producing Cellular Concrete Using Preformed Foam
C 869	Standard Specification for Foaming Agents Used in Making Preformed Foam for Cellular Concrete
C 1074	Standard Practice for Estimating Concrete Strength by the Maturity Method
C 1157	Standard Performance Specification for Hydraulic Cement
C 1585	Standard Test Method for Measurement of Rate of Absorption of Water by Hydraulic Cement Concretes
D 2434	Standard Test Method for Permeability of Granular Soils (Constant Head)
D 4694	Standard Test Method for Deflections with a Falling-Weight-Type Impulse Load Device
D 5084	Standard Test Methods for Measurement of Hydraulic Conductivity of Saturated Porous Materials Using a Flexible Wall Permeameter
D 5334	Standard Test Method for Determination of Thermal Conductivity of Soil and Soft Rock by Thermal Needle Probe Procedure

ACI

SP-29	Lightweight Concrete
523.1R	Guide for Cast-in-Place Low-Density Cellular Concrete
523.2R	Guide for Precast Cellular Concrete Floor, Roof, and Wall Units
523.3R	Guide for Cellular Concretes Above 50 lb/ft 3 (800 kg/m^3)

CAN/CSA Standards

A 3001	Cementitious Materials Used in Concrete

A 23.1 Concrete Materials and Methods of Concrete Construction/Test methods and Standard Practices for Concrete

3. DEFINITIONS

For this specification, the following definitions apply:

Asphalt concrete	Material placed immediately above the granular base made up of asphalt cement.
Cellular concrete	In its simplest form, is comprised of cement, fly ash and/or slag, water, and air bubbles.
Cold weather	Conditions when the air temperature is at or below 5 °C in the shade and when air temperature is likely to fall below 5 °C within 24 hours.
Hot weather	Conditions when the air temperature is at or above 28 °C in the shade and when air temperature is likely to rise above 28 °C within 24 hours.
Curing	The maintenance of a satisfactory moisture content and temperature in cellular concrete for a suitable period during its early stages following placing. This enables the development of desired properties and assures satisfactory hydration and hardening of the cellular concrete.
Contractor	A company that undertakes a contract to provide materials and labour for a roadway construction project.
Differential icing	The occurrence of slippery conditions on insulated pavement sections, while adjacent conventional pavement sections have dry surfaces.
Engineer	A professional engineer licensed by the Professional Engineers in their respective province to practice and is designated by owner to administer

contract.

Falsework	Any temporary structural support, including bracing, used to support all or part of the formwork or of the structure during its construction or rehabilitation until it becomes self-supporting.
Formwork	The mould into which the fresh concrete is placed.
Granular base	Material placed immediately above the subbase made up of crushed stones to specification.
LCCS	Lightweight Cellular Concrete Subbase.
Pavement	The hard upper layer of a roadway, typically comprised of asphalt or concrete.
Slurry	Refers to a specific mixture of cement, fly ash and/or other supplementary cementing materials and water.
Subbase	Material placed immediately above the subgrade.
Subgrade	The natural soil upon which the subbase is to be placed.

4. MATERIALS

4.1 Portland cement

The cement shall fulfill the requirement of the following standards: CAN/CSA A3001 for Type GU, GUL, HE, HS, and InterCem GUb cement in Canada, ASTM C 150 for Portland cement, ASTM C 595 for Blended cement, and ASTM C 1157 for hydraulic cement [2, 47].

4.2 Pozzolans

In the production of LCCS, supplementary cementitious materials such as fly ash, silica fume, high reactivity metakaolin, or ground granulated blast furnace slag may be used to not

only improve flowability and reduce the heat of hydration, but also reduce bleeding, segregation, and increase strength. However, trial batches shall be used to confirm final properties. The supplementary cementitious materials shall follow the requirement of CAN/CSA A 3001.

4.3 Water

The quality and cleanliness of water are significant in the production of the mixture. The mixing water shall be in accordance with CSA Standard A23.1 or ASTM C94/94M. Water with questionable quality may affect the preformed foam, the setting time, and the strength of the LCCS [2] and should be tested to ensure that the mix meets the required compressive strength.

4.4 Admixtures

Chemical admixtures (e.g., accelerators or retarders) conforming to ASTM C494 may be used with LCCS. Trial batches should be used to confirm admixture dosage and compatibility with the foam [2].

4.5 Preformed foam

Pre-formed foam is essential in cellular concrete as it can control the plastic density of the mix [259]. It consists of a foaming agent, water, and compressed air to help produce foam [32]. The foam shall have a homogeneous bubble structure to provide concrete with reasonable strength [36]. TThe foam structure shall be capable of resisting the pressure of the base mix until the initial setting time of the cement is reached, and the air bubbles are surrounded by strong skeleton of concrete [209, 138].

The preformed foam is created by mixing the foaming agent with water and passing it through the foam generator [2]. The foaming agent shall conform to ASTM C 796 and ASTM C 869, which covers the laboratory testing of the performance of the foaming agent and provides the method of how to evaluate the performance of the foaming agent.

5. PHYSICAL PROPERTIES

5.1 Fresh density

The fresh density or as-cast density of the LCCS shall be measured by calculating the density of the mix using a known volume container. ASTM C 796 describes the procedure of how the measurement of the density shall be taken. The fresh density shall be monitored and maintained within the range of $\pm 10\%$ of the designed density. Density measurements shall be measured and recorded once per 50 cubic meters, or once per ready mix truck (for wet mix) [47]. Method for sampling and testing the material to ensure quality should conform to ASTM C 513 or ASTM C796 and ASTM C 495.

5.2 Dry density

The dry density of the LCCS shall be determined following the procedure prescribed in ASTM C 796 and ASTM C 495.

5.3 Maturity

The maturity method is a technique for estimating the strength of the concrete via the strength-maturity relationship. The strength-maturity relationship shall be obtained by performing a compressive strength test following ASTM C 495 and recording the temperature history of the mix (ASTM C 1074). For instance, the ultimate strength when fully cured for the 475 kg/m^3 density LCCS with a cement/slag ratio of 4, and a w/c ratio of 0.50 was estimated to be 2 MPa.

5.4 Compressive strength

The determination procedures for compressive strength for LCCS shall follow ASTM C796 and ASTM C 495. For road applications, the typical density of the LCCS is between 400 and 600 kg/m^3 [63]. Compressive strength for these densities ranges between 0.5 and 2.5 MPa depending on different mix compositions [32, 2]. LCCS with less than 0.5 MPa compressive strength could be used in cases where a thicker granular / asphalt layer is placed over top, or where a top lift of LCCS with a higher density is used.

5.5 Modulus of elasticity

The modulus of elasticity in pavement design represents how much the concrete will compress under load [234]. The modulus of elasticity (E-value) of cellular concrete is lower than normal weight concrete. The E-value of LCCS shall be determined in accordance with ASTM C 469, and the E-value for 400 kg/m^3, 475 kg/m^3, and 600 kg/m^3 density LCCS were investigated by the University of Waterloo lab [174]. The results ranged from 637 to 824 MPa for 400 kg/m^3, 794 to 1,279 MPa for 475 kg/m^3, and 1,310 to 1,738 MPa for 600 kg/m^3 density LCCS, which follows the typical range of the past research that the E-value of LCCS range between approximately 600 to 1800 MPa for densities between 400 to 600 kg/m^3 [32]. By comparison, a typical granular subbase (i.e., granular B) has a modulus of elasticity of approximately 200 MPa. Therefore, using LCCS instead of granular subbase results in a stiffer subbase layer.

5.6 Poisson's ratio

Poisson's ratio is one of the parameters that have been used to calculate the stress, strain, and displacement within the pavement structure [234] and is one of the input factors in pavement design for performance prediction (AASHTO 93 and MEPDG). To determine the Poisson's ratio of LCCS, the test procedure shall follow ASTM C 469. LCCS Poisson's ratio has been found to be 0.25, 0.27, and 0.26 for 400, 475 and 600 kg/m^3 respectively [174].

5.7 Splitting tensile strength

The test method for determining the splitting tensile strength of LCCS shall conform to ASTM C 796 and ASTM C 496. The tensile strength of LCCS is reported to have a positive relationship with its densities and a strong connection with its compressive strength. Test results from the University of Waterloo lab found that the splitting tensile strength for LCCS is 0.16 MPa for 400 kg/m^3 density, 0.20 for 475 kg/m^3 density, and 0.30 for the 600 kg/m^3 density [174].

The results correspond to the typical ratio of tensile strength to compressive strength, which is between 0.2 and 0.4 [8].

5.8 Modulus of rupture

The concrete flexural strength (or modulus of rupture) is the maximum value of allowable stress before the concrete fractures in pavement design [234]. It is necessary to understand the flexural strength of LCCS material before applying it to the pavement structure [92]. The modulus of rupture is a crucial parameter in rigid pavement design and flexible pavement when a cement-treated base material is used. The typical range for flexural strength ratio to cellular concrete's compressive strength is 0.25 to 0.35 [252]. To determine modulus of rupture for LCCS, the testing protocol shall be in accordance with ASTM C 78. Test results from the University of Waterloo lab showed that the flexural strength of LCCS is 0.22 for 400 kg/m^3, 0.28 for 475 kg/m^3, and 0.39 for 600 kg/m^3 density, which is 19% to 25% to its compressive strength and follow the trend from past research [174].

5.9 Drying shrinkage

It is reported that the lack of aggregate causes cellular concrete to generate ten times more drying shrinkage than normal weight concrete [209]. The drying shrinkage would increase when the density reduces [32, 158, 52]. However, the reduction of drying shrinkage can be achieved by replacing cement content with pozzolanic materials such as fly ash and slag [118, 49]. Moreover, drying shrinkage is not usually considered critical in cellular concrete used for geotechnical applications. The reason is its bearing capacity is not significantly decreased when any shrinkage cracking occurs 5(ACI 523.1R)[2]. Drying shrinkage for LCCS shall be determined in accordance with ASTM C157.

5.10 Thermal insulation

The bubble structure of LCCS makes it a good thermal insulation material and has low thermal conductivity compared to normal concrete. According to BCA and ACI, the thermal conductivity of cellular concrete ranges from 0.1 to 0.16 W/m/K for 400 to 640 kg/m^3 dry densities [32, 2]. A technical report [46] from the industry indicated that the thermal conductivity for oven-dried samples with cast densities of 400 to 600 kg/m^3 ranged from 0.05 to 0.09 W/m/K for ASTM D5334 and 0.076 to 0.101 for ASTM C 518. These values are typically 5% to 30% of the normal weight concrete [219].

5.11 Workability

LCCS is considered to have good workability due to its ease-to-pour, self-levelling, and self-consolidating ability [189, 2], which could save construction time and excludes the need for vibration during placement.

The workability of LCCS is typically visually evaluated, and, aimed at achieving appropriate viscosity of the mix. To measure workability, a sample of fresh mix LCCS is placed in an open-ended cylinder 75 mm in diameter and 150 mm long. The cylinder is raised vertically to allow

the material to spread. The spread is then measured in two directions, averaged, and reported to the nearest 5mm [38]. Currently, no minimum workability requirements for a desirable mix have been established [8].

5.12 Permeability

The permeation of cellular concrete is one of the indices to evaluate its durability. Generally, low-density cellular concrete has a low coefficient of permeability (k) and is related to the water absorption of cellular concrete [131]. Reported values from ACI 523.1R range from 1×10^{-4} to 1×10^{-5} mm/s (ASTM D 2434). Technical report [46] also showed that 400 kg/m^3, 475 kg/m^3, and 600 kg/m^3 density LCCS has a permeability of 6.02×10^{-6} cm/s, 1.4×10-6 cm/s, and 5.7×10^{-7} cm/s in accordance with ASTM D 5084. Permeability testing for LCCS shall be in accordance with modified testing as described in ACI 523.1R. Alternatively, the NCAT field permeameter kit and procedure could also be used to determine the permeability of LCCS. Results from the University of Waterloo lab found that the coefficient of permeability for LCCS ranged from 0 to 0.035 for 600 kg/m^3 to 400 kg/m^3 density [174].

5.13 Water absorption

The water absorption of LCCS is one of the indices to evaluate its durability of LCCS. The testing procedure is in accordance with ASTM C 769. The water absorption of LCCS may be twice as high as normal weight concrete at similar water-to-binder ratio [8]. For oven-dried LCCS samples at 400 kg/m^3 to 600 kg/m^3 densities, the water absorption was found to be 24.5% to 33%. However, the water absorption for non-oven-dried samples ranged from 6.5 to 10% [174].

5.14 Sorptivity

Sorptivity explains the water absorption and transport in material via capillary action [8]. Sorptivity of LCCS is dependent upon pore structure, filler type, permeation mechanism, foam agent, and curing conditions [209]. Cellular concrete sorptivity is observed to increase with an increase in foam volume and the addition of fly ash into the mixes in place of sand [121]. It was found that the 400 kg/m^3 and 475 kg/m^3 density LCCS had higher sorptivity than the 600 kg/m^3 density sample [174].

5.15 Freeze and thaw resistance

Cellular concrete is considered to have excellent freeze-thaw resistance due to the hollow voids which hold the expansive forces resulting from freeze water [36]. It was found that the strength, depth of initial penetration, absorption, and absorption rate of the cellular concrete at low density provide good freeze-thaw resistance. The freeze and thaw resistance of the LCCS shall be evaluated using ASTM C 666 Procedure B, which freezes in air and thaws in water. However, the insulation property of low density LCCS expands the required freezing time to the target temperature. Therefore, extending the freezing time to about nine hours is recommended while keeping the thawing time at about two hours [244]. The modified freezing and thawing procedure was applied in the freeze-thaw test performed at the University of Waterloo Lab. It

Table 11.1: Typical values of various LCCS properties [174]

Property	**Test Standard**	**Density(kg/m^3)**		
		400	475	600
Compressive Strength (MPa)	ASTM C 495	0.7-1.0	1.1-1.5	1.6 - 2.2
Modulus of rupture (MPa)	ASTM C 78	0.2 - 0.25	0.27 - 0.29	0.37 - 0.45
Modulus of elasticity (MPa)	ASTM C 469	637 – 824	794 – 1,279	1,310 – 1,738
Poisson's ratio	ASTM C 469	0.25	0.27	0.26
Splitting tensile strength (MPa)	ASTM C 496	0.14 - 0.17	0.18 - 0.22	0.24 - 0.35
Permeability (k)	NCAT Permeameter	0.035	0.012	0
Water absorption (oven dry)	ASTM C 796	28-36%	26-34%	23-25%
Water absorption (non-oven dry, 28 days)	ASTM C 796	8.9-10.8%	8.7-10.4%	6.8-7.3%
Damping ratio	ASTM D 4015	1.35%- 1.90%	2.77% - 3.20%	1.92%- 2.26%
Drying shrinkage (%)	ASTM C 157	0.18	0.12	0.09

was found that the 475 kg/m^3 and 600 kg/m^3 density samples were not deteriorated after 180 cycles, showing LCCS's excellent freeze-thaw resistance. However, 400 kg/m^3 density samples failed in the first 45 cycles [174]. Therefore, it is recommended to follow the requirement from ACI, which is the relative dynamic modulus of elasticity of LCCS shall exceed 70% after 120 cycles [2].

5.16 Damping ratio

The dynamic characteristic of LCCS is important as cellular concrete is typically used in many geotechnical applications. The damping ratio for cellular concrete is dependent on the specimen unit weight during testing [245]. The testing procedure is in accordance with ASTM D 4015. The test could determine the damping ratio of the LCCS at low amplitude (very small strain). Test results indicated that LCCS with density from 400 to 600 kg/m^3 has a material damping ratio between 1.35% to 3.2%. Although 475 kg/m^3 density, LCCS has the highest damping ratio compared to 400 and 600 kg/m^3 densities. The difference was considered minimal as they all fall below 5% and are similar to soft rock and other soil materials such as hard clay, which typically has a damping ratio of 1.5% and up to 5% at very small shearing strain [174].

5.17 Summary of typical LCCS properties

Table 1 presents typical values of various LCCS properties. These results have specifically been obtained for road subbase application and are cured for 28 days prior to testing except for the damping ratio which tested at 120 days. The cement/slag ratio was 4, and the w/c ratio was 0.50. The results will vary if other Pozzolans are used and in different proportions.

6. DESIGN CONSIDERATIONS AND SUBMISSION REQUIREMENTS

6.1 General

As a result of its lightweight and insulating properties, LCCS is commonly used to reduce or prevent roadway settlement and/or frost action. Key design considerations include density selection and thickness.

6.2 Density Selection

LCCS may be placed within a range of densities, depending on the project's needs. Density selection must consider design requirements for load reduction, buoyancy, insulation, and strength. A density of 475 kg/m^3 is commonly used because it strikes a good balance between unit weight, insulating value, and strength. Where practical, densities may be adjusted within the LCCS layer to optimize performance. For example, 400 kg/m^3 could be used within the lower lifts of LCCS to optimize load reduction, while the final lift could use 600kg/m^3 to enhance load carrying capacity.

6.3 Design thickness

Pavement thickness is a critical design parameter in pavement design. The determination of pavement layer thickness depends on several factors such as material properties, environmental conditions, and traffic conditions [234]. This section outlines three methods currently in use within Canada, and how the LCCS material could be incorporated in each method.

The thickness of the asphalt concrete and granular base layers over the LCCS will be based on traffic loading and the potential for differential icing. These layers will be in accordance with minimum design requirements for the location it is being incorporated. Provincial standards must be followed to ensure appropriate design. The thickness for all the layers needs to be determined based on the preferred pavement design method. For example, thickness for asphalt concrete and granular base layer in the AASHTO 93 method should be determined based on their structural number under different ESALs and reliability. For MEPDG, the designed thickness should meet Provincial performance criteria.

6.3.1 AASHTO 93 Method

In the AASHTO 93 pavement design procedure, it is important to retrieve the structural number of each layer's material. Therefore, it is important to determine the structural number of LCCS with the intention of thickness design. However, AASHTO 93 does not provide the structural number for LCCS. Nonetheless, the determination of the structural number of LCCS can be achieved by performing in-field Falling Weight Deflectometer (FWD) test. The FWD is a non-destructive test equipment that is capable of back calculating the moduli of the pavement layer and shall be performed in accordance with ASTM D4694. Once the moduli of each pavement layer are obtained, the effective structural number of the existing pavement can be calculated.

Based on a field test performed in Ontario, Canada, an effective structural number of 0.20 was obtained for 475 kg/m^3 density LCCS [88]. Another test section in the Region of Waterloo,

Ontario indicated a layer coefficient of 0.22 for 475 kg/m^3 density LCCS. These are considered typical average values when designing a pavement structure incorporating the 475 kg/m^3 density LCCS as subbase. For comparison, asphalt and granular base layers usually have structural layer coefficients of 0.38 and 0.12, respectively. However, it should be noted that depending on the mix design (i.e., proportions, foaming agent) and how the cellular concrete is produced, the material may meet density requirements, but not the specified strength. The relationship between compressive strength and elastic modulus should be used instead as it has been indicated that the compressive strength and elastic modulus have positive relationship, which is specified in past research [8, 175]. Under this circumstance, the minimum compressive strength can be specified to achieve the desired modulus of elasticity. Further guidance is presented in Section 6.4.

6.3.2 Mechanistic-Empirical Design Method

Currently, the AASHTOWare software which is based on the Mechanistic-Empirical pavement design method does not have provisions for LCCS material as a pavement layer. However, since LCCS is a cementitious material, it may be suitable to categorize it as a cement stabilized base or chemically treated material when using the AASHTOWare. It is noted that the cement-treated and other pozzolanic stabilized materials should be treated as separate layers when used as a base layer for structural support [11]. The LCCS layer could be considered as an unbound material with constant layer modulus and moisture insensitive if it is designed to provide long-term strength and durability. Alternatively, the LCCS layer could be classified as a chemically stabilized structural layer capable of providing structural support [11].

6.3.3 Granular Base Equivalency (GBE) Method

Granular Base Equivalency (GBE) equates the strength of the pavement materials in terms of their thicknesses. "The GBE thickness is the required overall structural pavement thickness expressed in terms of an equivalent thickness of Granular A (according to MTO Pavement Design Guide). GBE is calculated using Equation B.1.

$$H_e = a_1 h_1 + a_2 h_2 + a_3 h_3 \tag{11.1}$$

where:

H_e = the equivalent granular thickness.

a_1, a_2, a_3 = strength coefficients of the asphalt layer, base layer, and subbase layer.

h_1, h_2, h_3 = the actual thicknesses of the asphalt layer, base layer, and subbase layer.

To determine the strength coefficient (equivalency factors) for a typical pavement (control section) with the traditional granular material as subbase layer, typical design parameters specific to the location of the road section in Canada shall be utilized.

To calculate the required baseline pavement thickness that would produce the same GBE value as the control section for a roadway incorporating LCCS as subbase material, potential

strain values beneath the control section's subbase is required. This can be simulated using tested pavement design software, such as WESLEA, that can predict potential strain values for typical designs at the bottom of the subbase layer. The predicted microstrain values produced at the bottom of the subbase layers for various thicknesses are determined. This same process is used to determine strain values for the LCCS sections which use the same layer properties and thicknesses for all the pavement layers except the subbase layer. In determining the LCCS layer properties, laboratory results for Modulus of Elasticity and Poisson's ratio are utilized in the design. The simulated values for strain and corresponding thickness for the Control and LCCS sections are then interpolated to determine thicknesses that would provide the same level of strain. The Strength Coefficient for the LCCS layer using the GBE formula (equation 1) can then be obtained.

When designing for a weak subgrade with the Resilient Modulus of less than 30 MPa, GBE Expert values for the design traffic should not be less than 800 for 15 years [182].

An example of input parameters and strength coefficient for typical pavement design and comparable LCCS designs is presented in Table 2.

6.4 Compressive Strength Specifications

This section provides guidance with respect to the establishment of compressive strength specifications. It should be noted that the following information is dependent on a cement/slag ratio of 4 and a water/cementitious ratio of 0.5.

Typical average 28-day compressive strengths are approximately within 0.7 – 1.0 MPa for 400 kg/m^3 ; 1.1 – 1.5 MPa for 475 kg/m^3 and 1.6 – 2.2 MPa for 600 kg/m^3 . Minimum 28-day compressive strengths shall be established based on the required structural contribution of the LCCS for a given project. Typical minimum 28-day compressive strengths are 0.35, 0.5, and 1.2 MPa for 400, 475, and 600 kg/m^3 LCCS, respectively.

To estimate LCCS Modulus of Elasticity (MOE) based on minimum unconfined compressive strength (UCS) for densities ranging between 400 and 600 kg/m^3, the following relationship could be employed [174].

$$y = 677.43x + 122.16 \tag{11.2}$$

where:

y = Modulus of elasticity

x = Minimum UCS of LCCS

For instance, assuming the minimum UCS for 475 kg/m^3 LCCS is 0.5 MPa, using Equation B.2, the corresponding MOE is 461 MPa.

To further determine the structural layer coefficient of the LCCS material, Equation B.3 could be utilized. The calculation is built on the AASHTO layer coefficient as presented by the U.S. Department of Transportation Federal Highway Administration [50].

$$a = 0.14 \times (\frac{E}{207})^{0.333} \tag{11.3}$$

where:

a = Structural Layer Coefficient

E = layer Modulus of Elasticity in MPa

The corresponding minimum structural layer coefficient is thus 0.18, with typical values of 0.20 or greater.

6.5 Submission requirements

The contractor shall submit the following requirements to the engineer at least 30 days before LCCS pouring begins [93]:

- Certifications. Certifications for Portland cement, supplementary cementitious material and preformed foam as required by contract documents/ engineer.
- Specifications. Manufacturers' data and specifications for equipment including capacities to be used in mixing, hauling, and placing of LCCS.
- Plant layout. If central-plant mixing, submit layout of plant location showing mixing plant, cement and Pozzolan storage and water supply.
- Third-party test reports that establish compliance of the mix design with compressive strength, permeability, and durability properties. It is not necessary to repeat specialized tests such as permeability and freeze-thaw for each project, but the cellular concrete supplier should have these third-party test reports for a representative mix design (CEMATRIX). In a case where special or new materials are used as substitutes for typical components, trial batches should be produced to ensure optimum LCC mixture [153].

7. Equipment

7.1 Description

Since LCCS is a special type of concrete and its application within the pavement structure is quite different from typical concrete, specific types of equipment are required. This section describes the types and requirements for equipment used in the production and application of LCCS.

Equipment selection type shall be based on application and contract specifications and must conform to all necessary health and safety requirements. The specialized batching, mixing, and placing equipment shall be automated and certified for the purpose by the manufacturer of the LCCS. Lightweight cellular concrete subbase (LCCS) may be produced using either "dry" or "wet" mix processes.

7.2 Dry-mix method

Dry-mix processes are commonly used to produce LCCS for high volume and/or high production rate projects. Dry-mix refers to the process whereby all the constituents of the LCCS are blended on site, first by mixing the cement and water into a slurry, followed by injecting the foam and pumping the LCCS into place. Cement is delivered to the site using bulkers. Bulk cement weight measurements shall be determined by onboard instrumentation that operates within a tolerance of 1.5% per batch. Dust suppression systems shall conform to OSHA 29 CFR 1926 and 1910.

Dry-mix equipment should be capable of producing 100 cubic meters or greater per hour, continuously, from one piece of equipment. The equipment should also be able to pump through hoses or pipes up to a flat linear distance of 1,000 meters. [47].

7.3 Wet-mix method

"Wet" mix processes use a cement and water slurry batched by a ready-mix supply company. Once onsite, the temperature, density, and viscosity of the slurry from each truck are measured to confirm compliance with the requirements to make LCCS. After quality is verified, the slurry is delivered into the LCC equipment, which then injects foam into the slurry and pumps the LCCS into place.

Production capacity should be at least 75 cubic meters per hour, continuously, from one piece of equipment. The pumping distance should be at least 200 meters. [47].

7.4 Addition of foam and placement

LCCS must be pumped by a positive displacement type such as a progressive-cavity or peristaltic pump. The pump hose should be large enough (usually at least 2 inches in diameter) to enable uniform delivery at the placement point without damage to the LCCS structure. [2]. A foam generator shall be used to continuously generate preformed foam which shall be injected and mixed with the cementitious slurry downstream of the positive displacement slurry pump. The equipment shall be calibrated to produce a precise and predictable volumetric rate of foam with a stable uniform bubble structure. [47].

8 Construction

8.1 Preparation of subgrade

Before LCCS placement begins, the area to be paved shall be graded and shaped according to design specifications. The subgrade shall be compacted to ensure firmness and ability to support

LCCS without yielding [2]. Snow and ice shall be removed from areas before LCCS pour. The placement area shall be free of standing water during placement of cellular concrete and until backfill is placed on top of the cellular concrete [47].

8.2 Forms

Wooden forms are often used to contain LCCS during placement. These forms must be adequately secured to the subgrade and able to withstand cellular concrete hydrostatic pressure. Forms may require lining the contact surface with LCCS with an impermeable membrane such as poly sheeting or the like to prevent leakage [47]. Forms are typically removed after placement of LCCS.

Where LCCS is placed on a slope, nonwoven geotextile fabric partitions supported by rebar stakes are commonly used to stabilize the material. This method may also be used to partition the LCCS lift into smaller volumes.

8.3 Placing

Lift thickness is influenced by the specific application, layout, casting procedure, mix design, cement content and ambient temperature [2]. LCCS shall be placed within one or two hours to avoid disrupting setting time [47].

LCCS shall not be placed during heavy or prolonged precipitation. Groundwater control is essential during the placement of LCCS until a sufficient cover is placed to prevent flotation [47].

A nonwoven geotextile fabric can be used to prevent infiltration of the LCCS into underlying or adjacent granular drainage layers.

Any item to be fully or partially encased in the LCCS shall be properly set and stable before LCCS installation [47].

8.4 Finishing

LCCS surface shall be smooth and free from ridges and projections that could adversely affect the layers above. LCCS can be placed with a maximum slope of 1% . Greater slopes will require profiling via steps with formwork or mechanically grading to the required slope percent with a bulldozer or milling machine [47]. Finish surfaces shall be within +/-25mm of design grades as per drawings.

8.5 Placement in cold weather conditions

LCCS may be placed during freezing conditions, provided measures are taken to prevent damage to the LCCS until sufficient strength has been attained.

These measures should achieve the purpose of early hydration aids which is to maintain the LCCS above 5 °C during initial curing. No cold weather protection measures are required where the minimum daily temperature during early-stage hydration is above 5 °C.

Where the internal temperature of the LCCS is below 5 °C, curing will cease. Permanent damage to the LCCS could occur if its temperature falls below 0 °C during initial curing.

Curing of LCCS will typically generate heat; therefore, below 5 °C air temperatures do not necessarily indicate that the LCCS has stopped curing. Other factors that must be considered for cold weather protection include the following:

- Thicker lifts of LCCS generate more hydration heat.
- New lifts of LCCS will often be placed on existing lifts, which will continue to generate heat and insulate the current pour from heat loss.
- Additional time may be required to allow the LCCS to cure before placement of another lift.

When considering hydration aid methods, site-specific methods should be pre-determined by the LCCS supplier and the contractor at the time of construction, based on site conditions.

Where the placement of tarps directly on the LCCS is not practical, the area where LCCS is to be placed must be enclosed and heated to greater than 5 °C. The enclosure and heating must be in place prior to LCCS placement [47].

8.6 Curing

Loading of, or traffic on the LCCS shall be prevented until the material has attained sufficient strength to withstand the loads with no damage. The rate of strength gain will be influenced by the mix design, pour dimensions, and temperatures during curing. Backfill can commence when LCCS supports foot traffic without leaving an indentation.

8.7 Traffic

To prevent damage to the LCCS, foot traffic is not allowed during initial curing. In high traffic areas, precautions such as fencing may be required.

Traffic or other heavy equipment on newly poured LCCS shall be prevented until sufficient strength is gained to withstand the loads with no damage. Construction equipment must not be allowed to drive directly on the cellular concrete until the first lift of asphalt concrete is placed. The roadway shall not be opened to traffic until the full pavement structure is in place.

8.8 Surfacing and bases

Base course placement can commence when foot traffic can be supported without leaving an indentation. Backfill material must be placed in such a manner as to prevent damage to the LCCS. For the base layer directly above the LCCS layer, vibrating compaction shall be avoided. The initial granular base layer shall not be less than 150 mm thick. Vibratory compaction may be used on the asphalt layer.

8.9 Maintenance

The contractor shall maintain the LCCS material in good condition until all work is completed and accepted. Maintenance shall include protecting the LCCS material in cold and hot weather conditions and immediately repairing any defects that may occur. Such maintenance shall be done by the contractor at his own expense or as specified by contract terms and conditions.

9. Inspection and testing

9.1 Description

Testing and Quality Control procedures for LCCS shall be consistent with or surpass requirements according to the American Society for Testing and Materials (ASTM), Canadian Standards Association (CSA) and American Concrete Institute (ACI). LCCS supplier is required to have documented quality control procedures, including processes for training and certification of QC professionals. The LCCS supplier must provide a dedicated onsite PC representative that is certified according to the above-noted process.

9.2 Quality Procedures

9.2.1 General

A summary of precautions and quality control procedures for LCCS is provided below:

- Foam-generating nozzle, water meter and scales shall be calibrated before the project and during the project when there is a reason for its necessity [16, 18].
- Avoid excessive mixing of material, which could yield density and consistency changes.
- Add ingredients in proper proportioning during continuous mixture for uniformity [136].
- Allowance shall be made for density changes due to placing methods or conditions (extreme weather, pumping distances).
- Production and installation shall be done by a specialized contractor with previous experience.
- If the slurry is delivered by ready-mix, density, temperature, and viscosity must be verified before use to confirm acceptability to produce quality cellular concrete.
- Slurry production from bulk powder on site shall have a density tolerance within 5% of the mix design value [153].

9.2.2 Density

During production, the wet (cast) density of the LCCS is measured, as follows:

- Density measurements shall be measured and recorded once per 50 cubic meters, or once per ready mix truck (for wet mix).
- The density shall be maintained within +/- 10% of the design density.

9.2.3 Compressive Strength

During production, specimens of LCCS are captured to verify compliance with compressive strength requirements, according to the following procedures:

- Cylindrical specimens of 75 mm diameter by 150 mm shall be cast and measured for compressive strength at 28 days in accordance with ASTM C495 for every 100 cubic meter production [153].
- Specimens shall be stored in an undisturbed condition within 15 minutes of the casting area and not moved for 24 hours.
- Initial curing temperature of 25 to 30 °C for 24 to 96 hours is required for the specimens.
- Specimens shall be cured in 80% to 100% humidity room at 18 to 27 °C.

9.3 Reporting

A turnover package must be submitted at most 60 days from project completion. Information to be included in a package shall include at a minimum, the measured cast densities of cylinders, cast dates, location of samples, cylinder dimensions, cylinder mass, and 28-day compressive strength [47].

10. Measurement and Payment

10.1 Measurement

This work shall be measured in cubic meters determined by multiplying the known volume of slurry by the ratio of slurry density to average LCCS density [47].

10.2 Payment

Payment shall be on an all-in unit rate basis per cubic meter placed. The unit rate shall include materials, production, placement, and testing of LCCS.

References

[1] Abbas M Abd and Suhad M Abd. Modelling the strength of lightweight foamed concrete using support vector machine (svm). *Case studies in construction materials*, 6:8–15, 2017.

[2] American Concrete Institute (ACI). Guide for cast-in-place low density cellular concrete, 2006.

[3] Ibrahim Adwan, Abdalrhman Milad, Zubair Ahmed Memon, Iswandaru Widyatmoko, Nuryazmin Ahmat Zanuri, Naeem Aziz Memon, and Nur Izzi Md Yusoff. Asphalt pavement temperature prediction models: A review. *Applied Sciences*, 11(9):3794, 2021.

[4] Changfa Ai, Ali Rahman, Chuan Xiao, Enhui Yang, and Yanjun Qiu. Analysis of measured strain response of asphalt pavements and relevant prediction models. *International Journal of Pavement Engineering*, 18(12):1089–1097, 2017.

[5] Mohammad Z Alavi, Mohammad R Pouranian, and Elie Y Hajj. Prediction of asphalt pavement temperature profile with finite control volume method. *Transportation Research Record*, 2456(1):96–106, 2014.

[6] D ALDRIDGE. Introduction to foamed concrete: What, why, and how. use foam. *Concrete. Construction, Thomas Telford Ltd*, 2005.

[7] Arminda Almeida, John JM Moreira, João Pedro Silva, and Carlos GV Viteri. Impact of traffic loads on flexible pavements considering ecuador's traffic and pavement condition. *International Journal of Pavement Engineering*, 22(6):700–707, 2021.

[8] YH Mugahed Amran, Nima Farzadnia, and AA Abang Ali. Properties and applications of foamed concrete; a review. *Construction and Building Materials*, 101:990–1005, 2015.

[9] Lingshi An, Feng Zhang, Yongchang Geng, and Bo Lin. Field measurement of dynamic compressive stress response of pavement-subgrade induced by moving heavy-duty trucks. *Shock and Vibration*, 2018, 2018.

[10] ARA. Methodology for the development of equivalent pavement structural design matrix for municipal roadways including maintenance rehabilitation schedules and life cycle cost analysis. Technical report, Applied Research Associates, 2015.

[11] ERES Consultants Division ARA, Inc. Guide for mechanistic–empirical design of new and rehabilitated pavement structures. *Final Rep., NCHRP Project 1-37A*, 2004.

[12] Shobha Rani Arangi and RK Jain. Review paper on pavement temperature prediction model for indian climatic condition. *Int. J. of Innovative Research in Adv. Engineering*, 2(8):1–9, 2015.

[13] Arul Arulrajah, Mahdi M Disfani, Farshid Maghoolpilehrood, Suksun Horpibulsuk, Artit Udonchai, Monzur Imteaz, and Yan-Jun Du. Engineering and environmental properties of foamed recycled glass as a lightweight engineering material. *Journal of Cleaner Production*, 94:369–375, 2015.

[14] Arian Asefzadeh, Leila Hashemian, and Alireza Bayat. Development of statistical temperature prediction models for a test road in edmonton, alberta, canada. *International Journal of Pavement Research and Technology*, 10(5):369–382, 2017.

[15] ASTM. Standard test method for compressive strength of lightweight insulating concrete. 2012.

[16] ASTM. Standard test method for foaming agents for use in producing cellular concrete using preformed foam. 2012.

[17] ASTM. Standard guide for calculating in situ equivalent elastic moduli of pavement materials using layered elastic theory, 2015.

[18] ASTM. Standard specification for foaming agents used in making preformed foam for cellular concrete. Am. Soc. Test. Mater. USA, 2016.

[19] ASTM. Standard test method for measurement of rate of absorption of water by hydraulic-cement concretes. Technical report, 2020.

[20] C ASTM. Standard test method for sieve analysis of fine and coarse aggregates. *ASTM C136-06*, 2006.

[21] C ASTM et al. Standard test method for static modulus of elasticity and poisson's ratio of concrete in compression. *Annual book of ASTM standards*, 4:469, 2002.

[22] D Astm. Standard practice for roads and parking lots pavement condition index surveys. 2011.

[23] D ASTM. 4694-09: Standard test method for deflections with a falling-weight-type impulse load device. *American Society for Testing and Materials, USA*, 2015.

[24] D ASTM. 4695-03: Standard guide for general pavement deflection measurements. *American Society for Testing and Materials, USA*, 2015.

[25] Jim W. Hall Jr. Athar Saeed and Walter Barker. Performance-related tests of aggregates for use in unbound pavement layers. Technical report, 2001.

[26] Sergey Averyanov. Analysis of construction experience of using lightweight cellular concrete as a subbase material. Master's thesis, University of Waterloo, 2018.

[27] Sergey Averyanov, Frank Mi Way Ni, Eskedil Melese, and Susan Tighe. Construction experience analysis of using cematrix lightweight cellular concrete as a subbase material. In *CSCE General Conference 2018, Held as Part of the Canadian Society for Civil Engineering Annual Conference 2018*, pages 179–185. Canadian Society for Civil Engineering, 2018.

[28] H Awang, ZS Aljoumaily, N Noordin, and MZ Al-Mulali. The mechanical properties of foamed concrete containing un-processed blast furnace slag. In *MATEC Web of Conferences*, volume 15, page 01034. EDP Sciences, 2014.

[29] Bansal, Jan and Sven 2019. Differential Frost Heave Modelling .

[30] P Barbi, Guangyuan Zhao, Seyedata Nahidi, Jessica Achebe, and Susan Tighe. Adaptation strategies on flexible pavement design practices due to climate change in canada. In *Transportation Association of Canada 2021 Conference and Exhibition-Recovery and Resilience: Transportation after COVID-19*, 2021.

[31] Alireza Bayat and Mark Knight. Field evaluation and analysis of flexible pavement structural responses under dynamic loads. *Road materials and pavement design*, 13(1):26–37, 2012.

[32] BCA. *Foamed concrete- Composition and properties*. British Cement Association, 1994.

[33] Jean-Pascal Bilodeau, Guy Doré, Francois Perron Drolet, and Diane Chaumont. Correction of air freezing index for pavement frost protection design to consider future climate changes. *Canadian Journal of Civil Engineering*, 43(4):312–319, 2016.

[34] Rocky Bilotta, Jesse E Bell, Ethan Shepherd, and Anthony Arguez. Calculation and evaluation of an air-freezing index for the 1981–2010 climate normals period in the coterminous united states. *Journal of Applied Meteorology and Climatology*, 54(1):69–76, 2015.

[35] Peter J Bosscher, Hussain U Bahia, Suwitho Thomas, and Jeffrey S Russell. Relationship between pavement temperature and weather data: Wisconsin field study to verify superpave algorithm. *Transportation research record*, 1609(1):1–11, 1998.

[36] KC Brady, GRA Watts, and M Roderick Jones. *Specification for foamed concrete*. TRL Limited Crowthorne, UK, 2001.

[37] TW Bremner, PM Carkner, H Michael, and A Litvin. Guide for precast cellular concrete floor, roof, and wall units. *Manual of concrete practice*, pages 2–6, 1997.

[38] William E Brewer. Controlled low strength materials (clsm). In *Concrete in the Service of Mankind*, pages 664–675. CRC Press, 1996.

[39] SF Brown. State-of-the-art report on field instrumentation for pavement experiments. *Transportation Research Record*, (640), 1977.

[40] KJ Byun, HW Song, SS Park, and Y Song. Development of structural lightweight foamed concrete using polymer foam agent. *ICPIC-98*, 9, 1998.

[41] ASTM C513. Standard test method for obtaining and testing specimens of hardened lightweight insulating concrete for compressive strength. Technical report, 2019.

[42] CAC 2016. General Use (GU) and Portland Limestone (GUL) Cements.

[43] Campbell Scientific 2005. Campbell Update.

[44] Lafarge Canada. Richmond cement plant - gu and gul cements environmental product declaration (epd). Technical report, 2019.

[45] Transport Canada. Transportation 2030: A strategic plan for the future of transportation in canada. Technical report, 2017.

[46] CEMATRIX. Thermal conductivity testing of cellular concrete. amec foster wheeler. no. tb162029. Technical report, 2016.

[47] CEMATRIX. Cematrix lightweight self-compacting flowable closed cell cellular concrete specification. Technical report, n.d.

[48] Karim Chatti and Doseung Lee. Development of a preventive maintenance strategy for minimizing roughness-related pavement damage. *Transportation research record*, 1769(1):39–45, 2001.

[49] Prinya Chindaprasirt and Ubolluk Rattanasak. Shrinkage behavior of structural foam lightweight concrete containing glycol compounds and fly ash. *Materials & Design*, 32(2):723–727, 2011.

[50] Barry R Christopher, Charles W Schwartz, Randy Boudreaux, Ryan R Berg, et al. Geotechnical aspects of pavements. Technical report, United States. Federal Highway Administration, 2006.

[51] David M Cole, Lynne H Irwin, and Thaddeus C Johnson. Effect of freezing and thawing on resilient modulus of a granular soil exhibiting nonlinear behavior. *Transportation Research Record*, 809:19–26, 1981.

[52] Concrete Society. Materials Standing Committee. *Foamed Concrete: Application and Specification: a Report from the Materials Standing Committee of the Concrete Society*. Concrete Society, 2009.

[53] Billy Connor. Comparison of polystyrene expanded and extruded foam insulation in roadway and airport embankments. Technical report, 2019.

[54] Jean Côté and Jean-Marie Konrad. A numerical approach to evaluate the risk of differential surface icing on pavements with insulated sections. *Cold regions science and technology*, 43(3):187–206, 2005.

[55] Jean Côté and Jean-Marie Konrad. Granular protection design to minimize differential icing on insulated pavements. *Canadian geotechnical journal*, 43(3):260–272, 2006.

[56] ASTM D698. Standard test method for laboratory compaction characteristics of soil using standard effort, 2012.

[57] Giorgia Dalla Santa, Fabio Peron, Antonio Galgaro, Matteo Cultrera, David Bertermann, Johannes Mueller, and Adriana Bernardi. Laboratory measurements of gravel thermal conductivity: An update methodological approach. *Energy Procedia*, 125:671–677, 2017.

[58] Jesper Sand Damtoft, Jacques Lukasik, Duncan Herfort, Danielle Sorrentino, and Ellis Martin Gartner. Sustainable development and climate change initiatives. *Cement and concrete research*, 38(2):115–127, 2008.

[59] Martin Deckỳ, Marian Drusa, Katarína Zgútová, Matej Blaško, Matej Hájek, and Walter Scherfel. Foam concrete as new material in road constructions. *Procedia engineering*, 161:428–433, 2016.

[60] Barry Jo Dempsey. *A heat-transfer model for evaluating frost action and temperature related effects in multilayered pavement systems*. University of Illinois at Urbana-Champaign, 1969.

[61] Brian K Diefenderfer, Imad L Al-Qadi, and Stacey D Diefenderfer. Model to predict pavement temperature profile: development and validation. *Journal of Transportation Engineering*, 132(2):162–167, 2006.

[62] MM Disfani, Arul Arulrajah, MW Bo, and N Sivakugan. Environmental risks of using recycled crushed glass in road applications. *Journal of Cleaner Production*, 20(1):170–179, 2012.

[63] B Dolton, M Witchard, D Luzzi, and TJ Smith. Application of lightweight cellular concrete to reconstruction of settlement prone roadways in victoria, 2016.

[64] Brad Dolton and S McIntosh. Reconstruction of a high-volume bus lane using cellular concrete. In *Proceedings of the 71st Canadian Geotechnical Conference and the 13th Joint CGS/IAH-CNC Groundwater Conference, Edmonton, Alberta, Canada, September 23th-26th*, 2018.

[65] H Donovan, F Kanji, and B Dolton. Performance of a trial section reconstructed using cellular concrete in the city of edmonton. In *TAC 2018: Innovation and Technology: Evolving Transportation-2018 Conference and Exhibition of the Transportation Association of Canada*, 2018.

[66] Guy Dore, Jean Marie Konrad, Marius Roy, and Nelson Rioux. Use of alternative materials in pavement frost protection: Material characteristics and performance modeling. *Transportation research record*, (1481), 1995.

[67] M Drusa, M Decky, et al. Designing and quality control of earth structures on transport constructions. *Edis Uniza*, 522, 2013.

[68] J Eisenmann and A Hilmer. Influence of wheel load and inflation pressure on the rutting effect at asphalt-pavements: experiments and theoretical investigations. In *International conference on the structural design*, 1987.

[69] Mohab El-Hakim. Instrumentation and overall evaluation of perpetual and conventional flexible pavement designs. Master's thesis, University of Waterloo, 2009.

[70] John El Khoury, Barbar Akle, Samer Katicha, Ahmad Ghaddar, and Makram Daou. A microscale evaluation of pavement roughness effects for asset management. *International Journal of Pavement Engineering*, 15(4):323–333, 2014.

[71] Ahmed Ebrahim Abu El-Maaty. Temperature change implications for flexible pavement performance and life. *International Journal of Transportation Engineering and Technology*, 3(1):1–11, 2017.

[72] UN Environment, Karen L Scrivener, Vanderley M John, and Ellis M Gartner. Eco-efficient cements: Potential economically viable solutions for a low-co2 cement-based materials industry. *Cement and Concrete Research*, 114:2–26, 2018.

[73] EPA 1996. Large Stationary Diesel And All Stationary Dual-fuel Engines. AP-42, Vol. I, CH 3.4.

[74] EPA 2008. Non Roads 2008a Technical reports.

[75] David C Esch. Control of permafrost degradation beneath a roadway by subgrade insulation. 1972.

[76] Steven R Evett. Soil water measurement by time domain reflectometry. *Encyclopedia of water science*, pages 894–898, 2003.

[77] Devid Falliano, Dario De Domenico, Giuseppe Ricciardi, and Ernesto Gugliandolo. Experimental investigation on the compressive strength of foamed concrete: Effect of curing conditions, cement type, foaming agent and dry density. *Construction and Building Materials*, 165:735–749, 2018.

[78] FDOT. Instrumentation of florida's accelerated pavement testing facility. *FDOT-State Materials Office*, 2011.

[79] FHWA 2022. Bridges and Structures. U.S Department of Transportation.

[80] DA Field, T Ruban, A Johnston, D Dixon, and D Lewycky. Edmonton experience with bottom ash and other insulating materials for mitigation of frost heave induced damage in pavements. In *2011 Conference and Exhibition of the Transportation Association of Canada. Transportation Successes: Let's Build on them. 2011 Congress et Exhibition de l'Association des Transports du Canada. Les Succes en Transports: Une Tremplin vers l'AvenirTransportation Association of Canada (TAC)*, 2011.

[81] David JM Flower and Jay G Sanjayan. Green house gas emissions due to concrete manufacture. *The international Journal of life cycle assessment*, 12(5):282–288, 2007.

[82] International Organization for Standardization. Buildings and constructed assets-service life planning-part 5. *Life cycle costing*, 2004.

[83] Delwyn G Fredlund, Hendry Rahardjo, and Murray D Fredlund. *Unsaturated soil mechanics in engineering practice*. John Wiley & Sons, 2012.

[84] H Christopher Frey. Quantification of uncertainty in emission factors and inventories. *Unpublished manuscript, Department of Civil, Construction, and Environmental Engineering, North Carolina State University, Raleigh, NC Retrieved from https://www. researchgate. net/publication/228618100_Quantification_of_Uncertainty_in_Emission_ Factors_and_Inventories*, 2007.

[85] H Christopher Frey, William Rasdorf, and Phil Lewis. Comprehensive field study of fuel use and emissions of nonroad diesel construction equipment. *Transportation Research Record*, 2158(1):69–76, 2010.

[86] Geocomp 2022. Pavement Instrumentation.

[87] A Giannakou and MR Jones. Potential of foamed concrete to enhance the thermal performance of low-rise dwellings. In *Innovations and Developments In Concrete Materials And Construction: Proceedings of the International Conference held at the University of Dundee, Scotland, UK on 9–11 September 2002*, pages 533–544. Thomas Telford Publishing, 2002.

[88] F Griffiths and M Popik. Pavement evaluation-cematrix site dixie road, caledon, ontario. *Thurber Engineering Ltd*, 2010.

[89] Negar Tavafzadeh Haghi, Leila Hashemian, and Alireza Bayat. Effects of seasonal variation on the load-bearing capacity of pavements composed of insulation layers. *Transportation Research Record*, 2579(1):87–95, 2016.

[90] Negar Tavafzadeh Haghi, Leila Hashemian, and Alireza Bayat. Seasonal response and damage evaluation of pavements comprised of insulation layers. *International Journal of Pavement Research and Technology*, 12(2):170–177, 2019.

[91] Negar Tavafzadeh Haghi, Somayeh Nassiri, Mohammad Hossein Shafiee, and Alireza Bayat. Using field data to evaluate bottom ash as pavement insulation layer. *Transportation Research Record*, 2433(1):39–47, 2014.

[92] Matej Hajek, Martin Decky, Marian Drusa, Lucia Orininová, and Walter Scherfel. Elasticity modulus and flexural strength assessment of foam concrete layer of poroflow. In *IOP conference series: Earth and environmental science*, volume 44, page 022021. IOP Publishing, 2016.

[93] Gregory E Halsted, David Robert Luhr, and Wayne S Adaska. *Guide to cement-treated base (CTB)*. 2006.

[94] J Harvey, A Kendall, IS Lee, N Santero, T Van Dam, and T Wang. Pavement life cycle assessment workshop: discussion summary and guidelines (technical memorandum: Ucprc-tm-2010-03). *Pavement Research Center, University of California, Davis, California, USA*, 2010.

[95] John Harvey, Joep Meijer, Hasan Ozer, Imad L Al-Qadi, Arash Saboori, Alissa Kendall, et al. Pavement life cycle assessment framework. Technical report, United States. Federal Highway Administration, 2016.

[96] Robert L Hayden and Herbert N Swanson. Styrofoam highway insulation on colorado mountain passes. 1972.

[97] Mahsa Hedayati and Sahadat Hossain. Data based model to estimate subgrade moisture variation case study: Low volume pavement in north texas. *Transportation Geotechnics*, 3:48–57, 2015.

[98] Vimy Ina Henderson. *Evaluation of the performance of pervious concrete pavement in the Canadian climate*. PhD thesis, University of Waterloo, 2012.

[99] Chris A Hendriks, Ernst Worrell, David De Jager, K Blok, and Pierce Riemer. Emission reduction of greenhouse gases from the cement industry. In *Proceedings of the fourth international conference on greenhouse gas control technologies*, pages 939–944. IEA GHG R&D Programme Interlaken, Austria, 1998.

[100] Kristian Dahl Hertz and Anne Bagger. Co2 emissions from super-light structures. In *International Association for Shell and Spatial Structures (IABSE-IASS) Symposium 2011*, 2011.

[101] Kristian Dahl Hertz and Philip Halding. *Sustainable light concrete structures*. Springer, 2022.

[102] Inge Hoff, A Watn, E Øiseth, A Emdal, and KO Amundsgård. Light weight aggregate (lwa) used in road pavements. In *Bearing Capacity of Roads, Railways and Airfields*, pages 1013–1022. CRC Press, 2020.

[103] Suksun Horpibulsuk, Apirat Wijitchot, Anek Nerimitknornburee, SL Shen, and Cherdsak Suksiripattanapong. Factors influencing unit weight and strength of lightweight cemented clay. *Quarterly Journal of Engineering Geology and Hydrogeology*, 47(1):101–109, 2014.

[104] Arpad Horvath. Palate—pavement life-cycle tool for environmental and economic effects, 2007.

[105] M Shabbir Hossain, Alex K Apeagyei, et al. Evaluation of the lightweight deflectometer for in-situ determination of pavement layer moduli. Technical report, Virginia Transportation Research Council, 2010.

[106] Yang Hsien Huang et al. *Pavement analysis and design*, volume 2. Pearson Prentice Hall Upper Saddle River, NJ, 2004.

[107] Yunyan Huang, Mohamad Molavi Nojumi, Leila Hashemian, and Alireza Bayat. Performance evaluation of different insulating materials using field temperature and moisture data. *Transportation Research Record*, 2675(9):595–607, 2021.

[108] Deborah N Huntzinger and Thomas D Eatmon. A life-cycle assessment of portland cement manufacturing: comparing the traditional process with alternative technologies. *Journal of cleaner production*, 17(7):668–675, 2009.

[109] S Immanuel and David H Timm. Measured and theoretical pressures in base and subgrade layers under dynamic truck loading. In *Airfield and Highway Pavement: Meeting Today's Challenges with Emerging Technologies*, pages 155–166, 2006.

[110] American Concrete Institute. Aci 523.3 r-14 guide for cellular concretes above 50 lb/ft 3 (800 kg/m3). American Concrete Institute Farmington Hills, MI, USA, 2014.

[111] ASM Institute. Cement and structural concrete products: Life cycle inventory update# 2, 2005.

[112] Asphalt Institute. *Superpave TM Mix Design*. Superpave Series SP-2, Lexington, Kentucky, USA, 1996.

[113] Md Islam, Rafiqul A Tarefder, et al. Measuring thermal effect in the structural response of flexible pavement based on field instrumentation. *International Journal of Pavement Research & Technology*, 6(4), 2013.

[114] Md Rashadul Islam, Sanjida Ahsan, and Rafiqul A Tarefder. Modeling temperature profile of hot-mix asphalt in flexible pavement. *International Journal of Pavement Research and Technology*, 8(1):47, 2015.

[115] Nan Ji Jin, Kyu-Seok Yeon, Seung-Ho Min, and Jaeheum Yeon. Using the maturity method in predicting the compressive strength of vinyl ester polymer concrete at an early age. *Advances in Materials Science and Engineering*, 2017, 2017.

[116] Peerapong Jitsangiam, Korakod Nusit, Suphat Chummuneerat, Prinya Chindaprasirt, and Preda Pichayapan. Fatigue assessment of cement-treated base for roads: An examination of beam-fatigue tests. *Journal of Materials in Civil Engineering*, 28(10):04016095, 2016.

[117] Chester W Jones, DG Miedema, and Joel S Watkins. Frost action in soil foundations and control of surface structure heaving. 1982.

[118] M Roderick Jones, Michael J McCarthy, and Aikaterini McCarthy. Moving fly ash utilisation in concrete forward: A uk perspective. In *Proceedings of the 2003 International Ash Utilization Symposium*, pages 20–22. University Press of Kentucky Lexington, KY, USA, 2003.

[119] M Roderick Jones, Kezban Ozlutas, and Li Zheng. Stability and instability of foamed concrete. *Magazine of Concrete Research*, 68(11):542–549, 2016.

[120] MR Jones. Foamed concrete for structural use. In *Proceedings of one day seminar on foamed concrete: properties, applications and latest technological developments, Loughborough University*, pages 27–60, 2001.

[121] MR Jones and A McCarthy. Preliminary views on the potential of foamed concrete as a structural material. *Magazine of concrete research*, 57(1):21–31, 2005.

[122] MR Jones and A McCarthy. Heat of hydration in foamed concrete: Effect of mix constituents and plastic density. *Cement and concrete research*, 36(6):1032–1041, 2006.

[123] Roderick Jones, Li Zheng, Amarnath Yerramala, and Kharidu Srinivasa Rao. Use of recycled and secondary aggregates in foamed concretes. *Magazine of concrete research*, 64(6):513–525, 2012.

[124] Sajan K Jose, Mini Soman, and Y Sheela Evangeline. Influence of mixture composition on the properties of foamed concrete. *Materials Today: Proceedings*, 42:399–404, 2021.

[125] MCG Juenger, Frank Winnefeld, J Lt Provis, and JH Ideker. Advances in alternative cementitious binders. *Cement and concrete research*, 41(12):1232–1243, 2011.

[126] S Karl and J-D Wörner. Foamed concrete—mixing and workability. In *Special Concretes-Workability and Mixing*, pages 220–226. CRC Press, 1993.

[127] E Kearsley and M Visagie. Properties of foamed concrete as influenced by air-void parameters. *Concr. Beton*, 101:8–14, 2002.

[128] EP Kearsley. The use of foamcrete for affordable development in third world countries. *Concrete in the service of mankind: Appropriate concrete technology*, 3:232, 1996.

[129] EP Kearsley and P Booysens. Reinforced foamed concrete-can it be durable? *Concrete Beton*, (91), 1998.

[130] EP Kearsley and PJ Wainwright. The effect of high fly ash content on the compressive strength of foamed concrete. *Cement and concrete research*, 31(1):105–112, 2001.

[131] EP Kearsley and PJ Wainwright. Porosity and permeability of foamed concrete. *Cement and concrete research*, 31(5):805–812, 2001.

[132] EP Kearsley and PJ Wainwright. The effect of porosity on the strength of foamed concrete. *Cement and concrete research*, 32(2):233–239, 2002.

[133] Brian R Keeble. The brundtland report:'our common future'. *Medicine and war*, 4(1):17–25, 1988.

[134] Zafrul H Khan, Md Rashadul Islam, and Rafiqul A Tarefder. Determining asphalt surface temperature using weather parameters. *Journal of Traffic and Transportation Engineering (English Edition)*, 6(6):577–588, 2019.

[135] Hyeong-Ki Kim, JH Jeon, and Haeng-Ki Lee. Workability, and mechanical, acoustic and thermal properties of lightweight aggregate concrete with a high volume of entrained air. *Construction and Building Materials*, 29:193–200, 2012.

[136] Paul Klieger. *Significance of tests and properties of concrete and concrete-making materials*, volume 169. ASTM International, 1994.

[137] Sachi Kodippily, Susan L Tighe, Theunis FP Henning, and John Yeaman. Evaluating pavement performance through smart monitoring–effects of soil moisture, temperature and traffic. *Road Materials and Pavement Design*, 19(1):71–86, 2018.

[138] IT Koudriashoff. Manufacture of reinforced foam concrete roof slabs. In *Journal Proceedings*, volume 46, pages 37–48, 1949.

[139] EK Kunhanandan Nambiar and K Ramamurthy. Fresh state characteristics of foam concrete. *Journal of materials in civil engineering*, 20(2):111–117, 2008.

[140] Yee Loon Lee, Kau Soon Goh, Heng Boon Koh, and Bakar Ismail. Foamed aggregate pervious concrete–an option for road on peat. 2009.

[141] Qing Li, Fengxiang Qiao, and Lei Yu. Clustering pavement roughness based on the impacts on vehicle emissions and public health. *Journal of Ergonomics*, 5(146):1000146, 2015.

[142] Qing Li, Fengxiang Qiao, and Lei Yu. Impacts of pavement types on in-vehicle noise and human health. *Journal of the Air & Waste Management Association*, 66(1):87–96, 2016.

[143] Genovaitė Liobikienė and Mindaugas Butkus. The european union possibilities to achieve targets of europe 2020 and paris agreement climate policy. *Renewable Energy*, 106:298–309, 2017.

[144] Albert Litvin et al. Sp-029: Lightweight concrete. *Special Publication*, 29, 1971.

[145] Hongwei Liu, Pooneh Maghoul, and Ahmed Shalaby. Optimum insulation design for buried utilities subject to frost action in cold regions using the nelder-mead algorithm. *International Journal of Heat and Mass Transfer*, 130:613–639, 2019.

[146] Michael Yong Jing Liu, U Johnson Alengaram, Mohd Zamin Jumaat, and Kim Hung Mo. Evaluation of thermal conductivity, mechanical and transport properties of lightweight aggregate foamed geopolymer concrete. *Energy and Buildings*, 72:238–245, 2014.

[147] Qingfan Liu. *Field measurement and finite element simulation of pavement responses to standard and reduced tire pressure*. University of Manitoba (Canada), 2011.

[148] Andreas Loizos, Manfred N Partl, Tom Scarpas, and Imad L Al-Qadi. *Advanced Testing and Characterization of Bituminous Materials, Two Volume Set*. CRC Press, 2009.

[149] Amara Loulizi, Imad L Al-Qadi, and Mostafa Elseifi. Difference between in situ flexible pavement measured and calculated stresses and strains. *Journal of transportation engineering*, 132(7):574–579, 2006.

[150] Pan Lu and Denver Tolliver. Pavement treatment short-term effectiveness in iri change using long-term pavement program data. *Journal of transportation engineering*, 138(11):1297–1302, 2012.

[151] Erland O Lukanen, Chunhua Han, and Eugene L Skok Jr. Probabilistic method of asphalt binder selection based on pavement temperature. *Transportation research record*, 1609(1):12–20, 1998.

[152] Erland O Lukanen, Richard Stubstad, Robert C Briggs, and Braun Intertec. Temperature predictions and adjustment factors for asphalt pavement. Technical report, Turner-Fairbank Highway Research Center, 2000.

[153] MLJ Maher and JB Hagan. Constructability benefits of the use of lightweight foamed concrete fill (lfcf) in pavement applications. In *Proceedings of the Annual Conference—Canadian Society for Civil Engineering*, volume 2, pages 1354–1362, 2016.

[154] Attapole Malai and Sompote Youwai. Stiffness of expanded polystyrene foam for different stress states. *International Journal of Geosynthetics and Ground Engineering*, 7(4):1–11, 2021.

[155] Rajib B Mallick and Tahar El-Korchi. *Pavement engineering: principles and practice*. CRC Press, 2008.

[156] Medgar Marceau, Michael A Nisbet, and Martha G Van Geem. Life cycle inventory of portland cement manufacture. Technical report, Portland Cement Association Skokie, IL, USA, 2006.

[157] Chris Marshall, Roger Meier, and Michael Welch. Seasonal temperature effects on flexible pavements in tennessee. *Transportation research record*, 1764(1):89–96, 2001.

[158] Aikaterini McCarthy. *Thermally insulating foundations and ground slabs for sustainable housing using foamed concrete*. PhD thesis, University of Dundee, 2004.

[159] Fred C McCormick. Ratioanl proportioning of preformed foam cellular concrete. In *Journal Proceedings*, volume 64, pages 104–110, 1967.

[160] G McGovern. Manufacture and supply of ready-mix foamed concrete. In *One Day Awareness Seminar on Foamed Concrete: Properties, Applications and Potential, University of Dundee, Scotland*, pages 12–25, 2000.

[161] H Miller, C Cabral, M Kestler, R Berg, and R Eaton. Calibration of a freeze-thaw prediction model for spring load restriction timing in northern new england. In *Cold Regions Engineering 2012: Sustainable Infrastructure Development in a Changing Cold Environment*, pages 369–379. 2012.

[162] Heather J Miller, Christopher Cabral, Maureen A Kestler, and Richard Berg. Aurora spr-3 (042), phase 1: Review of seasonal weight restriction models for comparison and demonstration project. *Transportation Research Board 94th Annual MeetingTransportation Research Board*, (15-2845), 2015.

[163] Qingyan Min. Quantifying greenhouse gas mitigation measures during provincial highway design, construction, and maintenance activities. Master's thesis, University of Waterloo, 2020.

[164] Manuel JC Minhoto, Jorge C Pais, Paulo AA Pereira, and Luís G Picado-Santos. Predicting asphalt pavement temperature with a three-dimensional finite element method. *Transportation Research Record*, 1919(1):96–110, 2005.

[165] Mizan Moges, Amr Ayed, Giannin Viecili, and Amir Abd El Halim. Review and recommendations for canadian lcca guidelines. In *TAC 2017: Investing in Transportation: Building Canada's Economy–2017 Conference and Exhibition of the Transportation Association of Canada*, 2017.

[166] Mizan Moges, Amr Ayed, Giannin Viecili, and Amir Abd El Halim. Review and recommendations for canadian lcca guidelines. In *TAC 2017: Investing in Transportation: Building Canada's Economy–2017 Conference and Exhibition of the Transportation Association of Canada*, 2017.

[167] Maziah Mohammad. *Development of foamed concrete: enabling and supporting design.* PhD thesis, University of Dundee Scotland, UK, 2011.

[168] A Montepara, G Tebaldi, Alessandro Marradi, and Giacomo Betti. Effect on pavement performance of a subbase layer composed by natural aggregate and rap. *Procedia-Social and Behavioral Sciences*, 53:980–989, 2012.

[169] Trevor Moore, Steven Jagdat, Tom Kazmierowski, and Leonard Ng. Quality metrics for recycled concrete aggregates in municipal roads. 2014.

[170] EK Kunhanandan Nambiar and K Ramamurthy. Influence of filler type on the properties of foam concrete. *Cement and concrete composites*, 28(5):475–480, 2006.

[171] EK Kunhanandan Nambiar, K Ramamurthy, et al. Shrinkage behavior of foam concrete. *Journal of materials in civil engineering*, 21(11):631–636, 2009.

[172] N Narayanan and K Ramamurthy. Structure and properties of aerated concrete: a review. *Cement and Concrete composites*, 22(5):321–329, 2000.

[173] Filzah Nasir. Integration of environmental costs in ontario's pavement management systems. Master's thesis, University of Waterloo, 2018.

[174] Frank Mi-Way Ni. *Lightweight Cellular Concrete: Applicability of Pavement Subbase Layer Materials.* PhD thesis, University of Waterloo, 2021.

[175] Frank Mi-Way Ni, Abimbola Grace Oyeyi, Sergey Averyanov, Susan Tighe, Brad Dolton, and Jim Li. Properties of ultra-low density lightweight cellular concrete containing slag. Technical report, 2019.

[176] Frank Mi-Way Ni, Abimbola Grace Oyeyi, and Susan Tighe. Structural capacity evaluation of lightweight cellular concrete for flexible pavement subbase. *Road Materials and Pavement Design*, pages 1–17, 2021.

[177] Balwinder Nimana, Christina Canter, and Amit Kumar. Life cycle assessment of greenhouse gas emissions from canada's oil sands-derived transportation fuels. *Energy*, 88:544–554, 2015.

[178] American Association of State Highway Transportation Officials. Mechanistic-empirical pavement design guide: A manual of practice. *AASHTO: Washington, DC, USA*, 2008.

[179] American Association of State Highway Transportation Officials. R30, mixture conditioning of hot mix asphalt (hma), 2010.

[180] American Association of State Highway Transportation Officials. Standard practice for preparation of cylindrical performance test specimens using the superpave gyratory compactor (sgc), 2013.

[181] American Association of State Highway Transportation Officials T342. Standard method of test for determining dynamic modulus of hot mix asphalt (hma), 2011.

[182] Ministry of Transportation of Ontario. Pavement design and rehabilitation manual, 2013.

[183] Ministry of Transportation of Ontario. Green pavement design rating system," reference guide for new, reconstruction and rehabilitation of ontario pavement structures. Technical report, 2014.

[184] Ministry of Transportation Ontario. Manual for assessment of surface defects of in-place recycled pavement mats. 2015.

[185] Ministry of Transportation Ontario. Ontario's default parameters for aashtoware pavement me design interim report. 2019.

[186] University of Waterloo 2011. Indirect tensile strength and resilient modulus testing of cematrix cellular concrete. unpublished test report. Technical report, 2013.

[187] Md Azree Othuman and YC Wang. Elevated-temperature thermal properties of lightweight foamed concrete. *Construction and Building Materials*, 25(2):705–716, 2011.

[188] Abimbola Grace Oyeyi, Frank Mi-Way Ni, Daniel Pickel, and Susan Tighe. Lightweight cellular concrete as a subbase alternative in pavements: Instrumentation plan, installation and preliminary results. In *Transportation Association of Canada and ITS Canada 2019 Joint Conference and Exhibition*, 2019.

[189] Kezban Ozlutas. *Behaviour of ultra-low density foamed concrete*. PhD thesis, University of Dundee Scotland, UK, 2015.

[190] Dong-Yeob Park, Neeraj Buch, and Karim Chatti. Effective layer temperature prediction model and temperature correction via falling weight deflectometer deflections. *Transportation Research Record*, 1764(1):97–111, 2001.

[191] Hee Mun Park and Y Richard Kim. Prediction of remaining life of asphalt pavement with falling-weight deflectometer multiload-level deflections. *Transportation research record*, 1860(1):48–56, 2003.

[192] Jeong Jun Park, Eun Chul Shin, and Byoung Jo Yoon. Development of frost penetration depth prediction model using field temperature data of asphalt pavement. *International Journal of Offshore and Polar Engineering*, 26(04):341–347, 2016.

[193] Arthur C. Parola and Colin J. Apelt. debris forces on highway bridges. Technical report, 2000.

[194] William Paterson. A transferable causal model for predicting roughness progression in flexible pavements. *Transportation Research Record*, (1215), 1989.

[195] Pavement Interactive 2022. Frost Action.

[196] Edward Penner. Experimental pavement structures insulated with a polyurethane and extruded polystyrene foam. *Physics of Snow and Ice: proceedings*, 1(2):1311–1322, 1967.

[197] Oshani Perera, Barbara Morton, and Tina Perfrement. Life cycle costing in sustainable public procurement: A question of value. 2009.

[198] Rohan W Perera, Abdalla S Al-Rawashdeh, et al. Investigation of increase in roughness due to environmental factors in flexible pavements using profile data from long-term pavement performance specific pavement studies 1 experiment. Technical report, United States. Federal Highway Administration, 2017.

[199] Rohan W Perera and Starr D Kohn. Ride quality performance of asphalt concrete pavements subjected to different rehabilitation strategies. In *Airfield and Highway Pavement: Meeting Today's Challenges with Emerging Technologies*, pages 789–800, 2006.

[200] Daniel Pickel. *Precast concrete inlay panels: rehabilitation strategy for high-volume highways in Ontario*. PhD thesis, University of Waterloo, 2018.

[201] Daniel Pickel, Susan Tighe, Warren Lee, and Rico Fung. Highway 400 precast concrete inlay panel project: Instrumentation plan, installation, and preliminary results. *Canadian Journal of Civil Engineering*, 45(10):889–898, 2018.

[202] Linda M Pierce, James E Bruinsma, Kurt D Smith, Monty J Wade, Karim Chatti, Julie Vandenbossche, et al. Using falling weight deflectometer data with mechanistic-empirical design and analysis, volume iii: Guidelines for deflection testing, analysis, and interpretation. Technical report, United States. Federal Highway Administration, 2017.

[203] Portland Cement Association 2016. Environmental Product Declaration: Portland Cements.

[204] Portland Cement Association 2022. Freeze-Thaw Resistance.

[205] Nadia Pouliot and Yves Savard. High density expanded polysterene boards as road insulation, phase i. *Performance Evaluation of Expanded Polystyrene on Road 161 ins St-Martyrs-Canadiens*, 2003.

[206] National Cooperative Highway Research Program. Manual for fwd testing in the long-term pavement performance program. (report no. shrp-p-661). pcs law engineering and braun intertec pavement, inc. national research council, washington, dc. Technical report, 1993.

[207] National Cooperative Highway Research Program. Mepdg-guide for mechanistic-empirical design of new and rehabilitated pavement structures. transportation research board, national research council. Technical report, 2004.

[208] Yinghong Qin and Jacob E Hiller. Modeling temperature distribution in rigid pavement slabs: impact of air temperature. *Construction and building materials*, 25(9):3753–3761, 2011.

[209] K Ramamurthy, EK Kunhanandan Nambiar, and G Indu Siva Ranjani. A classification of studies on properties of foam concrete. *Cement and concrete composites*, 31(6):388–396, 2009.

[210] EPBD Recast. Directive 2010/31/eu of the european parliament and of the council of 19 may 2010 on the energy performance of buildings (recast). *Official Journal of the European Union*, 18(06):2010, 2010.

[211] T Richard, Joseph Dobogai, T Gerhardt, and W Young. Cellular concrete-a potential load-bearing insulation for cryogenic applications? *IEEE Transactions on Magnetics*, 11(2):500–503, 1975.

[212] Richway 2022. CRETEFOAMER Cellular Concrete Calculator .

[213] Thomas Norton Rumney and RA Jimenez. Pavement temperatures in the southwest. *Highway Research Record*, 361:1–13, 1969.

[214] Thorbjorg Saevarsdottir and Sigurdur Erlingsson. Water impact on the behaviour of flexible pavement structures in an accelerated test. *Road Materials and Pavement Design*, 14(2):256–277, 2013.

[215] Farhad Salour. *Moisture influence on structural behaviour of pavements: Field and Laboratory Investigations*. PhD thesis, KTH Royal Institute of Technology, 2015.

[216] Farhad Salour and Sigurdur Erlingsson. *Pavement structural behaviour during spring thaw: interpretation of FWD measurements by monitoring environmental data from county road 126 at Torpsbruk*. Statens väg-och transportforskningsinstitut, 2012.

[217] Farhad Salour and Sigurdur Erlingsson. Investigation of a pavement structural behaviour during spring thaw using falling weight deflectometer. *Road Materials and Pavement Design*, 14(1):141–158, 2013.

[218] Farhad Salour and Sigurdur Erlingsson. *Impact of groundwater level on the mechanical response of a flexible pavement structure: a case study at the Torpsbruk test section along county road 126 using Falling Weight Deflectometer*. VTI, 2014.

[219] Kamarul Aini Mohd Sari and Abdul Rahim Mohammed Sani. Applications of foamed lightweight concrete. In *MATEC Web of Conferences*, volume 97, page 01097. EDP Sciences, 2017.

[220] Michael W Sayers. Guidelines for conducting and calibrating road roughness measurements. Technical report, University of Michigan, Ann Arbor, Transportation Research Institute, 1986.

[221] Michael W Sayers. The little book of profiling: basic information about measuring and interpreting road profiles. Technical report, University of Michigan, Ann Arbor, Transportation Research Institute, 1998.

[222] Adam C Schneider. Sustainable alternative materials in unbound granular layers of pavement structures. Master's thesis, University of Waterloo, 2017.

[223] P Segui, J-P Bilodeau, J Côté, and G Doré. Thermal behavior of flexible pavement containing foam glass aggregates as thermal insulation layer. In *Cold Regions Engineering 2019*, pages 204–212. American Society of Civil Engineers Reston, VA, 2019.

[224] Kevan Shafizadeh and Fred Mannering. Acceptability of pavement roughness on urban highways by driving public. *Transportation Research Record*, 1860(1):187–193, 2003.

[225] Nayyar Zia Siddiki, Daehyeon Kim, and Rodrigo Salgado. Use of recycled and waste materials in indiana. *Transportation research record*, 1874(1):78–85, 2004.

[226] K Krishna Bhavani Siram and K Arjun Raj. Concrete+ green= foam concrete. *International Journal of civil engineering and technology*, 4(4):179–184, 2013.

[227] Scott H Smith and Stephan A Durham. A cradle to gate lca framework for emissions and energy reduction in concrete pavement mixture design. *International Journal of Sustainable Built Environment*, 5(1):23–33, 2016.

[228] Ontario Provincial Standard Specifications. Material specification for aggregates-base, subbase, select subgrade, and backfill material. *OPSS. PROV*, 1010, 2013.

[229] Ontario Provincial Standard Specifications. Material specification for aggregates-base, subbase, select subgrade, and backfill material. *OPSS. PROV*, 1010, 2013.

[230] Statistics Canada 2010. Appendix A: Conversion Factors.

[231] Yin H. Antle C. E. Stoffels, S. M. and S. W. Lim. Integrating condition measurement variability in network pavement management. draft final report. Technical report, 2006.

[232] Bambang Suhendro. Toward green concrete for better sustainable environment. *Procedia Engineering*, 95:305–320, 2014.

[233] Pajtim Sulejmani, Safwat Said, Sven Agardh, and Abubeker Ahmed. Impact of temperature and moisture on the tensile strain of asphalt concrete layers. *International Journal of Pavement Engineering*, 22(13):1711–1719, 2021.

[234] Transportation Association Canada (TAC). Transport asset design and management guide. Technical report, 2013.

[235] MR Taha, S Hardwiyono, NI Md Yusoff, MR Hainin, J Wu, and KAM Nayan. Study of the effect of temperature changes on the elastic modulus of flexible pavement layers. *Research Journal of Applied Sciences, Engineering and Technology*, 5(5):1661–1667, 2013.

[236] AS Tarasov, Elsabe P Kearsley, AS Kolomatskiy, and HF Mostert. Heat evolution due to cement hydration in foamed concrete. *Magazine of concrete research*, 62(12):895–906, 2010.

[237] Christina Tatarniuk and D Lewycky. A case study on the performance of high load polystyrene as roadway insulation in edmonton, alberta, canada. In *Conference and Exhibition of the Transportation Association of Canada-Transportation Successes: Let's Build on Them*, page 121, 2011.

[238] Negar Tavafzadeh Haghi, Leila Hashemian, and Alireza Bayat. The effect of insulation layers on pavement strength during non-freeze–thaw season. *International Journal of Pavement Engineering*, 19(6):543–552, 2018.

[239] S Taylor and G Halsted. Guide to lightweight cellular concrete for geotechnical applications. *PCA Special Rep. No. SR1008P. Washington, DC: Portland Cement Association*, 2021.

[240] R Core Team. R: A language and environment for statistical computing. r foundation for statistical computing, vienna, austria. *http://www. R-project. org/*, 2022.

[241] Susan Tighe. Guidelines for probabilistic pavement life cycle cost analysis. *Transportation research record*, 1769(1):28–38, 2001.

[242] Susan L Tighe et al. Accelerated testing and instrumentation: A canadian case study. In *9th International Conference on Managing Pavement Assets*, 2015.

[243] Susan Louise Tighe, Lynne Cowe Falls, Ralph Haas, and Donaldson MacLeod. Climate impacts and adaptations on roads in northern canada. Technical report, 2006.

[244] Paul J Tikalsky, James Pospisil, and William MacDonald. A method for assessment of the freeze–thaw resistance of preformed foam cellular concrete. *Cement and concrete research*, 34(5):889–893, 2004.

[245] Binod Tiwari, Beena Ajmera, Ryan Maw, Ryan Cole, Diego Villegas, and Peter Palmerson. Mechanical properties of lightweight cellular concrete for geotechnical applications. *Journal of Materials in Civil Engineering*, 29(7):06017007, 2017.

[246] Transportation Association of Canada (TAC). Transportation Asset Management Best Practices for Canada.

[247] Takashi Tsuchida and Kazuhiko Egashira. *The lightweight treated soil method: new geomaterials for soft ground engineering in coastal areas*. CRC Press, 2004.

[248] J-C Turtschy. Advanced model for analytical design of european pavement structures. Technical report, 2000.

[249] E Tutumluer. Practices for unbound aggregate pavement layers. nchrp synthesis 445. *Transportation Research Board, Washington, DC*, 2013.

[250] Ishfaq Mohi ud Din, Mohammad Shafi Mir, and Mohammad Adnan Farooq. Effect of freeze-thaw cycles on the properties of asphalt pavements in cold regions: a review. *Transportation Research Procedia*, 48:3634–3641, 2020.

[251] L Uzarowski and G Moore. Sustainable pavements-making the case for longer design lives for flexible pavements. In *2008 Annual Conference of the Transportation Association of CanadaTransportation Association of Canada (TAC)*, 2008.

[252] Rudolph C Valore et al. Cellular concretes part 1 composition and methods of preparation. In *Journal Proceedings*, volume 50, pages 773–796, 1954.

[253] SK Vanapalli, DG Fredlund, DE Pufahl, and AW Clifton. Model for the prediction of shear strength with respect to soil suction. *Canadian geotechnical journal*, 33(3):379–392, 1996.

[254] PV Vijay and Justin S Smith. Mechanical concrete for enhancing the properties of pavement base/subbase. In *Geo-Congress 2019: Geotechnical Materials, Modeling, and Testing*, pages 287–295. American Society of Civil Engineers Reston, VA, 2019.

[255] Harold L Von Quintus, Ahmed Eltahan, and Amber Yau. Smoothness models for hot-mix asphalt-surfaced pavements: Developed from long-term pavement performance program data. *Transportation research record*, 1764(1):139–156, 2001.

[256] Perera R W and Elkins G E. Ltpp manual for profile measurements and processing. Technical report, Federal Highway Administration McLean, Virginia, 2008.

[257] Hao Wang, Rashmi Gangaram, et al. Life cycle assessment of asphalt pavement maintenance. Technical report, Rutgers University. Center for Advanced Infrastructure and Transportation, 2014.

[258] Zilong Wang and Hao Wang. Life-cycle cost analysis of optimal timing of pavement preservation. *Frontiers of Structural and Civil Engineering*, 11(1):17–26, 2017.

[259] Tiong-Huan Wee, Daneti Saradhi Babu, T Tamilselvan, and Hwee-Sin Lim. Air-void system of foamed concrete and its effect on mechanical properties. *ACI materials journal*, 103(1):45, 2006.

[260] Moira A Wilson, WD Hoff, and Christopher Hall. Water movement in porous building materials—x. absorption from a small cylindrical cavity. *Building and Environment*, 26(2):143–152, 1991.

[261] Ernst Worrell, Lynn Price, Nathan Martin, Chris Hendriks, and Leticia Ozawa Meida. Carbon dioxide emissions from the global cement industry. *Annual review of energy and the environment*, 26(1):303–329, 2001.

[262] WOWA 2022. Bank of Canada Interest Rate.

[263] Dayong Wu, Changwei Yuan, and Hongchao Liu. A risk-based optimisation for pavement preventative maintenance with probabilistic lcca: a chinese case. *International Journal of Pavement Engineering*, 18(1):11–25, 2017.

[264] Ying Xu and Yi-Chang Tsai. Financial consequences of delaying pavement rehabilitation: Case study using ltpp data. *Journal of transportation engineering*, 138(8):975–982, 2012.

[265] Grigorij Yakovlev, Jadvyga Kerienė, Albinas Gailius, and Ingrida Girnienė. Cement based foam concrete reinforced by carbon nanotubes. *Materials Science [Medžiagotyra]*, 12(2):147–151, 2006.

[266] Yassaman Yousefi. Engineering and environmental assessment of foam glass lightweight aggregate for pavement application. Master's thesis, University of Waterloo, 2019.

[267] Bin Yu. *Environmental implications of pavements: a life cycle view*. University of South Florida, 2013.

[268] Wei Yu, Xu Liang, Frank Mi-Way Ni, Abimbola Grace Oyeyi, and Susan Tighe. Characteristics of lightweight cellular concrete and effects on mechanical properties. *Materials*, 13(12):2678, 2020.

[269] Nur Izzi Md Yusoff, Emmanuel Chailleux, and Gordon D Airey. A comparative study of the influence of shift factor equations on master curve construction. *International Journal of Pavement Research and Technology*, 4(6):324, 2011.

[270] Imen Zaabar and Karim Chatti. Estimating vehicle operating costs caused by pavement surface conditions. *Transportation Research Record*, 2455(1):63–76, 2014.

[271] Jieru Zhang, Gengyuan Liu, Bin Chen, Dan Song, Jing Qi, and Xinyu Liu. Analysis of co2 emission for the cement manufacturing with alternative raw materials: A lca-based framework. *Energy Procedia*, 61:2541–2545, 2014.

[272] Zhuang Zhuo. *Design and Analysis of Flexible Insulated Pavement for Cold Region Applications*. Rowan University, 2021.

[273] Zinta Zimele, Maris Sinka, Aleksandrs Korjakins, Diana Bajare, and Genadijs Sahmenko. Life cycle assessment of foam concrete production in latvia. *Environmental & Climate Technologies*, 23(3), 2019.

[274] Gang Zuo, Eric C Drumm, and Roger W Meier. Environmental effects on the predicted service life of flexible pavements. *Journal of Transportation Engineering*, 133(1):47–56, 2007.

Appendices

Appendix A

Instrumentation

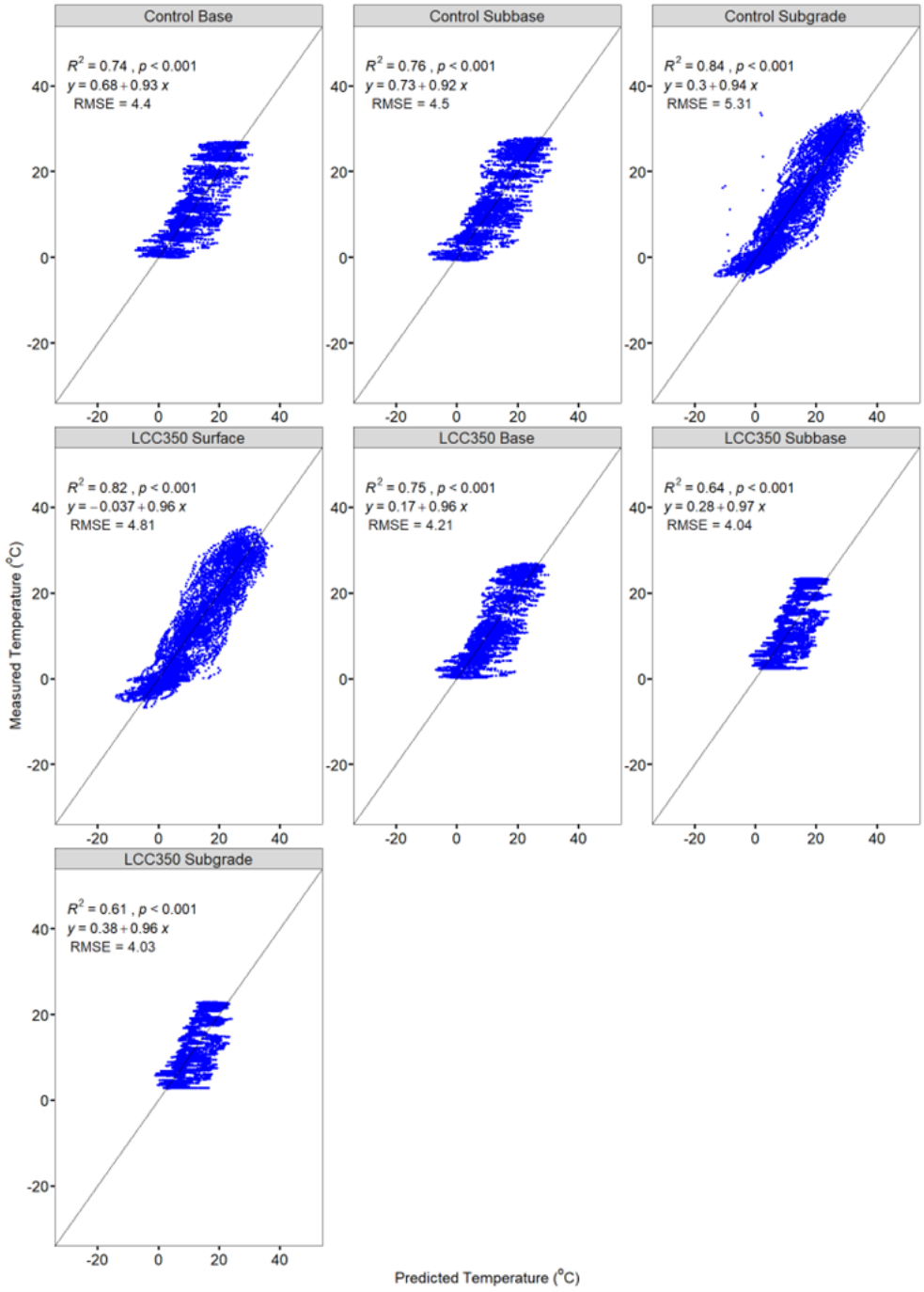

Figure A.1: Erbsville hourly temperature validation with regression models

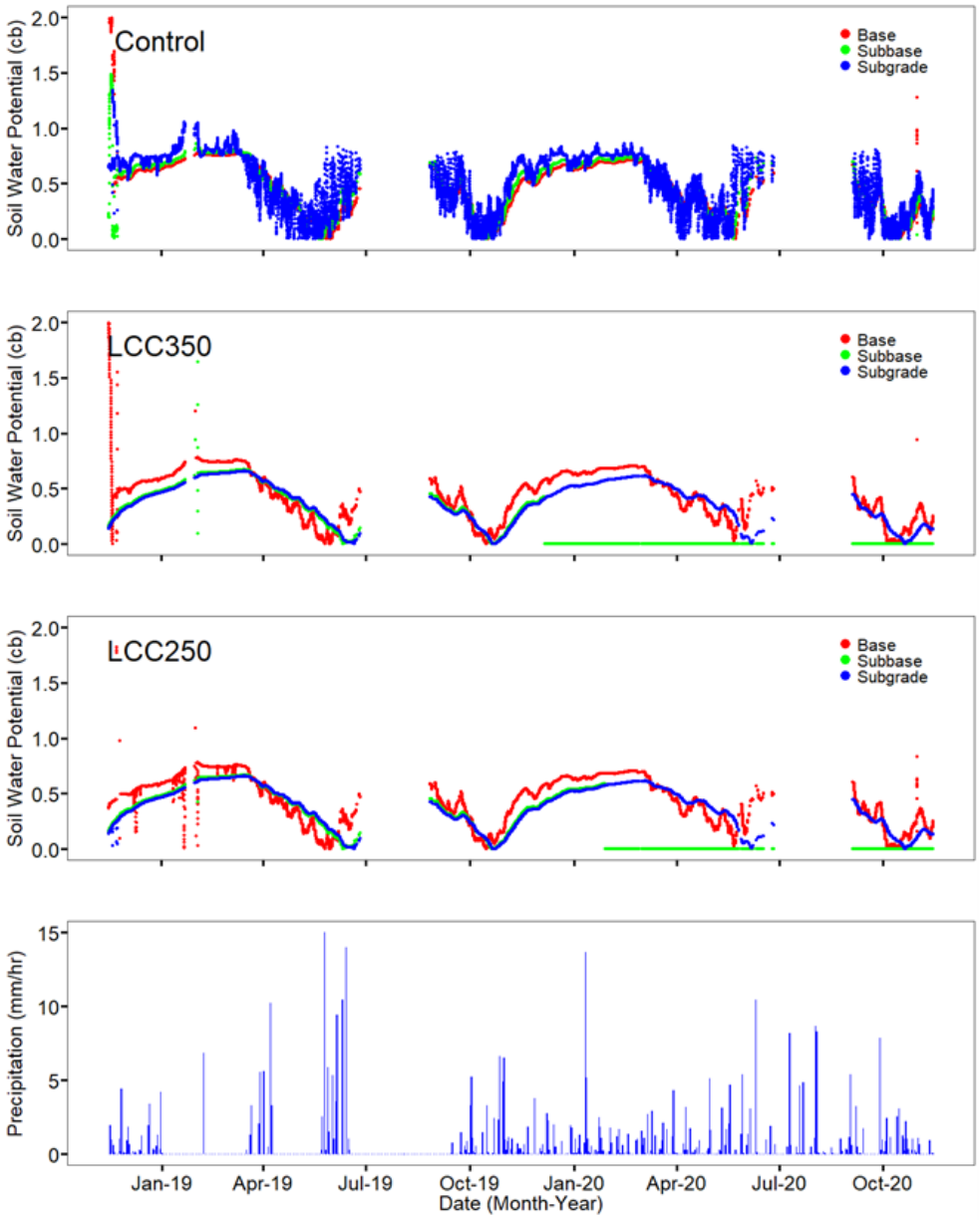

Figure A.2: Erbville precipitation and moisture

Appendix B

Least Square Difference Calculation

Sample Calculation: (Adapted from Pickel, 2018 [200]) Consider the following Elastic Modulus values for each of the three sections at Erbsville that were tested (Table B.1).

Table B.1: Erbsville Elastic Modulus values

Control	**LCC400**	**LCC475**	**LCC600**
#1	548.00	832.33	723.33
#2	506.67	690.33	565.00
#3	521.00	774.00	638.50
#4	574.00	859.33	727.33
#5	775.00	774.33	671.33
#6		825.67	797.67
#7		924.33	918.33
Mean	584.93	811.48	720.21

To determine the 5% LSD Value:

1. Set the significance level b = 0.05 for 5% significance (95% confidence).
2. Set k = 3 as the total number of sections (Control, LCC350, LCC250).
3. Set N = 19 as the total number of results for the three sections.
4. Calculate n = 6.33 as the average number of results for each support condition.

5. Calculate "α" for use in the t-test calculation:

$$\alpha = 1 - (1 - b)^{(\frac{1}{k})} = 1 - (1 - 0.05)^{(\frac{1}{3})} = 0.01695 \tag{B.1}$$

6. Calculate the t-statistic as:

$$t_{\alpha, N-k} = t_{0.01695,16} = 2.66 \tag{B.2}$$

7. Calculate the mean square within groups as the sum of squares divided by the degrees of freedom with number of sections (i.e., N – k = 16).

   Note: a one-way or single-factor ANOVA analysis was carried out using EXCEL to calculate these values:

   Anova: Single Factor, Table B.2 and Table B.3

Table B.2: SUMMARY

Groups	**Count**	**Sum**	**Average**	**Variance**
Control	#1	548.00	832.33	723.33
LCC350	#2	506.67	690.33	565.00
LCC250	#3	521.00	774.00	638.50

Table B.3: ANOVA

Source of Variation	**SS**	**df**	**MS**	**F**	**P**$-value$	**F**$_{crit}$
Between Groups	149731.53	2	74865.766	7.5141134	0.0049992	3.6337235
Within Groups	159413.65	16	9963.3533			
Total	309145.18	18				

8. Calculate the standard error (SE) of the difference between two means:

$$SE = \sqrt{\frac{2(MS)}{N-k}} = \sqrt{\frac{2(9963.35)}{16}} \cong 56.09 \tag{B.3}$$

   Calculate the 5% LSD:

$$5\%LSD = t_{stat} \times SE = (2.66)(56.09) = 149.47 \tag{B.4}$$

This 5% LSD represents the smallest significant difference between two means in the given set of values. Therefore, the mean Modulus of Control and LCCC250 and LCC350 and LCC250 are not significantly different since the difference of their means is approximately 135.28 and 91.26 respectively, which is smaller than the 5% LSD. However, the mean Modulus difference of the Control and LCC350 sections is significantly higher with differences in mean of 226.54. This is higher than the 5% LSD. This means that the Control and LCC350 section are distinctively different.

Time	Section Relationship	SB Left Wheel Path			SB Right Wheel Path			
		Difference in mean	95% LSD	P-value	Difference in mean	95% LSD	P-value	Comment
Sep-22	LCC600-LCC475	0.31	0.31	0.004	0.23	0.47	0.000	Some difference
	LCC600-LCC400	0.08			1.00			
	LCC600-Control	0.24			0.16			
	LCC475-LCC400	0.39			0.78			
	LCC475-Control	0.07			0.06			
	LCC400-Control	0.32			0.84			
Feb-22	LCC600-LCC475	0.05	0.40	0.020	0.03	0.47	0.012	Some difference
	LCC600-LCC400	0.37			4.10			
	LCC600-Control	0.10			0.05			
	LCC475-LCC400	0.32			4.07			
	LCC475-Control	0.15			0.02			
	LCC400-Control	0.47			4.05			
Apr-22	LCC600-LCC475	0.33	0.43	0.012	0.00	0.72	0.000	Some difference
	LCC600-LCC400	0.43			1.33			
	LCC600-Control	0.13			0.22			
	LCC475-LCC400	0.10			1.33			
	LCC475-Control	0.46			0.22			
	LCC400-Control	0.56			1.54			
Jun-22	LCC600-LCC475	0.08	NA	0.292	0.40	0.47	0.012	Some difference
	LCC600-LCC400	0.02			0.08			
	LCC600-Control	0.12			0.40			
	LCC475-LCC400	0.07			0.48			
	LCC475-Control	0.20			0.00			
	LCC400-Control	0.13			0.47			

Figure B.1: Notre Dame southbound section least square difference analysis

Time	Section Relationship	NB Left Wheel Path			NB Right Wheel Path			
		Difference in mean	95% LSD	P-value	Difference in mean	95% LSD	P-value	Comment
Sep-22	LCC600-LCC475	0.33	0.33	0.013	0.39	0.42	0.020	Difference exists within the LCC sections
	LCC600-LCC400	0.05			0.48			
	LCC600-Control	0.20			0.41			
	LCC475-LCC400	0.38			0.10			
	LCC475-Control	0.13			0.02			
	LCC400-Control	0.25			0.08			
Apr-22	LCC600-LCC475	0.09	0.45	0.001	0.35	0.61	0.000	Some difference
	LCC600-LCC400	0.58			0.42			
	LCC600-Control	0.51			1.13			
	LCC475-LCC400	0.49			0.07			
	LCC475-Control	0.42			0.78			
	LCC400-Control	0.07			0.71			
Jun-22	LCC600-LCC475	0.17	NA	0.226	0.08	0.72	0.001	Some difference
	LCC600-LCC400	0.14			0.95			
	LCC600-Control	0.06			0.86			
	LCC475-LCC400	0.31			0.86			
	LCC475-Control	0.12			0.78			
	LCC400-Control	0.19			0.09			

Figure B.2: Notre Dame Drive northbound section least square difference analysis

Seasonal Relationship	Control	LCC350	LCC250	Comments
Dec 18 - June 19	769	1818	1842	Significant difference
Dec 18 - Oct 19	680	1695	1729	Significant difference
Dec 18 - Feb 22	665	360	88	No significant difference except Control
Dec 18 - Apr 22	693	1623	1729	Significant difference
Dec 18 - June 22	608	1582	1680	Significant difference
June 19 - Oct 19	89	123	113	No significant difference
June 19 - Feb 22	1434	1458	1930	Significant difference
June 19 - Apr 22	76	195	113	No significant difference
Jun 19 - Jun 22	161	236	162	No significant difference
Oct 19 - Feb 22	1345	1335	1817	Significant difference
Oct 19 - Apr 22	13	72	0	No significant difference
Oct 19 -June 22	72	112	49	No significant difference
Feb 22 - Apr 22	1358	1263	1817	Significant difference
Feb 22 - June 22	1273	1222	1768	Significant difference
Apr 22 - June 22	85	41	49	No significant difference
95% LSD	**583**	**504**	**191**	
P value	0.000	0.000	0.000	

Figure B.3: Erbsville Seasonal Difference in Mean LWD measured Elastic Modulus and LSD Analysis

Appendix C

General Additive Model Results

```
Family: gaussian
Link function: identity

Formula:
Layer_Temp ~ s(Temperature) + s(Moisture)

Parametric coefficients:
            Estimate Std. Error t value Pr(>|t|)
(Intercept)  12.5728     0.0118    1065   <2e-16 ***
---
Signif. codes:  0 '***' 0.001 '**' 0.01 '*' 0.05 '.' 0.1 ' ' 1

Approximate significance of smooth terms:
                edf Ref.df        F p-value
s(Temperature) 8.919  8.998 54087.33  <2e-16 ***
s(Moisture)    7.267  8.156    31.56  <2e-16 ***
---
Signif. codes:  0 '***' 0.001 '**' 0.01 '*' 0.05 '.' 0.1 ' ' 1

R-sq.(adj) =  0.757   Deviance explained = 75.7%
-REML = 4.6495e+05  Scale est. = 21.862    n = 156993

Family: gaussian
Link function: identity

Formula:
Pressure ~ s(Layer_Temp) + s(Moisture)

Parametric coefficients:
            Estimate Std. Error t value Pr(>|t|)
(Intercept)  1.30225    0.01715   75.92   <2e-16 ***
---
Signif. codes:  0 '***' 0.001 '**' 0.01 '*' 0.05 '.' 0.1 ' ' 1

Approximate significance of smooth terms:
                edf Ref.df       F p-value
s(Layer_Temp) 8.976  9.000 1020.11  <2e-16 ***
s(Moisture)   8.685  8.968   31.27  <2e-16 ***
---
Signif. codes:  0 '***' 0.001 '**' 0.01 '*' 0.05 '.' 0.1 ' ' 1

R-sq.(adj) =  0.114   Deviance explained = 11.5%
-REML = 2.1448e+05  Scale est. = 21.382    n = 72680

Family: gaussian
Link function: identity

Formula:
Strain ~ s(Layer_Temp) + s(Moisture)

Parametric coefficients:
            Estimate Std. Error t value Pr(>|t|)
(Intercept)  29.4929     0.3996   73.81   <2e-16 ***
---
Signif. codes:  0 '***' 0.001 '**' 0.01 '*' 0.05 '.' 0.1 ' ' 1

Approximate significance of smooth terms:
                edf Ref.df       F p-value
s(Layer_Temp) 8.941  8.998 617.300  <2e-16 ***
s(Moisture)   1.035  1.068   0.049   0.878
---
Signif. codes:  0 '***' 0.001 '**' 0.01 '*' 0.05 '.' 0.1 ' ' 1

R-sq.(adj) =  0.0462   Deviance explained = 4.63%
-REML = 7.252e+05  Scale est. = 18301     n = 114629
```

Figure C.1: General Addictive Model results

Appendix D

Life Cycle Assessment

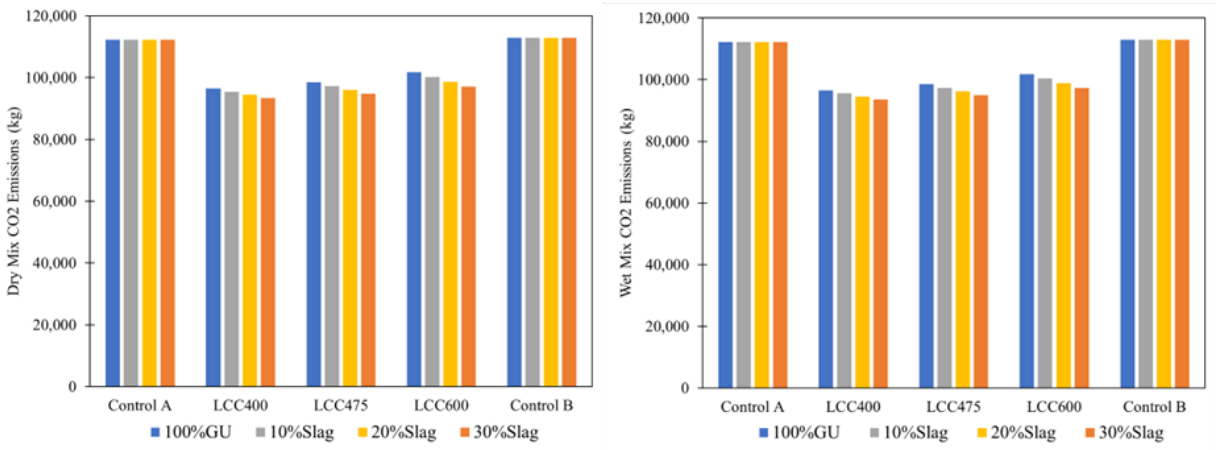

Figure D.1: Sensitivity to change in LCC slag content